Identification of Hindbrain Neural Substrates for Motor Initiation in the hatchling *Xenopus laevis* Tadpole

Giulia Messa

A thesis submitted in partial fulfilment of the requirements of the University of Kent and the University of Greenwich for the Degree of Doctor of Philosophy

December 2021

DECLARATION

I certify that this work has not been accepted in substance for any degree, and is not concurrently being submitted for any degree other than that of Doctor of Philosophy being studied at the Universities of Greenwich and Kent. I also declare that this work is the result of my own investigation except where otherwise identified by references and that I have not plagiarised the work of others.

17/12/2021

ABSTRACT

Animal survival profoundly depends on the ability to detect stimuli in the environment, process them and respond accordingly. In this respect, motor responses to a sensory stimulation evolved into a variety of coordinated movements, which involve the control of brain centres over spinal locomotor circuits. The hatchling *Xenopus* tadpole, even in its embryonic stage, is able to detect external sensory information and to swim away if the stimulus is considered noxious. To do so, the tadpole relies on well-known ascending sensory pathway, which carries the sensory information to the brain. When the stimulus is strong enough, descending interneurons are activated, leading to the excitation of spinal CPG neurons, which causes the undulatory movement of swimming.

However, the activation of descending interneurons that marks the initiation of motor response appears after a long delay from the sensory stimulation. Furthermore, the long-latency response is variable in time, as observed in the slow-summating excitation measured in descending interneurons. These two features, *i.e.* long-latency and variability, cannot be explained by the firing time and pattern of the ascending sensory pathway of the *Xenopus* tadpole. Therefore, a novel neuronal population has been proposed to lie in the hindbrain of the tadpole, and being able to 'hold' the sensory information, thus accounting for the long and variable delay of swim initiation. In this work, the role of the hindbrain in the maintenance of the long and variable response to trunk skin stimulation is investigated in the *Xenopus* tadpole at developmental stage 37/38. A multifaceted approach has been used to unravel the neuronal mechanisms underlying the delayed motor response, including behavioural experiments, electrophysiology analysis of fictive swimming, hindbrain extracellular recordings and imaging experiments.

Two novel neuronal populations have been identified in the tadpole's hindbrain, which exhibit activation patterns compatible with the role of delaying the excitation of the spinal locomotor circuit. Future work on cellular properties and synaptic connections of these newly discovered populations might shed light on the mechanism of descending control active at embryonic stage.

Identifying supraspinal neuronal populations in an embryonic organism could aid in understanding mechanisms of descending motor control in more complex vertebrates.

CONTENTS

LIST OF FIGURES

1 Locomotion in Vertebrates

Locomotion is one of the fundamental features of the animal kingdom. It appeared early during the evolution and can lead to very different final outputs, from the interminable migrations of whales and birds around the globe, to the slow crawling of snails and slugs in our gardens, to the humans' walk to grab a coffee.

Indeed, even the more ancient animals are able to move in order to satisfy their needs, with the necessities of food, shelter and breeding above all. Some of these simpler animals still survive nowadays, as they have evolved to perfectly fit in their ecological niche. This has allowed researchers to study the locomotion mechanisms of a variety of animals, including nudibranchs (Sakurai and Katz, 2015, Sakurai and Katz, 2016), the lamprey (Grillner et al., 2008, Dubuc et al., 2008), the embryonic stages of newts and frogs (Roberts et al., 2010, Roberts et al., 2019) and fish (Fetcho et al., 2008, Berg et al., 2018). Experiments on mammals have been carried out on cats (Shik et al., 1968, Noga et al., 1988, Opris et al., 2019), and mice (Kiehn, 2006, Arber, 2012) (Kiehn, 2016). Intuitively, the type of locomotion one animal can perform is strictly linked to its body characteristics, like shape, weight and the kind of appendices it has, if there are appendices. Nevertheless, the building blocks of the locomotor circuit are conserved among animals, especially among vertebrates (Jung and Dasen, 2015, Katz, 2016, Kiehn, 2006).

Locomotion, and movements in general, are the physical actions that animals, including humans, take to perform behaviours. These can be innate behaviours, for example escaping from a predator, or goal directed behaviours, such as searching for food. In both cases, the motor output rises from the interaction between neuronal activity at a central level (both in the brain and in the spinal cord), and the activation of motor neurons, that ultimately cause muscle contraction. Indeed, the ultimate physiological cause of locomotion in all vertebrates is the contraction of specific muscles, for a certain amount of time and in a particular sequence, which allows the displacement of the whole body.

1.1 Central Pattern Generator

From a neural circuit point of view, locomotion is maintained by neurons in the spinal cord forming the so-called Central Pattern Generator (CPG), a neuronal network that was firstly

identified in invertebrates, and that is able to organize rhythmic movement if sufficient excitation is provided (Wilson and Wyman, 1965, Grillner, 2006). Indeed, early experiments in the spinalized cat demonstrated the capability of the spinal cord circuit to elicit coordinated movements without the input of brain centres, and this was later proven to be true for the lamprey, the *Xenopus* tadpole, and the zebrafish (Orlovskiĭ, 1970, Buchanan James and Grillner, 1987, Roberts et al., 2010, Eklöf-Ljunggren et al., 2012). The CPG of vertebrates consists of motor neurons, which directly elicit muscles contraction, and of diverse classes of interneurons, both excitatory and inhibitory (Goulding, 2009, Grillner and El Manira, 2020). Overall, the rhythmicity of the locomotion circuit can be summarized by the alternation of in-phase excitation and mid-cycle inhibition (Goulding, 2009, Grillner and El Manira, 2020).

Because the architecture of the CPG is formed by local neuronal circuits repeated along the spinal cord, it has been proposed that this circuit is formed by segmental neuronal pools, that can drive locomotion in distinct sectors of the spinal cord (Grillner, 2006, Dougherty and Kiehn, 2010b). More recent evidence from the zebrafish and mice challenged this model and led to accept the view of the CPG as a continuous circuit, with rostral and caudal segments concatenated to each other. In fact, if the rhythmic aspect of the zebrafish locomotion is retained in disconnected spinal segments, this is not true for the overall coordination of the movement, which is lost when rostral and caudal portion of the spinal cord are severed (Wiggin et al., 2014). Spinal neurons in mice provide anatomical evidence for the importance of a globally patterned locomotion, with interneurons sending projections to distant segments, and conversely, motor neurons receiving connections from distant interneurons (Stepien and Arber, 2008, Tripodi et al., 2011).

The excitatory and inhibitory CPG neurons that drive swimming in the lamprey (Grillner and Matsushima, 1991) and in the *Xenopus* tadpole (Roberts, 2000) also run across multiple segments of the animal's body, favouring the idea of a linked circuit along the spinal cord even in simpler organisms. It is now widely accepted that the overarching locomotor circuit is formed by long-ranging connections and local modules, and the coordination across all these elements is needed in order to achieve a functional motor output.

1.1.1 Swimming

Swimming is one type of locomotion that has been studied in depth because of its relatively simpler features if compared to movements in limbed animals. Although experiments on

nudibranchs shed light on the mollusks' motor circuits (Sakurai and Katz, 2015, Sakurai and Katz, 2016), the three swimming animals that have been, and still are, instrumental to understand how locomotion is initiated and sustained in vertebrates are the lamprey, the *Xenopus* laevis tadpole, and more recently, the zebrafish (*Danio rerio*). These three animal models swim by bending their elongated bodies in a rhythmic fashion, with waves of side-to-side alternating contractions that propagate from the head to the tail (Fetcho, 1992). The resulting undulatory movement opposes to the lateral pressure of water against the body, making the animal swim forward. Both the lamprey and the *Xenopus* tadpole show continuous movement during swimming episodes, with muscles on the opposite sides of the body contracting rhythmically and alternatively (Grillner and Matsushima, 1991, Roberts et al., 2010). The larval zebrafish instead, swims in a 'beat and glide' manner, with short episodes of active swimming followed by brief periods of inactivity (Saint-Amant and Drapeau, 1998, Buss and Drapeau, 2001). The adult zebrafish instead, swims continuously and stops by decreasing the undulatory movements instead of stopping abruptly (Gabriel et al., 2008).

The CPG circuit that is active during swimming has been described first in the lamprey and in the tadpole, and it consists of excitatory and inhibitory premotor neurons, and motor neurons. Glutamatergic premotor neurons have descending axons, which run ipsilaterally in the spinal cord and rhythmically excite motor neurons. Glycinergic inhibitory commissural interneurons ensure rhythmic activation of the excitatory components on the two sides of the spinal cord, and thus they coordinate the opposing contractions that ultimately cause movement (Grillner and Matsushima, 1991, Roberts et al., 2010). As the *Xenopus laevis* tadpole is the model organism used in this work, its swimming behaviour and the CPG neurons underlying it are further explained in chapter 2.

1.1.2 Locomotion in Limbed Animals

Terrestrial limbed animals display a great variety of locomotor behaviours, among which are walking, running but also jumping or galloping. Each of these movements involves precise coordination both between the left and right limbs, as well as between the forelimbs and the hindlimbs, as different patterns in their movement give rise to different locomotion modalities. For example, while walking a cat's limbs coordination is different from the limbs coordination observed during running. The mammalian locomotor system is much more complex than the one controlling swimming in fish and tadpoles, as it has to maintain the activity of four limbs,

which also need to be coordinated among each other depending on the environmental necessities. Furthermore, the coordinated contraction of muscles around the joints within each limb adds another level of complexity to the mammalian locomotor system. Early studies demonstrated that the CPG that controls the forelimbs is located in the cervical spinal cord and similarly, the CPG that controls the hindlimb is found in the lumbar spinal cord (Grillner and Zangger, 1979, Andersson and Grillner, 1981). These delocalized centres are connected to each other by long projections of genetically diverse neuronal populations, namely the $V0_v$ population, which provides the excitatory commissural connections and the $V2_a$ population, which instead provides the ipsilateral projections (Goulding, 2009, Kiehn, 2006, Kiehn, 2016).

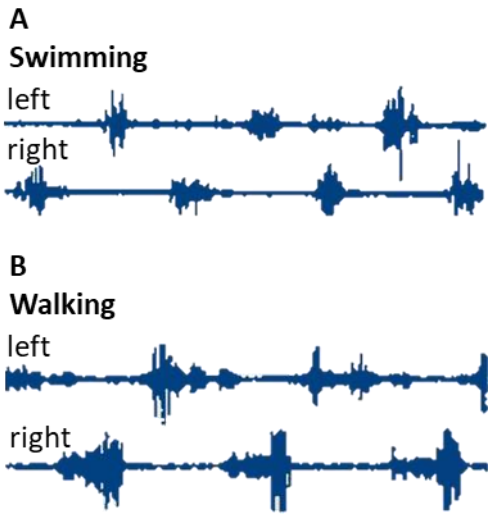

Figure 1.1 Locomotor rhythm in swimming and walking.

A) *Example of electrical activity recorded in the left and right muscles of the lamprey during swimming.*

B) *Example of electrical activity recorded in the cat hindlimb during walking. In both recordings, rhythmic muscle contraction is alternate to produce locomotion. Adapted from (Orlovsky et al., 1999) in (Goulding, 2009).*

1.2 Brain Circuits for Locomotor Control

Although the spinal circuits that sustain locomotion have been largely unravelled at least in simpler organisms as the lamprey and the tadpole, the brain circuits that exert control over the spinal circuits are still under investigation. A vast portion of the early and recent work on brain control of locomotion has been carried out on mammals, mostly cats and mice, but it was quickly observed that the basic mechanisms are shared also with non-mammal vertebrates (Grillner and Robertson, 2016, Katz, 2016). In the following paragraphs, a description of the mammalian

motor control circuit is reported, followed by a parallel description of motor control mechanisms in two swimming animals, lamprey and zebrafish.

1.2.1 Locomotor Control in Mammals

1.2.1.1 The Mesencephalic Locomotor Region

Early experiments on cats allowed the identification of a midbrain area that, when electrically stimulated could elicit coordinated locomotion, which was also functional in adapting speed and gait (Shik Ml Fau - Severin et al., 1966, Shik and Orlovsky, 1976). This brain region was named MLR (Mesencephalic Locomotor Region), and it integrates incoming signals from different brain areas in order to coordinate movements which are suitable for the external environment (Ryczko and Dubuc, 2013, Jordan, 1998). More recent studies on mice identified a glutamatergic neuronal population in the MLR, which expresses the vesicular transported for glutamate VGluT2 and that is responsible for eliciting locomotion (Roseberry et al., 2016, Caggiano et al., 2018). Indeed, optogenetic activation of these neurons led to locomotion, whilst their inhibition prevented motor activity in mice (Roseberry et al., 2016). Furthermore, the VGluT2-positive population in the MLR is divided into two sub-categories, which drive quick and slow locomotion respectively. Both the CnF (Cuneiform nucleus) and the PPT (prepontine nucleus) are anatomical regions that encompass the MLR and where VGluT2 neurons are present. When these glutamatergic neurons were selectively activated with optogenetics in one or the other area of the MLR, two different outcomes were recorded. After the activation of CnF neurons, quick locomotion that adapted to increasing stimulation frequency was elicited. On the contrary, when the PPT was activated, slow locomotor response was recorded, which failed to initiate at low frequency stimulation (Caggiano et al., 2018). The latter response was also shown to drive slow explorative behaviour in a hole-board test (File and Wardill, 1975, Kliethermes and Crabbe, 2006), thus linking one neuronal population to a specific behaviour in mice (Caggiano et al., 2018).

1.2.1.2 Basal Ganglia

Upstream of the MLR in the motor control pathway of mammals, lie the basal ganglia. Although the motor cortex sends projections to the MLR, experiments on several animals, including cats and rodents, demonstrated that removing the motor cortex does not impair the ability of the animal to move (Schaltenbrand and Cobb, 1931, Bjursten et al.). Nevertheless, this locomotor

ability is retained only if the basal ganglia are intact (Schaltenbrand and Cobb, 1931, Bjursten et al.). The mammals' basal ganglia are a forebrain structure, formed by the striatum, the globus pallidus (divided in pars externa and pars interna, GPe and GPi, respectively), the substantia nigra pars reticulata (SNr) and the subthalamic nucleus (STN) (Grillner and El Manira, 2020). Experimental work over the years has proven that the basal ganglia is a brain region that can determine motor selection and whether locomotion happens or not (Albin et al., 1989, DeLong, 1990{Grillner, 2016 #156).

The output projections of the basal ganglia depart from the SNr and GPi and consist in GABAergic neurons which are tonically active in resting conditions (Hikosaka and Wurtz, 1983, Stephenson-Jones et al., 2011, Surmeier et al., 2011). These neurons provide continuous inhibition to the brain motor centres, including the MLR (Garcia-Rill et al., 1983, Grillner et al., 2005), thus also silencing the VGluT2 neurons responsible for locomotion (Roseberry et al., 2016, Caggiano et al., 2018).

The striatum is the input area of the basal ganglia (Gerfen and Surmeier, 2011, Grillner et al., 2005, Kreitzer and Malenka, 2008), where another GABAergic population lies, namely the medium spiny neurons (MSNs) (Albin et al., 1989, Kreitzer and Malenka, 2008). Contrary to GABAergic neurons in the SNr and GPi, striatal MSNs are hyperpolarised at rest, and they are activated only following strong excitation (Surmeier et al., 2011). This population expresses two types of dopamine receptors (DR), either DR1 or DR2, which in turn define two neuronal pathways in the basal ganglia (Gerfen Charles et al., 1990, Surmeier et al., 1996, Gerfen and Surmeier, 2011). The neurons expressing DR1 run directly from the striatum to the GPi and the SNr, thus forming the so-called direct pathway. Conversely, the indirect pathway consists in DR2-positive neurons, which connect the striatum to the GPe and the STN, from where projections reach the GPi and SNr (Mogenson et al., 1985, Wu et al., 1993).

Both the direct and the indirect pathway neurons are active at locomotor initiation, and they activate heterogeneously the MLR neurons via the SNr, resulting in a combination of excitation and inhibition (Cui et al., 2013, Freeze et al., 2013, Jin et al., 2014, Barbera et al., 2016, Klaus et al., 2017). Among the SNr neurons that receive synaptic inputs from MSNs, only the cells that are silenced by the optogenetic activation of DR1 neurons were shown to be correlated to motor initiation. On the contrary, neurons in the SNr that were excited by the activation of DR2 neurons were correlated to movement arrest (Freeze et al., 2013). It was further demonstrated that DR1

and DR2 show opposite responses to dopamine, affecting the probability of activation of MSNs in the direct or indirect pathway (Parker et al., 2018).

Dopaminergic neurons in the SNc (Substantia Nigra pars compacta) reach the striatal MSNs neurons and they have been shown to fire not only tonically, but also in phasic bursts prior to locomotion (da Silva et al., 2018, Howe and Dombeck, 2016). Indeed, the optogenetic activation of dopaminergic SNc neurons increased the probability of movement initiation in mice, but their inhibition was not sufficient to stop locomotion (da Silva et al., 2018). Instead, the inhibition of dopaminergic neurons makes animals at rest less prone to initiate movement (da Silva et al., 2018, Howe and Dombeck, 2016).

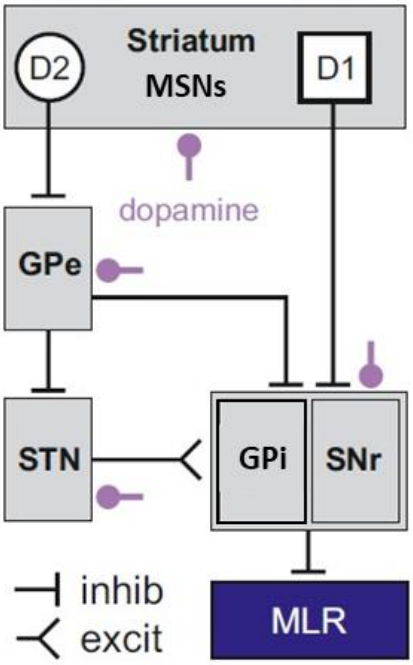

Figure 1.2 The basal ganglia circuit in mammals

GABAergic MSNs in the striatum are activated by strong depolarization and control the MLR via a direct or indirect pathway, depending on the dopamine receptor expressed by MSNs. Neurons expressing the D1 receptor project directly to the GPi and SNr, inhibiting them. This will in turn remove the inhibition on the MLR. Conversely, neurons expressing the D2 receptor inhibit the GPe, which in turn release the GPI and the SNr from its own inhibition, ultimately silencing the MLR. (MSNs= medium spiny neurons; GPe= globus pallidum pars externa; STN= subthalamic nucleus; GPi= globus pallidum pars interna; SNr= substantia nigra pars reticulata). Adapted from (Ferreira-Pinto et al., 2018).

1.2.2 Locomotor Control in the Lamprey

The lamprey is the most ancient vertebrate specie alive, and it has been, and still is, an instrumental animal model to decipher the neuronal mechanism of locomotion (Rovainen, 1979, Buchanan James and Grillner, 1987). Even in this animal, brain regions with the same functionality of the MLR and the basal ganglia are present, supporting the idea that locomotor behaviours and locomotor control have developed early on during evolution.

Although the lamprey reticulospinal (RS) neurons that excite spinal CPG, including motor neurons, have been long known (Brodin et al., Buchanan James and Grillner, 1987), it was only more than ten years later that the MLR was identified in the lamprey (Sirota et al., 2000, Brocard and Dubuc, 2003). As it happens with mammalian locomotion, electrical stimulation of the lamprey's MLR elicits coordinated swimming. In this ancient vertebrate, the MLR is a very small brain region, located in the caudal mesencephalon, which was shown to be able to start swimming after AMPA microinjection, leading to propose that the descending connections were glutamate mediated (Sirota et al., 2000). Intracellular recordings of RS neurons following MLR stimulation, together with backfilling staining of projections, provided evidence for a direct connection from the MLR to RS neurons (Sirota et al., 2000, Brocard and Dubuc, 2003), thus for a direct control of the MLR on locomotor behaviour in the lamprey.

GABAergic neurons have been identified in the lamprey forebrain, which sends GABAergic projections that reach the MLR (Robertson et al., 2006, Ménard et al., 2007). The forebrain region where these GABAergic neurons lie has been proposed to serve as the input layer (the striatum in mammals) of the basal ganglia in the lamprey (Robertson et al., 2006, Ménard et al., 2007, Grillner et al., 2008). Similar to mammals, the dopaminergic system plays an important role in the mechanism of motor control in lamprey (Ryczko and Dubuc, 2017). Indeed, dopaminergic projections from the posterium tuberculum (PT), homologous of the SNc and the VTA (ventral tegmental area) in mammals, were found to be both ascending to the striatum (Ryczko and Dubuc, 2013), as well as descending to the MLR (Ryczko and Dubuc, 2013, Pérez-Fernández et al., 2014, Ryczko and Dubuc, 2017). When this dopaminergic region was stimulated, a dopamine release was detected in the MLR, followed by the activation of RS neurons (Ryczko and Dubuc, 2013). Furthermore, the microinjection of DR1 antagonist in the MLR reduced the locomotor output, while bath applied dopamine had the opposite results (Ryczko and Dubuc, 2013). Recently, a novel dopamine-mediated pathway has been unveiled in

the lamprey, with dopaminergic projections that run from the PPT directly to RS neurons (Ryczko et al., 2020). Also in this pathway, the blockade of DR1 caused the RS neurons to be less active and it impaired locomotion (Ryczko et al., 2020). So far, the lamprey is the only organism where this 'short' pathway has been documented, even if dopaminergic projections have been found around Mauthner cells in zebrafish (McLean and Fetcho, 2004b, McLean and Fetcho, 2004a).

1.2.2.1 Sensorimotor control

The lamprey model organism has also been exploited to study mechanism of sensorimotor control, *i.e.* the motor output that the animal produces in response to a sensory stimulation to the skin (Dubuc et al., 1993a, Di Prisco et al., 1995, Viana Di Prisco et al., 2000). Cutaneous stimulation is detected by sensory neurons and the sensory information enters the CNS either via the dorsal roots, in the case of stimulation to the skin that covers the body of the animal (Dubuc et al., 1993b), or via the trigeminal nerve, in case of stimulation to the head skin (Glenn Northcutt, 1979, Viana Di Prisco et al., 2005).

When the cutaneous stimulation is delivered to the body, a disynaptic pathway is activated to achieve the excitation of motor circuit in the spinal cord of the lamprey. The afferent fibers of the dorsal roots reach the brainstem to the level of the dorsal column nucleus (Dubuc et al., 1993b), with a few fibers running more rostral and reaching the octavolateralis area (Ronan and Northcutt, 1990, Dubuc et al., 1993b) . In the dorsal column nucleus and in the octavolateralis area alar plate neurons are activated by the afferent fibers, and in turn excite the RS neurons (Dubuc et al., 1993b, Pflieger and Dubuc, 2004), by glutamatergic synapses (Dubuc et al., 1993b, Viana Di Prisco et al., 2005). In turn, RS project caudally into the spinal cord and drive the spinal CPG neurons (Brodin et al., Buchanan James and Grillner, 1987). Similar to the neuronal pathway for body stimulation, when the cutaneous stimulation is delivered to the head the pathway that activate spinal CPG neurons is disynatpic. In this case, the trigeminal afferent fibers form the descending root of the trigeminal nerve, which in turn excite the RS neurons in the brainstem (Glenn Northcutt, 1979, Viana Di Prisco et al., 2005). In the locomotor response to a cutaneous stimulus, both via the excitation of alar plate neurons (in case of stimulation of the body), or via the descending root of the trigeminal nerve (in case of stimulation of the head), the synapses from relay neurons to RS neurons are of dual nature, glutamatergic and glycinergic (Dubuc et al., 1993b, Viana Di Prisco et al., 2005).

1.2.3 Locomotor Control in Zebrafish

1.2.3.1 Escape response

One of the best studied mechanisms of motor control in vertebrates is the startle response in zebrafish. Differently from the execution of the basal ganglia-driven planned movement in mammals, the startle response is triggered by external stimulation, and consists in an escape response. One pair of large neurons, the Mauthner cells (Mauthner, 1859, Eaton and Emberley, 1991), was identified as the primary responsible for one typical response in zebrafish, called C-start response. Once stimulated, the fish bends its head towards the side opposite to stimulation, followed by one bend on the stimulated side, which will eventually become rhythmic swimming (Hale et al., 2016). This typical response is fast and has the purpose of escaping a predator. Indeed, Mauthner cells are anatomically positioned in the fourth rhombomere (Mauthner, 1859, Eaton and Emberley, 1991), an area where they can receive multiple sensory information, *i.e.* inputs from the ipsilateral vestibulococlear cranial nerve, from somatosensory neurons, from the visual system and from the lateral line system (Hale et al., 2016). Mauthner neurons have large commissural axons that run caudally into the spinal cord, on the side opposite to their respective somata (Mauthner, 1859, Eaton and Emberley, 1991).

When one of the Mauthner neuron fires one action potential, the animal quickly bends to the opposite side, thanks to direct synaptic contact between Mauthner cells and motor neurons in the spinal cord (Fetcho and Faber, 1988, Kimura et al., 2006). The spinal motor neurons can also be activated by Mauthner cells indirectly, via the excitatory CiD (Circumferential Descending) and the inhibitory CoLo (Commissural Local) interneurons. CiD axons run ipsilaterally and caudally for several segments into the spinal cord, where they have synaptic connections with motor neurons (Fetcho and Faber, 1988, Hale et al., 2001). At the same time, CoLo interneurons inhibit motor neurons on the non-bending side of the body (Fetcho and Faber, 1988, Liao and Fetcho, 2008). In order to allow the first bend to happen quickly and reliably, Mauthner cells need to be prevented from firing multiple action potentials. This is achieved with their inhibition by several types of interneurons, *i.e.* CNR (Cranial Relay) neurons (Koyama et al., 2011) and PHP (Passive Hyperpolarizing Potential) collateral neurons, together with PHP commissural neurons and SFNs (Spiral Fibers Neurons) (Koyama et al., 2011).

Additionally, two other pairs of interneurons that drive the startle response are present in the fifth and sixth rhombomeres, just caudally to Mauthner neurons (Lee et al., 1993). These cells,

named MiD2cm and MiD3cm, together with Mauthner neurons, have been shown to be activated on the same side after head stimulation. On the contrary, when stimulation was given to the zebrafish tail, only Mauthner neurons were activated (O'Malley et al., 1996, Liu and Fetcho, 1999). Confirmation that Mauthner cells, MiD2cm and MiD3cm neurons are differentially responsible for motor response to stimulation at different body sites came from ablation experiments. Indeed, when Mauthner neurons were ablated, response to tail stimulation was impaired, whilst head stimulation response was normal. Conversely, ablation of MiD2cm and MiD3cm cells caused impaired motor response after head stimulation (Liu and Fetcho, 1999).

Recently, it has been shown that neurons lying in the nMLF (nucleus of the Medial Longitudinal Fasciculus) are responsible for the transition from the first contralateral bend, mediated by Mauthner cells, into forward swimming (Xu et al., 2021).

The nMLF is a rostral cluster of reticulospinal neurons, which lie in the midbrain of the zebrafish and whose cells send axons, both ipsilateral and contralateral, into the spinal cord (Gahtan and O'Malley, 2003, Gahtan et al., 2005, Wang and McLean, 2014). The nMLF is implicated in various behaviours of the zebrafish, from escape response to prey capture, with different nMLF neurons relaying sensory information into the brainstem and ultimately into the spinal cord. For example, prey capture, which is driven by visual information (Bianco et al., 2011, Antinucci et al., 2019), fails if certain neurons in the nMLF are ablated, namely the MeLr and MeLc cells (Gahtan et al., 2005).

As mentioned above, the nMLF is also involved in escape response. In fact, after stimulation of one Mauthner cell, neurons in the ipsilateral and contralateral nMLF were activated. This is achieved by the synaptic connection between Mauthner cells and the CNR neurons, which project rostrally reaching the nMLF (Xu et al., 2021). Additional evidence for the importance of this circuit came from the laser ablation of CNR neurons, which led to the failing of swimming, both in an *ex vivo* preparation and in the freely moving animal. Laser ablation of the bilateral nMFL cells activated by CNR neurons also caused the animals to fail the swimming response (Xu et al., 2021).

In addition to the quick response to stimulation mediated by Mauthner neurons system, the zebrafish responds to weaker stimulation by bending preferentially on the same side of

stimulation, and this response is slower than the one mediated by Mauthner neurons (Eaton et al., 1984, Gahtan et al., 2002, Burgess and Granato, 2007, Koyama et al., 2016). A bilateral population of ipsilaterally projecting neurons has been identified, which lie in the hindbrain and preferentially activate swimming on the same side of stimulation and with longer latency (Marquart et al., 2019). Although slower than the startle response mediated by Mauthner cells, this ipsilateral response is still fast, and falls into the category of escape responses, which are different from the planned motor execution that has been studied in mammals (Marquart et al., 2019).

1.2.3.2 Role of dopaminergic System

Based on the evidence that the mechanisms found in the mammals' basal ganglia are conserved (Lemon, 2008, Grillner and Robertson, 2016), the dopaminergic system has been under investigation for its role in the motor control of the zebrafish. Evidence for a dopaminergic role in motor control came from pharmacological studies on freely moving larvae, which decreased their spontaneous swimming activity after incubation of toxins that bind to dopamine receptors (Farrell et al., 2011, Irons et al., 2013). Further experiments identified hypothalamic neurons that express *th2* (tyrosine hydroxylase 2, used as a marker for dopaminergic neurons). When theses dopaminergic neurons were ablated, the spontaneous swimming in zebrafish larvae decreased (McPherson et al., 2016, Barrios et al., 2020). The hypothalamic *th2*-positive population was found to be heterogeneously activated in correlation to both spontaneous and stimulus-evoked locomotion, and four subgroups were identified based on anatomical and functional features. Three of these groups (cells lying in the posterior tuberculum and in the intermediate and caudal hypothalamus) showed shorter projections and were proposed to have sensory-motor features, as they are activated by sensory stimulation and/or motor activity (Barrios et al., 2020). Instead, the fourth dopaminergic population, residing in the preoptic nucleus, has longer projections that reach the nMLF. The latter, indeed, gets activated when the preoptic nucleus is stimulated. Additional confirmation of this connections came from intracellular recording from MeLr neurons (in the nMLF), which showed activation following the stimulation of *th2* expressing neurons (Barrios et al., 2020). Moreover, because *th2*-positive neurons are generated till adulthood in the zebrafish, it was possible to observe that the regeneration of these dopaminergic neurons can reinstate a normal locomotor activity in fishes where *th2*-positive neurons were previously ablated (Barrios et al., 2020).

2 The *Xenopus laevis* tadpole

2.1 Behaviour of the *Xenopus* tadpole

Just after the time of hatching (at developmental stage 37/378), tadpoles spend 99% of their time remaining still. Either they hang from the water surface or from solid object thanks to the mucus secreted by the cement gland (Lambert et al., 2004a), or they lie on the bottom of ponds (or tanks, when held in captivity in the lab). This behaviour allows energy conservation, which is a feature of major importance for the *Xenopus* embryos, as they do not feed until stage 45. In fact, during the first days of their life, tadpoles take their nutrients from the yolk, which is stored in all cells in the form of yolk platelets (Jorgensen et al., 2009). Yolk platelets are membrane-bound organelles containing vitellogenin (Brooks and Wessel, 2002, Smolenaars et al., 2007), whose intracellular proteolysis provides amino acids, lipids and ions to the developing cells (Ohlendorf et al., 1977, Wiley and Wallace, 1981, Montorzi et al., 1995, Thompson and Banaszak, 2002).

Even though the tadpole does not need to look for food, it needs to avoid predators, which in nature are the adults of its own species, and big insects such as damselflies and dragonflies. Adult individuals of the *Xenopus laevis* are mostly nocturnal predators, which move on pond floors. On the contrary, predator insects are diurnal, and they will reach the tadpoles from above the water surface. In this scenario, it is clear that, as early as the time of hatching, the tadpole needs to be able to detect sensory stimuli and react to them in order to survive. In freely moving tadpoles, their swimming response to stimulation seems to be advantageous for escaping both predators moving on the bottom of ponds, as well as flying insects coming from outside the water. In fact, when a tadpole lying at the bottom of a tank is stimulated on one side of its body, it swims upwards in a very reliable spiralling movement (Roberts, 2000). On the contrary, when the tadpole is hanging on the water surface and it is touched on the head, it flexes and swims downwards (Roberts, 2000). On either case, the tadpole's behaviour is functional for escaping predators, as it swims away from the source of stimulation.

After the sensory information is detected, it is taken to the CNS and the swimming response is activated when a noxious stimulus is detected. The tadpole's swimming consists of an

undulatory movement of the body along its longitudinal axis, with the two sides contracting in a perfectly rhythmically manner.

When the sensory stimulation received by the tadpole is strong and repetitive, a different behaviour is initiated. This has been called 'struggling behaviour' (Kahn et al., 1982b) and it is performed by the tadpole when it is grabbed by a predator. Struggling is a more turbulent movement than swimming (Kahn et al., 1982b, Green and Soffe, 1996), as the aim of this behaviour is to set the tadpole free from the predator grasp.

Both swimming and struggling movements are driven and sustained by spinal neurons, which form a well-known CPG circuit stretching from the caudal brain to the tail. Thanks to its simplicity and amenability, the anatomy of the spinal cord of the *Xenopus* embryo has been described in detail, and only eight types of neurons have been found. These are part of the CPG circuit (motor neurons, descending interneurons, ascending and commissural inhibitory neurons) or take part in the sensory pathway (Rohon-Beard neurons, dorsolateral ascending and dorsolateral commissural neurons). The last neuronal population consists in a population of GABA-positive neurons, named Kolmer-Agduhr cells, which reside on the spinal cord floor and contact the spinal fluid in the neurocoele with fine cilia (Roberts and Clarke, 1982).

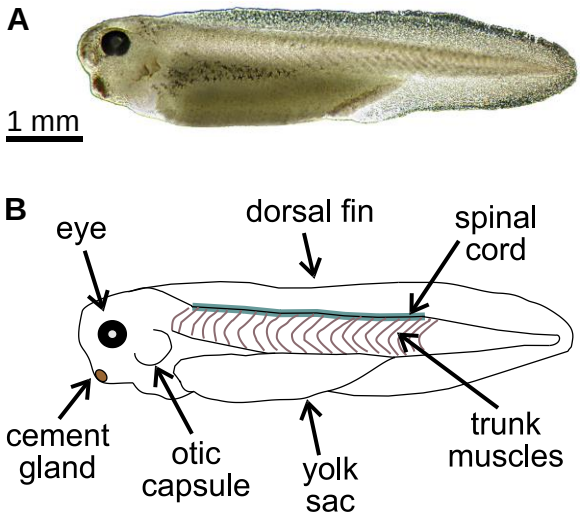

Figure 2.1 Anatomy of the Xenopus laevis tadpole.

A) *Picture of a Xenopus laevis tadpole lying on one side;* ***B)*** *schematic of the Xenopus tadpole with annotation of the most important anatomical hallmarks. Scale bar is the same for A and B.*

2.2 The Tadpole's Central Pattern Generator

The *Xenopus* tadpole swims in a series of rhythmic bends that propagate along its longitudinal axis, allowing the undulatory body movement that propels the animal in the water. Although the experiments focusing more on the ethological importance of the tadpole locomotion have been carried out in freely swimming animals (Jamieson and Roberts, 2000), the identities of neurons involved in swimming and how they are organized into the CPG spinal circuit have been unveiled in immobilized tadpoles. Indeed, most of the studies on locomotor circuit in the tadpole rely on experimental preparations that allow electrophysiology extracellular recording of ventral root (VR) bursts from the sides of the animal's trunk. In this preparation, one or more suction electrodes are attached to the trunk muscle at the intermyotomal cleft, where motor neurons axons exit the spinal cord and innervate the muscle fibers (Roberts and Clarke, 1982). In such preparation, the recorded VR bursts are a very reliable indication of the so called 'fictive swimming', *i.e.* swimming in a immobilized animal (fig. 2.2). Moreover, VR can be monitored simultaneously on both sides of the body when two suction recording electrodes are placed one facing the other at the same longitudinal level on the trunk muscles. Thanks to this simple preparation, the rhythmic and phasic features of the tadpole's swimming were identified early on, and anatomical studies on fixed samples and intracellular recording coupled with pharmacological studies were carried out to disentangle the spinal locomotor circuit in the tadpole.

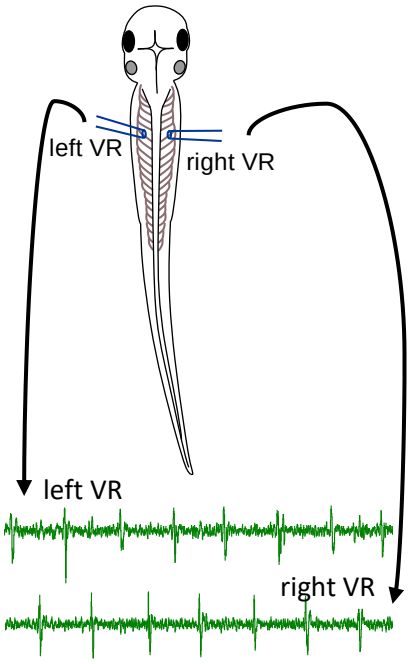

In the next paragraphs, a description of the spinal CPG neurons is reported, and how they regulate each other to sustain swimming and struggling is described in detail. Following, detailed explanations of the different sensory pathways and sensory neurons present in the hatchling tadpole are reported.

Figure 2.2 Fictive swimming in the Xenopus tadpole. *Two recording electrodes are attached at the myotomal cleft on the opposite side of the tadpole's body. Left and right VR electrical activities show the rhythmic and alternating bursts of fictive swimming.*

2.2.1 Motor Neurons

Motor neurons are the cells directly responsible for the contraction of trunk muscles in the *Xenopus* tadpole, and thus they effectively sustain the undulatory movement of its swimming. Motor neurons lie in the ventral sector of the spinal cord, where they form a continuous longitudinal column of cells, which sometime can be stacked in dorso-ventral direction (Roberts and Clarke, 1982, Soffe and Roberts, 1982a). The dendrites of motor neurons spread laterally into the marginal zone of the spinal cord, without reaching the dorsal areas (Roberts and Clarke, 1982). Motor neurons' axons run ipsilaterally to the somata and caudally into the marginal zone without giving rise to secondary branches (Soffe and Roberts, 1982b). Axons then turn sideways, leaving the spinal cord in tight bundles, and innervate the myotomes by entering at the intermyotomal cleft (Roberts and Clarke, 1982).

Motor neurons do not show spontaneous activity, and they fire one action potential at each swim cycle, in phase with ipsilateral VR burst (Soffe and Roberts, 1982b, Soffe and Roberts, 1982a, Dale and Roberts, 1984, Soffe, 1987, Soffe, 1990). When motor neurons are activated intracellularly by depolarizing current injection, they fire only one action potential, but if the current is injected repetitively, they fire one action potential at each pulse (Soffe, 1990). During fictive swimming, motor neurons receive 1) rhythmic EPSPs in phase with VR bursts on the same side of the tadpole's body, 2) mid-cycle inhibition from commissural neurons and 3) tonic, background excitation (Soffe and Roberts, 1982a, Soffe and Roberts, 1982b, Dale and Roberts, 1984, Soffe, 1987).

EPSPs recorded from motor neurons are largely due to glutamate excitation delivered from descending interneurons (dINs, see paragraph 2.2.2). This glutamate-mediated excitation was shown to have a slow NMDA component, and a faster AMPA and kainate component (Dale and Roberts, 1984, Perrins and Roberts, 1995a, Perrins and Roberts, 1995b), with AMPA receptors contributing to a minimum extent (Perrins and Roberts, 1995b, Perrins and Roberts, 1995a). Indeed, early pharmacological experiments demonstrated that when NMDA and kainate receptors were activated by their respective agonists, motor neurons were depolarized and a motor output similar to fictive swimming was recorded (Dale and Roberts, 1984). On the contrary, when AMPA agonist was applied to the spinal cord, no reliable motor output was detected, although motor neurons were depolarized (Dale and Roberts, 1984).

Later studies provided evidence for a strong cholinergic component of the excitation recorded in motor neurons. Pharmacological experiments demonstrated that acetylcholine application depolarize motor neurons via muscarinic (mAch) receptors (Perrins and Roberts, 1994), and that this component makes up the 20% of the excitation received by motor neurons. This cholinergic element is due to reciprocal excitation among motor neurons, which are the only cholinergic cells in the spinal cord of the tadpole. In fact, motor neurons provide cholinergic rhythmic excitation to other motor neurons on the same side of the spinal cord (Perrins and Roberts, 1994, Perrins and Roberts, 1995a, Perrins and Roberts, 1995b). Moreover, motor neurons are electrically coupled to other ipsilateral motor neurons within 70 µm of distance, and this electrical component constitute the 50% of the excitation they receive (Perrins and Roberts, 1995a, Perrins and Roberts, 1995b).

Motor neurons also receive mid-cycle inhibition from commissural glycinergic interneurons (cINs, see paragraph 2.2.3) (Roberts and Clarke, 1982, Soffe and Roberts, 1982b, Perrins and Roberts, 1995a). Experiments with strychnine and bicuculline (glycine and GABA antagonists respectively) showed that, although motor neurons have both glycine and GABA receptors, the inhibition they receive is mediated by glycine only (Soffe, 1987). Indeed, glycine antagonist eliminated the mid-cycle IPSPs recorded in motor neurons, while GABA antagonist application did not have any effect on motor neurons inhibition or on fictive swimming (Soffe, 1987).

2.2.2 Descending Interneurons

In the *Xenopus* tadpole, descending interneurons (dINs) are a population of interneurons that form a longitudinal column in the ventral spinal cord and continues rostrally into the hindbrain (Dale and Roberts, 1985, Roberts and Alford, 1986). They were firstly identified as the cells providing excitation to motor neurons in the spinal cord during locomotion (Dale and Roberts, 1985), and they were described as part of the spinal CPG for swimming. Indeed, they fire one long action potential in every swim cycle in phase with the ipsilateral VR burst (Dale and Roberts, 1985, Roberts and Alford, 1986, Li et al., 2006), they are tonically depolarized, and they receive mid-cycle inhibition (Li et al., 2006).

They have long ipsilaterally descending axons, and a population of the dINs found in the hindbrain (Roberts and Alford, 1986), which can be called reticulospinal interneurons (hdINs, hindbrain dINs), also have ipsilaterally ascending axons (Li et al., 2006, Soffe et al., 2009). The anatomical features of dINs allow them to provide excitation to spinal CPG neurons, which is

needed to sustain swimming. Indeed, thanks to their long descending axons running along the spinal cord, they contact all classes of spinal interneurons (commissural IN, ascending INs and other dINs), as well as they make synapses onto motor neurons (Roberts and Alford, 1986, Li et al., 2006, Li et al., 2009). Intracellular recordings from these classes of spinal neurons have revealed that they receive both glutamatergic excitation, as well as multi components EPSPs (Li et al., 2004c). The multi component feature of the EPSPs is caused by dINs excitation and has been studied by means of agonists and antagonists of AMPA, NMDA and nAch receptors, and it has been shown to be the result of a corelease of glutamate and acetylcholine from the same vesicles in dINs post synaptic compartments (Li et al., 2004c). Hence, it was proposed that glutamate and acetylcholine receptors are colocalized on synaptic sites of spinal neurons post synaptic to dINs (Li et al., 2004c).

In addition of making synapses with spinal interneurons and motor neurons, dINs contact each other multiple times, on their somata and along their dendrites and axons (Li et al., 2006, Li et al., 2009). On these contact sites, dINs have gap junctions that make them an electrically coupled population (Li et al., 2009). The electrical coupling on dINs is bidirectional, just slightly stronger in the rostro-caudal direction, and it weakens as distance between two dINs increases (Li et al., 2009). In the hatchling tadpole, electrical coupling in dINs is of extreme importance for the maintenance of swimming. When blockers of gap junctions were perfused on the spinal cord, the dINs population was still able to fire action potentials, but their activation during locomotion was less reliable, with almost half of the dINs investigated that failed to fire in a few swimming cycles (Li et al., 2009). Electrical coupling has also proven to be essential for the maintenance of rhythmicity during swimming, as when gap junctions were blocked, dINs lying in proximity of each other did not show synchronous firing. This prevented the coordinated activation of other spinal CPG neurons, resulting in shorter and unreliable episodes of fictive swimming (Li et al., 2009).

Another important feature of the tadpole's dINs is their ability to provide feedback excitation onto other dINs (Li et al., 2006). This depends crucially on the fact that a population of dINs lying in the hindbrain has an ascending axon (Roberts and Alford, 1986, Li et al., 2006, Soffe et al., 2009) in addition to the descending axon present in all dINs. These ascending projections allow the dINs to receive positive feedback excitation via NMDA receptors. This feedback excitation

provides background depolarization, which in turn allows dINs' rebound firing (Li et al., 2006, Li et al., 2009).

The reticulospinal dINs population that resides in the hindbrain (hdINs) has been shown to be the first to be activated as swimming starts (Soffe et al., 2009). Latency was measured for dINs and non-dINs activation at the start of locomotion, and it was found that, in a portion of hdINs, spikes were discharged before EPSPs could be recorded in the same neurons. This led the authors (Soffe et al., 2009) to propose that this portion of hdINs is activated first at locomotor initiation, probably not always the same cells, and that they can excite and drive the rhythmic activation of other dINs and of spinal CPG neurons during swimming.

Although it is difficult to obtain genetic information on the *Xenopus* tadpole neurons, dINs express the transcription factor Chx10 (Li and Soffe, 2019, Roberts et al., 2012). Staining with antibody against Chx10 revealed a population of spinal neurons that extended longitudinally into the hindbrain, and when neurons occupying the same location were recorded intracellularly, they were shown to have dINs features (Li and Soffe, 2019). Despite of the fact that direct evidence of dINs to be *chx10* positive is lacking, it is plausible that the tadpole's dINs are homologous to the excitatory V2a neurons in zebrafish (see paragraph 2.3.1.)

2.2.3 Premotor Inhibitory Interneurons

Two inhibitory classes of interneurons are present in the tadpole's spinal cord: the commissural interneurons (cINs) and the ascending interneurons (aINs).

Commissural INs have unipolar somata, which lie in the dorso-medial portion of the spinal cord, and they extend caudally into the tail. Their axons grow ventrally before crossing contralaterally and branching both in rostral and caudal direction (Soffe et al., 1984, Dale and Roberts, 1985, Dale et al., 1986, Roberts et al., 1988, Yoshida et al., 1998). Early recordings from cINs showed they have rhythmic firing during swimming, in phase with ipsilateral motor neurons activation (Soffe et al., 1984, Dale and Roberts, 1985). For this reason, and because they were stained with antibodies against glycine (Dale et al., 1986, Roberts et al., 1988), they were proposed to be inhibitory interneurons, which could regulate swimming rhythm (Soffe et al., 1984, Dale et al., 1986, Roberts et al., 1988). Indeed, they have the typical firing pattern of CPG neurons, firing one action potential every swim cycle and receiving mid-cycle inhibition. Thanks to their commissural axons, they provide mid-cycle inhibition to CPG neurons on the opposite side of

the spinal cord, producing reciprocal left-right inhibition which will ultimately lead to the rhythm of undulatory swimming (Soffe et al., 1984, Yoshida et al., 1998). When cINs were stained in whole-mount preparations using antibody against glycine (Yoshida et al., 1998), varicosities along the axons were reported very frequently. These are synaptic sites, and as the cINs axons run rostrally and caudally, they come in contact with spinal neurons active during swimming, which then receive mid-cycle inhibition. One important evidence in favour of cINs providing inhibition to the opposite side came from experiments on tadpole preparation where the spinal cord was cut longitudinally along the midline (Soffe, 1989). In doing so, all commissural sources of inhibition were deleted, and indeed, although swimming episodes started after stimulation, no mid-cycle inhibition was recorded on CPG neurons (Soffe, 1989). Moreover, the two sides of the spinal cord were not coupled anymore, *i.e.* they were still able to give rise to VR burst but they were not rhythmically coupled (Soffe, 1989). A similar result was achieved by microperfusion of the glycine antagonist strychnine (Perrins and Soffe, 1996). Following local strychnine administration on the spinal cord, mid-cycle inhibition could not be recorded from neurons active during swimming, although the swim episode was not disrupted (Perrins and Soffe, 1996). Although none of the spinal CPG neurons fire on post-inhibitory rebound, the population of dINs in the caudal hindbrain and rostral spinal cord does (Soffe, 1990, Li et al., 2006). This dINs population receives strong mid-cycle inhibition from cINs during swimming, providing the conditions for post-inhibitory firing (Li et al., 2006). This mechanism can help dINs to sustain the rhythmic excitation needed by CPG neurons, and to maintain their own rhythmic firing (Roberts et al., 2008).

Their anatomy, as well as functional studies on cINs, point to the fact that functional commissural inhibitory connections are key to maintain the swimming pattern in the *Xenopus* tadpole (Soffe et al., 2001, Li et al., 2001, Roberts et al., 2008).

The second class of spinal inhibitory interneurons in the tadpoles consists of aINs. As for cINs, aINs also have unipolar cell bodies lying in the medial portion of the spinal cord, but contrary to cINs, they have only ipsilateral axons which run both rostrally and caudally (Li et al., 2001). Recordings from dlc neurons have shown that they are inhibited during the early phase of a swimming episode, and this inhibition is provided by aINs (Li et al., 2001, Li et al., 2002). Anatomically, aINs axons contact dlc somata, and the latencies of the IPSPs recorded in dlc are short and constant; these features indicate that the connection aINs-dlc is monosynaptic (Li et

al., 2002). Differently from cINs, aINs firing is less reliable. During swimming, aINs receive mid-cycle inhibition from cINs, and they fire on-cycle, but later than the activation of motor neurons (Li et al., 2002). As a population, aINs are active at high swimming frequencies (as it happens at the beginning of swimming), but the majority of these neurons turn silent after a few swim cycles (Li et al., 2002, Roberts et al., 2008). This leads to a greater inhibition of dlc neurons during the early phases of a swimming episode, and it has been explained as a mechanism to turn off the sensory pathway (dlc cells in this case) whilst motor response is being established (Seki et al., 2003). This will limit the effect of a possible second stimulation to act on the just-established motor output. Once swimming becomes sustained, aINs inhibition on dlc is released, allowing the tadpole to receive a second sensory stimulation (Roberts et al., 2008).

CPG neurons in the spinal cord also receive glycinergic inhibition from aINs (Li et al., 2004a). IPSPs were recorded in CPG neurons with variable latency during swimming, but always during the so called 'early-cycle' (Li et al., 2004a), which is the first part of swim cycle, from the start (when CPG neurons are activated) until before the appearance of mid-cycle inhibition. Thanks to paired recordings, it has been shown that these early IPSPs are produced by aINs (Li et al., 2004a). This is also supported by aINs anatomy, with their axons running in the marginal zone and contacting all classes of spinal interneurons (Li et al., 2004a, Roberts et al., 2008). Lastly, aINs express the transcription factor *engrailed*. Immunohistochemical analysis (Li et al., 2004a) using serum against the proteins En-1 and En-2 revealed the same characteristic anatomy of aINs. AINs are probably homologous to the inhibitory CiAs neurons in zebrafish (see paragraph 2.3.1), although no direct genetic evidence of aINs expressing *engrailed* is present in the tadpole.

2.2.4 Kolmer-Agdhur Cells

Kolmer-Agdhur (KA) cells are a population of highly conserved neurons, which lie on the floor of the spinal cord and contact the spinal fluid in the neurocoele with fine cilia (Kolmer, 1921, Kolmer, 1925, Agduhr, 1922). In the tadpole, these neurons were found as GABA-positive cells, and they have ipsilateral ascending axons (Roberts and Clarke, 1982, Dale et al., 1987), as observed in other vertebrates (Yang et al., 2020). From early staining, KA cells were found to lie in a bilateral column, usually one-cell thick, that runs from the tail to the rostral spinal cord. No cell bodies of KA cells were found rostrally to the spinal cord, but a few of their axons could reach the hindbrain (Roberts and Clarke, 1982, Dale et al., 1987).

In the larval zebrafish, KA cells have been shown to initiate spontaneous swimming without the involvement of brain descending mechanisms. In fact, the optical activation of KA neurons alone was enough to elicit swimming, even in the spinalized animal (Wyart et al., 2009). It was later demonstrated that KA cells contact motor neurons, thus eliciting swimming in the spinal cord (Fidelin et al., 2015, Hubbard et al., 2016, Djenoune and Wyart, 2017). Being KA cells GABAergic, this is a further confirmation that GABA, at early developmental stages, has indeed an excitatory function (Brustein and Drapeau, 2005, Ben-Ari, 2002).

In the *Xenopus* tadpole, KA cells have not been investigated beside the initial work on their anatomy (Roberts and Clarke, 1982, Dale et al., 1987). Even if it is possible that they could play a role in eliciting swimming, giving the early embryonic stage of the tadpole and the fact that they have been stained for GABA (Dale et al., 1987, Roberts and Clarke, 1982), this has not been tested so far. KA cells thus, are not included among the sensory neurons of the tadpole.

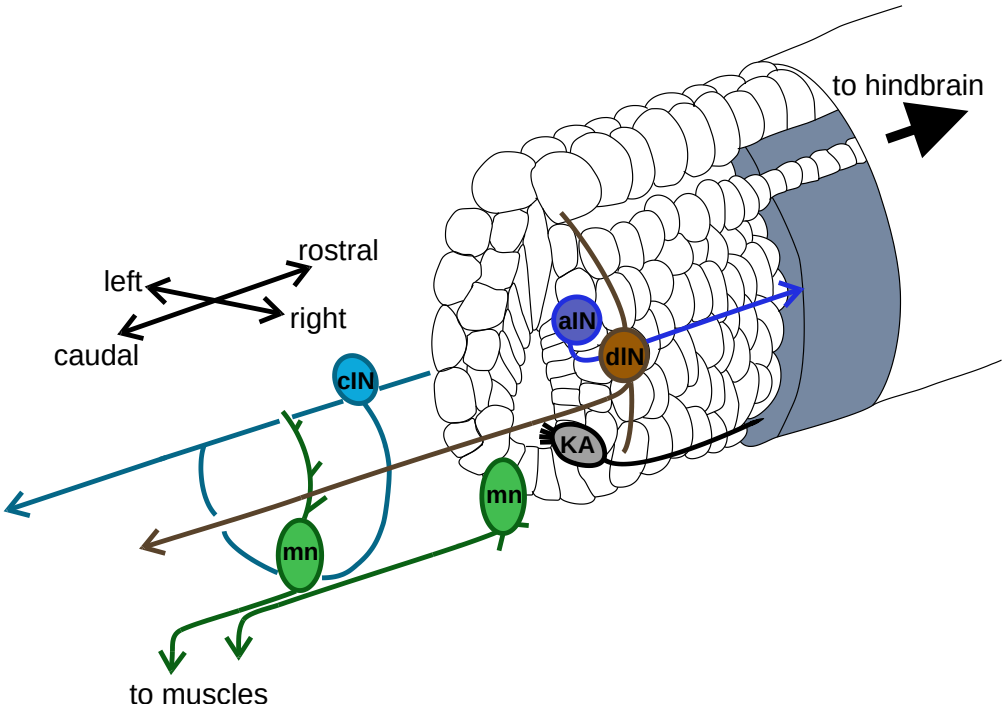

Figure 2.3 Anatomy of CPG neurons in the spinal cord of the Xenopus tadpole.
Schematic of the CPG neurons in the spinal cord of the tadpole with axonal and dendritic projections. In dorso-ventral direction: aINs (violet) have ipsilateral ascending axons that inhibit CPG neurons on the same side of the spinal cord; cINs (blue) have commissural ascending and descending axons that inhibit CPG neurons on the opposite side of the opposite side of the spinal cord; dINs (brown) have ipsilateral descending axons that excite motor neurons(mn); motor

neurons (green) exit the spinal cord and excite muscle fibers; KA cells (grey) have dendritic cilia in the neurocoele and an ascending axon. Note, KA cells are not CPG neurons and they have been included for anatomy illustration purposes. Grey band covering the side of the spinal cord represents the marginal zone, where ascending and descending projections run. Adapted from (Roberts, 2000).

2.3 The tadpole swimming behaviour

In the *Xenopus* tadpole, when a strong enough sensory stimulation is detected and transferred to the CNS, the swimming circuit in its spinal cord is activated. The spinal CPG neurons of the tadpole have three main common features: 1) they are silent when the animal is at rest, and are active only during swimming; 2) they fire one action potential in each swim cycle (with the exception of aINs) and 3) they receive mid-cycle inhibition. Motor neurons, inhibitory interneurons and dINs all show these features (Roberts et al., 2010). As described in paragraph 2.2.3, aINs can fire more than once per cycle. These interneurons provide inhibition to the secondary sensory neurons (dla and dlc) during the initial phases of a swimming episode, but they also inhibit motor neurons on the same side of the spinal cord (Li et al., 2004a). The inhibition of sensory neurons secures a functional swim initiation, preventing secondary stimulation to interfere with the stabilization of swim cycles (Roberts et al., 2008). On the other hand, aINs inhibition on ipsilateral motor neurons prevents them from firing more than once per cycle (Li et al., 2004a), aiding their synchronous firing.

Every CPG neuron on the same side of the spinal cord fires one action potential in phase with the VR burst, thus in phase with muscle contraction. Because cINs also fire in such manner, they can provide mid-cycle inhibition to the CPG neurons on the opposite side of the spinal cord (Soffe et al., 1984, Yoshida et al., 1998). By looking at the two sides of the spinal cord together (fig. 2.4), one can appreciate how rhythmicity is achieved during swimming in the *Xenopus* embryo. In fact, as the CPG circuit on one side fire, the CPG neurons on the opposite side are inhibited (mid-cycle inhibition). Altogether these phasic excitation and inhibition lead to a rhythmic VR burst and muscle contraction, which enables the undulatory propulsive movement of the tadpole in the water.

When the tadpole starts to swim, its body contractions appear firstly on the rostral segments and then propagate towards the caudal portions of the body (Kahn et al., 1982b, Kahn et al.,

1982a, Tunstall and Roberts, 1991). This rostro-caudal delay increases linearly with distance along the longitudinal axis of the tadpole's body (Tunstall and Roberts, 1991). Calculations considering the distance covered by descending axons, the number of synapses made and neurons conductance (Tunstall and Roberts, 1991) revealed that the mathematically calculated delay is much higher than the rostro-caudal delay recorded in fictive swimming experiments (17 ms vs 4-10 ms, (Tunstall and Roberts, 1991)). A longitudinal gradient of both excitation and inhibition in motor neurons has been recorded during swimming (Tunstall and Roberts, 1991). Indeed, two features of major importance for coordinated swimming are the fast AMPARs-mediated excitation and the glycinergic mid-cycle inhibition of CPG neurons. Both these features were found to decline in the more caudal segments, with the glycinergic inhibition that seemed not to be present after the 12th myotomal segment (Tunstall and Roberts, 1994). The NMDA component of CPG excitation is also involved in the rostro-caudal delay; when NMDA was applied to the caudal portion of the spinal cord, a decrease in the delay was reported. On the contrary, when NMDA was delivered globally to the spinal cord, no effect was detected (Tunstall and Roberts, 1991). Experiments on tadpoles where the spinal cord was transected at progressively more caudal segments (Tunstall and Roberts, 1994) showed that the portion of spinal cord till the 5th segment has itself enough oscillatory properties to sustain CPG activation, possibly because of a drive that it receives from the brain. The spinal cord portion comprised between the 5th and the 10th segment also has shown enough tonic drive and mid-cycle inhibition to actively sustain swimming, but external drive is necessary, otherwise swimming cannot be evoked (Tunstall and Roberts, 1994). Lastly, the portion of spinal cord caudal to the 10th segment does not show IPSPs (Tunstall and Roberts, 1994). For this reason, spinal CPG neurons in the more caudal area have been proposed to act as passive elements in the sustaining of swimming, as they would fire only when driven by the more rostral regions (Tunstall and Roberts, 1994).

One likely explanation for the rostro-caudal delay recorded in the swimming of the *Xenopus* tadpole comes from neurons anatomy and morphology. In fact, early anatomical studies showed that the number of both inhibitory and excitatory neurons decreases in the caudal spinal cord (Roberts and Alford, 1986, Dale et al., 1986, Roberts et al., 1988). Moreover, caudal CPG interneurons have shorter axons (Roberts and Alford, 1986, Dale et al., 1986, Roberts et al., 1988), thus providing less opportunities for synaptic contacts among them. Another possibility is that a developmental gradient is present at this embryonic stage. As observed in muscles and

pigmentation (Nieuwkoop and Faber, 1956), neuronal cells also show a spatial gradient in differentiation (Dale et al., 1986, Roberts et al., 1988). This feature might account for a non-self-sustaining caudal CPG population (Tunstall and Roberts, 1994).

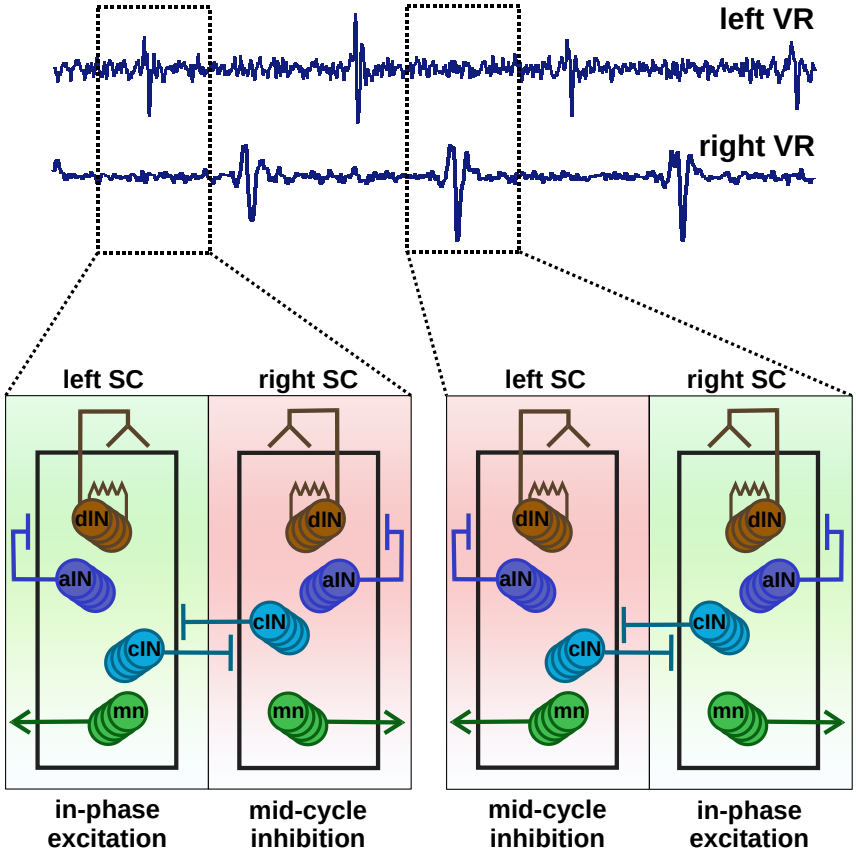

Figure 2.4 In-phase excitation and mid-cycle inhibition alternation drive swimming in the tadpole.

Scheme depicting the activation/inhibition mechanism of CPG neurons in the spinal cord of the tadpole. dINs (brown) are electrically coupled and sustain the excitation of other CPG neurons on the same side of the spinal cord (in-phase excitation); aINs (violet) inhibit CPG neurons on the same side, while cINs (blue) inhibit the CPG circuit on the opposite side providing mid-cycle inhibition; motor neurons (mn, green) excite muscles. While one VR burst is detected on the left side (left VR), the CPG circuit on the left side of the spinal cord (left SC) is excited (green, in phase-excitation). At the same time the right side of the spinal cord (right SC) receives mid cycle inhibition (red). On the contrary, when a VR burst is detected on the right VR, CPG neurons on the right side of the spinal cord receive in-phase excitation (green), while the left side CPG neurons receive mid-cycle inhibition (red).

2.3.1 The CPG and swimming behaviour in the zebrafish

Like the tadpole, the zebrafish swims by alternating left-right movements (Fetcho, 1992) with a rostro-caudal delay present from the larval stages to adults (Saint-Amant and Drapeau, 1998, Buss and Drapeau, 2001, Masino and Fetcho, 2005). In the adult zebrafish, swimming frequency decreases if compared to the swimming in larvae (frequency in adults 1-21 Hz *versus* 20-60 Hz in larvae; (Kyriakatos et al., 2011, Ampatzis et al., 2013, Saint-Amant and Drapeau, 1998, Buss and Drapeau, 2001, Masino and Fetcho, 2005)). This is due to the developmental changes that occur in the zebrafish musculature, which transitions from the red slow and white fast fibres in the embryo, to the red slow, pink intermediate and white fast fibres in the adult (van Raamsdonk et al., 1982, Devoto et al., 1996, Jackson and Ingham, 2013). Accordingly, motor neurons and premotor excitatory neurons develop to connect to the different muscle fibres.

As it happens in the *Xenopus* tadpole spinal cord, where the ventral areas are occupied by motor neurons and other CPG cells (aINs, cINs and dINs), the ventral domain of the zebrafish spinal cord also gives rise to neurons that sustain locomotion (Bernhardt et al., 1990, Hale et al., 2001). Five ventral domains are detectable in the zebrafish spinal cord, of which one gives rise to two types of motor neurons, and the remaining four (named V0 to V3) to other eight classes of interneurons (Bernhardt et al., 1990, Hale et al., 2001, Drapeau et al., 2002). Two motor neuron types appear at different stages, both rising from the same ventral domain (Myers, 1985, Myers et al., 1986, Menelaou and McLean, 2012): the primary early born motor neurons and the secondary late born motor neurons. Contrary to the *Xenopus* embryo, whose motor neurons are not differentiated in more than one type, the larval zebrafish activates one or the other type according to the type of swimming. Indeed, primary motor neurons are active in fast swimming and escape response, while secondary motor neurons are active during slow swimming (Myers, 1985, Myers et al., 1986, Kimura et al., 2006, McLean et al., 2007, McLean et al., 2008, McLean and Fetcho, 2009).

The neuronal population that differentiates from the V1 domain (Circumferential Ascending neurons, CiAs) is formed by inhibitory glycinergic neurons homologue to aINs in the tadpole. Indeed, they share the cellular anatomy, both CiAs and aINs use glycine as a neurotransmitter, and both express the transcription factor *engrailed* (Li et al., 2004a, Higashijima et al., 2004, Kimura et al., 2006).

Excitatory V2a neurons (Circumferential Descending neurons, CiDs) express the transcription factor *chx10* (Higashijima et al., 2004) (Kimura et al., 2006)), as dINs do in the *Xenopus* tadpole (Li and Soffe, 2019). The V2a population also shares other important features with the tadpole's dINs. In fact, V2a neurons have direct synapses to motor neurons (dINs also connect directly to motor neurons, (Dale and Roberts, 1985, Soffe et al., 2009)) and they are necessary and sufficient to drive swimming in the zebrafish (Eklöf-Ljunggren et al., 2012, Ljunggren et al., 2014). V2a interneurons ca be further divided into two sub-categories: ventral and dorsal V2a neurons. The dorsal V2a population is only able to maintain swimming at high frequency, while the ventral V2a population can initiate and maintain swimming at all speeds (Eklöf-Ljunggren et al., 2012, Ljunggren et al., 2014, Sternberg et al., 2016, Menelaou and McLean, 2019). This functional distinction is reflected by the different connections the two V2a populations have with motor neurons. Indeed, ventral V2a neurons have synapses with both primary and secondary motor neurons, while dorsal V2a neurons only connect to primary motor neurons (Svara et al., 2018).

The zebrafish spinal V0 domain gives rise to both excitatory (ventral, V0v) and inhibitory neurons (dorsal, V0d) (Satou et al., 2012, Juárez-Morales et al., 2016, Björnfors and El Manira, 2016).

The V0d inhibitory neurons all share the same anatomy, *i.e.* they all have bifurcating projections (Satou et al., 2012, Juárez-Morales et al., 2016, Björnfors and El Manira, 2016). One population of inhibitory interneurons is formed by the glycinergic V0d (CoBL, Commissural Bifurcating Longitudinal) neurons that maintain the left-right alternation during swimming (McLean et al., 2007, Hale et al., 2001, Satou et al., 2012, Satou et al., 2020). Recently, another neuronal population has been unveiled in the larval zebrafish for the maintenance of left-right alternation: the dI6 (interneurons that rise from the sixth dorsal domain of the spinal cord) neurons that express the transcription factor *dmrt3a*. These interneurons also have commissural projections and, together with V0d neurons, fire rhythmically inhibiting the CPG and motor neurons on the opposite side of the spinal cord (Satou et al., 2020). Both V0d and dI6/*dmrt3a* zebrafish neurons have the same role played by cINs in the *Xenopus* tadpole, where the axons of these glycinergic neurons cross the spinal cord and rhythmically inhibit CPG inteneurons and motor neurons that lie contralaterally (Soffe et al., 1984, Yoshida et al., 1998).

V0v excitatory neurons can be divided into three classes based on their anatomy, which also corresponds to different timing of differentiation, as well as involvement in swimming at

different speed in the adult animal. V0v ascending neurons are the first to appear and they are active during fast swimming, V0v bifurcating neurons are involved in swimming at intermediate speed, and V0v descending, which are the last to appear, are active during slow swimming (Satou et al., 2012). These three categories are already present at the larval stage, but they lack the different anatomy of their adult counterparts (Satou et al., 2012, Björnfors and El Manira, 2016).

Overall, the *Xenopus* tadpole at stage 37/38 shares some distinctive features with the zebrafish regarding their respective locomotor systems, implying that the basic mechanisms of CPG are the same. However, the spinal motor neurons and interneurons of the zebrafish, even in its larval stage, are more complex and diversified. This entails the more abundant behaviours that the zebrafish can perform to satisfy its needs, such as preying. The hatchling tadpole is still a young embryo and its neuronal circuits are developed just enough to sustain a few basic behaviours like swimming or struggling (see below). Nevertheless, it offers the possibility to study mechanisms conserved in vertebrates at a very early stage of development.

2.4 The struggling behaviour

In the unfortunate event of being grasped by a predator, the hatchling tadpole responds with a series of strong bendings aimed at setting itself free. This behaviour, named struggling, was initially observed when strong mechanical stimulation was given to the head of tadpole (Kahn et al., 1982b). After this stimulation, animals started strong alternating movements, similarly to swimming contractions, but slower and of greater amplitude (Kahn et al., 1982b). Even if this was a rare event, coiled movements were also observed, with the tail of the tadpole touching the head (Kahn et al., 1982b). Other features of struggling are the long bursts observed in VR discharges, and the caudal-rostral phase delay. Differently from swimming initiation, the sensory stimulation able to start struggling is stronger and repetitive, and can be delivered to the head (Kahn et al., 1982b) or to the trunk skin (Soffe, 1991, Soffe, 1993, Green and Soffe, 1996, Soffe, 1996, Soffe, 1997, Li et al., 2007). Also differently to swimming, struggling is maintained only during the time of repetitive stimulation: when the stimulus is stopped, the pattern of contractions transition, more smoothly than abruptly, to the well-known rhythmic swimming (Kahn et al., 1982b, Soffe, 1993). The same repetitive skin stimulation can start struggling both at the start of an episode, when the stimulus is delivered to an animal at rest, as well as during ongoing swimming (Soffe, 1991). The caudo-rostral delay is inverse compared to

the rostro-caudal delay present in swimming, as struggling waves of movement start at the level of the anus, then propagate rostrally (Green and Soffe, 1996). The caudo-rostral delay is affected by the cycle duration, and it has been defined 'phase delay' (Green and Soffe, 1996). This feature is different from the constant rostro-caudal delay measured during swimming, which is not affected by changes in the cycle period (Green and Soffe, 1996). Considering all these preliminary information, it seemed clear that struggling was a behaviour *per se*, probably sharing some neuronal underpinnings with swimming, but completely different from the swimming behaviour initiated by the tadpole in response to a brief stimulation.

Applications of both AMPA and NMDA antagonists showed that struggling is driven by glutamatergic excitation, and that NMDA receptors activation is neither sufficient nor necessary to start struggling (Soffe, 1996). When AMPA agonist was locally applied on segments of the spinal cord, struggling was evoked at the level of drug application, but failed to be evoked in more rostrally segments (Soffe, 1996). Conversely, swimming could be recorded in rostral segments following the same procedure with lower concentration of drug (Soffe, 1996). These experiments suggested that possible ascending connections are not enough to drive struggling following the caudo-rostral pattern (Soffe, 1996). Experiments using different concentration of the AMPA agonist also demonstrated that the behavioural output (swimming or struggling) is linked to a different agonist concentration, thus to a different level of excitation of the system (Soffe, 1996). In fact, for lower concentration, thus low excitation level, tadpoles displayed coordinated swimming. On the contrary, for higher AMPA agonist concentration, struggling was evoked (Soffe, 1996). Because of the different type of stimulation leading to swimming or struggling (brief vs repetitive stimulation), and because the secondary sensory dlc neurons (see paragraph 2.5.2) were never found to fire during struggling (Soffe, 1993), Rohon-Beard neurons (RB; see paragraph 2.5.2) firing was investigated. RB neurons are primary sensory neurons, which detect skin stimulation and fire one or two action potential in response to the brief stimulus that leads to swimming (Roberts and Clarke, 1982). When struggling was evoked after repetitive skin stimulation, single RB neurons showed a maintained discharge of action potentials, and more than two RB neurons with multiple firing were needed to reliably initiate struggling (Soffe, 1997).

Although the main players of the spinal CPG circuit are the same active in swimming (motor neurons, cINs and aINs), two additional neuronal classes have been discovered to drive the struggling response in the *Xenopus* tadpole (Li et al., 2007).

The first class, named ecINs (excitatory commissural interneurons), were found to fire repetitively when a 40 Hz electrical stimulation was delivered to the skin (Li et al., 2007). These neurons have somata placed dorsally in the spinal cord, and axons that run ventrally and cross to the opposite side of the spinal cord, where they give rise to an ascending and descending branch (Li et al., 2007). When a 40 Hz skin stimulation was used, ecINs received a summation of excitation from RB neurons, and the majority of them fired multiple rhythmic action potentials, while others were more tonically active. Because the same neurons were not activated after brief stimulation that led to swimming, it was suggested that ecINs are secondary sensory neurons, selectively recruited in the struggling behaviour (Li et al., 2007).

The second neuronal class found to account for the initiation of struggling is dINrs (repetitive firing dINs; (Li et al., 2007)). These are not anatomically different from 'regular' dINs, but they are never active during swimming. Instead, they fire more than three action potentials at every cycle during struggling (Li et al., 2007). Their action potentials are shorter, and when a depolarizing current is injected, they sustain high frequency firing, contrarily to dINs, which in the same conditions never fire more than once (Li et al., 2007). Whilst during struggling dINrs are strongly active, they are silent during swimming, with only a few weakly activated (Li et al., 2007). After single stimulation, dINrs are not activated, but when repetitive stimulation is provided, they receive summating excitation from RB neurons via ecINs (Li et al., 2007). As for dINs, dINrs also excite CPG neurons on the same side of the spinal cord, but they do so by releasing of glutamate on AMPA and NMDA receptors only, whilst dINs co-release glutamate and Ach (Li et al., 2004c). The multipolar somata of dINrs lie in the caudal hindbrain and rostral spinal cord, and they only project descending axons (never ascending, which instead is the case for hdINs (Soffe et al., 2009)). Although it does not happen in swimming because of the brief EPSPs they receive, CPG neurons have the ability to fire repetitively if they are kept under continuous depolarization. Indeed, when dINrs provide longer excitation to CPG neurons during struggling, they fire more spikes per cycle, giving rise to the long bursts recorded in the VR (Li et al., 2007).

In light of the discovery of these novel populations, ecINs and dINrs, it is now clear that both are selectively recruited when a repetitive and strong stimulation is given to the tadpole, leading to struggling. These findings ruled out an early possibility of modulation of the swimming circuit, which would have caused the transition from swimming into struggling (Soffe, 1991, Soffe, 1993). On the contrary, even if the same neurons of the CPG spinal circuit are active in both behaviours, the two neuronal populations that act presynaptically to CPG are immediately and selectively activated depending on the strong and repetitive stimulation, and the motor output is directly struggling (Li et al., 2007).

2.5 Sensory Pathways for Swimming Initiation

The hatchling tadpole relies on a simple, yet very functional sensory system, which enables it to respond to different stimuli from the environment. For its survival in nature, this embryo needs to escape predators, which are mainly the adult individuals of its own species and big insects such as dragonflies. In this context, it appears clear that tadpoles need to have a sensory system in place so that they can detect whether predators are approaching and quickly swim off.

Despite having lateral eyes, at stage 37/38 those are not yet connected to the brain (Grant et al., 1980, Holt and Harris, 1983), so that the tadpole cannot rely on sight for detecting potential predators. Nevertheless, this animal possesses receptors on the skin and one light sensitive organ, which are designated to enable the detection of external sensory stimuli.

In the next paragraphs, the pineal eye, and the sensory pathways in the trunk and head skin of the *Xenopus* tadpole are described. As the aim of this thesis is to study descending control on motor initiation after stimulation on the trunk skin, major interest has been given to neuronal processes of sensory detection lying in the skin, and a detailed explanation is given in paragraph 2.5.2. Lastly, the skin of the *Xenopus* embryo is electrically excitable, providing a primitive sensory mechanism. The excitatory properties of the skin and how they communicate with the CNS in the developing tadpole is discussed in paragraph 2.5.4.

2.5.1 The Pineal Eye Pathway

The pineal eye, or pineal organ, is indeed an organ present in the larval stages of several vertebrates such as newts, salamanders and frogs. In all these animals, the pineal eye is formed by extraretinal photoreceptors, which are responsive to changes in light intensity.

When the light is dimmed above a tadpole, the pineal eye mediates the start of swimming. This mechanism for the start of locomotion was initially proposed to serve as an escape response (Roberts, 1978, Foster and Roberts, 1982), but later studies on large groups of tadpoles suggested that the initiation of swimming mediated by the pineal eye responds to a different ecological need. In fact, by recording the behaviour of large numbers of *Xenopus* embryos, freely moving in a 20 cm deep volume of water, it was shown that the tadpoles respond to light dimming by swimming upwards (Jamieson and Roberts, 2000), attaching to the water surface with their cement gland. In the same work (Jamieson and Roberts, 2000), it was demonstrated that tadpoles prefer to attach on the bottom surface of an object which casts shadow on the water. Because ecological studies on the *Xenopus* tadpoles are missing, only suggestions can be made to explain the behaviour observed in laboratory experimental conditions. Jamieson and colleagues (Jamieson and Roberts, 2000) proposed that, because one of the main predators of tadpoles are adult frogs, which are nocturnal predators and move at the bottom of ponds, the embryos would escape them by swimming upwards and attaching to the water surface. Moreover, because attaching with the cement gland to a solid object is more stable than attaching to the water surface, the tadpoles might prefer to attach under objects which cast shadow, as leaves of aquatic plants would do in natural environments.

In the *Xenopus* tadpole, the pineal eye is present from developmental stage 33 (Roberts, 1978) until stage 44 (Jamieson and Roberts, 2000). At stage 45 the lateral eyes become functional (Beazley et al., 1972), and the pineal eye disappears. At developmental stage 37/38, the pineal eye is a flatten vesicle that lies dorsally at the border between forebrain and midbrain; it joins the brain via a thin stalk and its cavity is connected ventrally to the brain ventricles (Roberts, 1978). Pineal eye activity has been studied by means of multi-unit extracellular recordings; it produces a background activity, which increases to burst activity when light is dimmed, and drops when light intensity is raised (Roberts, 1978).

Immunohistochemistry and pharmacological experiments showed that the photoreceptors in the pineal eye of the tadpole use glutamate as a neurotransmitter, and that both NMDA and AMPA receptors are present (Jamieson and Roberts, 2000). These photoreceptors project into the lumen of the organ, where they make synapse with ganglion cells (Foster and Roberts, 1982). Ganglion cells send tightly bundled lateral axons out of the caudal sector of the pineal eye, which then branch and project to an area around the border of the midbrain and the forebrain (Foster and Roberts, 1982, Jamieson and Roberts, 1999). The same activity recorded on the pineal eye, was recorded in cells that lie in the most rostral area of the midbrain, the diencephalic/mesencephalic descending (D/MD) neurons (Jamieson and Roberts, 1999). These are small cells that mostly lie in one cluster in the ventral midbrain, but a few sparse cells have been reported to spread in the caudal forebrain (Jamieson and Roberts, 1999). The location of D/MD neurons is the same anatomical position where pineal ganglion axons stop (Foster and Roberts, 1982, Jamieson and Roberts, 1999) so, considering that their electrical activity mirrors the activity of the pineal eye both at rest and when swimming starts following light dimming (Jamieson and Roberts, 1999, Roberts, 2000), it is plausible that the D/MD neurons act postsynaptically to the pineal ganglion cells. Because D/MD neurons do not project caudally past the fifth myotomal cleft (Nordlander et al., 1985), it has been proposed they have synaptic contact with cells in the hindbrain, which in turn will excite the swimming centre in the spinal cord (Jamieson and Roberts, 1999, Roberts, 2000). To unveil this, more anatomical and functional studies are still needed.

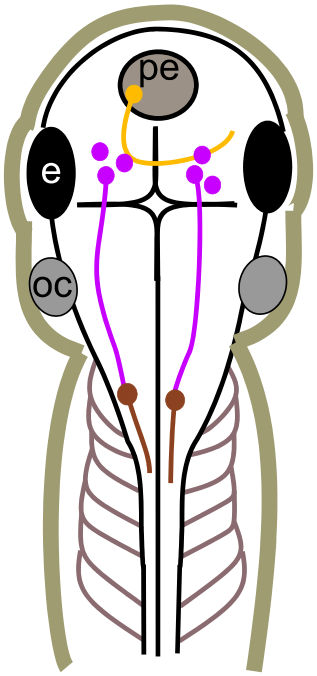

Figure 2.5 The pineal eye pathway for swimming initiation.
Pineal ganglion cells (in yellow) are activated by photoreceptors in the pineal eye (pe) and send axons caudally. D/MD neurons (in purple) in the ventral midbrain and caudal forebrain are excited by ganglion cells and in turn excite CPG in the hindbrain (dINs, in brown). e=eye, oc=otic capsule.

2.5.2 The Trunk Skin Sensory Pathway

The tadpole's body is wholly covered in a thin layer of epidermal cells, which in the trunk host among them sensory projections coming from neurons that lie in the superficial layer of the spinal cord. These are **Rohon-Beard** (RB) cells, which have been firstly identified by means of immunohistochemistry, and whose anatomy and function have been largely studied (Clarke et al., 1984). The cell bodies of RB neurons lie in a double longitudinal column in the most dorsal layer of the spinal cord and, rostrally, they reach the hindbrain till the level of the second myotomal cleft (Clarke et al., 1984). Each RB neuron has neurites that exit from the spinal cord, branch into smaller projections, and penetrate the skin running in between the external and internal layer of epidermal cells. These projections are unmyelinated 'free nerve-endings' (Sillar and Roberts, 1988), and they provide each RB neuron with a receptive field of around 1200 μm^2 on the skin surface (Clarke et al., 1984). RB cells have long axons that run longitudinally in the marginal zone of the spinal cord, both in rostral and caudal direction (Clarke et al., 1984). RB neurons are excited by touch on the skin, for example a manually delivered stroke or poke with a fine hair, and are also excited by electrical stimulation delivered to the skin with an electrode (Clarke et al., 1984). In both cases, RB cells respond to stimulation in a 'rapid transient' manner, *i.e.* by firing one or few impulses during the stimulation, but without maintaining their firing response. Indeed, repetitive stimulation of these neurons is ineffective, unless a recovery time of at least one minute is given to the animal (Roberts et al., 1987). When RB neurons are stimulated by a depolarizing intracellular current (Clarke et al., 1984), a single spike is evoked and this is sufficient to initiate fictive swimming in the immobilized tadpole. During ongoing swimming, RB neurons are silent and they do not show inhibition (Clarke et al., 1984). Initially, RB cells were found to be positive for substance P staining (Clarke et al., 1984), but later studies unveiled the glutamatergic nature of their synaptic connections to interneurons in the spinal cord. Indeed, by means of pharmacological experiments using agonists of glutamate receptors, it was shown that RB cells use glutamate as neurotransmitter (Sillar and Roberts, 1988).

The interneurons that act postsynaptically to RB cells have been initially defined based on their anatomy and position in the spinal cord (Clarke and Roberts, 1984). Two types of these interneurons are present in the hatchling tadpole, both lying dorso-laterally in the more superficial layer of the spinal cord. The first class is defined as **dorsolateral commissural** (dlc) interneurons and the second class consists of **dorsolateral ascending** (dla) interneurons. Both these classes of spinal neurons have dendrites that run in the dorsal half of the marginal zone

(Li et al., 2001), where they can make contact with RB axons running both rostrally and caudally (Clarke and Roberts, 1984). Dorsolateral commissural interneurons have axons that proceed ventrally towards the spinal cord floor, where they cross contralaterally (Roberts and Clarke, 1982). Backfilling with neurobiotin of these neurons showed that their axons, once reached the contralateral side of the spinal cord, branch to give rise to a rostrally projecting axon and to a shorter caudal one (Li et al., 2001). Rostrally projecting axons from dlc interneurons reach the hindbrain, but can also proceed further to the midbrain and forebrain (Li et al., 2001). Dorsolateral ascending interneurons have axons that run ipsilaterally to the soma and project rostrally to the hindbrain, and can also reach the midbrain and the forebrain (Li et al., 2001). Contrary to RB cells, when dlc interneurons were stimulated intracellularly to produce a few action potentials (Clarke and Roberts, 1984), swimming was never initiated in the immobilized tadpole.

Both dlc and dla interneurons have dendrites running in the dorsal part of the marginal zone, where they come in contact with the long rostrally and caudally projecting axons of RB primary sensory neurons. Indeed, intracellular recordings on dlc cells showed EPSPs summating to reach an action potential after electrical stimulation of the skin within the receptive field of one RB neuron (Clarke and Roberts, 1984). The latency of EPSPs was measured in the range of 5-10 ms (Roberts and Sillar, 1990), which is compatible with the conductance of the very fine and non-myelinated free ends of RB neurons lying in the skin. Conversely, when the electrical stimulus was applied to an area of the skin where RB neurons were surgically removed, neither action potentials nor EPSPs were recorded in dlc neurons (Clarke and Roberts, 1984). In dla interneurons, the latency of response from the delivery of an electrical stimulation to the skin was measured at 3-8 ms (Li et al., 2004b), again in accordance with the anatomy and the physiological properties of RB neurons afferent projections. Direct evidence is present for RB-dla connections, as pair recordings were made on these two classes of neurons (Li et al., 2004b). Current injection in RB cells produced EPSPs in dla neurons at a latency indicative of monosynaptic interaction (~1.5 ms, (Li et al., 2004b)). Intracellular recordings from dlc and dla interneurons (Clarke and Roberts, 1984, Roberts and Sillar, 1990, Li et al., 2004b) showed that both classes receive summating EPSPs, which will in turn lead to the firing of one or a few action potentials at short latency from skin stimulation.

EPSPSs recorded in dlc are of dual component type, with a fast rise and slow fall (Sillar and Roberts, 1988), due to the activation of different receptors by the release of glutamate from RB presynaptic compartment. Pharmacological studies using broad antagonists for glutamate receptors, as well as NMDA, AMPA and kainate-specific antagonists, demonstrated that dlc neurons express all three types of glutamate receptors, and that the different kinematic of the three receptor types allows the temporal summation of EPSPs (Roberts and Sillar, 1990). Moreover, dlc cells receive synaptic inputs along their dendrites from more than one RB neuron, which have small receptive field in the skin but long axons that run rostrally and caudally along the spinal cord. Vice versa, RB neurons will excite more than one dlc cell as they project long axons in the marginal zone. As a result, thanks to the anatomical position of both RB axons and dlc dendrites running longitudinally in dorsal part of the marginal zone, the sensory information coming from skin stimulation will be detected by RB free ends, amplified by the several RB-dlc connections, and then conveyed to the opposite side of the spinal cord via dlc interneurons (Roberts and Sillar, 1990).

EPSPs recorded in dla interneurons are also of a dual component type, comparably to EPSPs recorded in dlc (Clarke Jd Fau Hayes and Roberts, 1984, Li et al., 2004b). As in pharmacological experiments on dlc, the application of NMDA and AMPA antagonists abolished the summation of EPSPs in dla interneurons, preventing the firing of action potentials (Li et al., 2004b). In this case, specific NMDA or AMPA antagonists were used (D-AP5 and NBQX, respectively) so that it was possible to identify an early rising component due to the activation of AMPA receptors, and a slower and longer component due to NMDA receptors activation (Li et al., 2004b). Dla dendrites run ipsilaterally to the soma, and longitudinally in the same area of the marginal zone where RB axons and dlc dendrites also lie (Clarke Jd Fau Hayes and Roberts, 1984, Li et al., 2004b). This layout, as for RB-dlc connections, allows dla cells to be contacted by several RB projections, and conversely one RB neuron makes synaptic contact with more than one dla, creating the basis for a simple sensory pathway in the skin, ipsilateral to stimulation (Li et al., 2004b).

Both dlc and dla interneurons receive IPSPs during ongoing fictive swimming (Roberts and Sillar, 1990, Li et al., 2004b). This inhibition originates from aINs and it is stronger at the beginning of a swim episode, when swimming frequency is higher (Li et al., 2002, Li et al., 2004b). Dla and dlc are excited by RB neurons to fire only one or two action potential at short latency from

stimulation, and the glycinergic inhibition they receive has been firstly proposed as a sensory gating mechanism (Roberts and Sillar, 1990, Li et al., 2004b). In fact, it is beneficial during ongoing locomotion to gate the access of sensory stimulation so that the behavioural motor output is not affected. On the other hand, if stimulation is delivered to the skin during later phases of fictive swimming (*i.e.* not at the start of the swimming episode), dla are activated and swim frequency increases (Li et al., 2004b), showing that these neurons can contribute to the increase of speed of swimming in the freely moving animal.

Altogether, RB primary sensory neurons, dla and dlc sensory interneurons constitute a simple mechanism that detects stimulation in the skin, transfer the sensory information into the spinal cord both ipsilaterally (via dla) and contralaterally (via dlc). Dla and dlc finally convey the sensory input to higher brain centres, as their axons project rostrally to the hindbrain, but also to the midbrain and the forebrain (Clarke Jd Fau Hayes and Roberts, 1984, Li et al., 2004b).

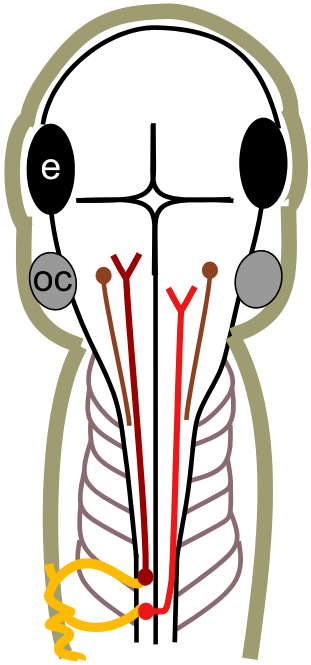

Figure 2.6 The trunk skin pathway for swimming initiation.

RB cells (in yellow) innervate the trunk skin, and get activated by sensory stimulation. In the spinal cord, RB axons excite dlc neurons (in light red), which have commissural axons that reach the brain. RB axons also excite dla neurons (in dark red), which have ipsilateral axons that reach the brain. Here, the dINs (in brown) are activated and start firing rhythmically to sustain swimming.

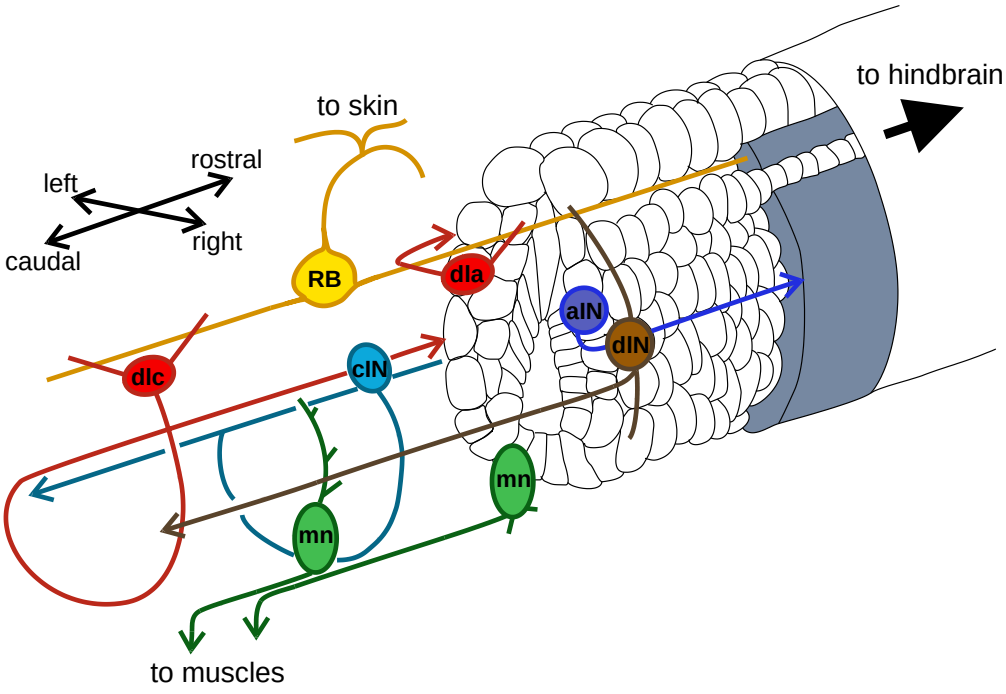

Figure 2.7 Anatomy of CPG and sensory neurons in the spinal cord of the Xenopus tadpole. *Schematic of the CPG neurons in the spinal cord of the tadpole with axonal and dendritic projections. Sensory pathway neurons are the more dorsally located: RB neurons (in yellow) have sensory projections that innervate the skin and long axons that excite dla and dlc (in red). Dla axons project directly to the hindbrain, and dlc cross to the opposite side of the spinal cord and then run to the hindbrain. More medially and ventrally located are CPG neurons: aINs (violet) have ipsilateral ascending axons that inhibit CPG neurons on the same side of the spinal cord; cINs (blue) have commissural ascending and descending axons that inhibit CPG neurons on the opposite side of the opposite side of the spinal cord; dINs (brown) have ipsilateral descending axons that excite motor neurons(mn); motor neurons (green) exit the spinal cord and excite muscle fibers; Grey band covering the side of the spinal cord represents the marginal zone, where ascending and descending projections run. Adapted from (Roberts, 2000).*

2.5.3 The Head Skin Sensory Pathway

As it happens with the trunk, the head of the *Xenopus laevis* tadpole is also covered in skin that hosts sensory projections. This allows the embryo to be responsive to external stimulation encountered anywhere on its body, providing a reliable aid towards its survival.

Early anatomical studies (Roberts, 1980, Davies et al., 1982) revealed dense trigeminal ganglion nerves in the head of the tadpole, which were described as two anatomically and functionally different classes (Hayes et al., 1983). The so called 'type I' projections run ipsilaterally to their soma in the trigeminal ganglion, and they branch in the skin (Roberts, 1980, Davies et al., 1982). In the more superficial layer of the skin, they often nearly encircle skin cells, with almost every skin cell to be in contact with type I projections (Hayes et al., 1983). 'Type II' projections were stained contralaterally to their originating trigeminal ganglion, but they also showed ipsilateral elongations (Hayes et al., 1983). Differently from type I, type II projections run more deeply into the skin and they never reach the most superficial layers. Usually, they lie and terminate in the extracellular space in the deep skin layer (Hayes et al., 1983). Both type I and type II projections are unmyelinated and they present varicosities with mitochondria (Hayes et al., 1983).

Because of their anatomy, and thanks to extracellular recordings following stimulation (Roberts, 1980, Davies et al., 1982), these two types of projections have been linked to functionally different sensory receptors. Type I have been proposed to work as movement detectors, as they largely innervate the superficial layer of the skin and respond to any small disturbance delivered to the skin, such as a light persistent stroke with a hair; these units are active as long as the mechanical stimulation moves along the skin (Roberts, 1980). Conversely, type II afferents run more deeply in the skin of the head, and they respond to local and rapid poke of the skin (Roberts, 1980).

More recently, a short direct pathway from the trigeminal sensory neurons to the spinal CPG circuit has been unveiled (Buhl et al., 2012). A consistent group of 14-23 unipolar neurons lying in the second and fourth rhombomeres was found to fire in response to head stimulation, but not to skin stimulation on the trunk or on the tail skin (Buhl et al., 2012). These cells have been named trigeminal interneurons (tINs), and they have axons which run ipsilaterally into the caudal hindbrain and reach the rostral sectors of the spinal cord (Buhl et al., 2012). Trigeminal interneurons (tINs) are silent at rest and fire in response to head stimulation which can be strong enough to lead to swimming, but they also fire at weaker stimulation. When a weak electrical

stimulation is delivered to the head, only a few tINs fire, and they fire only one action potential. As the stimulation increases, more units are activated and some units fire more action potential, occasionally giving rise to bursts (Buhl et al., 2012). Thus, tINs can also fire when swimming is not initiated after head stimulation, but they fire more reliably when the stimulus delivered is at threshold for swimming. Trigeminal interneurons have dendrites running in the same portion of the tadpole's head reached by the axons of trigeminal sensory neurons, and tINs activation has short latency after stimulation; for this reason it was proposed that tINs are monosynaptically activated by trigeminal sensory neurons (Buhl et al., 2012), whose afferents lie in the skin (Roberts, 1980, Davies et al., 1982, Hayes et al., 1983). Because perfusion with the AMPA antagonist NBQX led to the block of the larger rapid rise component of tINs activation, it was concluded that their excitation is glutamate mediated, mainly via AMPA receptors (Buhl et al., 2012). A smaller component of tINs excitation was visible whit NBQX perfusion, which led to propose that a second smaller portion of excitation can occur via NMDA receptors (Buhl et al., 2012). Thanks to paired recording from couples of tINs, it has been shown that these neurons do not excite each other, and they are not electrically coupled (Buhl et al., 2012). Nevertheless, different tINs can receive excitation from the same sensory afferent but, because single tINs have slightly different spike thresholds, some tINs fire after a certain stimulus, whilst others do not (Buhl et al., 2012). During ongoing swimming, tINs are not excited, instead they can receive IPSPs at variable swim phases. On-cycle and mid-cycle inhibition has been reported, as well as occasional IPSPs not coupled to swimming. Other tINs did not show inhibition at all during swimming (Buhl et al., 2012).

Paired recordings have also been instrumental in proving direct tINs-dINs connections (Buhl et al., 2012). As the tINs axons run caudally into the hindbrain and rostral spinal cord, they make synaptic contact with dINs, which are responsible for the activation of the spinal CPG circuit. As reported above, single tINs firing in response to head stimulation is unreliable, but they can fire more than one action potential after stimulus delivery. Moreover, at stronger stimulation, more tINs are recruited to fire. Therefore, because a few tINs make synapse on the same dIN, their EPSPs can sum in the dINs, both 1) spatially and 2) temporally. In fact, 1) different tINs receive sensory input from several sensory afferents innervating large portion of the head skin and 2) different tINs fire more than one action potential after stimulation (Buhl et al., 2012). This summation of excitation leads to a very reliable excitation in the dINs, which exciting each other

and being electrically coupled as a population (Li et al., 2009), can lead to a steady activation of spinal CPG neurons.

In conclusion, in the *Xenopus laevis* tadpole, swimming can be initiated by mechanical or electrical stimulation on the head. Sensory neurons have afferents lying in the head's skin, and contact a small group of ~20 tINs located on both sides at the level of the second/fourth rhombomeres. These tINs are excited variably depending on stimulus strength, and their EPSPs eventually sum in dINs. Ultimately, the activation of dINs marks the start of swimming, as they excited spinal CPG neurons.

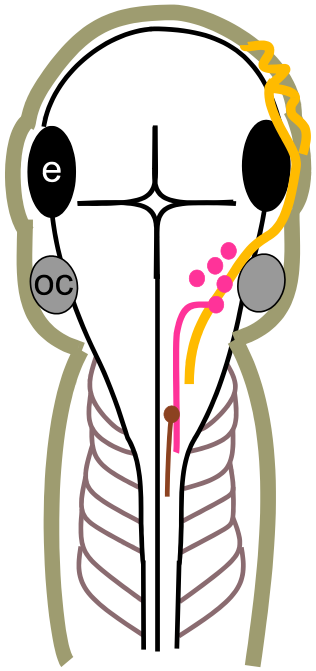

Figure 2.8 The head skin pathway for swimming initiation.

Trigeminal ganglion afferents (in yellow) lie in the skin on the tadpole's head and are activated by touch stimulation. They project caudally into the hindbrain, where they excite tINs (in pink). In turn, tINs axons run into the rostral spinal cord where they activate dINs (in brown), initiating the swimming response.

2.5.4 Skin Excitability Properties

Evidence of the excitable properties of the *Xenopus* tadpole skin have been long known (Roberts, 1969), but how and where this parallel sensory system enters the CNS was only more recently discovered (James and Soffe, 2011).

The tadpole skin is formed by two layers of epithelial cells and a basal lamina (Roberts, 1969). Initial experiments on skin preparation showed that all the skin cells are able to generate an electrical all-or-none impulse after a manual poke was delivered to the preparation (Roberts and Stirling, 1971). When the experiments were performed on tadpoles at stages where their muscles were developed enough to sustain movement, and if stimulation was strong enough, the stimulation caused swimming to start (Roberts, 1969, Roberts and Stirling, 1971). The skin impulse was not affected by changings in the stimulation strength and did not decrease during propagation (Roberts and Stirling, 1971). Impressively, the skin covering the whole body of embryos of developmental stages 26 to 38 was able to generate this impulse, including the epithelia of eyes, cement gland and dorsal fin (Roberts and Stirling, 1971). Considering that tadpoles hatch at developmental stage 37/38, the presence of such a sensory system at very early stages appeared unexpected. Nevertheless, it is worth noting that under adverse conditions, such as high temperature, overcrowding or high concentration of CO_2, the tadpoles can hatch earlier than stage 37/38. Thus, the skin impulse propagation was suggested to work as a primitive sensory system, in place during a time when the neuronal projections are still too short to reach peripheral areas (Roberts and Stirling, 1971, James and Soffe, 2011).

Further studies have shown that, as the brain and the spinal neurons develop, the skin impulse gains access to the CNS through different paths (James and Soffe, 2011). Because earlier evidence suggested that at stage 37/38 the skin impulse enters the brain via the trigeminal nerve (Roberts, 1996), brains of tadpoles from developmental stage 28 to stage 38 were severed just caudally to the otic capsule. Stimulation was delivered to an area of the tail, which was deprived from RB innervation by means of a horizontal cut (James and Soffe, 2011). Embryos of stage 28-31 responded very reliably to stimulation on the un-innervated skin, whilst tadpoles at stage 37/38 did not respond to stimulation. The number of reliable responses in tadpoles of stages 32 to 36 decreased sharply as the age increased (James and Soffe, 2011). This confirmed that at stage 37/38 the skin impulse access to the CNS is cranial, specifically via the trigeminal nerve (Roberts, 1996).

Because RB neurons were considered strong candidates for conveying the impulse into the CNS, single RB neurons were recorded in the same experimental conditions, in all developmental stages. RB neurons in early stages embryos (28-31) fired reliably with skin impulse, whilst RB cells in stage 37/38 tadpoles did not fire if the stimulation was delivered outside their receptive field; nevertheless swimming was initiated also in the latter case (James and Soffe, 2011). RB neurons in stage 32-36 tadpoles showed the same behaviour of RB cells in older animals if the recording was done on the soma, but they had opposite performance if the axonal activity was recorded. The authors proposed that in the 'in-between' stages, both immature and mature RB neurons can be present in the spinal cord, thus they will be still able (if immature) or not able anymore (if mature) to let the skin impulse into the spinal cord (James and Soffe, 2011).

2.6 The stopping Pathway

When the freely moving tadpole bumps with its head into a solid surface, it stops swimming. The same stopping response is observed if a short poke to the tadpole's head is delivered, both during free swimming, as well as during fictive swimming in immobilized tadpoles.

This implies a descending connection from the sensory neurons that lie in the head skin to the spinal CPG neurons responsible for swimming. Indeed, when a gentle pressure was delivered to the head, or the mucus was gently pulled from the cement gland, a burst of activity was recorded in the trigeminal ganglion, and after 1-2 swim cycles, VR activity consistently stopped (Boothby and Roberts, 1992). To confirm the involvement of trigeminal neurons in the stopping response, trigeminal nerves were severed on one or both sides (Boothby and Roberts, 1992, Lambert et al., 2004a). When only one side was lesioned, stimulation on the head was able to stop fictive swimming, but when trigeminal projections were cut on both sides, the tadpoles failed to stop after pressure on the head (Boothby and Roberts, 1992, Lambert et al., 2004a). In the tadpole, trigeminal neurons have caudal projections, which end in the hindbrain without reaching the spinal cord (Hayes et al., 1983). Also, trigeminal neurons are excitatory (Buhl et al., 2012), so it seemed plausible that a population of interneurons in the hindbrain would have an inhibitory effect on the spinal circuit to stop swimming activity.

Anatomical analysis revealed two hindbrain neuronal populations, which were stained for GABA (Boothby and Roberts, 1992). Both populations consist in two symmetrical clusters in the left and right hindbrain: the most rostral population lies in the second and third rhombomeres and has ipsilateral and contralateral descending axons, whilst the caudal cluster of GABAergic neurons reside caudally to the otic capsule and have only ipsilateral projections (Boothby and Roberts, 1992). Combinations of different lesions in the hindbrain confirmed that the neuronal pathway that leads to the stop of swimming can take both ipsilateral and contralateral path, referred to the side of the trigeminal nerve investigated (Boothby and Roberts, 1992, Lambert et al., 2004a). Both populations of these GABAergic hindbrain neurons (called midhindbrain neurons, MHRs; (Roberts et al., 1987, Boothby and Roberts, 1992)) respond to pressure on the head by increasing their firing, and have been proposed to act as inhibitory interneurons in the stopping pathway (Lambert et al., 2004a). Biotin filling of MHRs responding to pressure on the head, shed further light on their anatomy (Perrins 2002). MHRs have elongated multipolar somata and commissural and ipsilateral projections, which run caudally into the spinal cord (Roberts et al., 1987, Boothby and Roberts, 1992).

When pressure is delivered to the tadpole's head, MHR interneurons receive monosynaptic excitation from the trigeminal sensory neurons, and they fire one or a few action potentials (Perrins et al., 2002). Conversely, motor neurons and dINs receive IPSPs when the head or the cement gland receive pressure (Perrins et al., 2002, Li et al., 2003). Differently, inhibitory spinal interneurons (cINs and aINs) also receive IPSPs, but less reliably than dINs and motor neurons (Li et al., 2003). The direct evidence for MHRs being responsible for the stop of swimming came from their intracellular activation. In fact, when MHRs were activated by current injection (Perrins et al., 2002), swim stopped in 1-2 cycles, confirming that these GABAergic interneurons act postsynaptically to the trigeminal sensory neurons in the descending stopping pathway. Further evidence of MHRs' GABAergic transmission was reported in pharmacological studies using GABA and glycine antagonists (Perrins et al., 2002, Li et al., 2003). Indeed, when glycine-based transmission was blocked by strychnine, IPSPs were still recorded in spinal CPG neurons (Li et al., 2003). On the contrary, inhibition of spinal interneurons was not reported after the GABA antagonist bicuculline was perfused on the tadpole preparation (Perrins et al., 2002, Li et al., 2003).

During ongoing swimming, MHRs receive mid-cycle IPSPs (Perrins et al., 2002), which are most likely due to the ascending projections of spinal glycinergic cINs reaching the hindbrain (Yoshida et al., 1998). Although the function of this inhibition remains unclear, it has been proposed that it would diminish the probability of MHRs to fire an action potential while the animal is moving (Perrins et al., 2002). Nevertheless, if the tadpole encounters a strong enough stimulation, such as bumping into a solid object while swimming, excitation from the trigeminal sensory neurons will be conveyed to MHRs, they will be activated, and movement will stop.

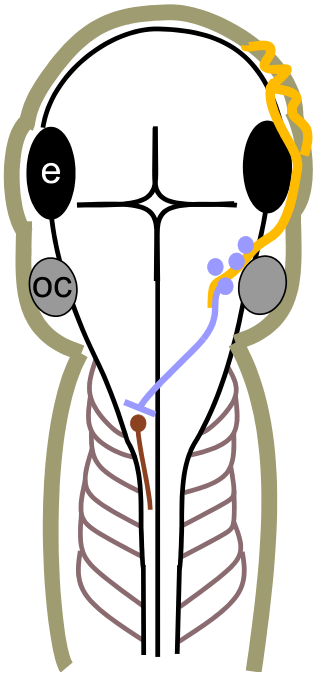

Figure 2.9 The stopping pathway.

The sensory projections of trigeminal ganglion neurons (in yellow) lie in the head skin and are activated by a strong manual poke, or when the tadpole bumps against a solid surface. Trigeminal neurons project into the hindbrain and activate the GABAergic MHR neurons (in lilac). MHR project caudally into the spinal cord and they inhibit dINs, causing the stop of swimming.

2.7 Tonic Inhibition of Locomotion

The stage 37/38 *Xenopus laevis* tadpole does not feed, and where the mouth will later develop, it has a dark pigmented gland secreting mucus: the cement gland. Thanks to the mucus it produces, the tadpole can hang to the water surface or to solid objects and remain still. The cement gland is anatomically formed by a pigmented columnar epithelium, with mucus-secreting cells in the superficial layer, and it is innervated by the unencapsulated terminals of the mandibular trigeminal nerve (Roberts et al., 1975). These sensory afferents reach the superficial layer of the gland and run for about 400 µm to the ventral lobe of the trigeminal ganglion (Roberts et al., 1975, Lambert et al., 2004b). Recordings from cell bodies lying in the ventral lobe of the trigeminal ganglion after pressure of the cement gland showed that these projections are unmyelinated, and that their receptive fields are confined in the cement gland, as stimulation on other area of the head did not evoke activity in the ventral area of the trigeminal ganglion (Roberts et al., 1975). These sensory receptors are not activated by electrical stimulation delivered directly to the cement gland, neither they work as chemical synapses as they still respond to pressure on the cement gland in high Mg^{++}/low Ca^{++} concentrations in perfusion saline (Roberts et al., 1975). Nevertheless, all the units investigated in early studies (Roberts et al., 1975) were activated by light pressure on the cement gland, and the majority of them also responded to the pulling of the mucus strand away from the animal's head. For these reasons, it has been proposed that the trigeminal afferents in the cement gland work as mechanosensory receptors, responding to mechanical distortion of the gland (Roberts et al., 1975). These units are also spontaneously active, and they increase their firing following stimulation. Specifically, the spontaneous activity recorded arise at the level of the afferent terminals, as localised microperfusion of anesthetic in the ventral lobe of the trigeminal ganglion did not eliminate spontaneous firing, but it did when it was applied to the terminals (Lambert et al., 2004b).

During stimulation of the cement gland, the tadpole is less responsive to other stimuli (Roberts et al., 1975, Boothby and Roberts, 1992, Lambert et al., 2004b). Behavioural observations (Boothby and Roberts, 1992) showed that when tadpoles are attached, the stimulation delivered to initiate swimming has to be stronger than when not attached. This was confirmed by multi-unit recording experiments carried out on a set up where a light weight could be attached (or detached) to the cement gland of the tadpole (Lambert et al., 2004b), thus

mimicking the animal's behaviour of attaching to the water surface or to solid objects with its mucus strand. The increased activity in cement gland units was sustained for the time of weight attachment (up to 60 minutes), and so was the reduced responsiveness to light dimming and trunk skin stimulation (Roberts et al., 1975, Lambert et al., 2004b). When fictive swimming was evoked after trunk skin stimulation or light dimming, no difference in the spontaneous activity of the units innervating the cement gland was reported (Lambert et al., 2004b). When the trigeminal nerve was severed on one side only, the reduced responsiveness during attachment was maintained, but it was lost when trigeminal nerves were cut on both sides of the tadpole (Lambert et al., 2004b).

MHRs, the hindbrain GABAergic interneurons responsible for the stop of swimming, have been found to be also responsible for the reduced responsiveness to stimulation following the tadpole's attachment through the cement gland (Roberts et al., 2008). Indeed, when the cement gland is stimulated with a light pressure, MHRs are excited (Perrins et al., 2002, Li et al., 2003). In the same conditions, motor neurons and dINs are inhibited, but no IPSPs have been recorded in dla sensory neurons (Li et al., 2003). Although it is possible that single MHR are involved in the stopping pathway caused by pressure on the head and other MHRs act towards the tonic inhibition observed during cement gland stimulation, the same hindbrain GABAergic population is responsible for both mechanisms (Roberts et al., 2008).

In order to understand the ecological advantages of the reduced responsiveness to stimulation during periods of attachment to the water or solid surfaces, behavioural experiments were carried out with one of the tadpoles' natural predators, the damselfly nymph (Zygoptera) (Lambert et al., 2004b). Tadpoles with both trigeminal nerves severed were predated more than control animals (Lambert et al., 2004b), pointing to the fact that the ability to remain still and attached to the water surface or solid objects provides ecological advantages to the *Xenopus* embryo.

2.8 Locomotor Control in the Tadpole

Differently from zebrafish larvae and other model organisms used in research on motor control, the tadpole at stage 37/38 does not swim spontaneously, so the activation of the spinal CPG

circuit is always caused by an external stimulus. Different pathways of sensory stimulation have been described in detail in this chapter; they include the initiation of swimming by stimulation of the skin on the trunk or head, and motor response to light dimming mediated by the pineal eye. Also differently from other model organisms, the hatchling tadpole does not need to feed, thus it does not perform hunting behaviour. This matches with the still undeveloped eyes and optic tectum, which do not allow visual information to be neither acquired, nor integrated with other sensory stimulation (Beazley et al., 1972). Indeed, the initiation of swimming caused by light dimming does not involve tectal neurons, and activates directly CPG neurons in the hindbrain and spinal cord via D/MD neurons (Jamieson and Roberts, 1999).

Although it has been abundantly reported that the tadpole can perform C-startle responses when stimulated mechanically (Sillar, 2009), and although Mauthner neurons are present in the stage 37/38 tadpole used in this work, their involvement in the escape response has never been reported in almost four decades of research on this organism's swimming behaviour. Mauthner neurons are present in the *Xenopus* at pre-hatching stages (30/31, (Nieuwkoop and Faber, 1956)), they then enlarge and their axons reach the spinal cord at stage 35/36 (van Mier and ten Donkelaar, 1984). Furthermore, Mauthner neurons remain even in the adult individuals of the *Xenopus laevis* (Cioni et al., 1989). In the tadpole, neuronal projections are unmyelinated (Yoshida, 1997) but the larger size of Mauthner neurons' axons could explain the fast C-response seen in the tadpole (Sillar, 2009, Sillar and Robertson, 2009). As now, no direct evidence for a role of Mauthner neurons in driving fast escape response has been shown in the tadpole. Nevertheless, their presence and features suggest that they could be responsible for a C-start response in the tadpole as they do in various other animals (Hale et al., 2016).

The dopaminergic system has been demonstrated to play an important role in the mechanism of locomotor control of mammals, lamprey and zebrafish (see paragraphs 1.2.2 and 1.2.3). At the very early stage of tadpole's development used in this work, dopaminergic neurons have never been reported, so it is reasonable to assume that the dopamine system does not have a role in the initiation of swimming in the stage 37/38 tadpole.

A population of reticulospinal neurons in the caudal hindbrain (hdINS) has been shown to fire first at swimming initiation, before the activation of other CPG neurons (Soffe et al., 2009, Koutsikou et al., 2018). Once swimming has started, hdINs fire one action potential at every swim cycle, together with the more caudally located dINs, providing the excitation needed to

the spinal CPG circuit (Roberts et al., 2010). Because these neurons are the first to fire at the start of locomotion, their activation has been investigated in detail. When the tadpole is stimulated electrically on the skin, hdINs receive EPSPs, which can summate and give rise to an action potential. If the summating effect is enough to lead to a first action potential, the hdINs will then continue to fire rhythmically, sustaining the CPG circuit. EPSPs recorded in hdINs are very variable, both in their amplitude and in their latency from stimulation (Koutsikou et al., 2018). Because hdINs, and dINs in general, are silent in resting conditions (Soffe et al., 2009, Li et al., 2006), it is very unlikely that background synaptic inputs contribute to the summation of these variable EPSPs. Interestingly, even when the skin stimulation failed to initiate a motor response (*i.e.* stimulation below threshold for swimming), EPSPs were recorded in hdINs. These EPSPs though, failed to depolarize the neurons to threshold for an action potential, thus swimming did not start (Koutsikou et al., 2018).

From an anatomical, temporal, and functional point of view, after skin stimulation and before hdINs activation, lies the sensory pathway. The ascending pathway that carries the sensory information from the tadpole's trunk skin to its brain is well known. It consists in primary sensory Rohon-Beard cells and secondary sensory dla and dlc neurons, which reach the brain (Buhl et al., 2012, Li et al., 2003). Although previous work failed to prove direct connections between the sensory pathway and hdINs (Buhl et al., 2015), it might be possible that the excitatory firing of dla and dlc can explain the EPSPs recorded in hdINs. This possibility has been tested (Koutsikou et al., 2018) and it has been shown that the firing latency and pattern of dla and dlc cannot sustain the variable and delayed EPSPs observed in hdINs. In fact, both dla and dlc fire only one, or two, action potentials following skin stimulation, at a constant and short latency from simulation (4-15 ms in (Koutsikou et al., 2018)). The summation of EPSPs recorded in hdINs occurs over a much longer time, which can last for ~100 ms (Koutsikou et al., 2018).

Because the known cellular populations in the *Xenopus* tadpole cannot explain the variable and delayed activation of hdINs, a new neuronal population was proposed to act between the sensory pathway and the hdINs; this population has been called extension neurons (ExNs), as it would extend the sensory stimulation in the time prior motor response (Koutsikou et al., 2018).

So far, no direct evidence for the presence of the ExNs population has been shown. Nevertheless, a computational model suggests that ExNs could sustain the variable and delayed excitation recorded in hdINs prior to swim initiation (Koutsikou et al., 2018). The model was built

on previously published computational models for the tadpole's various neurons and synapses (Sautois et al., 2007, Hull et al., 2016), to which a population of ExNs with recurrent excitation was added (Koutsikou et al., 2018). Briefly, a population of dlc excites the ExNs population, whose neurons are interconnected via AMPA and NMDA-mediated synapses. The ExNs have postsynaptic glutamatergic connections with hdINs, which will start to fire rhythmically if the threshold for activation is met. Thanks to the introduction of recurrent excitation in the ExNs population, the modelled hdINs were able to sustain their own firing, as it happens during swimming. Crucially, in order to reproduce the variability recorded in the hdINs EPSPs, only some ExNs in the model receive direct excitation from dlc neurons, whilst the excitation of the other ExNs is driven by the recurrent network they form across the ExNs population. In this scenario, ExNs act as 'procrastinators' in the process of swim initiation caused by skin stimulation, as they hold the sensory information within their recurrent network, allowing the summation of EPSPs in hdINs (Koutsikou et al., 2018).

The premises on which the computational model is built appear strong enough to investigate further the existence of ExNs, which is the overall aim of the experiments reported in this thesis.

3 Aim of the work

The overall aim of this work is to study the neural mechanisms of locomotor control in a simple vertebrate, the embryo of the *Xenopus laevis*. Specifically, the involvement of the caudal region of the brain of the tadpole, namely the hindbrain, will be investigated. The role played by hindbrain neuronal substrates in the activation of locomotor circuit will be studied in response to an external stimulation delivered to the skin of the *Xenopus* tadpole.

As illustrated in the previous chapter, both the spinal CPG circuit that sustains swimming, as well as the ascending sensory pathway that is activated by trunk skin stimulation, have been described in detail (Roberts et al., 2019). Nevertheless, a time gap exists in the activation of the descending pathway (dINs), after the firing of sensory neurons (fig. 3.1). Importantly, none of the already-known neuronal populations in the tadpole can account for this delayed swimming initiation (Koutsikou et al., 2018). A novel population, named extension neurons (ExNs), has been proposed to cover the role of 'holding' and 'extending' the sensory information in the tadpole's hindbrain, thus allowing the procrastination of the motor response. Accordingly, the hypothesis that has driven this work is that a novel neuronal population, namely the ExNs, resides in the hindbrain of the hatchling tadpole and a) fires in response to trunk skin stimulation, either at threshold for swimming or below the threshold for motor response; b) is activated after the sensory neurons but before swimming initiation; c) fires over a time long enough to activate dINs (Koutsikou et al., 2018, Ferrario et al., 2021).

Based on these premises, the main objectives of this thesis are:

1. to confirm the existence of the ExNs population in the hindbrain of stage 37/38 *Xenopu*s tadpole
2. to characterise ExNs firing pattern at the initiation of swimming
3. to locate the ExNs population in the hindbrain of the tadpole

Behavioural and electrophysiology *in vivo* experiments were performed on lesioned tadpoles to analyse the pattern of swimming initiation, and thus confirm the presence of putative ExNs in the hindbrain. This would also help to restrict the anatomical location of ExNs to discrete areas of the hindbrain (results presented in chapter 4). An extracellular, hindbrain-wide analysis of

firing activity in relation to motor response after trunk stimulation was carried out to identify putative ExNs units, and subsequently chracterise their activation patterns (results presented in chapter 5). *In vivo* calcium imaging and IHC on fixed samples were used to localize areas where putative ExNs can lie in the hindbrain of the *Xenopus* tadpole (results presented in chapter 6 and 7, respectively).

Completing the neuronal circuit that takes the sensory information to the tadpole's brain, and in turn sets the animal in motion, would bridge the gap in the knowledge available on embryonic descending motor control. On a larger scale, identifying the neurons responsible for the locomotor response in the *Xenopus* embryo will serve as a springboard to unravel how the building blocks of motor decision-making process develop and become integrate with the multiple sensory pathways in more complex vertebrates.

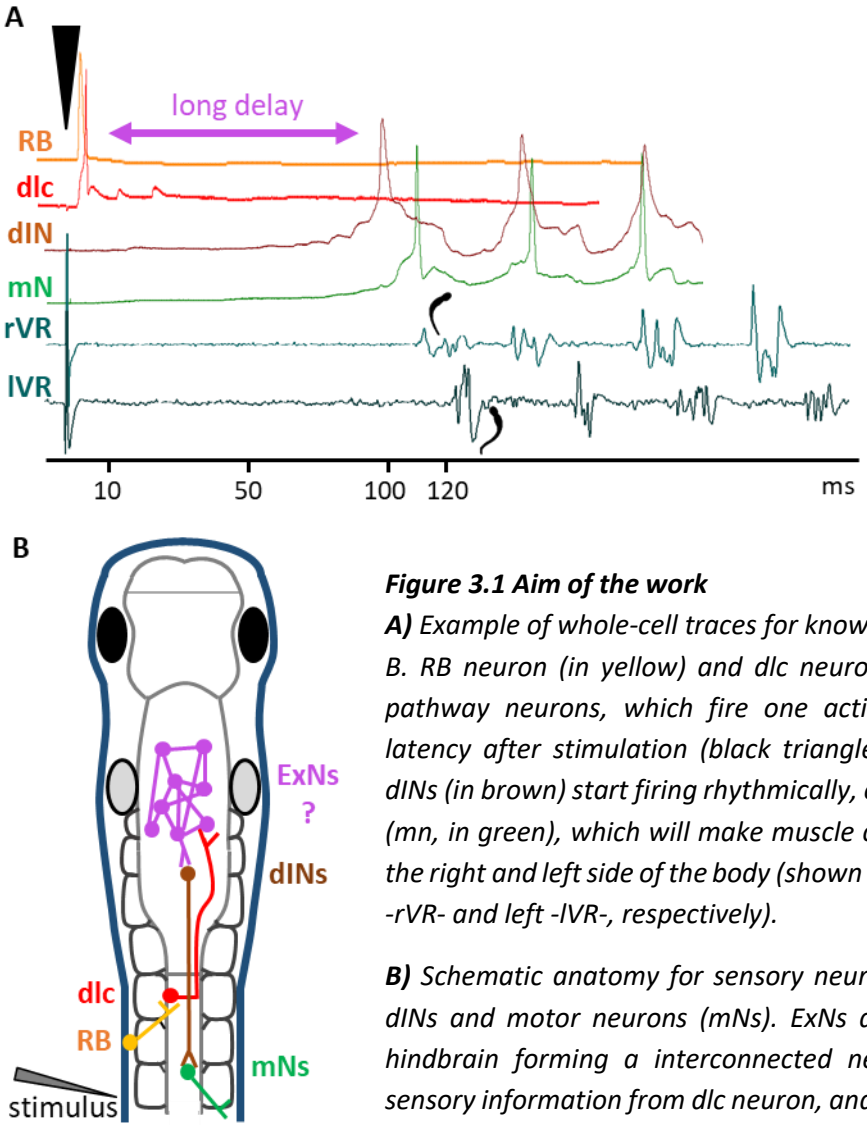

Figure 3.1 Aim of the work

A) *Example of whole-cell traces for known cell types depicted in B. RB neuron (in yellow) and dlc neuron (in red) are sensory pathway neurons, which fire one action potential at short latency after stimulation (black triangle). After a long delay, dINs (in brown) start firing rhythmically, exciting motor neurons (mn, in green), which will make muscle contract alternately on the right and left side of the body (shown here as VR bursts, right -rVR- and left -lVR-, respectively).*

B) *Schematic anatomy for sensory neurons (RB and dlc cells), dINs and motor neurons (mNs). ExNs are represented in the hindbrain forming a interconnected network, which receive sensory information from dlc neuron, and in turn activates dINs.*

4 Results: Hindbrain areas involved in motor response to skin stimulation

The experiments reported in this chapter were aimed to study the role of the hindbrain in the control of swimming initiation caused by an external stimulation to the trunk skin. The goal of these experiments was to identify anatomical areas in the hindbrain that might be 'hot spots' in the mechanism that regulate the start of swimming. These hypothetical hot spots would be the anatomical location of ExNs, the cellular populations proposed to be responsible for the descending motor control in the *Xenopus* embryo (Koutsikou et al., 2018).

The rationale of this study relies on the assumption that by lesioning different hindbrain areas, *i.e.* disconnecting certain neuronal populations from the swim-sustaining CPG circuit in the spinal cord, swim initiation would be controlled only by neurons and neuronal connections in the non-lesioned hindbrain. Conversely, failures in different aspects of swim initiation could be attributed to neurons lying in the hindbrain areas that were disconnected from the spinal CPG circuit.

Hence, the hindbrain was severed at different levels and behavioural experiments, as well as electrophysiology recordings, were carried out. Swim initiation was studied in freely moving animals, whilst fictive swimming was analysed with VR recordings in immobilized animals. In behavioural experiments, mechanical stimulation was manually delivered to the trunk skin of control and lesioned tadpoles, and slow-motion videos of the start of swimming were recorded. In extracellular recordings of fictive swimming, an electrical stimulus was delivered to the trunk skin, and ventral root activity was recorded on both sides of the tadpole's body. Two features of the initiation of movement were analysed in both experimental procedures: 1) the latency from stimulation to the first body movement, and 2) the side of the body where the first muscle contraction appeared. In fictive swimming recordings, latency was considered from stimulation to first ventral root burst, and the side of the body where the same first burst appeared was considered as the side of first muscle contraction. Both latency and side of first contractions were recorded and compared among control and lesioned animals.

The overall conclusion that could be drawn from the above-mentioned experiments is that putative neural populations involved in swim initiation are dispersed in the hindbrain. Indeed, it was not possible to define a discrete area in the hindbrain in which such neurons might lie. Nevertheless, the hindbrain was shown to be implicated in the mechanisms regulating the long and variable latency to the start of movement in the tadpole, as well as in processes that control the first asymmetrical activation of spinal CPG circuit.

4.1 Materials and Methods

Animal care

Experiments were performed on the South African clawed toad *Xenopus laevis* tadpoles at developmental stage 37/38, according to Nieuwkoop and Faber (Nieuwkoop and Faber, 1956). Fertilized eggs were purchased from the European *Xenopus* Resource Centre (EXRC, Portsmouth UK) and kept at 16-19° C in tap water treated with commercially available aquarium conditioner. Embryos were sorted according to the developmental stages and only healthy tadpoles were kept for subsequent experiments. Animal care and all experimental procedures on *Xenopus laevis* tadpoles were approved by the University of Kent Animal Welfare and Ethical Review Body (AWERB) committee (reference: 0037-SK-17, University of Kent AWERB).

Brain surgery

After being briefly anesthetized with MS-222 (ethyl 3-aminobenzoate methanesulfonate, Sigma-Aldrich; see Appendix 1 for solution details), tadpoles were pinned to a rotating Sylgard block in a saline-filled dish (see Appendix 1 for saline solution recipe, and pinning of the tadpole is illustrated in fig. 4.1B). The head skin was removed using handmade tungsten tools, and the trigeminal nerves were cut on both sides at the otic capsule level (fig. 4.1C); this precaution was taken to prevent the sensory stimulus to reach the brain via electrical conductance properties of the skin (Roberts and Stirling, 1971, James and Soffe, 2011). Further lesions were made with fine home-made tungsten tools as depicted in figure 4.1C. Specifically, lesions made were:

1) one longitudinal cut along the midline from the MHB to the obex, separating the left from the right side of the hindbrain;
2) one transversal cut along the MHB, leaving the hindbrain intact;
3) one transversal cut in the hindbrain at the first myotomal cleft, named zero cleft (0 cleft) level;

4) one transversal cut in the hindbrain at the second myotomal cleft, named second cleft (2nd cleft) level;
5) two staggered transversal partial cuts; the cut on left side was made at the MHB while the cut on the right side was at the 0 cleft level.

After surgery, all animals were allowed to recover for 10 minutes in saline at RT and were subsequently tested to ensure robust swimming before being used in further experiments.

Behavioural experiments

Following recovery after surgery, tadpoles were placed in a small Petri dish lined with Sylgard, in which a groove was made (fig. 4.2). The groove was shaped to accommodate the tadpole in upright position, with the yolk sac positioned into the groove and the tail hanging free without touching the Sylgard lining. During experiments, tadpoles were accurately positioned into the groove and a manual mechanical stimulus was given with a fine hair on the trunk skin at the level of the anus (fig. 4.2C). Tadpoles were stimulated on both sides of the trunk to minimize the effect of human error when touching the animal. Videos were recorded with a commercially available digital camera (Casio EX-FH100) at 420 fps in black and white mode. An LED light source was positioned beneath the Petri dish to enhance the contrast of the tadpole shape in single video frames. Video analysis was carried out on ImageJ software. Latency time (ms) from the touch of the hair to the first head's movement was calculated and the side of the first head's bend (ipsilateral or contralateral in respect to the given stimulus) was also assessed.

Electrophysiology

In addition to the brain lesions procedure described above, the skin covering muscles on both sides of the tadpole's body was removed to get access to the myotomal clefts. After surgery, animals were allowed to recover and tested for robust swimming. They were then immobilized in α-bungarotoxin (Invitrogen) for 50 minutes at room temperature (see Appendix 1 for details of α-bungarotoxin solution). Animals were pinned on a rotating Sylgard block in a small recording dish filled with saline. Two borosilicate glass suction electrodes (tip diameter approximately 70 µm) were attached to both sides of the tadpole's body approximately at the level of the 4th cleft to record ventral root activity. A third glass suction electrode was attached to the trunk skin on the right side of the body at the level of the anus to deliver electrical stimuli to the animal. A schematic view of electrodes positions can be seen in figure 4.3 Aii/Aiii. All electrodes were made from borosilicate glass capillaries (outer diameter 1 mm, inner diameter

0.58 mm; Clark Electromedical Instruments, UK), which were pulled in a micropipette puller (P-97, Sutter Instrument, USA) and cut at the desired length.

For staggered lesions, the position of the transversal cuts (MHB and 0 cleft level) was inverted in one group to allow the transfer of stimulation in the specular situations (referred to as L-R when the lesion at MHB was done on the left side and lesion at 0 cleft was on the right side; referred to as R-L lesion when the two transversal cuts were inverted). In the behavioural experiments, this was achieved by changing the side of manual stimulation. In electrophysiology experiments, electrical stimulation was given via a custom-made TTL pulse generator automatically driven through the software used for recording (Signal 7, CED, UK). Threshold stimulation was set as the smallest stimulus (both in intensity -V- and duration -ms-) which led to swimming initiation. Suprathreshold stimulation was defined as the intensity of threshold stimulus + 1V, with the same duration. Threshold intensity of the stimulus was tested in each animal prior experiments recording, and suprathreshold stimulus was calculated accordingly for each animal. All the animals started swimming with a threshold stimulus in the range of 3.5-4.5 V and 0.25-0.4 ms. Electrical signal from left and right VR was amplified, 50/60Hz noise was eliminated via a noise eliminator (HumBug, Digitimer, UK), and data were acquired in Signal 7 software, through a Power 1401 mkII (CED, UK) at a sample rate of 20000 Hz.

Data analysis

Slow motion videos were analysed in ImageJ and latency time for motor response was calculated in Microsoft Excel using the following equation: $latency\ (ms) = (N_{frames}/420\ fps)\ x\ 1000ms$. Electrophysiology experiments were analysed in Signal 7 (CED, UK). Following statistical analysis and graphs were made in Prism 9 (GraphPad Software, USA). Data were tested for normality with Shapiro-Wilk test and when normality criteria were not met, non-parametric analysis was used. Significance level was set at $p<0.05$ for all tests used.

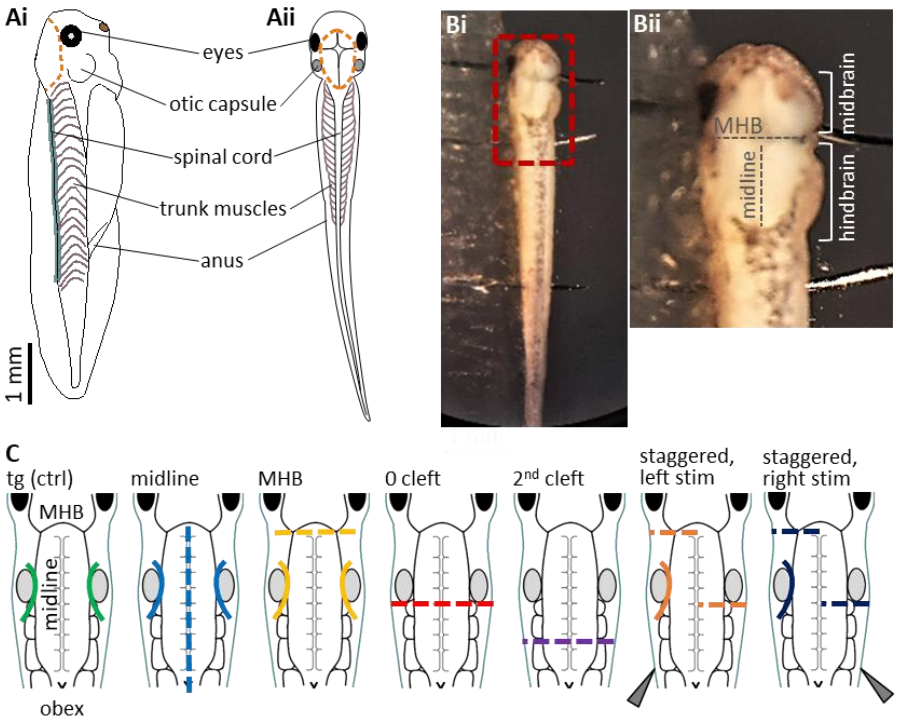

Figure 4.1 Anatomical schematic of brain surgery carried out on tadpoles for behavioural and electrophysiology experiments.

A) *Side (Ai) and top (Aii) view of the tadpole with anatomical hallmarks. Orange dashed lines on the head indicate skin removal to get access to the brain.*
Bi) *Picture of a tadpole pinned to the Sylgard block during experimental procedures. The skin was removed from the head to get access to the brain.* ***Bii)*** *Zoomed-in view of red dashed square in Bi. Midbrain and hindbrain are visible; midline and MHB are indicated by grey dashed lines.*
C) *Schematic of different brain lesions carried out on tadpoles for behavioural and electrophysiology experiments. Coloured dashed lines indicate where the tissue was severed. Grey pointed triangles in the animals with staggered lesions represent side of stimulation in behavioural experiments.*

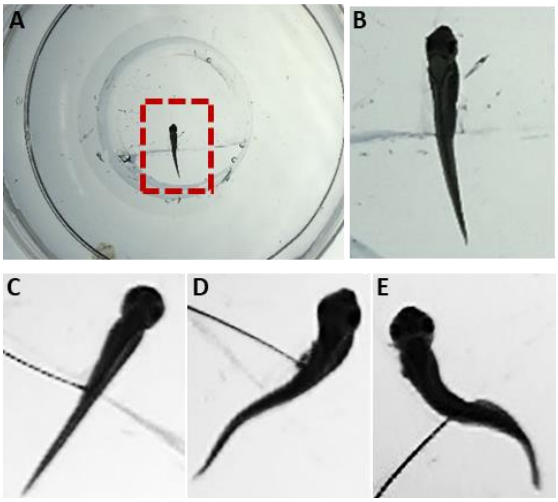

Figure 4.2 Behavioural experiments setup.
A) *The tadpole was placed in the middle of a round dish, whose floor was lined with Sylgard for half of the surface.* ***B)*** *Enlarged view of the red dashed square in A. The tadpole was positioned upright, with its tails hanging in the water.*
C) *Manual stimulation of the trunk skin of the tadpole on its left side.* ***D)*** *Example of an ipsilateral start: the first head bend is towards the same side of stimulation.* ***E)*** *Example of a contralateral start: the first head bend is towards the opposite side of stimulation.*

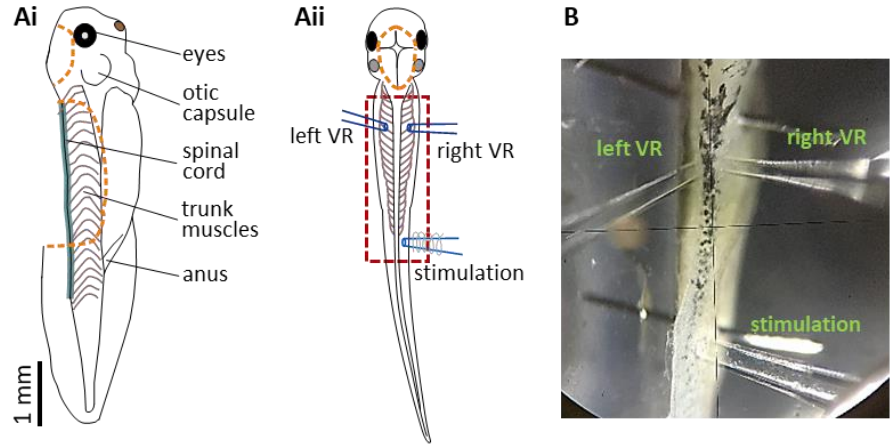

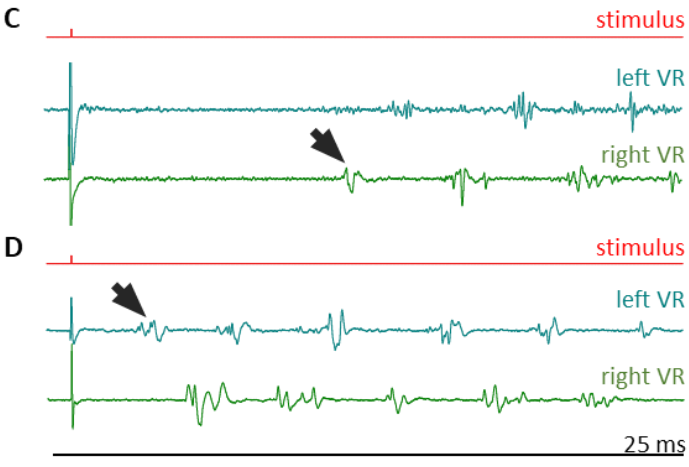

Figure 4.3 Fictive swimming experimental setup.
Ai) *Side view of the tadpole with anatomical hallmarks. Orange dashed lines indicate skin removal to get access to the brain and to the muscle clefts.* ***Aii)*** *Top view of the tadpole with electrodes positioned as in experimental conditions. Left and right VR electrodes were positioned facing each other approximately at the 4th myotomal*

cleft. Stimulating electrode was positioned on the right side at the level of the anus. Orange dashed line indicates skin removal; red dashed square area is replicated in panel B.
B) *Picture of the trunk of a tadpole pinned to the Sylgard block during experimental procedures. Right and left VR electrodes, as well as stimulating electrodes, are positioned as in Aii.*
C) *Example of an ipsilateral start (black arrow) of fictive swimming. The first VR burst is recorded on the right side of the body (right VR).*
D) *Example of a contralateral start (black arrow) of fictive swimming. The first VR burst is recorded on the left side of the body (left VR). In all experiments stimulation was delivered on the right side of the tadpole's body.*

4.2 Behavioural experiments

4.2.1 Results

Behavioural experiments (see 4.1 and 4.2 for schematic of experimental setup) confirmed that swim initiation is achievable in freely moving tadpoles even if the hindbrain is lesioned in various manners. All animals (total animals N=85) were able to initiate movement after touch stimulation was manually delivered to the trunk skin (fig. 4.4). Indeed, even tadpoles where most of the hindbrain was severed (2nd cleft lesion in fig. 4.4) still showed swim response to touch, in accordance with published results (Li et al., 2006).

Overall, lesions in the hindbrain caused a change in the latency from touch stimulation to the first head bend (fig. 4.4A, Kruskal-Wallis test p=0.0055). Lesion at the MHB and staggered lesion with stimulation delivered to the right side led to a longer latency to the first bend compared to control (fig. 4.4A, controls: median=109.5 ms; median values and median difference *vs* controls: 201.2 ms, +91.7 ms, p=0.0038 for MHB lesion, 192.9 ms, +83.4 ms, p=0.0353 for staggered lesion with right-side stimulation; Kruskal-Wallis test followed by Dunn's multiple comparison post-hoc test). The other lesions tested did not cause a significant increase in the latency to swim response (fig. 4.4A, median values and median difference *vs* controls: 150.0 ms, +40.5 ms, p>0.9999 for midline lesion, 163.1 ms, +53.6 ms, p>0.9999 for 0 cleft lesion; 160.7 ms, +51.2ms, p=0.2656 for second cleft lesion; 157.1 ms, +47.6ms, p= 0.8122 for staggered lesion with left-side stimulation; Kruskal-Wallis test followed by Dunn's multiple comparison post-hoc test). Interestingly, latency measurements were more variable in lesioned groups compared to control animals. Detailed changes in the variability of response times for all experimental groups are illustrated by median, 25% and 75% percentiles and interquartile range (IQR) values in table 1, Appendix 2.

Side preference of the first movement (*i.e.* whether the first head bend was recorded on the ipsilateral or contralateral side, referred to the side of stimulation) was analysed and percentages of ipsilateral and contralateral response are reported in fig.4.4B. Control animals showed a higher percentage of starting bends on the side contralateral to stimulation (30.3% ipsilateral bend *vs* 69.7% contralateral, 10 and 23 trials out of 33 total trials, respectively). The same preference was observed for all groups of lesioned animals (ipsilateral *vs* contralateral first bend; midline lesion: 30.0% *vs* 70.0% (9/30 *vs* 21/30 total trials); MHB lesion 28.1% *vs* 71.9% (9/33 *vs* 23/33 total trials); 0 cleft lesion 13.3% *vs* 86.7% (4/30 *vs* 26/30 total trials); second cleft lesion 36.7% *vs* 63.3% (11/30 *vs* 19/30 total trials); staggered lesion with left stimulation: 33.3% *vs* 66.7% (8/24 *vs* 16/24 total trials)). The only exception was found in the group with staggered lesion and stimulation on the right side, where the preference shifted to become higher for the ipsilateral side (71.0% ipsilateral *vs* 29.0% contralateral first bend, 22 and 9 trials out of 31 total trials).

Latency values were also analysed in accordance with the side of the first head movement (fig. 4.5). Control animals did not show a difference in latency depending on the side of the first bend (median values and median difference for ipsilateral *vs* contralateral responses: 119.0 ms *vs* 109.5 ms, -9.5 ms, p= 0.9468, Mann-Whitney unpaired test, two-tailed), and neither did lesioned tadpoles (median values and median difference for ipsilateral *vs* contralateral responses: midline lesion, 147.6 ms *vs* 185.7 ms, +38.1 ms, p=0.1224, MHB lesion, 195.2 ms *vs* 233.3 ms, +38.1 ms, p=0.7486; second cleft lesion: 211.9 ms *vs* 131.0 ms, +80.9 ms, p=0.1962, staggered lesion with stimulation on the left: 150.0 ms *vs* 277.4 ms, +127.4 ms, p=0.1576, staggered lesion with stimulation on the right: 221.4 ms *vs* 185.7 ms, +35.7 ms, p=0.7083; Mann-Whitney test unpaired test, two-tailed). An exception was recorded for tadpoles lesioned at the level of the otic capsule (0 cleft lesion, fig. 4.5 D), which showed a slower response when swimming started on the contralateral side (median values and median difference for ipsilateral *vs* contralateral response: 138.1 ms *vs* 325.0 ms, +186.9 ms, p=0.0036, Mann-Whitney unpaired test, two-tailed).

Figure 4.4 Latency and side preference in swimming initiation after mechanical stimulation in behavioural experiments.

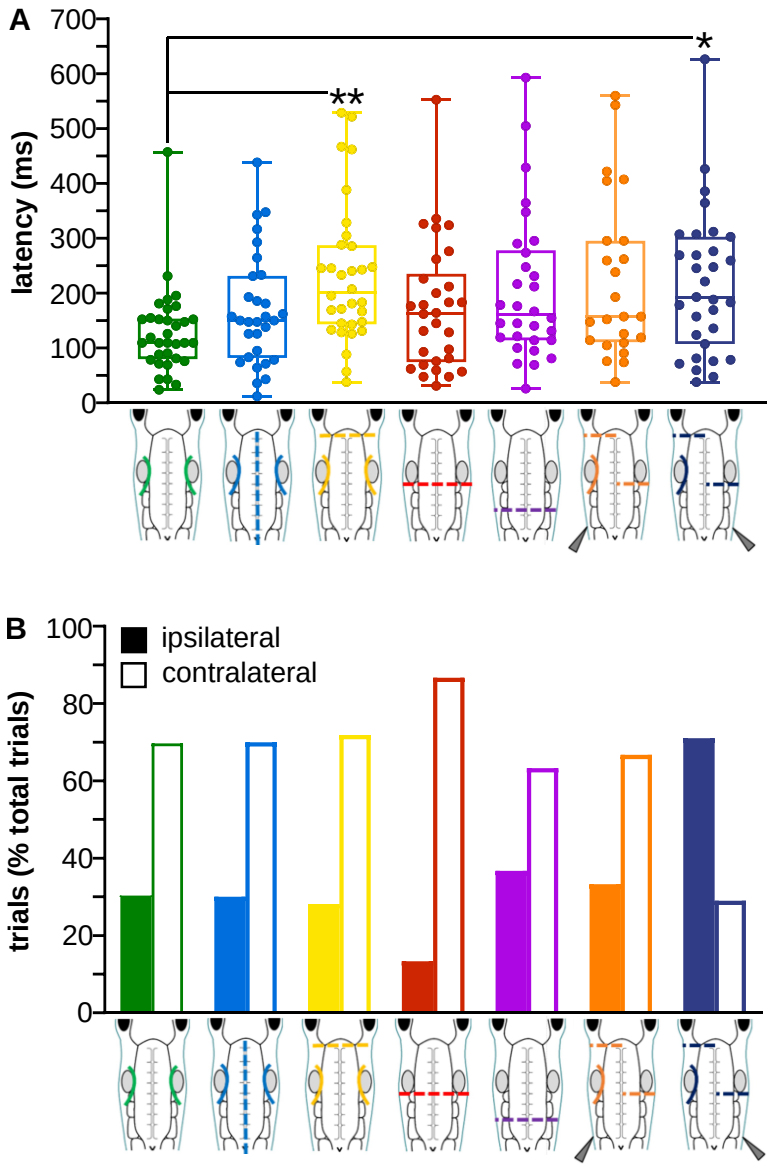

A) *Latencies (ms) for the first bend of the head after hair touch stimulation on trunk skin for control and lesioned animals, accordingly to the schematic below each bar. Single data points are reported; *p<0.05, **p<0.01 Kruskal-Wallis test followed by Dunn's multiple comparison post-hoc test. Multiple comparison adjusted p values: control vs MHB lesion p=0.0038, control vs staggered lesion, right stimulation p=0.0353. Single data points are plotted; boxes indicate 5-95 percentile; cross line in each box represents median value; error bars indicate minimum and maximum values. N numbers and median values for each experimental group are reported in the main text.*

B) *Percentage values (% total number of trials for each experimental group) for first head's bend direction after hair touch stimulation in control and lesioned animals, accordingly to the schematic below paired columns. Filled bars: ipsilateral first bend; White bars: contralateral first bend. Group percentages and raw data are reported in the main text.*

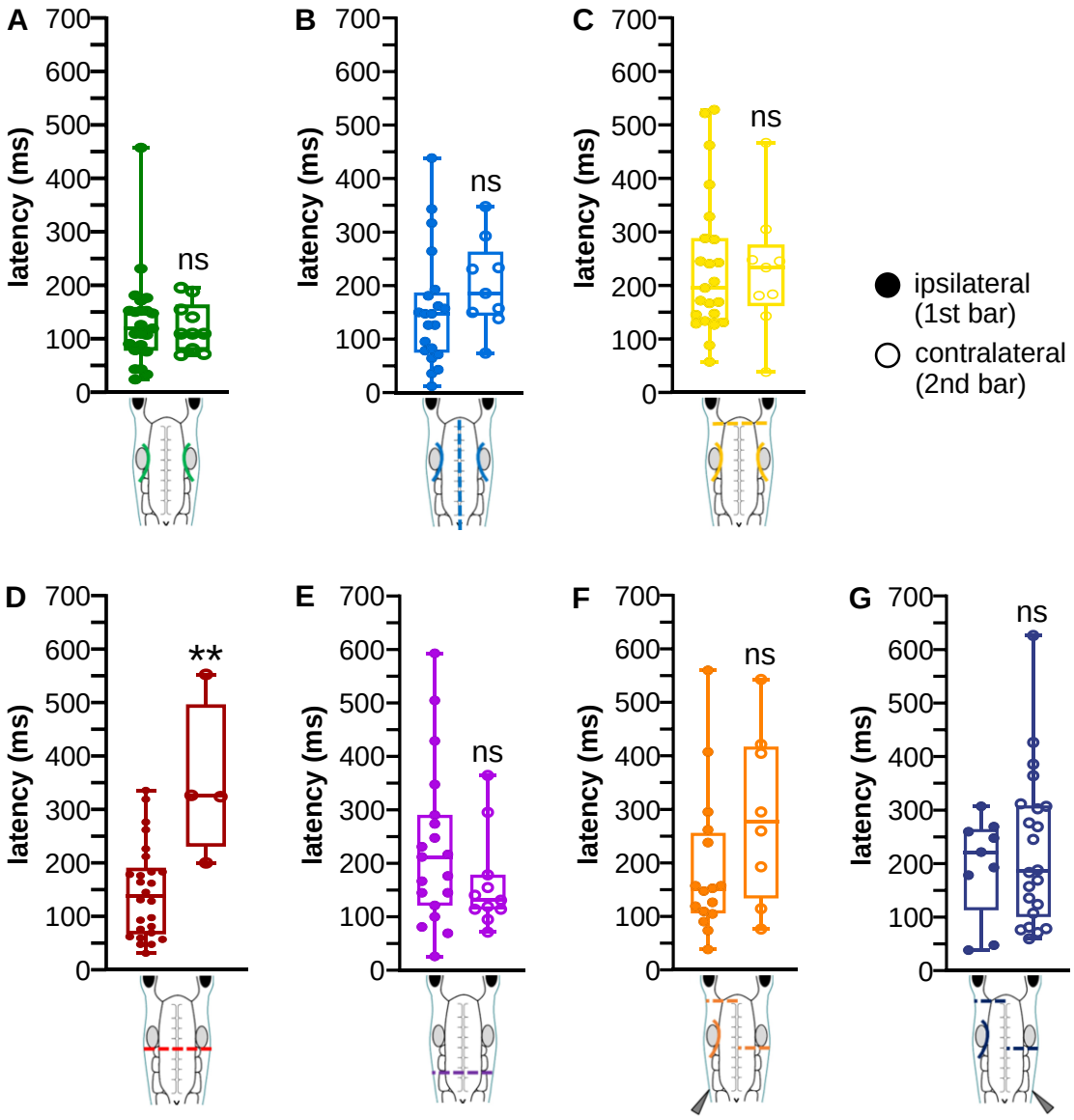

Figure 4.5 Latency according to side of first bend after mechanical stimulation in behavioural experiments.

A-B) *Latencies (ms) for the first bend of the head after hair touch stimulation for control and lesioned animals, accordingly to the schematic below each bar. First bars (solid circles) represent latencies for ipsilateral first bend, second bars (empty circles) represent latencies for contralateral first bend. **p<0.01 Mann-Whitney unpaired test, two-tailed. 0 cleft lesion ipsilateral vs contralateral p=0.0036. Single data points are plotted; boxes indicate 5-95 percentile; cross line in each box represents median value; error bars indicate minimum and maximum values. N numbers and median values for each experimental group are reported in the main text.*

4.2.2 Discussion

Hindbrain lesions led to shorter latency to swimming initiation

The behavioural experiments reported here show that lesions in the hindbrain cause a longer latency in the start of locomotion after a mechanical stimulus is delivered to the trunk skin of the freely moving animal (fig. 4.4 A). If we hypothesise that the hindbrain hosts a neuronal population involved in the holding of sensory information between the stimulus detection and the initiation of swimming, namely the ExNs, these behavioural results indicate that by removing or disconnecting part of this population, the overall delay for motor response is longer, although swim initiation is still possible. These results, showing that the tadpole's hindbrain can sustain swim initiation even after extensive removal of the rostral areas, (such as lesions at 0 cleft or at second cleft level) are in accordance with previous studies in immobilised tadpoles (Li et al., 2006) that considered the reticulospinal descending interneurons (hdINs) lying in the caudal hindbrain responsible for the drive of fictive swimming in the *Xenopus* embryo (Soffe et al., 2009).

However, motor response in lesioned animals was slower than in control animals. One possible explanation for this slow response is the partial disruption of ascending sensory connections and of descending swim-driving connections caused by the lesions. It might be possible that, because sensory neurons do not reach the rostral areas of the hindbrain, they only excite neurons in the more caudal areas, thus a smaller number of dINs will initiate and drive swimming. Nevertheless, if we assume that ExNs lie in the hindbrain, lesioning this area of the brain would have caused disruption to ExNs connections. Furthermore, if ExNs form a recurrent excitatory network in the hindbrain as it has been previously proposed (Koutsikou et al., 2018), disrupting ExNs connections by means of lesions would lead to a diminished capability of the hindbrain to hold the sensory information over the time prior swim initiation, thus they should cause a shorter latency in the lesioned animals. Instead, the lesioned animals in these experiments showed a longer response time (fig. 4.4 A).

Since none of the experimental groups revealed a significant difference in the latency to swimming compared to the other lesioned animal groups, it is not possible to identify one hindbrain area where the putative population responsible for the longer delay in the motor response could lie.

Swimming is preferentially initiated on the side contralateral to stimulation

The mechanical stimulation led control tadpoles to preferentially bend firstly on the side contralateral to the stimulus, a feature which is not affected by hindbrain lesions (fig.4.4 B). Interestingly, completely severing the hindbrain along the midline, thus eliminating any possible commissural connections, did not cause the side preference to shift towards an ipsilateral start. This can be explained by the fact that the side of the hindbrain contralateral to the stimulation can receive sensory stimulation via dlc neurons, secondary sensory neurons whose axons cross to the opposite side in the spinal cord (Roberts and Clarke, 1982, Li et al., 2001). This sensory information is then converted into motor response in the dINs, which drive CPG activation (Roberts and Alford, 1986, Li et al., 2006, Li et al., 2009) via their ipsilaterally descending axons, thus not affected by the lesion along the midline in the hindbrain.

Opposite response compared to controls (a preference for the ipsilateral side *vs* for the contralateral side in controls) was reported in animals with staggered lesion and stimulation on the right. With this lesion, the right side of the hindbrain, ipsilateral to the stimulation, was severed at the level of the otic capsule, while the left side was lesioned at the MHB. This lesion allowed dlc neurons to reach the more rostral area of the hindbrain on the contralateral side (referred to stimulation). On the contrary, dla axons were stopped at the otic capsule level, possibly facilitating a faster ipsilateral response.

Altogether the data on side preference indicate that on freely moving animals the preferred side for first bend is the one contralateral to stimulation, pointing to the possibility that the excitation in cells post-synaptic to dlc neurons summate quicker than the excitation released by dla, which run ascending and ipsilaterally from the spinal cord. This interpretation is nevertheless challenged by the results in animals with staggered lesion and stimulation on the right side, as discussed above. In this case, an accumulation of excitation would be quicker in neurons post-synaptic to dla, as the latter were severed to reach only half the distance allowed for dlc. This would then have favoured an ipsilateral motor response. Although clear comparisons on dla and dlc post synaptic excitation are not feasible within this study, it seems reasonable to propose that a balanced amount of dlc and dla axonal projections along the longitudinal axis of the hindbrain favours a motor response driven by dlc. However, when this balance is altered in favour of shorter dla connections, an ipsilateral response is more often recorded in freely moving tadpoles.

4.3 Fictive swimming experiments

The behavioural experiments reported in paragraph 4.2 showed that, in the freely moving animals, lesions in the hindbrain cause a longer delay in the motor response. This is in contradiction with the hypothesis of ExNs, which would temporally 'extend' the sensory information lying in the hindbrain of the tadpole. Therefore, in order to interrogate the behavioural experiments results, fictive swimming was analysed in electrophysiology experiments, where latency to the start of motor response in control and hindbrain-lesioned animals was analysed. Left and right ventral root activity was recorded following an electrical stimulation delivered to the trunk skin on the right side of the body (refer to fig. 4.3 for experimental setup); the first ventral root burst recorded was considered the start of swimming response.

4.3.1 Results

Initially, how control animals respond to threshold and suprathreshold stimulation was assessed. Control tadpoles revealed a shorter latency to first ventral root burst when stimulated with a suprathreshold stimulus (fig. 4.6 A; p=0.0023 Mann-Whitney unpaired test, two-tailed; median values: 100.9 ms for threshold, 27.82 ms for suprathreshold stimulation; median difference= -73.09 ms). Even if the latency values for lesioned animals were overall shorter and less variable when compared to controls' latency, hindbrain lesions did not completely abolish the ability of tadpoles to distinguish between stimuli intensities (fig. 4.6). Midline, 0 cleft and second cleft lesioned animals showed a significant difference in latencies in response to threshold or suprathreshold stimuli (fig.4.6 A,B,D,E) (median values for threshold *vs* suprathreshold stimulation: 53.93 *vs* 30.94 ms, median difference= -22.99 ms, p=0.0015 for midline lesion; 33.80 *vs* 27.36 ms, median difference= -6.447, p=0.0225 for 0 cleft lesion; 39.36 *vs* 26.90 ms, median difference= -12.46 ms, p=0.0052 for second cleft lesion; Mann-Whitney unpaired test, two-tailed). MHB and staggered lesioned animals failed to significantly change their response to different stimuli, resulting in comparable latencies to swim initiation after threshold and suprathreshold stimulation (fig. 4.6 C,F,G) (median values for threshold *vs* suprathreshold stimulation: 48.12 *vs* 38.92 ms, median difference= -9.155 ms, p=0.1802 for MHB lesion; 41.50 *vs* 24.08 ms, p=0.0549 for L-R staggered lesion; 38.12 *vs* 33.71 ms with p=0.8048 for R-L staggered lesion; Mann-Whitney unpaired test, two-tailed).

Because of the ability of the *Xenopus* embryo to discern between different stimulation intensities, a set of electrophysiology experiments on fictive swimming was carried out using threshold stimulation, whilst a second set of experiments was carried out using suprathreshold stimuli, and data were reported accordingly. In order to account for variability among individual tadpoles, threshold and suprathreshold stimuli were set in each experiment both in intensity (V) and duration (ms), as described in 'Materials and Methods' (paragraph 4.1).

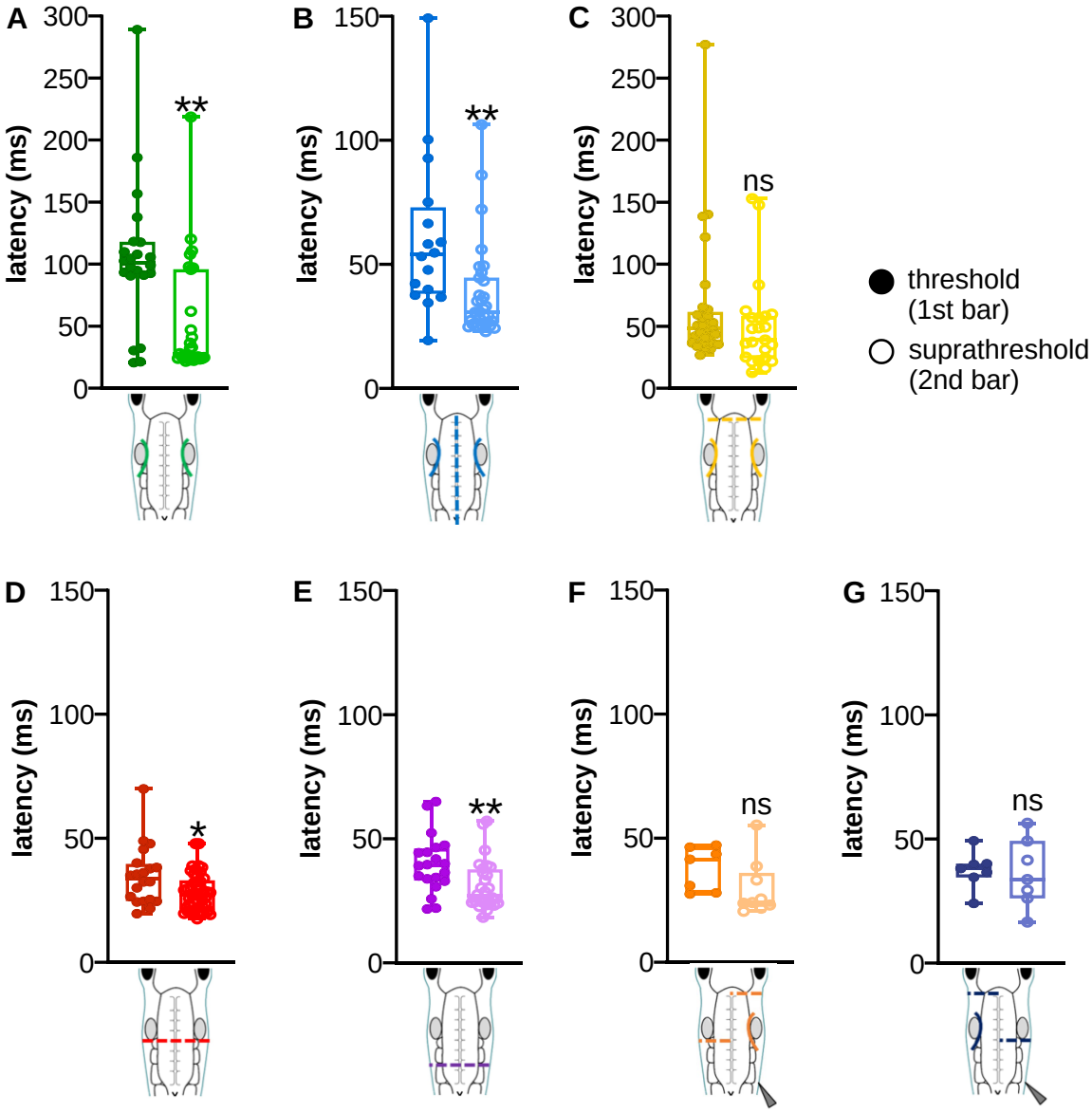

Figure 4.6 Swimming initiation after threshold and supra-threshold electrical stimulus in fictive swimming recording experiments.

A-G) *Latencies (ms) for the first VR burst after a threshold (first bars, solid circles in darker colours) and supra-threshold (second bars, empty circles in lighter colours) electrical stimulus*

*delivered to the trunk skin in control and lesioned animals, accordingly to the schematic on top-right of each graphs. Single data points are reported; boxes indicate 5-95 percentile; cross line in each box represents median value; error bars indicate minimum and maximum values. ns p>0.05; **p<0.01, *p<0.05 Mann-Whitney unpaired test, two-tailed. A) p=0.0023, control threshold vs suprathreshold stimulation; B) p=0.0015, midline lesion threshold vs suprathreshold stimulation; D) p=0.0225, 0 cleft lesion threshold vs suprathreshold stimulation; E) p=0.0052 2nd cleft lesion threshold vs suprathreshold stimulation.*

4.3.1.1 Threshold stimulation

Latency to the first ventral root burst recorded after threshold stimulation was shorter in animals with hindbrain severed at the level of 0 muscular cleft and second muscular cleft, as well as in tadpoles with staggered hindbrain lesions (fig. 4.7 A) (median values and median difference *vs* controls: 100.9 ms for control; 33.80 ms, median difference=-67.1 ms, $p<0.0001$ for 0 cleft lesion; 39.36 ms, median difference=-61.54 for second cleft lesion *p=0.0004*; 41.50 ms, median difference=-59.4 ms, $p=0.0156$ for L-R staggered lesion; 38.12 ms, median difference=-62.78 ms, $p=0.0151$ for R-L staggered lesion; Kruskal-Wallis test $p<0.0001$, followed by Dunn's multiple comparison post-hoc test). Lesions along the midline and of the MHB did not cause a significative reduction in the swimming response time (fig. 4.7 A) (median values and median difference vs controls: 53.93 ms, median difference=-46.97 ms, $p=0.683$ for midline lesion, 48.12 ms, median difference=-52.78 ms, $p=0.1417$ for MHB lesion; Kruskal-Wallis test $p<0.0001$, followed by Dunn's multiple comparison post-hoc test). Even if the median values for latencies reported in midline and MHB lesioned tadpoles were shorter than the controls', these two lesions did not abolish the variability in response times. Detailed changes in the variability of response times for all experimental groups are illustrated by median, 25% and 75% percentiles and interquartile range (IQR) values in table 2, Appendix 2.

The side of first ventral root burst was recorded as ipsilateral or contralateral to the stimulus delivered, and percentages for control and lesioned animals are reported in fig. 4.7 B. Control tadpoles showed a higher percentage of ipsilateral response (63.6% (14/22) ipsilateral, 36.4% 8/22) contralateral responses; trials n=22).

All the lesions tested caused synchronous first ventral root bursts to different extent (grey bars in fig. 4.7 B). Synchrony was defined as simultaneous ventral root bursts on both sides of the tadpole's body, and was recorded with different incidence in all groups of lesioned animals. The lesion that caused the highest percentage of synchronous swim response was L-R staggered

lesion (28.6%, 2/7). All other hindbrain lesions tested also led to a certain amount of synchronous responses (midline lesion: 12.5% (2/16), MHB lesion: 13.8% (4/29), 0 cleft lesion: 5.0% (1/20), second cleft lesion: 15.0% (3/20), R-L staggered lesion: 14.3% (1/7); percentages calculated over the total number of trials per experimental group fig. 4.7 B) As showed by controls, tadpoles with midline, second cleft and R-L staggered lesions showed higher percentage of ipsilateral response (midline: 50.0%, 8/16; second cleft: 50.0%, 10/20; R-L staggered lesions: 57.1%, 4/7) compared to percentages of contralateral first bursts (midline: 37.5%, 6/16; second cleft: 35.0%, 10/20; R-L staggered lesions: 14.3%, 1/7). On the contrary, tadpoles lesioned at MHB, 0 cleft and with L-R staggered lesion showed a higher percentage of contralateral response (ipsilateral *vs* contralateral responses: MHB= 34.5%, (10/29) vs 51.7% (15/29); 0 cleft= 45.0% (9/20) vs (50.0% 10/20), L-R staggered lesion=14.3% (2/7) vs 57.1% (4/7); percentages calculated over the total number of trials per experimental group fig. 4.7 B).

Furthermore, latency was plotted according to the side of first ventral root appearance (fig. 4.8). Mann-Whitney test was conducted on latency data of controls (ipsilateral or contralateral response only), whilst Kruskal-Wallis test was used for lesioned animals, whose responses were either ipsilateral, contralateral or synchronous. No significant differences were reported in the response times for ipsilateral contralateral or synchronous responses (fig. 4.8), except for animals lesioned at 0 cleft level (fig. 4.8 D, Kruskal-Wallis test p=0.041; non-significant Dunn's multiple comparisons test: ipsi vs contralateral response p=0.0627, ipsilateral vs synchronous response p>0.999, contralateral vs synchronous response p>0.999). Detailed p values for other lesioned groups are as follows: controls p=0.365, midline p=0.735, MHB p=0.186, 2nd cleft p=0.985, L-R p=0.590, R-L p=0.267.

Interestingly, whilst control animals showed a more variable latency to swim initiation in contralateral responses, all transverse hindbrain lesions (fig. 4.8; MHB, 0 cleft, second cleft, R-L and L-R staggered lesion) revealed a decreased variability in case of either ipsilateral, contralateral or synchronous response. Tadpoles lesioned along the midline showed slightly more variable latency in both ipsilateral and contralateral responses. Detailed changes in the variability of response times according to the side of first bend are illustrated for all experimental groups by median, 25% and 75% percentiles and interquartile range (IQR) values in table 3, Appendix 2.

Figure 4.7 Swimming initiation after threshold electrical stimulus in fictive swimming recording experiments.

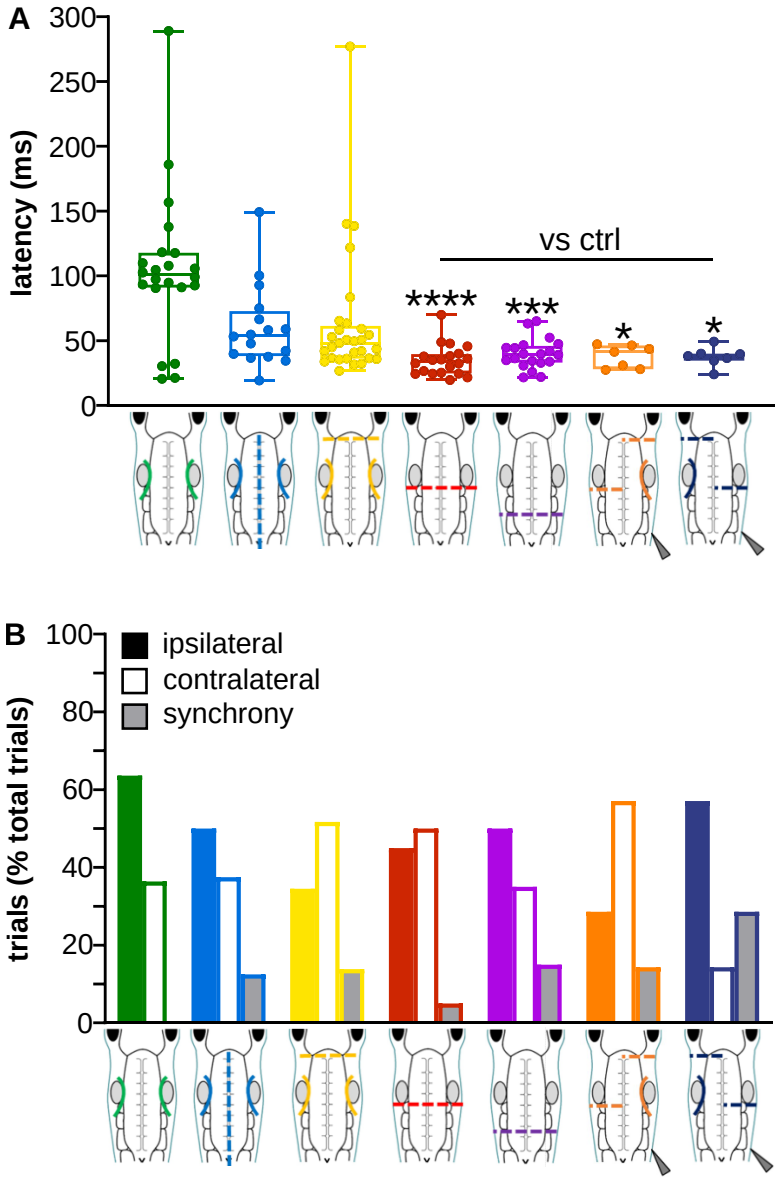

A) *Latencies (ms) for the first VR burst after a threshold electrical stimulus delivered to the trunk skin in control and lesioned animals, according to the schematic below each bar. Single data points are reported; *p<0.05, **p<0.01, ****p<0.0001 Kruskal-Wallis test followed by Dunn's multiple comparison post-hoc test. Multiple comparison adjusted p values vs controls: 0 cleft lesion p<0.0001, 2nd cleft lesion p=0.0014, L-R staggered lesion p=0.0156, R-L staggered lesion p=0.0151. Single data points are plotted; boxes indicate 5-95 percentile; cross-line in each box represents median value; error bars indicate minimum and maximum values.*

B) *Percentage values (% total number of trials for each experimental group) for first head's bend direction after hair touch stimulation in control and lesioned animals, accordingly to the schematic below paired columns. Filled bars: ipsilateral first VR burst; white bars: contralateral first VR burst; grey bars: synchronous first VR burst. Group percentages and raw data are reported in the main text.*

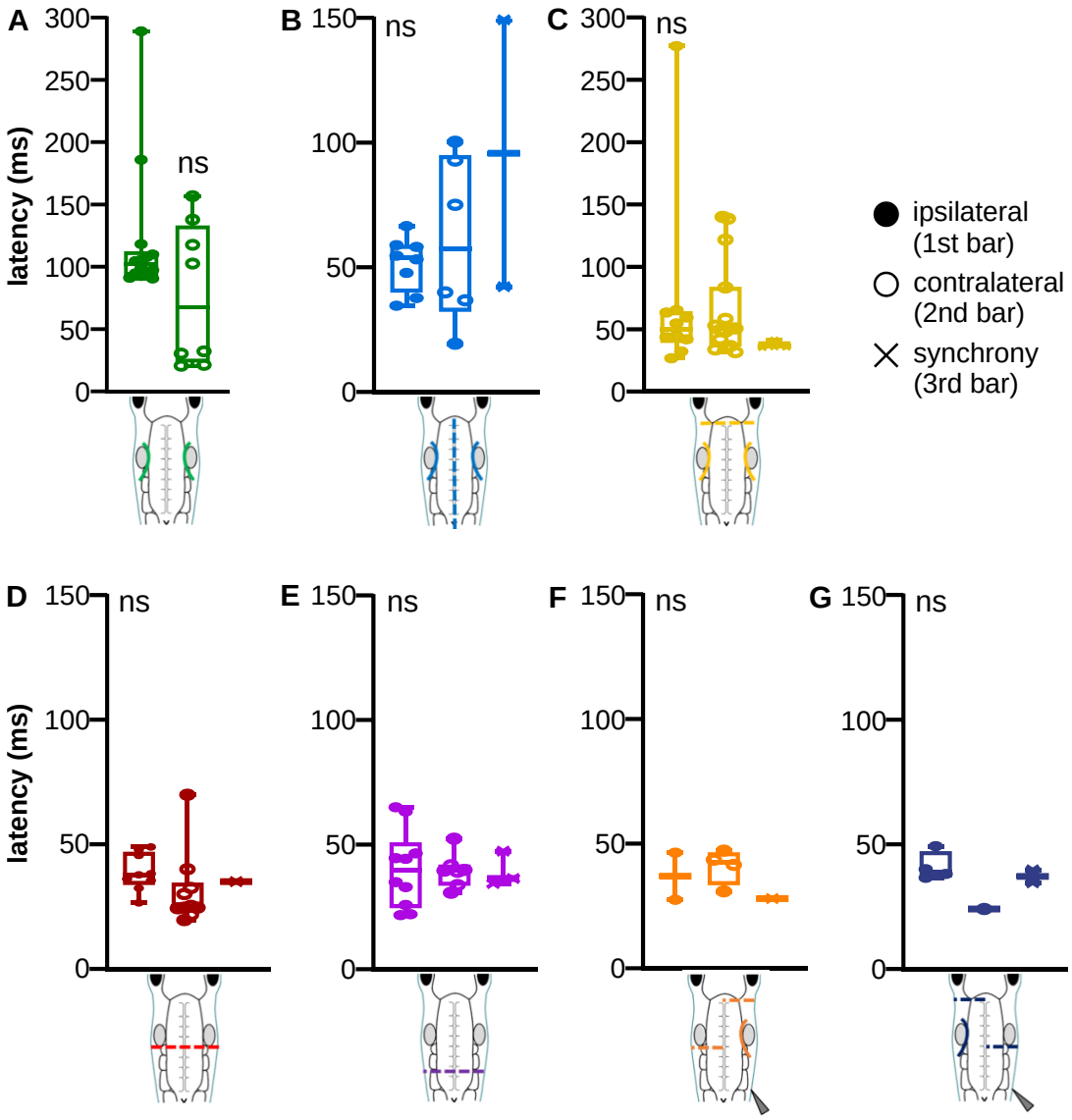

Figure 4.8 Latency to fictive swimming according to side of first VR burst after threshold stimulation.

A-G) *Latencies (ms) for the first VR burst after a threshold electrical stimulus delivered to the trunk skin in control and lesioned animals, accordingly to the schematic below each bar. First bars (solid circles) represent latencies for ipsilateral first VR burst, second bars (empty circles) represent latencies for contralateral first VR burst, third bars (crosses) represent VR bursts recorded simultaneously on both sides. Mann-Whitney test on controls, p>0.05; Kruskal-Wallis for lesioned animals p>0.05. See main text for single ns p values. Single data points are plotted; boxes indicate 5-95 percentile; cross-line in each box represents median value; error bars indicate minimum and maximum values. N numbers and median values for each experimental group are reported in the main text.*

4.3.1.2 Suprathreshold stimulation

When a suprathreshold electrical stimulus was delivered to the tadpoles, an overall significant difference in latency to swim response was reported (fig. 4.9 A; p=0.0148, Kruskal-Wallis test). However, none of the lesions tested significantly changed the latency to first ventral root burst, compared to controls (fig. 4.9 A; Dunn's multiple comparisons after Kruskall-Wallis test, p values for lesioned groups *vs* control as follows: midline p>0.0999, MHB p>0.0999, 0 cleft p=0.439, 2nd cleft p>0.0999, R-L p>0.0999, L-R p>0.0999). Nevertheless, hindbrain-lesioned animals showed a much less variable latency than control tadpoles. Median, 25% percentiles, 75% percentiles and IQR values for controls and lesioned animals are reported in table 4, Appendix 2.

Contrary to threshold stimulation (fig. 4.7 B), suprathreshold stimuli led control tadpoles to prefer the contralateral side as the side of first ventral root burst (4.9 B, 25.9% (7/27) ipsilateral *vs* 74.1% (20/27) contralateral responses). Experimental trials with synchronous excitation of ventral root on both sides were recorded for every lesion tested (fig. 4.9 B), with different incidence (midline lesion 38.7% (12/31), MHB lesion 18.2% (6/33), 0 cleft lesion 8.7% (4/46), second cleft lesion 14.3% (4/28), L-R staggered lesion 21.1% (4/19), R-L staggered lesion 5.9% (1/17)).

Differently from controls, none of the lesioned groups succeeded in maintaining a clear preference for the contralateral side (fig. 4.9 B; ipsilateral *vs* contralateral responses: midline= 29.0% (9/31) *vs* 32.3% (10/31); MHB= 39.4% (13/33) *vs* 42.4% (14/42); 2nd cleft= 39.3% (11/28) *vs* 46.48% (13/28), R-L= 41.2% (7/17) *vs* 52.9% (9/17)). Moreover, and contrarily to controls, 0 cleft and L-R staggered lesions caused the animals to have a higher percentage of ipsillateral first bursts (fig. 4.9 B; ipsilateral *vs* contralateral responses: 0 cleft= 56.5% (26/46) *vs* 34.8% (16/46), L-R 47.4% (9/19) vs 31.6% (6/19); percentages are calculated over the total number of trials per experimental group).

When latency data were plotted according with the side of first ventral root appearance, control animals revealed a significantly shorter response time for contralateral first burst (fig. 4.10 A; median values for ipsilateral vs contralateral responses: 107.9 *vs* 25.48 ms, median difference=-82.42 ms, *p<0.0001*, Mann-Whitney unpaired test, two-tailed). This difference in latency depending on the side of first burst was lost by animals with lesions (fig. 4.10). In fact, response time of lesioned animals was comparable no matter if the first burst appeared on the ipsilateral or contralateral side, or if synchronous bursts on both sides were recorded (p values for Kruskal-

Wallis tests run for the single experimental groups as follows: midline p=0.086, MHB p=0.211, 0 cleft p=0.544, 2nd cleft p=0.710, L-R p=0.702, R-L p=0.862). Detailed changes in the variability of response times according to the side of first bend are illustrated for all experimental groups by median, 25% and 75% percentiles and interquartile range (IQR) values in table 5, Appendix 2.

Figure 4.9 Swimming initiation after supra-threshold electrical stimulus in fictive swimming recording experiments.

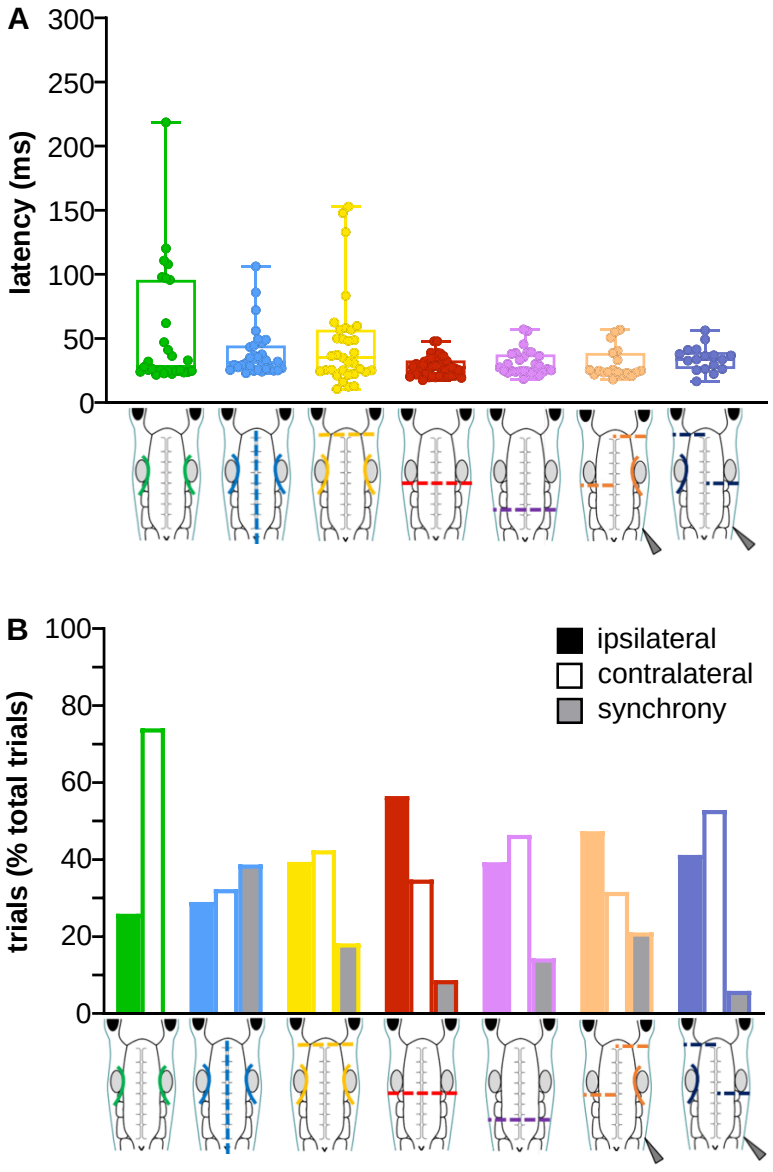

A) *Latencies (ms) for the first VR burst after a supra-threshold electrical stimulus delivered to the trunk skin in control and lesioned animals, accordingly to the schematic below each bar. Single data points are reported; Kruskal-Wallis test p=0.0148. Single data points are plotted; boxes indicate 5-95 percentile; cross line in each box represents median value; error bars indicate minimum and maximum values. N numbers and median values for each experimental group are reported in the main text.*

B) *Percentage values (% total number of trials for each experimental group) for first head's bend direction after hair touch stimulation in control and lesioned animals, accordingly to the schematic below paired coloumns. Filled bars: ipsilateral first VR burst; white bars: contralateral first VR burst; grey bars: synchronous VR first burst. Group percentages and raw data are reported in the main text.*

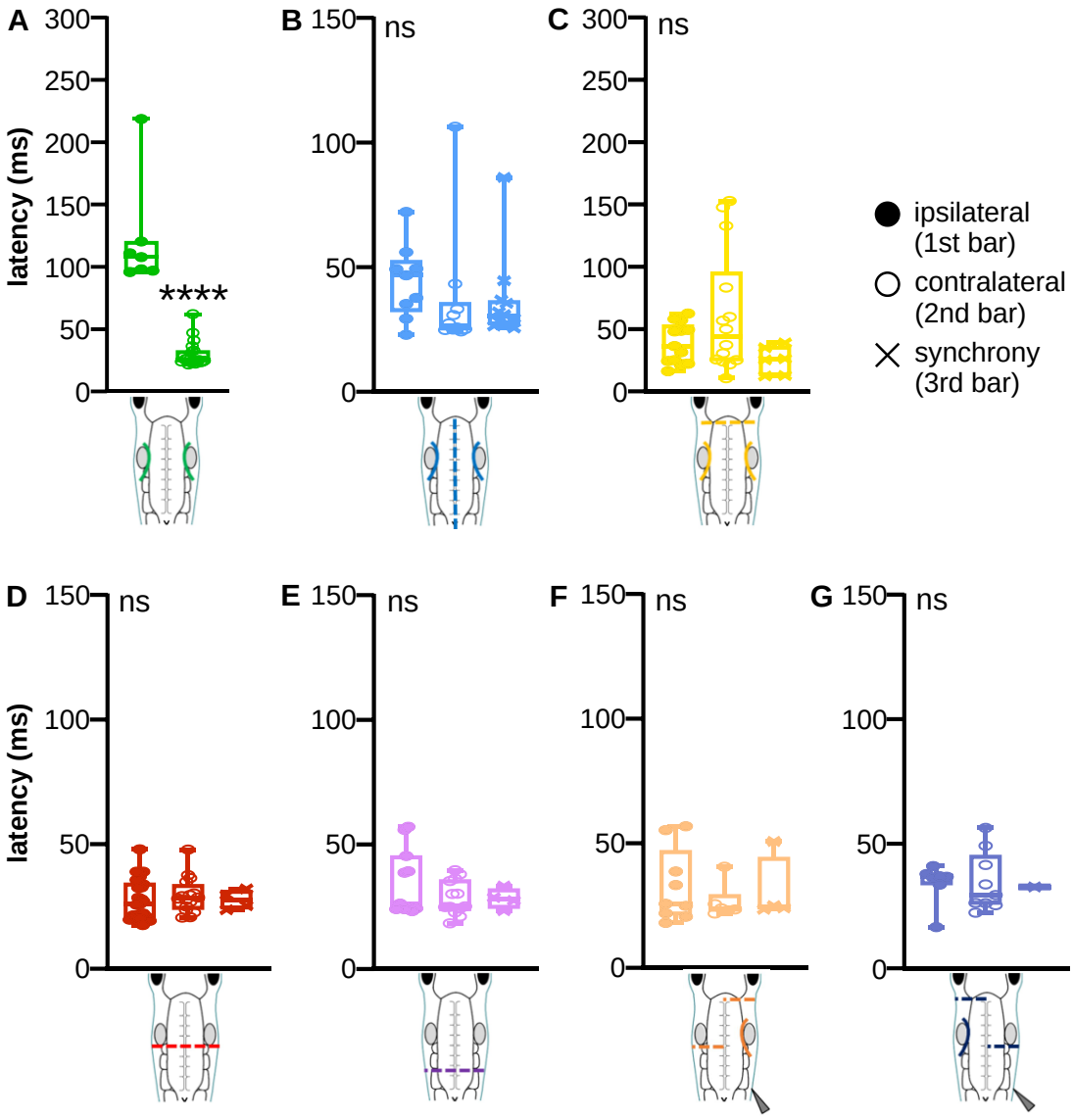

Figure 4.10 Latency to fictive swimming according to side of first VR burst after suprathreshold stimulation.

A-G) *Latencies (ms) for the first VR burst after a supra-threshold electrical stimulus delivered to the trunk skin in control and lesioned animals, accordingly to the schematic below each bar. First bars (solid circles) represent latencies for ipsilateral first VR burst, second bars (empty circles) represent latencies for contralateral first VR burst, third bars (crosses) represent VR bursts recorded simultaneously on both sides. ****p<0.0001 Mann-Whitney unpaired test, two-tailed; control ipsilateral vs contralateral p<0.0001. Single data points are plotted; boxes indicate 5-95 percentile; cross line in each box represents median value; error bars indicate minimum and maximum values. N numbers and median values for each experimental group are reported in the main text.*

4.3.1.3 Synchronous Initiation of Swimming

The simultaneous activation of both sides of the body observed in lesioned animals (both after threshold and suprathreshold stimulation, fig. 4.8 B and 4.9 B, respectively) would cause the freely moving animal not to swim off immediately, as to do so, the rhythmic and anti-phasic activation of left and right muscles is required. The latency to the first burst of rhythmic swimming was plotted for control and lesioned tadpoles, following either threshold or suprathreshold stimulation. Even when only the functional (as in propelling swimming movement) first bursts were considered, lesioned animals did not completely revert to control levels (fig. 4.11, 4.13). Indeed, after both a threshold or a suprathreshold stimulation, the latencies recorded in lesioned animals were shorter than the latency of ipsilateral or contralateral first bends in control animals (fig. 4.11 threshold stimulation: $p<0.0001$; fig. 4.13 suprathreshold stimulation $p=0.0008$; Kruskal-Wallis test).

After threshold stimulation, only animals lesioned at the level of second cleft were able to achieve controls' latency (fig. 4.11; control vs 2nd cleft $p=0.162$, Dunn's multiple comparisons after Kruskal-Wallis test). Instead, animals lesioned at 0 cleft and tadpoles with staggered lesions did not succeed in delaying the swim initiation to the same extent of the controls (fig. 4.11; 0 cleft $p<0.0001$, L-R lesion $p<0.0001$, R-L lesion $p<0.0001$; Dunn's multiple comparisons vs controls after Kruskal-Wallis test). Tadpoles with lesion at the MHB and along the midline were able to sustain a delayed response even when the synchronous starts were considered (fig. 4.7 A), and they were found to have latencies comparable to the controls also when only the first asynchronous VR bursts were plotted (fig. 4.11; MHB $p>0.999$, midline $p>0.999$; Dunn's multiple comparisons vs controls, after Kruskal-Wallis test).

Latency to the first asynchronous VR burst was plotted for each experimental group according to the side of the body. After a threshold stimulation, neither controls nor the lesioned animals showed different latency for the activation of the ipsilateral or contralateral side (fig. 4.12; two-tailed Mann-Whitney test on each group; ipsilateral vs contralateral latency: controls $p=0.365$, midline $p=0.673$, MHB $p=0.808$, 0 cleft $p=0.095$, 2nd cleft $p=0.188$, L-R $p=0.976$, R-L $p=0.100$).

When only the first asynchronous VR burst was considered after suprathreshold stimulation, lesioning the hindbrain still had an effect on the latency to swim initiation (fig. 4.13; Kruskal-Wallis test $p=0.0008$), but none of the lesioned groups showed a significantly slower response to stimulation (midline $p>0.9999$, MHB $p>0.9999$, 0 cleft $p=0.695$, 2nd cleft $p>0.9999$, L-R lesion

p>0.9999, R-L lesion *p*>0.9999; Dunn's multiple comparisons vs controls, after Kruskal-Wallis test). Latency to the first asynchronous burst after suprathreshold stimulation was plotted according to the side of its appearance in fig. 4.14. Even when only first asynchronous bursts were considered, none of the lesioned groups showed the diversified response observed in the controls (fig. 4.14; two-tailed Mann-Whitney test on each group ipsilateral vs contralateral latency: controls *p*<0.0001, midline *p*=0.457, MHB *p*=0.465, 0 cleft *p*=0.707, 2nd cleft *p*=0.790, L-R *p*=0.513). The only exception was reported in animals with R-L staggered lesion, which showed a quicker response on the contralateral side (two-tailed Mann-Whitney test, *p*=0.048).

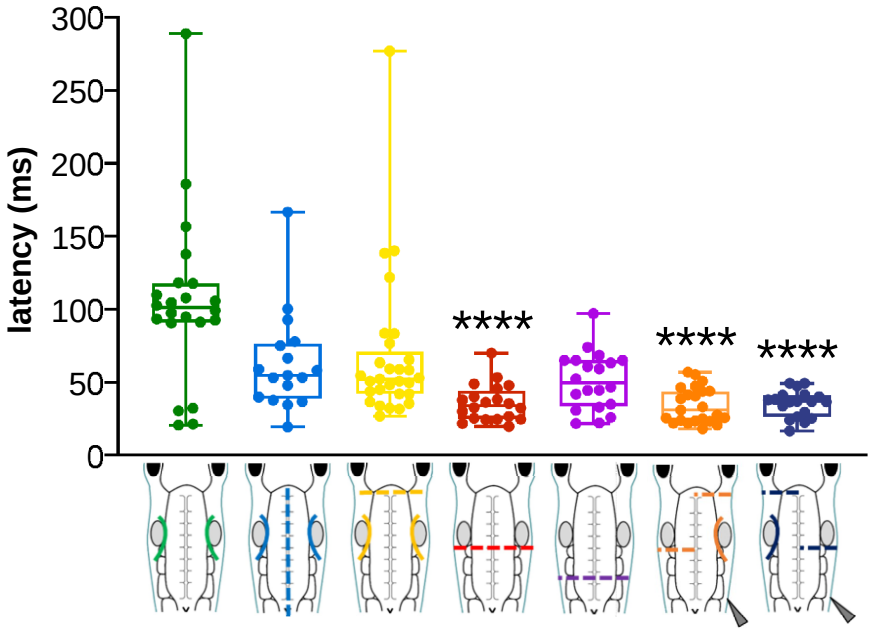

Figure 4.11 Latency to asynchronous starts in fictive swimming after threshold stimulation. *Latencies (ms) for the first non-synchronous VR burst after a threshold electrical stimulus delivered to the trunk skin in control and lesioned animals, according to the schematic below each bar. Kruskal-Wallis test p<0.0001, Dunn's multiple comparisons tests vs controls 0 cleft p p<0.0001, L-R lesion p<0.0001, R-L lesion p<0.0001. Non-significant p values (ns, p>0.05) are reported in the main text. Single data points are plotted; boxes indicate 5-95 percentile; cross line in each box represents median value; error bars indicate minimum and maximum value.*

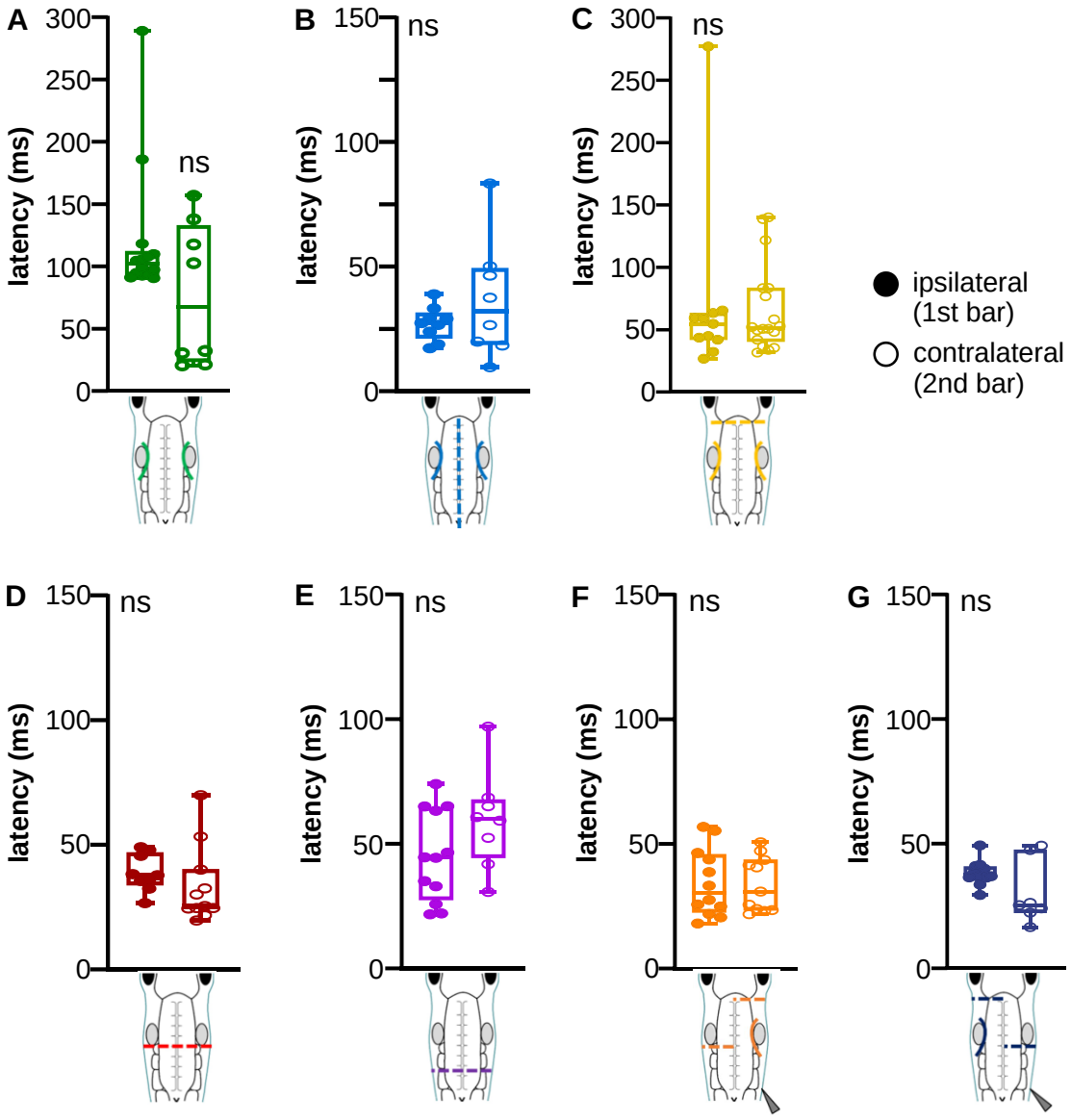

Figure 4.12 Latency to fictive swimming according to side of first non-synchronous VR burst after threshold stimulation.

A-G) *Latencies (ms) for the first non-synchronous VR burst after a threshold electrical stimulus delivered to the trunk skin in control and lesioned animals, according to the schematic below each bar. First bars (solid circles) represent latencies for ipsilateral first VR burst, second bars (empty circles) represent latencies for contralateral VR burst. Two-tailed Mann-Whitney test for each group ipsilateral vs contralateral response, non-significant (ns, p>0.05) p values are reported in the main text. Single data points are plotted; boxes indicate 5-95 percentile; cross line in each box represents median value; error bars indicate minimum and maximum value*

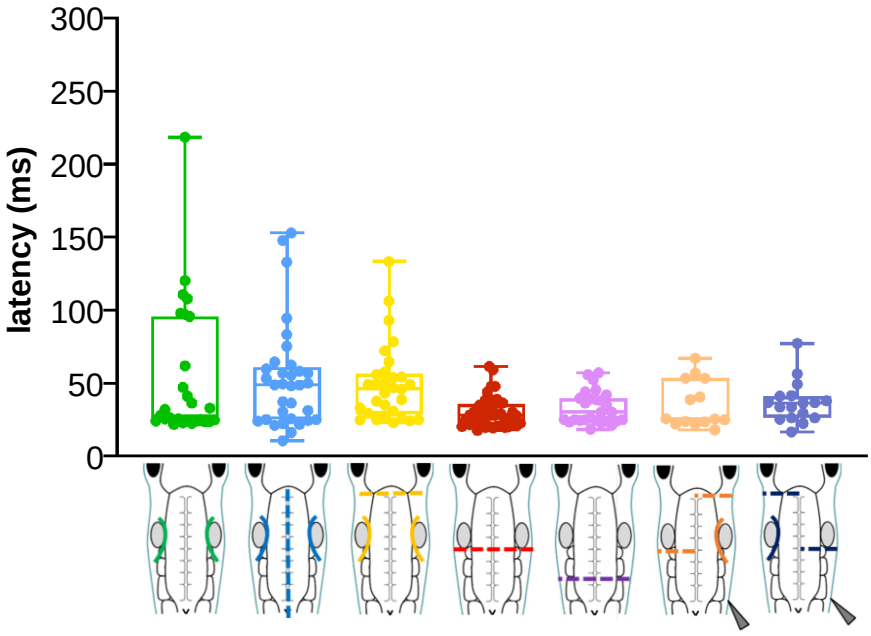

Figure 4.13 Latency to asynchronous starts in fictive swimming after suprathreshold stimulation.

Latencies (ms) for the first non-synchronous VR burst after a suprathreshold electrical stimulus delivered to the trunk skin in control and lesioned animals, according to the schematic below each bar. Kruskal-Wallis test p=0.0008, Dunn's multiple comparisons, non-significant (ns, p>0.05) p values for lesioned groups vs controls are reported in the main text. In A and B single data points are plotted; boxes indicate 5-95 percentile; cross line in each box represents median value; error bars indicate minimum and maximum value.

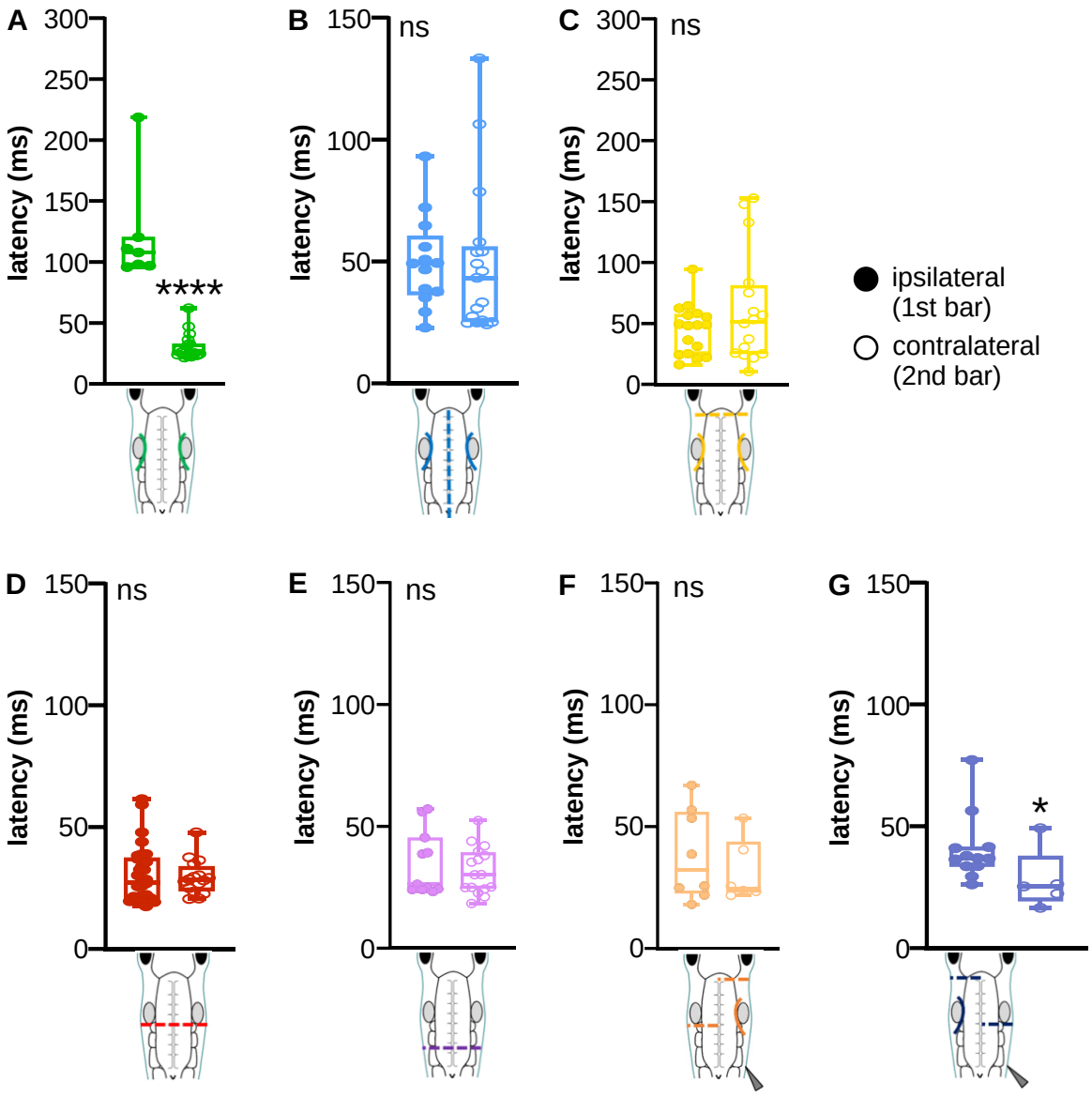

Figure 4.14 Latency to fictive swimming according to side of first non-synchronous VR burst after supra-threshold stimulation.

A-G) *Latencies (ms) for the first non-synchronous VR burst after a threshold electrical stimulus delivered to the trunk skin in control and lesioned animals, according to the schematic below each bar. First bars (solid circles) represent latencies for ipsilateral first VR burst, second bars (empty circles) represent latencies for contralateral first VR burst. Two-tailed Mann-Whitney test for each group ipsilateral vs contralateral response, controls p<0.0001; non-significant (ns, p>0.05) p values are reported in the main text. Single data points are plotted; boxes indicate 5-95 percentile; cross line in each box represents median value; error bars indicate minimum and maximum value*

4.3.2 Discussion

The experiments reported here show that control tadpoles have the ability of discerning different strength of sensory stimulation, as they responded differently both in the latency to swim initiation, as well as regarding the side preference for the first muscle contraction depending on the stimulus intensity (control groups in fig. 4.6, 4.7, 4.8). In fact, when an electrical stimulation was delivered to the trunk skin of controls at suprathreshold intensity, the motor response was initiated quicker than following a threshold stimulation. A switch in the preference for the side of first VR burst was also observed at different stimulation strength. Whilst threshold stimulation led control tadpoles to contract first on the ipsilateral side, suprathreshold stimuli caused the preference to switch to the contralateral side. These results are in agreement with previously published data, which found that at suprathreshold stimulation the preferred side was contralateral, and that ipsilateral and contralateral response did not show overlapping latencies measurements (Zhao et al., 1998). Glycinergic IPSPs have been recorded in motor neurons ipsilaterally to stimulation with very short delay, whilst no inhibition was found in motor neurons lying contralaterally (Zhao et al., 1998). Moreover, this inhibition was reported only at higher stimulus intensities, while no IPSPs were recorded on either side after a threshold stimulation (Zhao et al., 1998). Because the latency of IPSPs was too short to be attributed to CPG neurons active during swimming, it was proposed that aINs might be responsible for the ipsilateral inhibition prior to the initiation of swimming (Zhao et al., 1998). If this is the case, ipsilateral sensory pathway neurons (dla) would have synaptic contact with aINs, which in turn will inhibit motor neurons on the same side of stimulation. So far, this connection has not been established.

Although the results presented here do not provide the reasons underlying these differences, it is plausible from an ethological point of view that a strong stimulation (suprathreshold stimulus) will induce the tadpole to quickly orientate itself away from the noxious source (contralateral contraction, faster response), while a less intense stimulation (threshold stimulus) will be perceived as less dangerous, leading to a higher percentage of slower ipsilateral responses. In order to test this hypothesis, studies on the trajectory of swimming in freely moving animals are needed. Indeed, it is also possible that the side of first muscle contraction does not correlate with the overall swim path of a non-restrained animal. Briefly, the tadpole could show the first contraction on one side of its body, but it could end up swimming along a trajectory leaning to

the opposite direction. As now, no direct evidence for a correlation between the side of first contraction and the overall swimming pathway has been demonstrated in the tadpole.

Lesions in the hindbrain affect the ability of discerning stimulus strength

Only some of the experimental groups with hindbrain lesions retained the ability to discern different strength of stimulation by showing a shorter latency in the swim response after stronger stimulation (fig. 4.6 A). Even if the MHB lesioned animals were the only group to be able to sustain delayed motor response (compared to controls, note different Y axis in fig. 4.6 C), their response times were similar after a threshold and a suprathreshold stimulation.

Animals with transverse lesions at different levels of the hindbrain showed a faster and less variable motor response after a threshold stimulation (fig. 4.7A). It is not possible to rule out that this difference in latency might be due to the shorter distance dla and dlc are allowed to cover in the transected hindbrain, thus leading to a faster activation of the hdINs population which initiate swimming. Another possible explanation is that by removing extensive areas of the hindbrain, the ExNs population was largely eliminated from the hindbrain circuit controlling swim initiation, thus abolishing the holding of sensory information in the hindbrain, and forcing the motor response into a quicker, reflex-like locomotor initiation (Li et al., 2004a).

Ipsilateral and commissural connections in the hindbrain are involved in the correct motor initiation

Although the overall side preference did not completely switch (compared to controls), lesioning the hindbrain caused the appearance of some synchronous starts on both sides of the tadpoles' body after threshold and suprathreshold stimulation (fig. 4.7B and 4.9 B). Interestingly, this feature appeared not only in the animals lesioned along the midline. Indeed, a simultaneous activation of CPG neurons on both sides of the body could be reasonably explained by a lack of commissural communication in the hindbrain, which would lead to a synchronous excitation of hdINs on the left and right side. This explanation does not seem to be accurate enough, since all the experimental groups with transverse lesions only, but with intact commissural hindbrain connections, showed a certain percentage of synchronous start. Possibly, ExNs provide the time and the neuronal connections needed to select the side which will first initiate a functional motor response.

Latency data grouped according to the side of the respective VR first burst corroborate the hypothesis of a disperse ExNs population in the hindbrain, whose axonal projections might be both ipsilateral and commissural. In fact, the short latency to motor response seen in lesioned animals is observed in ipsilateral, contralateral and synchronous responses. Although animals where the two sides of the hindbrain were disconnected (midline lesion) showed a more variable ipsilateral, contralateral or synchronous start after a threshold stimulation, their quick responses point to the involvement of some hindbrain commissural connections in the holding of the sensory information before the initiation of locomotion. On the other hand, the non-variable and fast swim responses (ipsilateral, contralateral and synchronous) of animals with transverse lesions suggest that neural projections on the same side of the hindbrain also play an important role in ensuring the delay needed for a correct execution of the swimming response.

Stronger stimulation leads to a different type of motor response

When a suprathreshold stimulation was used to initiate swimming, control animals responded preferentially contracting on the contralateral side first, and the latency was significantly quicker than for ipsilateral responses (fig. 4.6 A). This observation is in accordance with previous works (Boothby and Roberts, 1995, Zhao et al., 1998), and seems to confirm the presence of a neural circuit, which is activated when the stimulation received is strong and that, via the inhibition of ipsilateral CPG neurons, drives mainly faster contralateral responses. The neurons involved in this mechanism are possibly located in the caudal area of the hindbrain or in the spinal cord, as no difference among the several experimental groups with transverse sections were observed. Even if controls showed a quicker response following strong stimulation, this is seen only in controls' contralateral responses, while is also maintained in the ipsilateral and synchronous responses of lesioned tadpoles (fig. 4.6 B-G). As discussed above, it is possible that by removing the ExNs population in the hindbrain of lesioned animals, their swimming initiation can only be driven by a fast and non-variable mechanism. In case of a strong stimulation, this reflex-like mechanism is the physiological path that control tadpoles took in the majority of the experimental trials, indicating that the ExNs population might be mostly involved in responses to less intense stimulation, when a delay in locomotion initiation is observed. Nevertheless, the ipsilateral response of control animals to suprathreshold stimulation might still be activated by a different neuronal pathway, possibly involving one additional level of interneurons. It is possible that dlc sensory neurons activate directly CPG neurons after a strong stimulus, since it has been proven they have NMDA-mediated synaptic connections (Li et al., 2004a). So far, no

direct connections between dla and CPG neurons have been reported. However, it is possible that, as ipsilateral responses in the tadpoles with transverse lesion showed the same short latency as contralateral start, the sensory dla neurons also have connections to CPG neurons. This neural circuit does not seem to be active in the controls, but it could be activated when more rostral neuronal populations are removed.

Comparison with an alternative circuit demonstrated in the Zebrafish

Recently, Liu and colleagues (Liu and Hale, 2017) have shown that swimming initiation in the zebrafish larvae is orchestrated by the activation of Mauthner neurons in the hindbrain and of inhibitory neurons in the caudal segments of the spinal cord. By means of whole cell recording (Liu and Hale, 2017), it was demonstrated that CoLo are activated shortly after stimulation, earlier than Mauthner neurons, and they provide inhibition to motor neurons in the opposite side of the spinal cord, in the caudal regions. The sensory RB neurons were shown to synapse with CoLo and to excite them in order to give rise to inhibition in motor neurons (Liu and Hale, 2017).

It cannot be excluded that a similar circuit might be present also in the *Xenopus* tadpole. Two classes of inhibitory neurons are present in the tadpole spinal cord: the cINs, which provide mid-cycle inhibition to CPG neurons lying in the opposite side of the spinal cord (Soffe et al., 1984, Yoshida et al., 1998), and the aINs, which have ipsilateral axons that inhibit dlc and CPG on the same side of the spinal cord (Li et al., 2001, Li et al., 2002). If cINs serve the same purpose of CoLo in the zebrafish, they could inhibit contralateral motor neurons in the more caudal segments of the spinal cord, allowing the first bend of swimming to happen rostrally and possibly explaining the higher percentage of contralateral first head bend recorded after a suprathreshold stimulation (fig. 4.9). Indeed, in order for swimming to start properly, a first rostral contralateral (in respect to stimulation) bend needs to be accompanied by a non-activation of the motor neurons that lie more caudally and on the same side. If this coordination fails, the undulatory movement cannot start functionally. Crucially, a direct synaptic connection between cINs and sensory pathway neurons dla in the tadpole has not been reported yet. A second possibility is that RB neurons directly connect to cINs, although evidence on this synaptic link are lacking.

One last possibility is that, in the tadpole, inhibition is carried to the side contralateral to stimulation not by the inhibitory cINs themselves (as CoLo do in the larval zebrafish (Liu and

Hale, 2017)), but rather by the sensory pathway neurons dlc, which are activated by RB cells and whose axons are commissural (Roberts and Clarke, 1982, Li et al., 2001). In fact, monosynaptic connections have been identified between dlc and aINs, although the synaptic input is inhibitory and goes from the aINs to dlc (Li et al., 2002). Nevertheless, the possibility that dlc could excite aINs, which in turn would inhibit motor neurons on the side opposite the stimulation is intriguing and should be further investigated.

Synchrony does not explain the shorter latency in electrophysiology experiments compared to behaviour

When synchronous VR bursts appear on both side of the tadpole's body, the actual motor outcome would be for the animal to be still until the phase/anti-phase rhythmic swimming is introduced. For this reason, episodes of synchrony cannot be observed in behavioural analysis, where the latency is measured as the first bend of the head. Thus, it is possible that the longer delay for swimming initiation reported for lesioned animals in behavioural experiments was due to underlying synchronous start that is not detected. To investigate this, the latency in electrophysiology experiments was calculated on the first VR burst of rhythmic swimming (fig. 4.11, 4.13), *i.e.* when the tadpole would have started the undulatory movement if not immobilised. Nevertheless, even taking synchrony into account, none of the lesioned animal groups showed latencies comparable to the values observed in behavioural experiments.

It is worth noting that the stimulation used during behavioural and electrophysiology experiments are of different natures; it is a manual poke with a hair *versus* an electrical stimulation delivered through a suction electrode, in behaviour and electrophysiology experiments, respectively. In both cases the primary sensory RB neurons in the skin will be activated, which excite dla and dlc secondary sensory neurons (Clarke and Roberts, 1984, Roberts and Sillar, 1990, Li et al., 2004b). However, it is possible that different types of stimulation evoke excitation in RB neurons with different timing. One aspect to take into account is that electrical stimulation spreads on the skin around the tip of the electrode, stimulating more RB neurons, which in turn excite more dla and dlc cells. On the contrary, a manually delivered poke with a hair only activates the RB sensory receptors lying in the area where the skin has been touched. One RB neuron still contacts and activates more than one dla and dlc (Clarke and Roberts, 1984, Roberts and Sillar, 1990, Li et al., 2004b), but it is plausible

that this secondary sensory excitation that reaches the brain is less strong than the one caused by electrical stimulation.

4.4 Conclusion

Three main aspects of swim initiation were analysed and found to be affected by lesions in the hindbrain: the latency from stimulation to motor response, the variability of this latency, the side preference for first muscle contraction. Although it is not possible to conclude that all these features are regulated by the same neuronal population, it is reasonable to suggest that at least some of the cells responsible lie in the hindbrain.

Here, no anatomical 'hot spots' for the putative population of ExNs could be defined in the brainstem of tadpoles. On the contrary, all the lesions performed on the hindbrain caused changes in the latency to swim initiation and in the side preference for first muscle contraction, with the most obvious effects of lesions being shown when swimming was triggered by a threshold stimulation. For this reason, subsequent experiments aimed at identifying ExNs in the hindbrain were carried out using threshold stimulation only. One other explanation for the unsuccessful attempt of locating ExNs by means of lesions, is that these neurons might have long projections, running both in ascending and descending direction across the hindbrain. It is also likely that ExNs projections are both ipsilateral and commissural.

5 Results: Novel hindbrain firing patterns at motor response to skin stimulation

In this chapter, extracellular recordings of hindbrain activity are reported. As it appears from data previously shown in this thesis (chapter 4), the putative neuronal population responsible for the initiation of swimming in the *Xenopus* tadpole could not be restricted to discrete areas of the hindbrain. For this reason, extracellular recordings were performed in the hindbrain, with the aim of identifying single units that showed characteristic firing patterns. Importantly, extracellular multi-unit recording was instrumental for the acquisition of electrical activity in the whole hindbrain, which allowed an unbiased analysis of firing patterns throughout the rostro-caudal axis.

As the overall goal here was to identify neurons controlling motor initiation, single units' firing was tested for correlation with swimming behaviour. The rationale of these experiments is that if a neuron is involved in the motor initiation, its firing would change when the animal starts to swim. Conversely, if a neuron is not involved in swimming control, its firing pattern would be stable both when movement happens, as well as when the animal is at rest.

Hindbrain extracellular recordings were acquired during four different motor states: 1) animal at rest, 2) delivery of a subthreshold stimulation, *i.e.* which did not lead to swim initiation, 3) delivery of a threshold stimulation, *i.e.* which led to swim initiation, 4) continuous, ongoing swimming. Spike sorting analysis was carried out to identify single firing units from multi-unit recordings. Subsequently, each unit was tested for changes in their spiking pattern during the four motor states mentioned above.

Two main novel neuronal populations were identified in the experiments described in this chapter, and each of these two neuronal classes were further classified in two subpopulations. These four populations showed features of ExNs, suggesting that a circuit for descending motor control is present in the hindbrain of the *Xenopus* tadpole.

5.1 Materials and methods

Animal care

Fertilized *Xenopus laevis* eggs were purchased from EXRC (Portsmouth, UK) and raised as described in the 'Materials and Methods' section of Chapter 3. All experiments were carried out on tadpole at developmental stage 37/38 (Nieuwkoop and Faber, 1956).

Animal surgery and Experimental setup

Stage 37/38 tadpoles were deeply anesthetized in α-bungarotoxin (Invitrogen) for 50 minutes at RT (see Appendix 1 for α-bungarotoxin details), and then pinned on a rotating Sylgard block in a small recording dish filled with saline. The skin covering the brain and trunk muscles on both sides was removed with fine tungsten needles. To prevent the sensory stimulus to reach the brain via electrical conductance properties of the skin (Roberts and Stirling, 1971, James and Soffe, 2011). trigeminal nerves were severed at both sides at the otic capsule level. Two borosilicate glass suction electrodes (tip diameter approximately 70 μm) were attached to both sides of the tadpole's body, approximately at the level of the 5th myotomal cleft, to record ventral root activity. A third glass suction electrode (tip diameter approximately 50 μm) was used to record extracellular hindbrain activity (fig. 5.1 B,C) During single experiments, the brain recording electrode was positioned in one of the three hindbrain areas depicted in fig. 5.1 D; the electrode's location was annotated based on its position relative to anatomical landmarks, *i.e.* the MHB, the otic capsule, the obex. Electrical stimulation was delivered through a suction electrode attached to the skin at the level of the anus (fig. 5.1.B) connected to a custom-made, software driven pulse generator. Both intensity (V) and duration (ms) of the stimulus given were set in each experiment as the smallest values which caused swimming initiation; all animals initiated swimming with a stimulation in the range of 3.5-4.5 V and 0.25-0.4 ms. Electrical signal from left and right VR was amplified and 50/60Hz noise was eliminated via a noise eliminator (HumBug, Digitimer, UK). Extracellular electrical activity from the hindbrain was amplified and filtered through Neurolog modules (preamplifier modules: NL100RK, NL100C, NL104; filters module: NL125; Digitimer, UK); 50/60Hz noise was eliminated (HumBug, Digitimer, UK). All data were acquired through a Power 1401 mkII (CED, Cambridge, UK), in Signal 7 (CED, UK) at a sampling rate of 20000 Hz.

Fictive swimming and hindbrain activity were recorded in four motor states (fig. 5.2):

1) at rest, when no stimulus was applied to the tadpole's skin and the ventral roots were silent;
2) stimulation/no start, when the stimulus delivered was not strong enough to produce fictive swimming;
3) stimulation/start, when the stimulus delivered triggered fictive swimming;
4) sustained swimming, when ventral root bursts indicated ongoing, continuous swimming

Data analysis

Spike sorting was run on hindbrain extracellular recordings (Spike2 10.00, CED, UK) and the resulting single units were visually evaluated for spike's shape consistency. Following quantitative analysis were performed on single units identified through spike sorting. The number of spikes fired by each unit was counted in 150 ms trials for each motor states (rest, stimulation/no start, stimulation/start, sustained swimming; fig. 5.2). Randomly chosen 150 ms repetitions throughout the recording were analysed for 'at rest' and 'sustained swimming' states. For the two states in which a stimulation was given, the time frame considered was stimulation (t=0) +150 ms. A minimum number of 4 trials were analysed for each motor state in each experiment. Two-way ANOVA with Geisser-Greenhouse correction was run on the number of single unit spikes counted in the different motor states (GraphPad Prism 8). The factors used in the two-way ANOVA were (1) stimulation and (2) swimming; each factor was either present or absent in the motor state considered. Two-way ANOVA was used to classify units based on their firing pattern in response to stimulation (stimulation/no start), swimming (sustained swimming), the combination of the two factors (stimulation/start), or the absence of those (rest) (fig. 5.2). Coefficient of variations of the number of spikes fired by one unit (CV=standard deviation/mean) were used to create all the heat maps in the figures presented. CV in 5 ms time bins was calculated in the 150 ms trials analysed for each motor state.

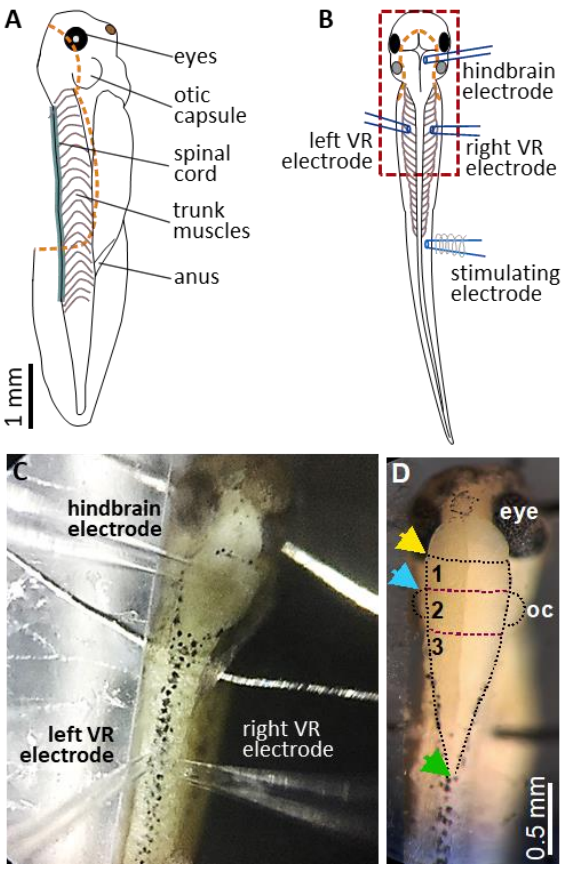

Figure 5.1 Hindbrain extracellular recordings experimental setup.

A) *Side view of the tadpole with anatomical hallmarks. Orange dashed lines indicate skin removal to get access to the brain and to the muscle clefts.* ***B)*** *Side view of the tadpole with electrodes positioned as in experimental conditions. Left and right VR electrodes were positioned facing each other approximately at the 5th myotomal cleft. Stimulating electrode was positioned on the right side at the level of the anus. Orange dashed line indicate skin removal; red dashed square area is replicated in panel C.*

C) *Picture of brain and trunk of a tadpole pinned to the Sylgard block during experimental procedures. Right and left VR electrodes, as well as stimulating electrodes, are positioned as in B.* ***D)*** *Picture of a tadpole's brain as it appears when the skin is removed. The hindbrain was visually divided into three sectors along the rostro-caudal axis using anatomical landmarks, i.e. MHB (yellow arrow), otic capsules (blue arrow) and obex (green arrow): rostral sector (1), otic capsule level (2) and caudal sector (3).*

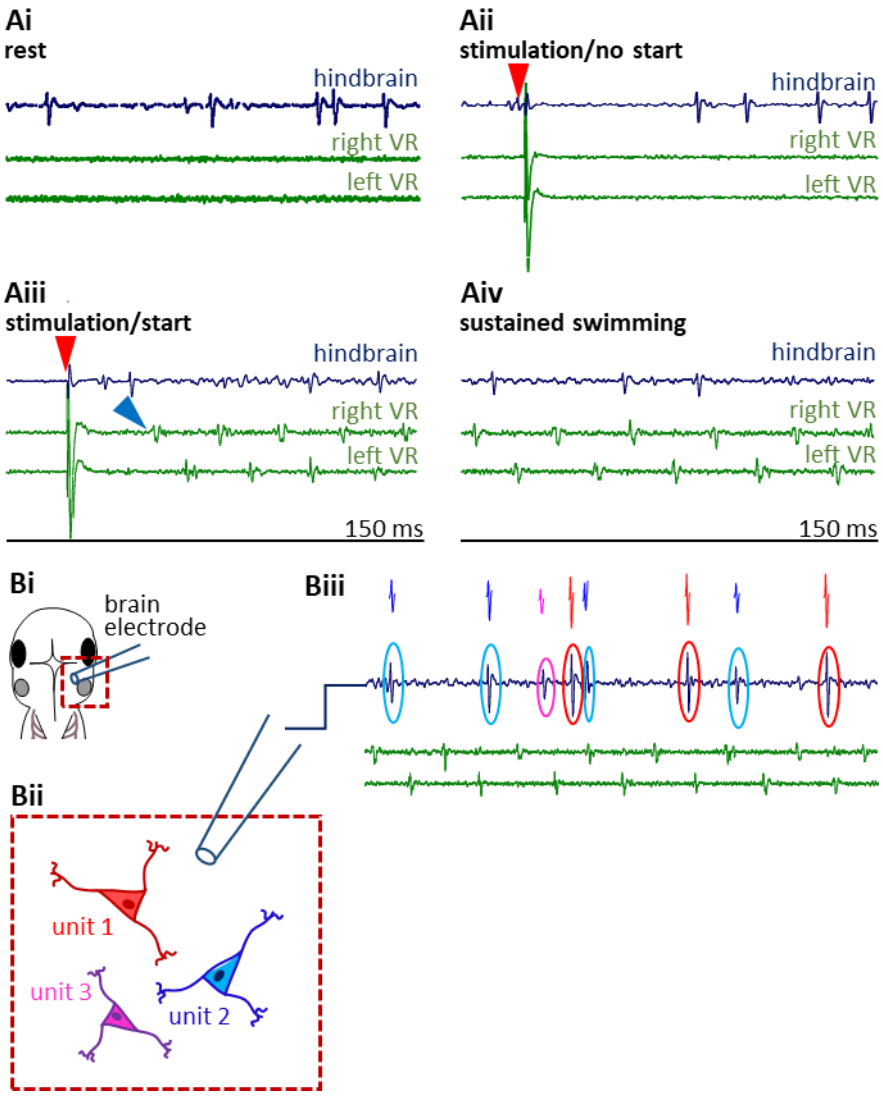

Figure 5.2 Hindbrain recordings experimental design.

A) *Examples of recordings in the four different motor states analysed (150 ms): rest, stimulation/no start, stimulation/start, sustained swimming. Raw traces for hindbrain extracellular activity (blue trace) and right and left VR recording (green traces) are presented. In Ai and Aii no fictive swimming is present, as indicated by the absence of VR bursts. In Aiii and Aiv fictive swimming is indicated by the rhythmic VR bursts. Red arrowheads indicate stimulus delivery, blue arrowhead in Aiii indicates the start of swimming.*

B) *Schematic for extracellular recordings in the hindbrain. Firing activity was recorded extracellularly in the hindbrain (Bi). Activity from different firing units was recorded (Bii) and subsequently analysed for spike sorting (Biii). Single unit firing patterns were then used in downstream analyses.*

5.2 Results

5.2.1 Hindbrain units firing patterns correlate with swim initiation

Extracellular recordings were carried out in the hindbrain in the four motor states described in 'Materials and Methods' and depicted in fig. 5.2 (rest, stimulation/no start, stimulation/start, swimming). Multi-unit recordings were then spike-sorted to identify single unit activity. A total number of 90 firing units in 18 animals were detected by spike sorting analysis. In order to keep track of the relative positions of firing units, the hindbrain was visually divided into three sectors along the rostro-caudal axis, following well-defined anatomical border. In rostro-caudal direction these sectors were: 1) rostral sector (from the MHB to the rostral edge of the otic capsule), 2) otic capsule sector (which comprised the area adjacent to the otic capsule) and 3) caudal sector (from the caudal edge of the otic capsule to the obex). The division of hindbrain sectors is depicted in fig. 5.1 D. Out of the total number of 90 units, 33 units in 7 animals were recorded in the rostral sector, 36 units in 6 animals were recorded at the otic capsule level, and 21 units in 5 animals were recorded in the caudal sector.

Statistical analysis was performed on the number of spikes fired by single units in order to differentiate units active in one (or more) motor state (rest, stimulation/no start, stimulation/start, swimming; fig. 5.2A).

54 units (60% of tot units, n tot units=90) resulted non-significant (p>0.05) neither for swimming, nor for stimulation factor when tested in a two-way ANOVA test (fig. 5.3A). These non-significant units were recorded in each hindbrain sector; 63.6% in the rostral area (21/33 sector's units), 72.2% (26/36 sector's units) at the otic capsule level, 33.3% (7/21 sector's units) in the caudal area (fig. 5.3 B, C and D, respectively). These units showed stable, low firing in every motor state tested (fig. 5.4A). For this reason, the non-significant units were considered as not implicated in the control of swim initiation, and therefore they were excluded from further analysis.

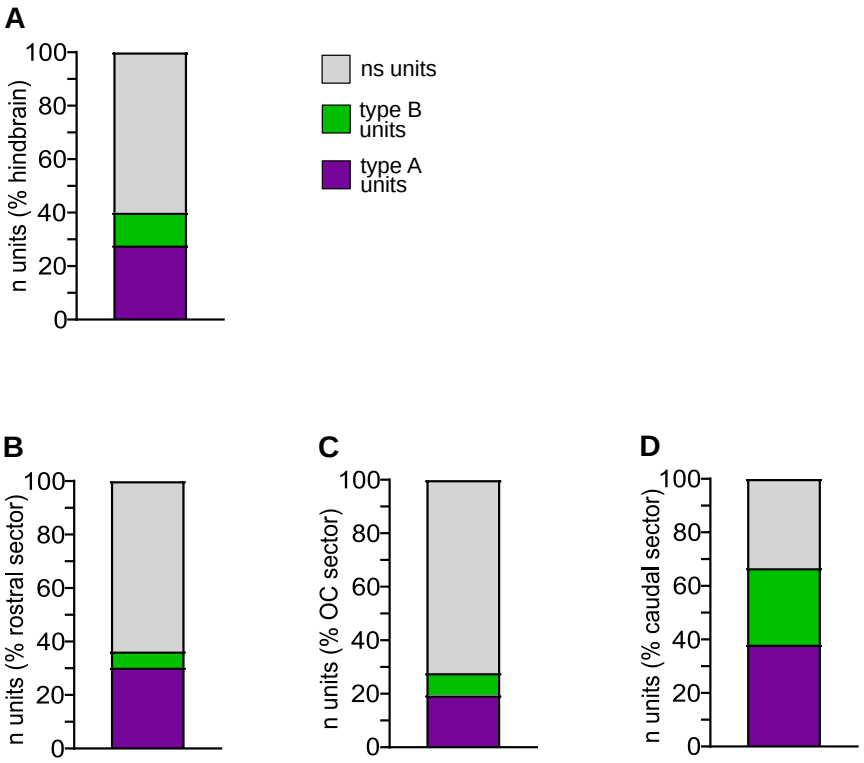

Figure 5.3 Hindbrain distribution of type A and type B units.

A-D) *Bar charts representing percentages for non-significant (ns, grey), type B (green) and type A units (violet) in the entire hindbrain (**A**), and in the different hindbrain sectors as depicted in fig. 5.1D (**B**, rostral sector; **C** otic capsule level; **D**, caudal sector). A) Percentages calculated over the total number of units recorded in the hindbrain (54/90 = 60.0% ns units; 11/90 = 12.2% type B units, 25/90 = 27.8% type A units); B-D) percentages calculated over the total number of units recorded in each of the hindbrain sectors (B - rostral sector, 21/33 = 63.6% ns units, 2/33 = 6.1% type B units, 10/33 = 30.3% type A units; C - otic capsule level, 26/36 = 72.2% ns units, 3/36 = 8.3% type B units, 7/36 = 19.4% type A units; D - caudal sector, 7/21 = 33.3% ns units; 6/21 = 28.6% type B units, 8/21 = 38.1% type A units).*

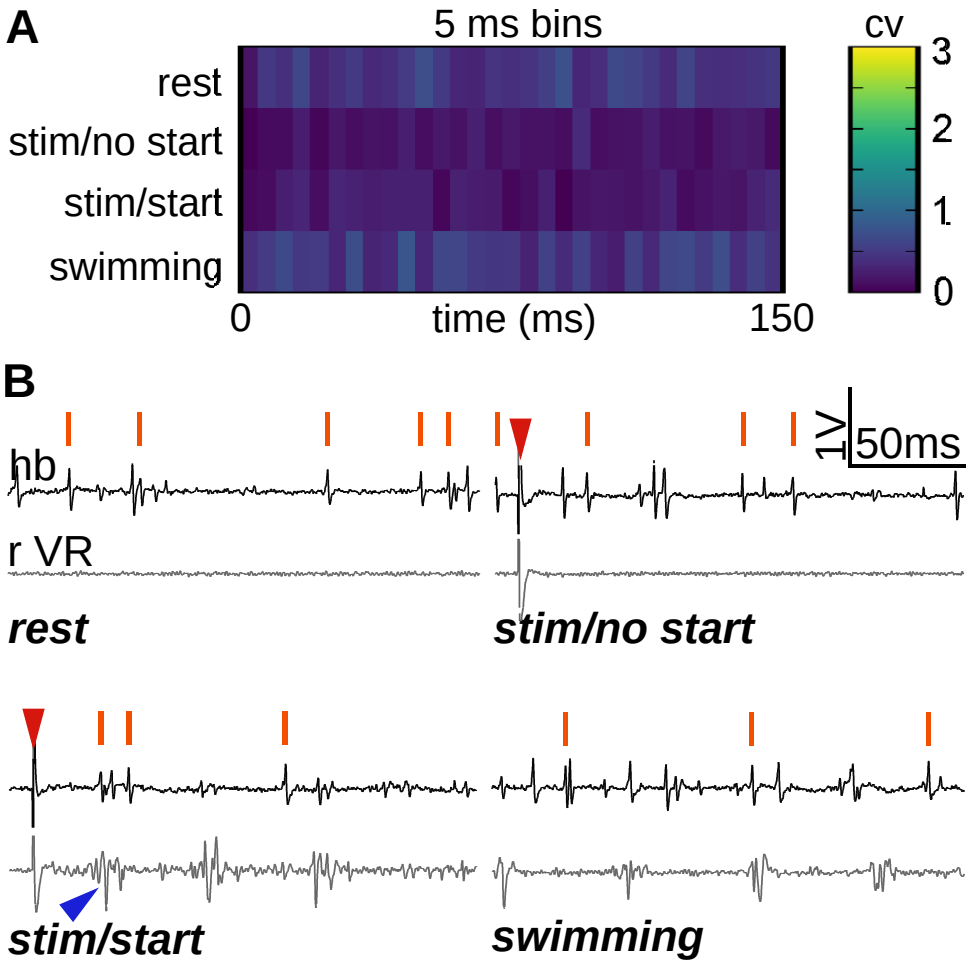

Figure 5.4 Neural activity of non-significant units is not correlated to swim behaviour.

A) *Average heat map of non-significant units recorded in the hindbrain (54 units in 14 animals, minimum of 4 trials per motor state per units). Coefficients of variation (CV=standard deviation/mean) were calculated for each time bin (5 ms) on the number of spikes fired by single units during the same 5 ms in the four motor states.*

B) *Examples of spikes fired by one non-significant unit recorded in the four motor states investigated (rest, stimulation/no start, stimulation/start, swimming). 200 ms are reported for each example. Orange lines indicate spikes fired by the unit, and they are presented above the respective extracellular hindbrain recording raw trace (black trace). Fictive swimming is shown by rhythmic bursts of the right VR (grey trace, rVR). Red arrowheads represent electrical stimulus; blue arrowhead indicates the start of swimming.*

25 units (27.8% of 90 units, recorded in 6 animals, fig. 5.3 A) showed significantly higher activity at the start of swimming in response to skin stimulation ('stimulus x swim interaction' units, $p<0.05$, two-way ANOVA). Such units were recorded throughout the hindbrain: they constituted the 30.3% of recorded units in the rostral area (10/33 sector's units), the 19.4% (7/36 sector's units) at the otic capsule level, and the 38.1% (8/21) of the units recorded in the caudal area (fig. 5.3). These units, with firing rate higher only at motor initiation, were named '**type A units**'. Type A units were highly active only when the electrical stimulus was strong enough to induce swimming in the tadpole (the experimental condition referred to as 'stimulation/start'), while they were mainly silent at rest, during sustained swimming, and when the stimulation failed to trigger swimming (fig. 5.5).

11 units (12% of 90 units, recorded in 8 animals, fig. 5.3 A) showed increased firing activity following trunk skin stimulation, both at the initiation of movement and during sustained swimming. These units did not show a significant 'stimulation x swimming' interaction in the two-way ANOVA test. Instead, they fired a different number of spikes in response to fictive swimming only ('swim effect' units, $p<0.05$ for swimming effect only, two-way ANOVA). These units, which were more active both at the start of movement as well as during continuous swimming, were named '**type B units'**. Type B units were mostly inactive when the animal was not swimming, *i.e.* at rest and when stimulation did not lead to swimming (fig. 5.6). As for type A, also type B units were recorded throughout the three hindbrain sectors (fig. 5.3A). In the rostral sector, 6.1% of the units were found to be type B units (2/33 sector's units, fig. 5.3B), at the otic capsule level type B units constituted the 8.3% of the units (3/36 sector's units, fig. 5.3C) and they made up the 28.6% of units recorded in the caudal area (6/21 units, fig. 5.3D).

Because CPG neurons are also activated as soon as swimming starts, three CPG units were recorded, one in each hindbrain area, and they were characterised to rule out the possibility for type B units to have CPG-like activity. The first feature of a CPG neuron is to be active only during swimming: the heat maps in fig. 5.7A shows that the three CPG units are silent when motor activity is not present (rest and stim/no start), but they start firing when swimming is initiated (stim/start, see also fig. 5.8) and sustained (swimming). Following a two-way ANOVA, the three units resulted with a significant swimming effect ($p<0.0001$ rostral unit, $p<0.0001$ otic capsule level unit, $p=0.0004$ caudal unit), and with a non-significant 'stimulation x swimming' interaction (rostral unit $p=0.5096$, otic capsule level unit $p=0.5561$, caudal unit $p= 0.0775$). The second

characteristic feature of CPG neurons is to fire rhythmically at the same frequency of ventral root bursts. When the tadpole swims, CPG units fire one spike at every muscle contraction, here monitored as ventral root bursts (fig.5.7 B). Differently from CPG units, type B units were not completely silent when the animal was not engaged in fictive swimming (fig. 5.6 A), and they did not fire rhythmically following ventral root bursts (fig. 5.6 B). In conclusion, none of the units categorised here as 'type B' show features of a CPG-like neuron.

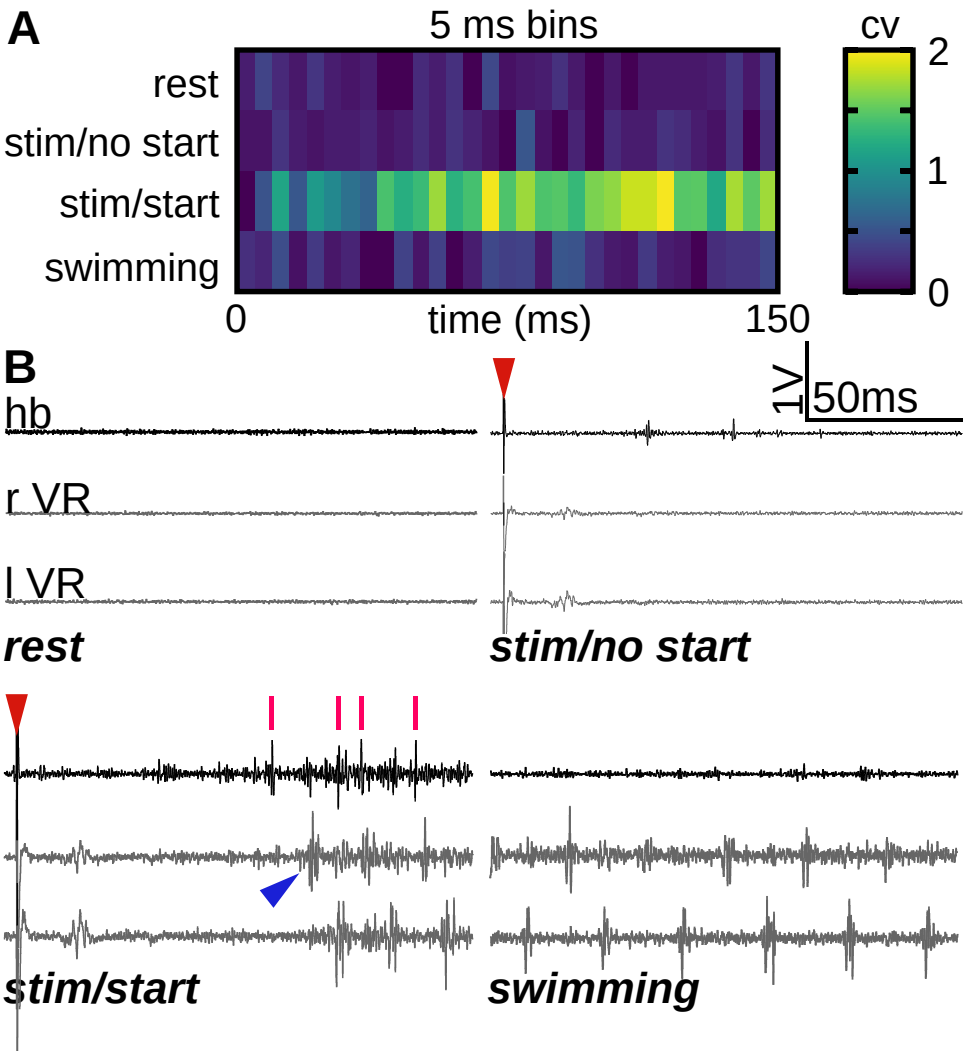

Figure 5.5 Type A units are activated at swimming initiation.

A) *Average heat map of type A units recorded in the hindbrain (25 units in 11 animals, minimum of 4 trials per motor state per units). Coefficients of variation (CV) were calculated for each time bin (5ms) on the number of spikes fired by single units during the same 5 ms in the four motor states.*

B) *Examples of spikes fired by one type A unit recorded in the four motor states investigated (rest, stimulation/no start, stimulation/start, swimming), 150 ms are reported for each example. Red lines indicate spikes fired by the unit, and they are presented above the respective extracellular hindbrain recording raw trace (black trace). Fictive swimming is shown by rhythmic right and left VR bursts (grey trace, rVR and lVR). Red arrowheads represent the electrical stimulus; blue arrowhead indicates the start of swimming.*

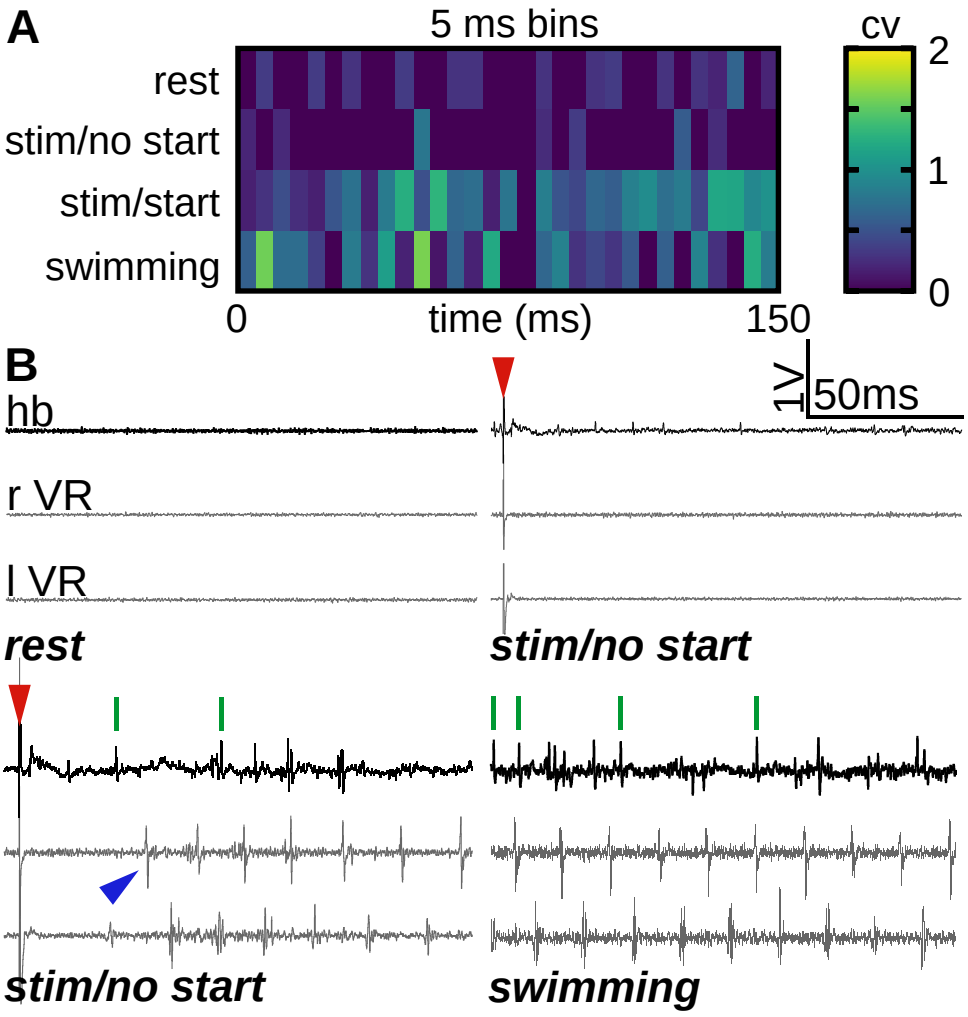

Figure 5.6 Type B units are activated at swimming initiation.

A) *Average heat map of type B units recorded in the hindbrain (11 units in 8 animals, minimum of 4 trials per motor state per units). Coefficients of variation (CV=standard deviation/mean) were calculated for each time bin (5 ms) on the number of spikes fired by single units during the same 5 ms in the four motor states.*

B) *Examples of spikes fired by one type B unit recorded in the four motor states investigated (rest, stimulation/no start, stimulation/start, swimming) 150 ms are reported for each example. Green*

lines indicate spikes fired by the unit, and they are presented above the respective extracellular hindbrain recording raw trace (black trace). Fictive swimming is shown by rhythmic right and left VR bursts (grey trace, rVR and lVR). Red arrowheads represent the delivery of the electrical stimulus; blue arrowhead indicates the start of swimming.

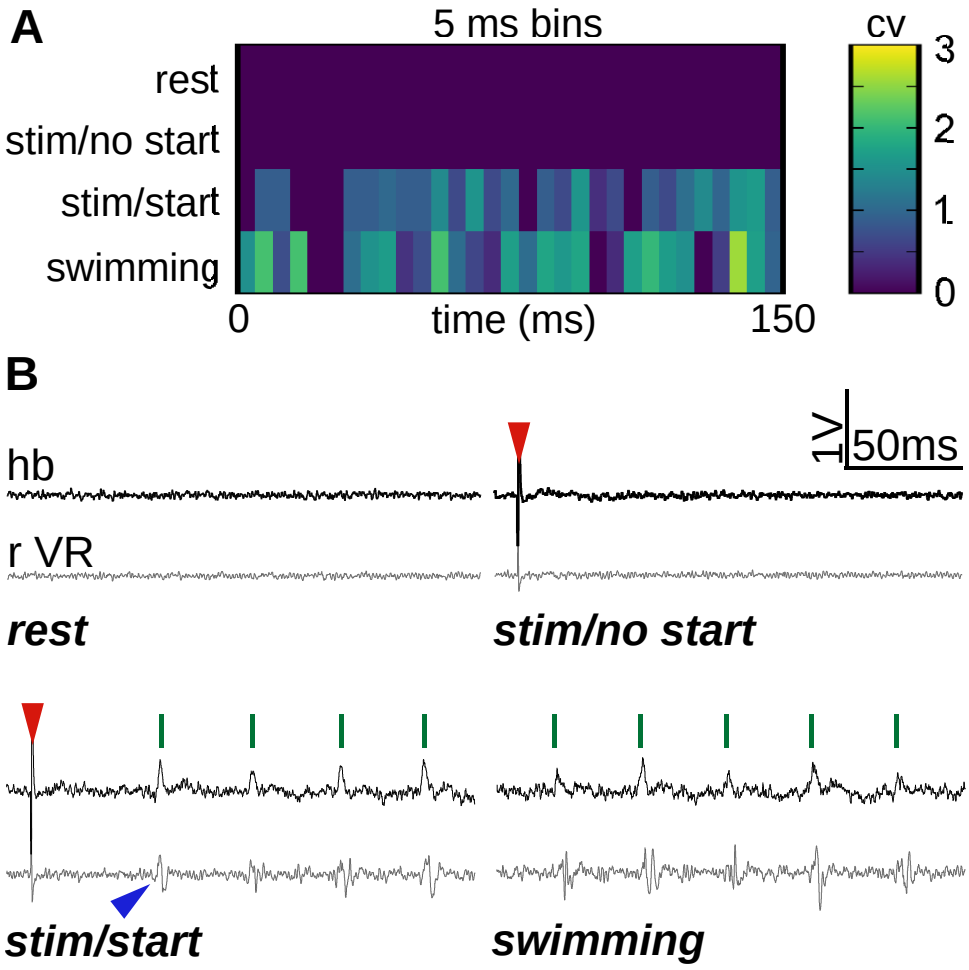

Figure 5.7 Central Patter Generator units.

A) *Average heat map of CPG units recorded in the hindbrain (3 units in 3 animals, minimum of 4 trials per motor state per units). CV were calculated for each time bin (5 ms) on the number of spikes fired by single units during the same 5 ms in the four motor states.*

B) *Examples of spikes fired by one CPG unit recorded in the four motor states investigated; 200 ms are reported for each example. Green lines indicate spikes fired by the unit, and they are presented above the respective hindbrain extracellular raw trace (black trace). Fictive swimming is shown by rhythmic bursts of the right VR (grey trace, rVR). Red arrowheads represent the electrical stimulus; blue arrowhead indicates the start of swimming.*

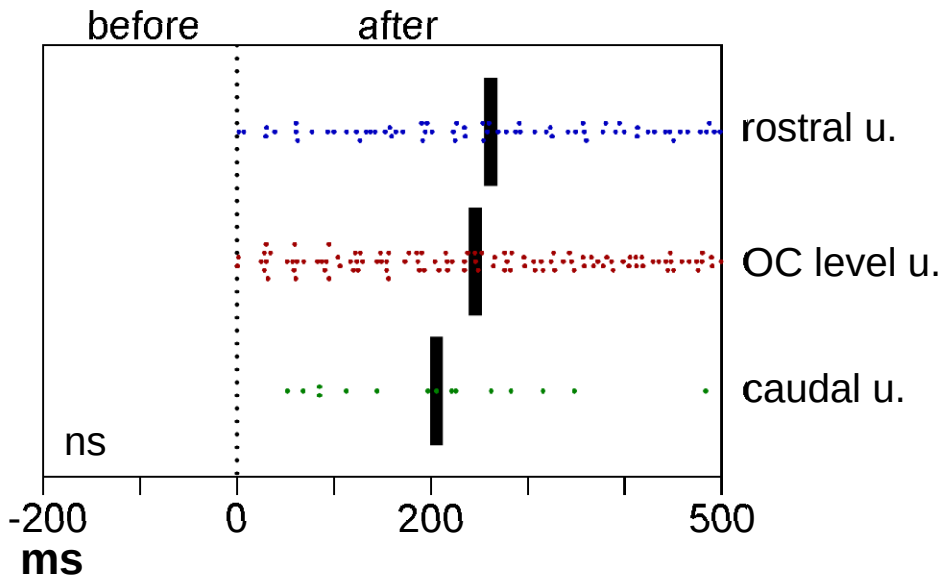

Figure 5.8 Central Patter Generator units.

Scatter plot of spikes fired by one rostral CPG unit (blue), one CPG unit recorded at the otic capsule level (red) and one caudal CPG unit (green) at the initiation of swimming. Dotted grey line (ms=0) marks the start of fictive swimming. Black solid lines indicate median values. Kruskal-Wallis test, p=0.356; rostral CPG unit 261.9 ± 141.5 ms; CPG unit at the otic capsule level 248.4 ± 143.9 ms; caudal CPG unit 205.9 ± 120.6 ms. Values expressed as median ± SD. 69 spikes from 1 rostral unit, 110 spikes from 1 unit at the otic capsule level, 15 spikes from 1 caudal unit.

5.2.2 Different firing patterns are recorded at swimming initiation

The timing of spikes fired by type A and type B units was analysed in the time gap between stimulus delivery and the start of fictive swimming (negative area of the graphs in fig. 5.9), and in the first 500 ms after swim initiation (positive area of the graphs in fig.5.9).

Importantly, type A and type B units produced spikes before the first ventral root burst (fig. 5.5B, 5.6 B). This early firing, *i.e.* before swimming has started, is the main feature a neuron has to display in order to be categorised as implicated in mechanism of motor initiation. Indeed, at least theoretically, neuronal populations that fire before the start of movement could act presynaptically to dINs in the *Xenopus* tadpole.

Following stimulation, type A units increased their firing to a peak (0.48 ± 0.21 Hz, mean ± SEM) 11 ms before swimming started, and then slowly decreased it to become silent during sustained swimming (fig. 5.9 A, violet trace). Type B units also increased their activity rate before the start of swimming (fig. 5.9 A, green trace), but no clear peak was found in their firing activity. Instead, type B units' firing rate was stable as swimming became continuous (0.06 ± 0.08 Hz 10 ms before start vs 0.06 ± 0.09 Hz 10 ms after swimming initiation; data expressed as mean ± SEM). The firing rate of type A units was found to be significantly different from type B firing units' firing rate over the time ranging from stimulation to the first 500 ms into fictive swimming (fig.5.9 A, Wilcoxon matched pairs signed rank test, $p<0.0001$).

Interestingly, spikes fired by type A units were recorded earlier than the spikes fired by type B units (fig. 5.9B). This feature, together with the difference in firing rate at motor initiation described above (fig. 5.9 A), strengthens the possibility that type A and type B units might form two distinct neuronal population which act in sequence in order to initiate swimming in the tadpole.

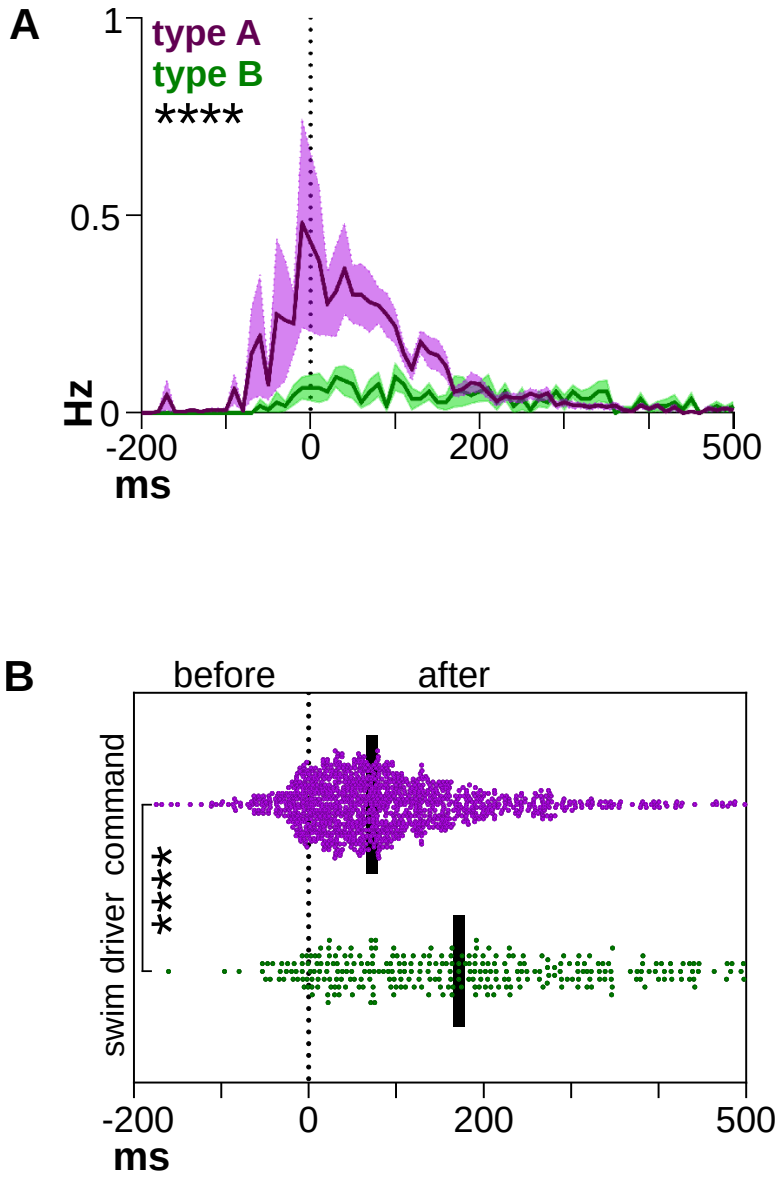

Figure 5.9 Type A and type B units are activated at different latencies.

***A**) Firing rates of type A (violet line) and type B units (green line) recorded before movement initiation and in the first 500 ms of sustained swimming. Dotted grey line (ms=0) marks the start of fictive swimming. Data are presented as mean (solid lines) ± SEM (shaded area). Wilcoxon matched pairs signed rank test, p<0.0001.; command units 0.0925 ± 0.0139, swim driver units 0.0299 ± 0.0031 (mean ± SEM). Command units N=25, swim driver units N=11; minimum 4 trials/unit. ****p<0.0001.*

***B)** Scatter plot of spikes fired by type A units (violet) and type B units (green) before movement initiation and during the first 500 ms of sustained swimming. Dotted grey line (ms=0) marks the start of fictive swimming. Black solid lines indicate median values (median ± SD= 72.69 ± 104.4 ms for type A units; median ± SD = 160.8 ± 144.3 ms for type B units). Kolmogorov-Smirnov test, p<0.0001; 1145 spikes from 25 type A units, 288 spikes from 11 type B units. ****p<0.0001.*

The activation time of type A units varied in the different hindbrain sectors (fig. 5.10 A, p=0.0003, repeated measures one-way ANOVA with Bonferroni correction for multiple comparisons; rostral vs OC level, mean diff.=0.0725; rostral vs caudal, mean diff.= 0.0376; OC level vs caudal, mean diff.= 0.1101). Type A units recorded in the central area of the hindbrain (at the otic capsule level) were the major responsible for the firing rate peak at swimming initiation, showing a peak of 1.28 ± 2.23 Hz recorded 10 ms before the start (fig.5.10 A, red line). Type A units detected in the rostral and caudal sectors increased their firing in a less abrupt fashion (fig. 5.10 A, blue and green line, respectively), contributing nevertheless to the overall augmented activity, prolonged after the initiation of swimming (0 to ~200 ms after the start, fig. 5.10 A). However, the distribution of spikes fired at the start of movement by type A units in the three hindbrain sectors did not differ (fig.5.10 B**,** p=0.0618, Kruskal-Wallis test; rostral units= 71.94 ± 93.29 ms; otic capsule level units= 65.97 ± 117.5 ms; caudal units= 78.32 ± 109.5 ms; data reported as median ± SD).

Also type B units showed a different timing of activation depending on their location in the hindbrain (fig. 5.11 A; p<0.0001, repeated measures one-way ANOVA with Bonferroni correction for multiple comparisons; rostral vs OC level, mean diff.= 0.0390; rostral vs caudal, mean diff.= 0.0137; OC level vs caudal, mean diff.= -0.0254). Type B units recorded in the rostral hindbrain showed a higher peak in firing activity than type B units recorded at the otic capsule level and in the more caudal hindbrain (fig. 5.11B, red and green line, respectively). However, type B units did not show a different timing in the onset of their firing activity depending on their position in the hindbrain (fig. 5.11 B, p=0.2837 Kruskal-Wallis test; rostral units= 127.8 ± 148.6 ms for; otic capsule level units= 190.2 ± 160.7 ms; caudal units= 162.2 ± 134.1 ms; data reported as median ± SD).

Because both type A and type B units showed firing activity distributed along the rostro-caudal axis of the hindbrain, the location of their respective neuronal populations was considered to be dispersed throughout the hindbrain.

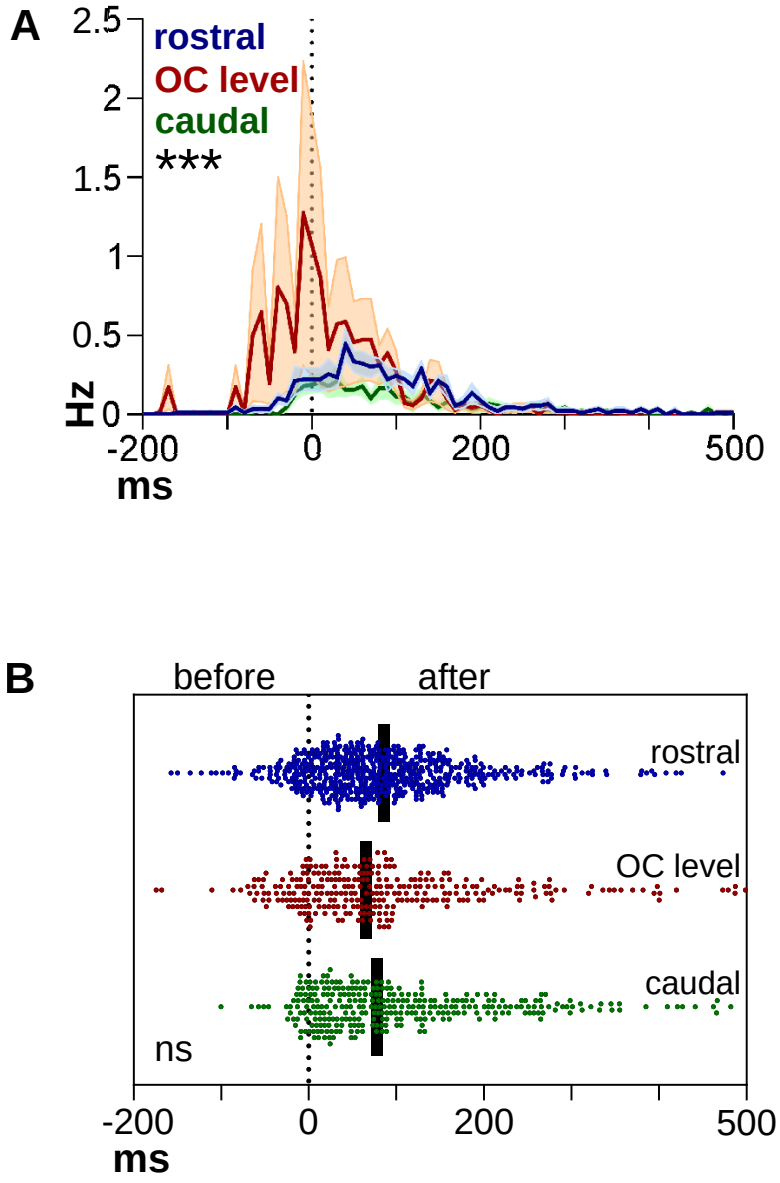

Figure 5.10 Type A units show different firing rates throughout the hindbrain.

A) *Firing rates of type A units recorded in the rostral sector (blue), at the otic capsule level (red) and in the caudal sector (green) of the hindbrain. Dotted grey line (ms=0) marks the start of fictive swimming. Data are presented as mean (solid lines) ± SEM (shaded area). Repeated measures one-way ANOVA with Bonferroni correction for multiple comparisons, p=0.0003; rostral vs OC level, mean diff.=0.0725; rostral vs caudal, mean diff.= 0.0376; OC level vs caudal, mean diff.= 0.1101. Rostral sector N=10 units; otic capsule level N=7 units; caudal sector N=8 units; minimum 4 trials per unit. ***p<0.001.*

B) *Scatter plot of spikes fired by type A units recorded in the rostral sector (blue), at the otic capsule level (red) and in the caudal sector (green) of the hindbrain. Dotted grey line (ms=0) marks the start of fictive swimming. Black solid lines indicate median values (median ± SD = 71.94 ± 93.29 ms for rostral units; median ± SD = 65.97 ± 117.5 ms for otic capsule level units; median ± SD= 78.32 ± 109.5 ms for caudal units). Kruskal-Wallis test, p=0.0618; 558 spikes from 10 rostral units, 284 spikes from 7 otic capsule level units, 303 spikes from 8 caudal units.*

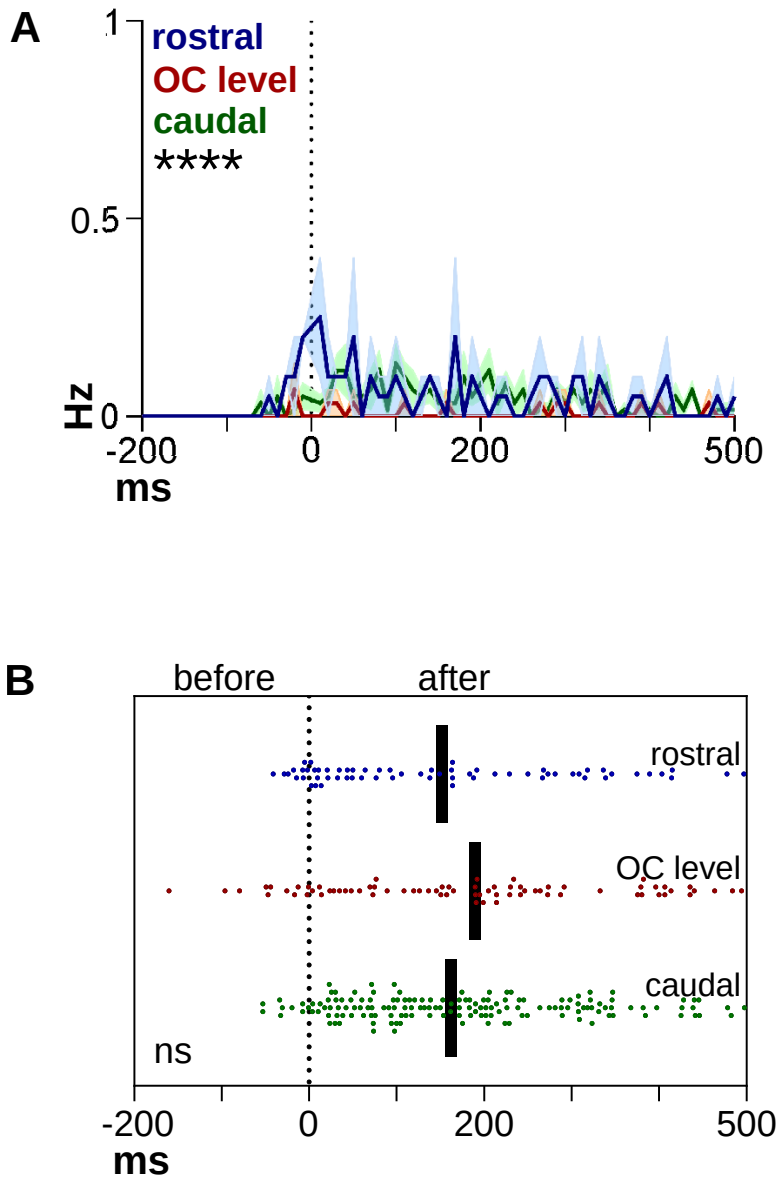

Figure 5.11 Type B units show different firing rates throughout the hindbrain.

A) *Firing rates of type B units recorded in the rostral sector (blue), at the otic capsule level (red) and in the caudal sector (green) of the hindbrain. Dotted grey line (ms=0) marks the start of fictive swimming. Data are presented as mean (solid lines) ± SEM (shaded area). Repeated measures one-way ANOVA with Bonferroni correction for multiple comparisons, p<0.0001; rostral vs OC level, mean diff.= 0.0390; rostral vs caudal, mean diff.= 0.0137; OC level vs caudal, mean diff.= -0.0254. Rostral sector N=2 units; otic capsule level N=3 units; caudal sector N=6 units; minimum 4 trials per unit. ****p<0.0001.*

B) *Scatter plot of spikes fired by type B units recorded in the rostral sector (blue), at the otic capsule level (red) and in the caudal sector (green) of the hindbrain. Dotted grey line (ms=0) marks the start of fictive swimming. Black solid lines indicate median values (median ± SD = 127.8 ± 148.6 ms for rostral units; median ± SD = 190.2 ± 160.7 ms for otic capsule level units; median ± SD = 162.2 ± 134.1 ms for caudal units). Kruskal-Wallis test, p=0.2837; 63 spikes from 2 rostral units, 73 spikes from 3 oc level units, 152 spikes from 6 caudal units.*

5.2.3 Neuronal subpopulations respond differently to subthreshold stimulation

Type A and type B units were further sorted into two subgroups, based on whether they were active or not following sub-threshold stimulation, *i.e.* during stimulation/no start trials. Type A and B units that were active both at threshold and sub-threshold stimulation (stimulation/start and stimulation/no start trials, respectively) were named 'level 1' populations (fig. 5.12 A, 5.13 A). On the other hand, type A and B units which were active only when the stimulus delivered led to fictive swimming (stimulation/start trials), were named 'level 2' populations (fig. 5.12 B, 5.13 B).

Level 1 and level 2 populations were found in both type A and type B units in the following numbers:
- type A: 11 level 1 units (44%, out of 25 type A units), 14 level 2 units (56%, out of 25 type A units); from now on referred to as 'type A_1' and 'type A_2'
- type B: 5 level 1 units (45.4%, out of 11 type B units), 6 level 2 units (54.6%, out of 11 type B units); from now on referred to as 'type B_1' and 'type B_2'

Type A_1 units showed increased firing in the stimulation/start trials (fig. 5.12 Ai and Aii), but were also slightly active when the stimulus delivered was not strong enough to cause swim initiation (fig. 5.12 Bi and Bii). On the contrary, type A_2 units were active only when the stimulation led to a motor response (fig. 5.12 Ai, Aii and Bi, Bii). In the time gap prior to swim initiation, spikes fired by type A_1 units were recorded at shorter latencies compared to those fired by type A_2 units (fig. 5.12 C, negative area of the graph; p=0.0187, Kolmogorov-Smirnov test on data recorded before swim initiation; type A_1 units= -25.75 ± 50.27 ms; type A_2 units= -17.19 ± 26.90 ms, data reported as median ± SD). After swimming had started, the temporal distribution of spikes fired by type A_1 and type A_2 units did not differ (fig. 5.12 C, positive area of the graph; p=0.0923, Kolmogorov-Smirnov test on data recorded after swim initiation; type A_1 units= 91.09 ± 94.18 ms; type A_2 units= 88.95 ± 104.5 ms, data reported as median ± SD).

Similarly, type B_1 units were activated when stimulation was delivered to the animal, irrespective of the motor outcome of the trial (*i.e.* with threshold or sub-threshold stimulation) (fig. 5.13 A and B). On the other hand, type B_2 units' firing was detected only when the electrical stimulus led to swimming (fig. 5.13 A and B). Contrary to type A units, both type B_1 and type B_2 units showed the same temporal distribution of spikes prior to movement initiation (fig. 5.13 C

negative area of the graph; *p*=0.1182, Kolmogorov-Smirnov test on data recorded before swim initiation; type B_1 units= -15.65± 11.20 ms, type B_2 units= -30.61 ± 38.49 ms, data reported as median ± SD), as well as after swimming had become continuous (fig. 5.13 C, positive area of the graph; *p*=0.0803, Kolmogorov-Smirnov test on data recorded after swim initiation; type B_1 units= 183.5 ± 152.7 ms, type B_2 units= 183.9 ± 125.3ms, data reported as median ± SD.

(next page) ***Figure 5.12 Differential activation of subpopulations of Type A units.***

Ai) *Firing rates of first (type A_1, pink line) and second level (type A_2, violet line) type A units recorded before movement initiation and in the first 500 ms of sustained swimming. Dotted grey line (ms=0) marks the start of fictive swimming. Data are presented as mean (solid lines) ± SEM (shaded area). Wilcoxon matched pairs signed rank test, p=0.0511; type A_1 units 0.0695 ± 0.0100 ms, type A_2 units 0.1094 ± 0.0180 ms (mean ± SEM). First level type A_1 units N=11, type A_2 units N=14; minimum 4 trials/unit.*

Aii) *Examples of spikes fired by one type A_1 unit (top trace, pink lines) and one type A_2 unit (bottom trace, violet lines), recorded in the stimulation/start motor state. Spikes fired by the units are presented above the respective extracellular hindbrain recording raw trace (hb, black trace). Fictive swimming is shown by rhythmic VR bursts (grey trace, VR). For clarity, only the VR with the first burst, marking swimming initiation, is shown here. Red arrowheads represent electrical stimulus; blue arrowhead indicates the start of swimming.*

Bi) *Firing rates of type A_1 (pink line) and type A_2 (violet line) units recorded in the first 500 ms after stimulation. Data are presented as mean (solid lines) ± SEM (shaded area). Wilcoxon matched pairs signed rank test, p<0.0001; type A_1 units 0.0149 ± 0.0018 ms, type A_2 units 0.0000 ± 0.0000 (mean ± SEM). Type A_1 units N=11, type A_2 units N=14; minimum 4 trials/unit. ****p<0.0001*

Bii) *Examples of spikes fired by one type A_1 unit (top trace, pink lines) and one type A_2 unit (bottom trace, no lines), recorded in the in the stimulation/no start motor state. Spikes fired by the units are presented above the respective extracellular hindbrain recording raw trace (hb, black trace). The absence of fictive swimming is shown by the silent VR (grey trace, VR). As both VR were silent in this case, for clarity only one VR is shown here. Red arrowheads represent electrical stimulus.*

C) *Scatter plot of spikes fired by type A_1 units (pink) and type A_2 units (violet) before movement initiation and during the first 500 ms of sustained swimming. Dotted grey line (ms=0) marks the start of fictive swimming. Black solid lines indicate median values. Kolmogorov-Smirnov test on data recorded before swim initiation, p=0.0187; type A_1 units -25.75 ± 50.27 ms; type A_2 units -17.19 ± 26.90 ms (median ± SD). 60 spikes from 11 type A_1 units, 120 spikes from 14 type A_2 units. Kolmogorov-Smirnov test on data recorded after swim initiation, p=0.0923; type A_1 units 91.09*

*± 94.18 ms; type A_2 units 88.95 ± 104.5 ms (median ± SD). 450 spikes from type A_1 units, 565 spikes from type A_2 units. *p<0.05.*

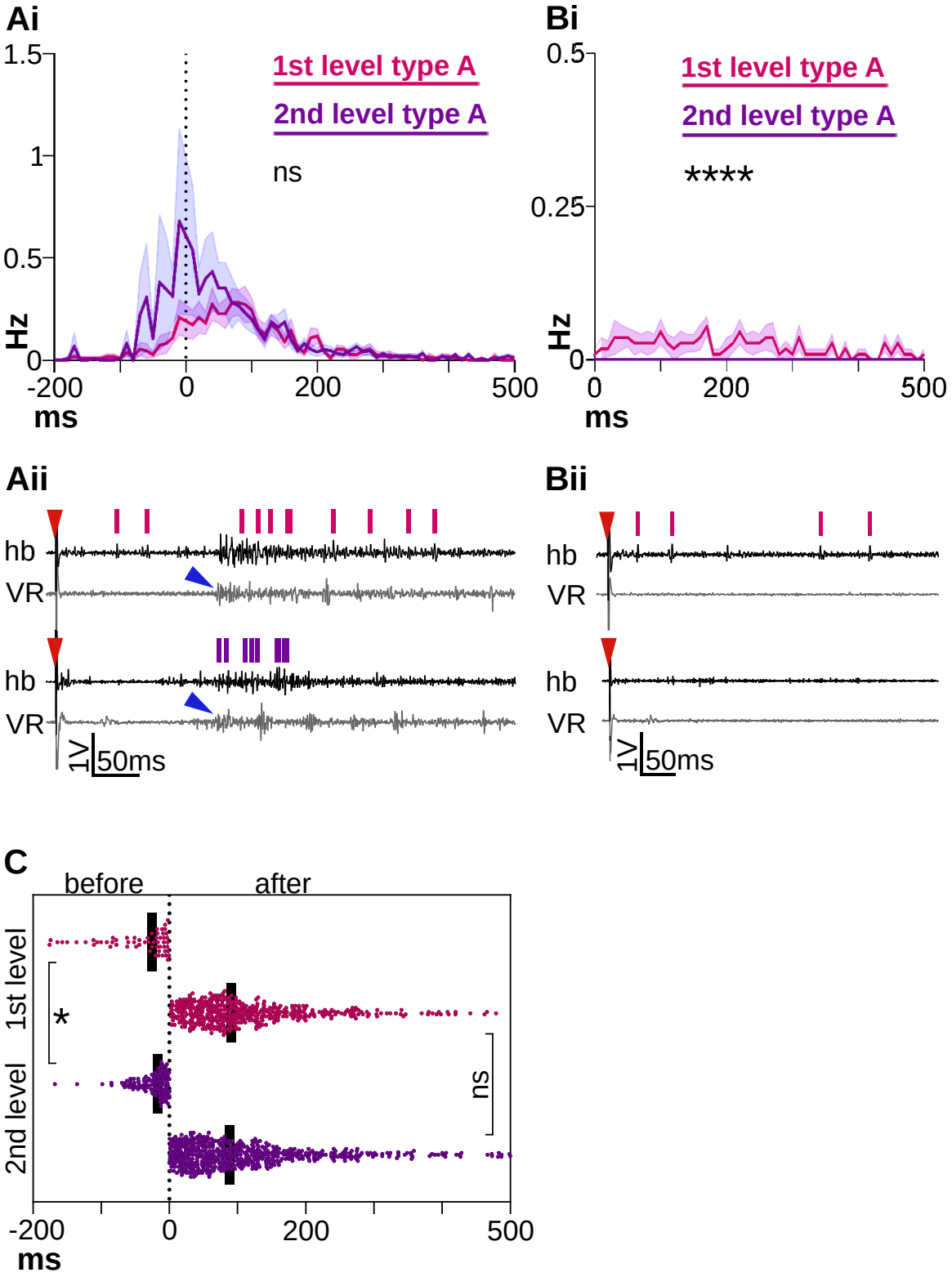

Figure 5.12 *(figure legend in the previous page)*

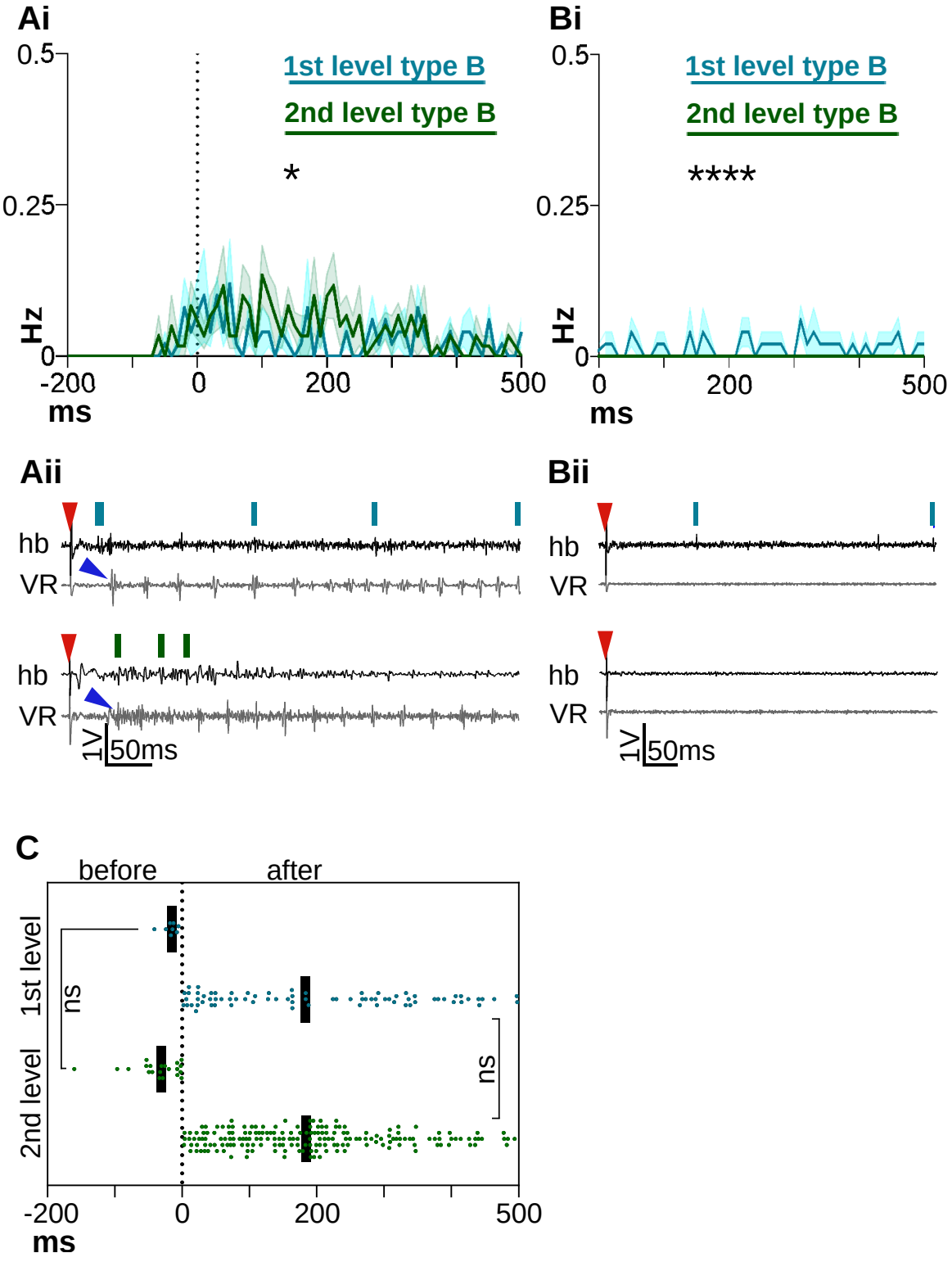

Figure 5.13 *(figure legend in the next page)*

Figure 5.13 Differential activation of subpopulations of Type B units.

Ai) *Firing rates of type B_1 (blue line) and type B_2 (green line) units recorded before movement initiation and in the first 500 ms of sustained swimming. Dotted grey line (ms=0) marks the start of fictive swimming. Data are presented as mean (solid lines) ± SEM (shaded area). Wilcoxon matched pairs signed rank test, p<0.0394; type B_1 units 0.0237 ± .0035, type B_2 units 0.0350 ± 0.0042 (mean ± SEM). Type B_1 units N=5, type B_2 units N=6; minimum 4 trials/unit. *p<0.05*

Aii) *Examples of spikes fired by one type B_1 unit (top trace, blue lines) and one type B_2 (bottom trace, green lines), recorded in the in the stimulation/start motor state. Spikes fired by the units are presented above the respective extracellular hindbrain recording raw trace (hb, black trace). Fictive swimming is shown by rhythmic VR bursts (grey trace, VR). For clarity, only the VR with the first burst, marking swimming initiation, is shown. Red arrowheads represent electrical stimulus; blue arrowhead indicates the start of swimming.*

Bi) *Firing rates of type B_1 (blue line) and type B_2 (green line) units recorded in the first 500 ms after stimulation. Data are presented as mean (solid lines) ± SEM (shaded area). Wilcoxon matched pairs signed rank test, p<0.0001; type B_1 units 0.0111 ± 0.0017, type B_2 units 0.0000 ± 0.0000 (mean ± SEM). Type B_1 units N=5, type B_2 units N=6; minimum 4 trials/unit. ****p<0.0001*

Bii) *Examples of spikes fired by one type B_1 (top trace, blue lines) and one type B_2 unit (bottom trace, no lines), recorded in the in the stimulation/no start motor state. Spikes fired by the units are presented above the respective extracellular hindbrain recording raw trace (hb, black trace). The absence of fictive swimming is shown by the silent VR (grey trace, VR). For clarity, only one VR is shown. Red arrowheads represent electrical stimulus.*

C) *Scatter plot of spikes fired by type B_1 (blue) and type B_2 units (green) before movement initiation and during the first 500 ms of sustained swimming. Dotted grey line (ms=0) marks the start of fictive swimming. Black solid lines indicate median values. Kolmogorov-Smirnov test on data recorded before swim initiation, p=0.1182; type B_1 units -15.65± 11.20 ms; type B_2 units -30.61 ± 38.49 ms (median ± SD). 8 spikes from 5 type B_1 units, 21 spikes from 6 type B_2 units. Kolmogorov-Smirnov test on data recorded after swim initiation, p=0.0803; type B_1 units 183.5 ± 152.7 ms; type B_2 units 183.9 ± 125.3ms (median ± SD). 75 spikes from 5 type B_1 units, 184 spikes from 6 type B_2 units.*

5.3 Discussion

Type A and B have ExNs features

The experiments reported in this chapter provide evidence for the presence of two novel populations, called type A and type B, which are involved in locomotor initiation in the hindbrain of the *Xenopus* tadpole. Type A and type B units were identified based on their firing pattern in response to trunk skin stimulation that caused (or not) swimming, and both types were shown to be associated with the initiation of swimming.

Although it has been demonstrated that other cellular populations fire at the initiation of swimming, the two novel neuronal types described here do not show firing patterns similar to the firing of known neurons. The ascending axons of primary and secondary pathway neurons (RB and dla/dlc cells, respectively) can reach the hindbrain (Roberts and Clarke, 1982, Clarke et al., 1984), but these neurons fire very briefly (one or two action potentials) immediately after the stimulus is delivered to the skin (Roberts and Clarke, 1982, Clarke et al., 1984). Moreover, dla and dlc neurons receive glycinergic inhibition from aINs during swimming, especially during its initial phase when swim frequency is higher (Li et al., 2002). For these reasons, it has been excluded that type A or type B activity could belong to the tadpole's sensory pathway as we know it.

It is also clear that type A and type B units do not show CPG-like activity, as they never fire rhythmically in phase with either the ipsilateral or contralateral VR bursts. Moreover, also differently from CPG neurons, the level 1 subpopulation of both type A and type B units (referred to as A_1 and B_1 units) fired when the stimulation delivered to the trunk skin did not lead to swimming initiations (subthreshold stimulation, 'stim/no start' trials). CPG neurons are activated only when and if the locomotor response is initiated, and no CPG firing is recorded if the stimulus is delivered at subthreshold intensities. Because of these differences, it has been excluded that neither type A nor type B units are part of the CPG circuit of the tadpole.

Type A and type B units showed the features proposed for ExNs (Koutsikou et al., 2018), which are: 1) firing activity in the time gap between stimulation and swimming initiation, 2) the ability to fire following threshold and subthreshold stimuli and 3) a firing pattern that is prolonged enough after stimulation to be able to sustain the activation of CPG in the early stages of swimming.

In the tadpole, the activation of dINs marks the initiation of swimming (Soffe et al., 2009). Intracellular recordings have previously shown an accumulation of excitation in single dINs following stimulation (Koutsikou et al., 2018), which will ultimately lead to the firing of the neuron and the activation of the dINs population through their electrical coupling (Li et al., 2009). From this moment onwards, the spinal CPG circuit is active and can self-sustain itself and thus the swimming behaviour (Li et al., 2009). However, when subthreshold stimulation is delivered to the tadpole's skin, dINs receive EPSPs that fail to trigger an action potential (Koutsikou et al., 2018). Type A and type B units show features that ideally place them presynaptically to dINs. Indeed, type A and B units 1) fire after stimulation and before swimming starts, 2) fire at variable latencies across experimental trials, possibly providing the accumulation of excitation reported in dINs, and 3) type A_1 and B_1 units fire following subthreshold stimulation, which will lead to fewer EPSPs in dINs that do not allow the cells to reach their firing threshold (Koutsikou et al., 2018).

The brain processes underlying simple decision making, such as how to decide when to initiate a movement, have been modelled as an accumulation of excitation in still-unknown brain areas of the mammal brain (Gold and Shadlen, 2007, Carpenter, 1999, Carpenter and Williams, 1995, Noorani and Carpenter, 2016). In particular, the LATER model has been proposed to explain the long and variable latencies prior the initiation of movement (the eye saccadic response is used in the model, (Carpenter, 1999, Carpenter and Williams, 1995, Noorani and Carpenter, 2016). Briefly, the authors ascribe the delayed motor response to an accumulation of signals in time, which ultimately lead to motor initiation. Altogether, the firing of type A and type B units in the *Xenopus* embryo can provide the accumulation of excitation over the time prior to swimming initiation, which is delayed after sensory stimulus detection (fig. 5.9A). Hence, the activity of these novel neuronal populations found in the embryonic stage of a lower vertebrate, recapitulate one established theory for motor decision-making in mammals (Svoboda and Li, 2018).

Proposed mechanism

In fig. 5.14, a supraspinal mechanism for descending motor control is illustrated, which includes the newly identified type A and B units, as well as their respective subpopulations, *i.e.* level 1 and level 2 units.

In the proposed hindbrain circuit, type A units work as sensory processors, being postsynaptic to the ascending sensory pathway neurons (dla and dlc). Instead, type B units are involved at a later stage, providing the necessary overall excitation to the dINs residing in the hindbrain. This 'dual stage' process is supported by the average spiking latency of type B units, which is longer than the latency for activation of type A units (fig. 5.9). The sensory information, initially detected in the skin by RB neurons, is carried to the hindbrain via the axons of dla and dlc neurons. Here, it is weighted and integrated by level 1 and 2 type A neurons (A_1 and A_2), which form the proposed sensory processing centre in the hindbrain of the tadpole. This is also in accordance with the computational model previously proposed to describe the ExNs population (Koutsikou et al., 2018). Indeed, in this model only some ExNs have direct connections with sensory pathway neurons, while the overall excitation of the ExNs population is achieved by interconnections among ExNs.

When the stimulus delivered is strong enough to evoke swimming (threshold stimulation, 'stimulation/start' trials), both type A_1 and type A_2 units are activated, and they excite type B_1 and B_2 units. Both subpopulations of type B units fire in response to a threshold stimulation, and they provide cumulative excitation to dINs in the hindbrain. The accumulation of excitation in the dINs allows them to reach their firing threshold, and ultimately to drive and sustain CPG activity during swimming (Koutsikou et al., 2018).

When the stimulus is delivered at subthreshold intensities ('stimulation/no start' trials), swimming response is not evoked. Nevertheless, type A_1 and type B_1 units are activated by dla and dlc neurons excitation; this is a unique feature of level 1 units, as type A_2 and type B_2 units do not fire following subthreshold skin stimulation. In these conditions, type A_1 and type B_1 units firing activity alone is not enough to cause the complete depolarisation of dINs, which will only show incoming EPSPs without reaching their firing threshold, thus not activating the CPG circuit of swimming. Difference in the electrical membrane properties of level 1 and 2 type A units could explain their firing patterns in response to threshold and subthreshold skin stimulation. In fact, different membrane properties can facilitate a more reliable firing activity in type A_1 population, whilst depolarisation in type A_2 population can be restrained to conditions of higher excitation. This will provide the hindbrain neuronal circuit with the means to discriminate between stimulus intensities. In this scenario, type A_1 and A_2 neurons will receive synaptic input from dlc and dla sensory neurons, even at subthreshold stimulation for swim initiation.

However, type A_2 neurons will not be activated because of their higher firing threshold. On the contrary, type A_1 neurons will fire at lower sensory stimulus intensities, and they will excite type B_1 neurons. However, this excitation will not be enough to support the accumulation of EPSPs in dINs necessary to reach their firing threshold, thus not allowing swim initiation.

A different firing likelihood for type A_1 and A_2 populations might also explain the slightly delayed firing of type A_2 units in the time before swimming initiation when a threshold stimulation is given to the trunk skin of the tadpole (fig. 5.12). In this case, sensory stimulation will activate both populations, but because of the higher firing threshold of type A_2 neurons, their firing onset will be slightly delayed compared to the activation of type A_1 neurons.

Potential role for inhibition

Work by Koyama and colleagues (Koyama et al., 2016) revealed how inhibition plays a vital role in ensuring the right execution of the startle response in the zebrafish. By means of whole cell recording and cell ablation, it has been demonstrated that a population of glycinergic neurons in the hindbrain, namely feedforward (FF) neurons, provide inhibition to the Mauthner cells, as well as to contralateral FF neurons (Koyama et al., 2016). Interestingly, each FF neuron connects to both Mauthner cells, with more synapses onto the contralateral one (Koyama et al., 2016). These FF neurons fire in response to a variety of sensory stimulation, and they have been demonstrated to drive the laterality of the start of swimming, *i.e.* on which side the first bend of the body will happen, thus taking part in a simple decision-making circuit, the decision being which side of the body will bend first (Koyama et al., 2016). It has been proposed that the circuit formed by inhibition of FF and of Mauthner cells works as a network motif, where mutual inhibition, together with lateral inhibition, provides the basis for a behavioural choice (whether the right or left side will bend first) in the zebrafish (Koyama et al., 2016, Koyama and Pujala, 2018), but also can account for multi-choice selection in more complex behaviour. In fact, GABAergic neurons in the midbrain have been proven to direct the switch-like response in the optic tectum, by a feedback inhibitory mechanism (Knudsen, 2011).

Although Mauthner neurons have not been reported to drive the slow and variable response to a skin stimulus in the *Xenopus* tadpole, there is the possibility that inhibition plays a role in the mechanism of motor initiation. Indeed, with the experimental procedures described in this chapter, the option that the recorded extracellular activity is of inhibitory type cannot be

completely ruled out. One other aspect to take into account is that the electrical activity recorded in the experiments presented here might be produced by passing contralateral axons, whose cell bodies might lie on the opposite side of the hindbrain. Based on the studies in zebrafish, it seems plausible that inhibition might play a role in the mechanism of locomotor control in the tadpole, and might contribute to the long delay between stimulation and the initiation of swimming.

Novel neuronal population hindbrain location

Although it is not possible to precisely locate the neurons somata in extracellular recording experiments, type B activity was mostly recorded in the caudal sector of the hindbrain, whilst type A activity was more dispersed along the longitudinal axis of the hindbrain (fig.5.3). This anatomical layout might partially reflect the function of the two neuronal populations: type A units will excite, and thus control, type B units, which in turn lie close enough to the dINs in the caudal part of the hindbrain, from where they project their descending axons into the spinal cord to drive CPG excitation.

5.4 Conclusion

The extracellular recording experiments presented in this chapter identified putative neuronal populations, which lie in the hindbrain of the tadpole and that show features previously indicated for the ExNs. Briefly, these features are 1) firing before the initiation of swimming, 2) firing both at threshold and at subthreshold stimulation, and 3) firing over a time that allows the activation of dINs. However, firing activity recorded extracellularly does not allow the precise location of these units' cell bodies, as electrical activity might have been recorded from other neuronal compartments, such from axonal projections running close to the tip of the electrode. Hence, the next chapters of this work are aimed to anatomically localise putative ExNs in the hindbrain of the tadpole.

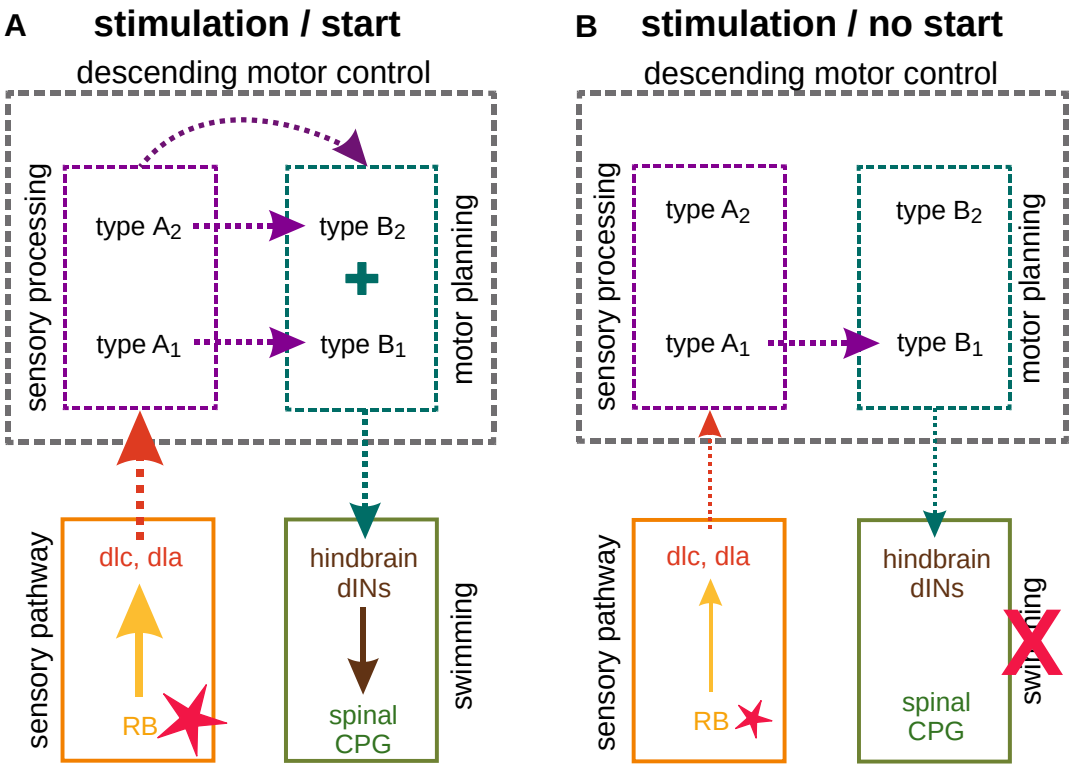

Figure 5.14 Proposed neural mechanism for motor descending control.

A) *Scheme of the proposed neural circuit active when a suprathreshold stimulus is delivered to the tadpole (stimulation/start). Solid arrows represent known synaptic connections, solid line boxes indicate known circuits (sensory pathway and swimming). Dotted arrows and boxes represent proposed connections and circuits in the hindbrain (sensory processing, motor planning, descending motor control). A higher firing rate in the various synaptic connections is represented by thicker arrows, compared to the same arrows in B. Red star represents stimulation that is strong enough to lead to swim initiation.*

B) *Scheme of the proposed neural circuit active when a subthreshold stimulus is delivered to the tadpole (stimulation/no start). Solid arrows represent known synaptic connections, solid line boxes indicate known circuits (sensory pathway and swimming). Dotted arrows and boxes represent proposed connections and circuits in the hindbrain (sensory processing, motor planning, descending motor control). A lower firing rate in the various synaptic connections is represented by thinner arrows, compared to the same arrows in B. Red star represents a weaker stimulation than in A, which does not lead to swim initiation. Red 'X' indicates that the tadpole does not start to swim.*

6 Results: Calcium Imaging Analysis of Hindbrain Neurons

The experiments reported in this chapter were carried out in in Dr. Wenchang Li's lab at the University of St Andrews (UK). In order to localise the ExNs identified by means of extracellular recordings (chapter 5), calcium imaging was employed. This technique allows to monitor fictive swimming while calcium transients in hindbrain neurons can be imaged through a high-resolution camera. Ideally, the neuronal activation following trunk skin stimulation defined for type A and type B units via extracellular recordings (in chapter 5) should be reproduced in these imaging experiments by a similar pattern of calcium transients detected in putative ExNs. This would provide a visual clue of the ExNs location in the hindbrain.

6.1 Materials and Methods

Animals

Tadpoles were obtained from the *Xenopus laevis* colony raised at the Institute of Psychology and Neuroscience (University of St Andrews). Briefly, mating was induced in pairs of adult *Xenopus laevis* by injection of human chorionic gonadotropin hormone (HCG, Sigma Aldrich; concentration used: 1000 U/mL in sterile water) into the dorsal lymph sacs. Embryos were raised in treated tap water at a temperature range of 17-20° C, and used for experiments at developmental stage 37/38 (Nieuwkoop and Faber, 1956).

Procedures for HCG injections were carried out in compliance with UK Home Office regulations; all experimental procedures performed on tadpoles were approved by the Animal Welfare Ethics Committee (AWEC) of the University of St Andrews.

Samples preparation

Tadpoles at developmental stage 37/38 were briefly anesthetised in MS-222 (Sigma Aldrich) dissolved in saline solution. The skin covering trunk muscles was removed and the animals were incubated for 50 minutes in α-bungarotoxin (Invitrogen) at RT. After immobilisation, tadpoles were pinned to a rotating Sylgard block in a dissection dish and surgery to expose the more ventral area of the hindbrain was performed with fine homemade tungsten needles. Firstly, the

skin covering the hindbrain and the rostral spinal cord was removed. The more dorsal brain tissue, consisting mostly of ependymal cells, was removed along the midline, causing the opening of the two sides of the hindbrain in the same fashion of the pages in a book. This procedure allows the exposure of the ventral portions of the brain and rostral spinal cord, where CPG interneurons lie. Tadpoles with exposed neurons were then incubated in a solution of Fluo-4 AM (Invitrogen) for 20 minutes at RT in the dark. The dye solution was prepared by dissolving 50 µg of Fluo-4 AM (Invitrogen) in 50 µL 20% Pluronic F-127 solution in DMSO (Invitrogen). 5 µL aliquots of this solutions were stored at -20°C, defrosted on the day of use, and diluted in 0.5 mL of fresh saline (final concentration of Fluo-4 AM 5 µM). After dye penetration, the tadpole was washed in fresh saline for 5 minutes at RT in the dark.

Imaging and fictive swimming recording

Calcium activity was imaged under an optic microscope (Olympus BX51WI) equipped with a 20X water immersion objective and a GFP filter. Blue light (λ=470 nm) used to excite the dye was transmitted to the sample from a LED light source (coolLED pE-2 excitation system, CoolLED, USA) at 100% intensity. Imaging was carried out with a Neos 5.5 high resolution camera (Andor, Oxford Instruments, UK) and image acquisition was performed in Solis software (Andor, Oxford Instruments, UK). The camera and the LED light source were automatically triggered by a sequence of pulses driven by an experimental protocol designed in Signal 6 (CED, Cambridge, UK). Specifically, the camera was set to record over a time of 5 seconds (at 10 Hz), starting 1.5 s before stimulation and recording for the 3.5 s following stimulation.

One skin stimulating suction electrode was positioned on the right side of the tadpole's body at the level of the anus and electrical pulses in the range of 50-400 µA were delivered to the animals through a current generator (DS3 Isolated current generator, Digitimer, UK). Threshold stimulation was set in each experiment as the lowest current intensity to initiate swimming after one pulse. Because no changes in fluorescence were detected after one pulse stimulation (even when it led to swim initiation), trains of 15 or 30 pulses at threshold intensity were used. Fictive swimming was monitored via suction electrode attached to the trunk muscle cleft, and data were acquired through a Power 1401 mkII (CED, UK) in Signal 6 (CED, UK) at a sampling rate of 10000 Hz. Electrodes were made from borosilicate glass capillaries (outer diameter=1.2 mm, inner diameter=0.94 mm; Warner Instruments, USA) whose tip opening measured ~60 µm.

Data analysis

Imaging of Calcium transient were acquired in Solis (Andor, Oxford Instruments, UK) and analysed in ImageJ. Background fluorescence was obtained from five ROIs placed in areas without fluorescence signal, and used to normalise fluorescence in ROIs. Briefly, mean values of the five background ROIs in each imaging frame was subtracted from the fluorescence of single ROI in the respective frame. Final analyses on fluorescence dynamics were performed on the adjusted values (ROI fluorescence – mean background fluorescence in the same frame). Changes in fluorescence signal were calculated on the adjusted values of each ROI using the formula $\Delta F/F = (F_{peak}-F_{rest})/F_{rest}$, where:

- F_{rest} is the average fluorescence signal in the five consecutive control frames before stimulation, when the tadpole was in resting condition
- F_{peak} is the average fluorescence signal in the consecutive frames that showed higher fluorescence intensity values. Because fluorescence intensity usually lasted for more than 1-2 seconds, the intensity values of a maximum of 20 consecutive frames were averaged to obtain the F_{peak}. Frames were considered to have peak intensity, and thus used to calculate the F_{peak}, if their fluorescence signal was higher than the value of fluorescence at rest, plus twice the standard deviation ($F_{peak} > F_{rest} + 2SD$). Peak fluorescence signals were always found after stimulation, and the numbers of frames with peak intensity values ranged from 14 to 20. Only in one case peak intensity was found in 4 frames.

Fluorescence changes ($\Delta F/F$) were then transformed into percentage values. Thus, the final number representing increase of signal is given as a percentage of the baseline signal. Data plotted in the graphs are intensity values normalised on the average intensity at rest (F_{rest}).

6.2 Results

A total number of 33 animals were used for calcium imaging experiments. In each animal a number of cells between 7 and 25 were detected in the hindbrain through fluorescence signal, resulting in a total number of 192 cells. Because of the very low probability of detecting cells responding to a one-pulse stimulation, trains of 15 or 30 pulses at threshold intensity were used. Stronger stimulation leads to a higher level of excitation in the sensory neurons that reach the brain, and ideally to higher probability of detecting cells that are activated in the hindbrain. Moreover, repeated stimulation often leads to struggling instead of swimming; during struggling

more CPG neurons are activated, and they fire in bursts (Li et al., 2007). This stronger activation could help with the detection of weak fluorescence transients. Although repetitive stimulation was used, most of the cells analysed (94.3%, 181/192) did not show changes in fluorescence after electrical stimulation which led to the initiation of swimming.

In total, 11 cells (5.7% of total N of cells, 11/192) in 7 different animals were found to change fluorescence intensity after stimulation which initiate swimming (fig. 6.1). Four neurons in three animals increased their fluorescence intensity after one pulse stimulation (fig. 6.1 A, ΔF/F= +84.37%, +50.03%, +48.61%, +96.98%, for cell 1, 2, 3 and 4 respectively). The remaining 8 neurons which showed increased signal were detected after a train of 15 pulses (4 neurons, fig. 6.1 B; ΔF/F= +54.33%, +86.36%, +19.46%, +112.67% for cell 5, 6, 7 and 8, respectively) or 30 pulses (3 neurons, fig. 6.1 C; ΔF/F= +39.97%, +105.92%, 134.34% for cell 9, 10 and 11, respectively).

The cells that were activated by one-pulse stimulation reached their peak intensity after 2.55 (cell 1), 2.35 (cell 2), 3.5 (cell 3) and 2.6 (cell 4) seconds from stimulation (fig.6.1 D). Neurons that were activated by a 15-pulses stimulation reached their peak fluorescence signal 1.9, 1.5, 2.3 and 1.8 seconds (cell 5, 6, 7 and 8, respectively) after the start of the pulse train. Lastly, cells that increased their fluorescence intensity after a 30-pulse stimulation did so at 1.6, 0.9 and 1 seconds (cell 9, 10 and 11, respectively) from the start of the stimulation. The timing of peaks fluorescence recorded in neurons activated by different stimulation were different (fig. 6.1 D, p=0.0034, one-way ANOVA); cells that responded to a one pulse stimulation did so with longer latency from stimulation than neurons that responded to 15 and to 30 pulses stimulation (Tukey's multiple comparisons test, one pulse stimulation *vs* 15 pulses stimulation: p=0.0431, mean difference= +0.8750 s; one-pulse stimulation *vs* 30 pulses stimulation: p=0.0028, mean difference= +1.583 s; one pulse stimulation: 2.750 ± 0.256 s; 15 pulses stimulation: 1.875 ± 0.165 s; 30 pulses stimulation: 1.167 ± 0.219 s; data reported as mean ± SEM). On the contrary, cells that responded to 15 pulses stimulation showed a latency to the fluorescence peak comparable to cells that were activated by 30 pulses stimulation (Tukey's multiple comparisons test, 15 pulses stimulation *vs* 30 pulses stimulation: p=0.1227, mean difference= +0.708 s; data reported as mean ± SEM).

The four neurons that responded to a one-pulse stimulation did so with different timing patterns. Cell 1 and 2 showed a more rapid increase in fluorescence signal (cell 1= 1.88 at the

start of the peak, 2.55 s from stimulation; cell 2= 1.549 at the start of the peak, 2.35 s from stimulation; normalized fluorescence values are reported), while cell 3 was activated more slowly (1.516 at the start of the peak, 3.5 s from stimulation). Cell 4 showed a higher activation than cell 3, but that was slower than cell 1 and 2 (1.87 at the start of the peak, 2.6 s from stimulation). Three of the neurons that responded to a 15-pulses stimulation showed similar patterns of activation, (cell 5= 1.50 at the start of the peak, 1.9 s from stimulation; cell 6= 1.79 at the start of the peak, 1.5 s from stimulation; cell 8= 2.00 at the start of the peak, 1.8 s from stimulation). Cell 7 showed a smaller increase of fluorescence signal (1.19 at the start of the peak, 2.3 s from stimulation). Lastly, the neurons that responded to a 30-pulses stimulation were activated more abruptly than what was observed with weaker stimulation (cell 9= 1.516 at the start of the peak, 1.6 s from stimulation; cell 10= 1.87 at the start of the peak, 0.9 s from stimulation; cell 11= 1.95 at the start of the peak, 1 s from stimulation).

Once the neurons were activated by one or 15-pulses stimulation, they kept an overall higher fluorescence signal during swimming (fig. 6.1 B). Differently, after the 30-pulses stimulation that activated cells 9,10 and 11, swimming started but stopped 2.2 seconds after stimulation (fig. 6.1 C, VR trace in red). At the same time, the fluorescence signal recorded in the neurons showed a decay in the fluorescence signal as swimming stopped.

Neurons that increased their fluorescence signal after skin stimulation were found dispersed in the hindbrain, without showing any localization pattern along the rostro-caudal axis. Cells that responded to one stimulation pulse were found in the central and caudal areas of the hindbrain (cells 3 and 4 central location, cell 2 caudal location). The neurons that responded to a 15 pulses stimulus were localized in the caudal and rostral hindbrain (caudal location: cells 5,6 and 8; rostral location: cell 7). The neurons that responded to a 30 pulses stimulation (cells 9, 10 and 11) were found in the rostro-central area of the hindbrain.

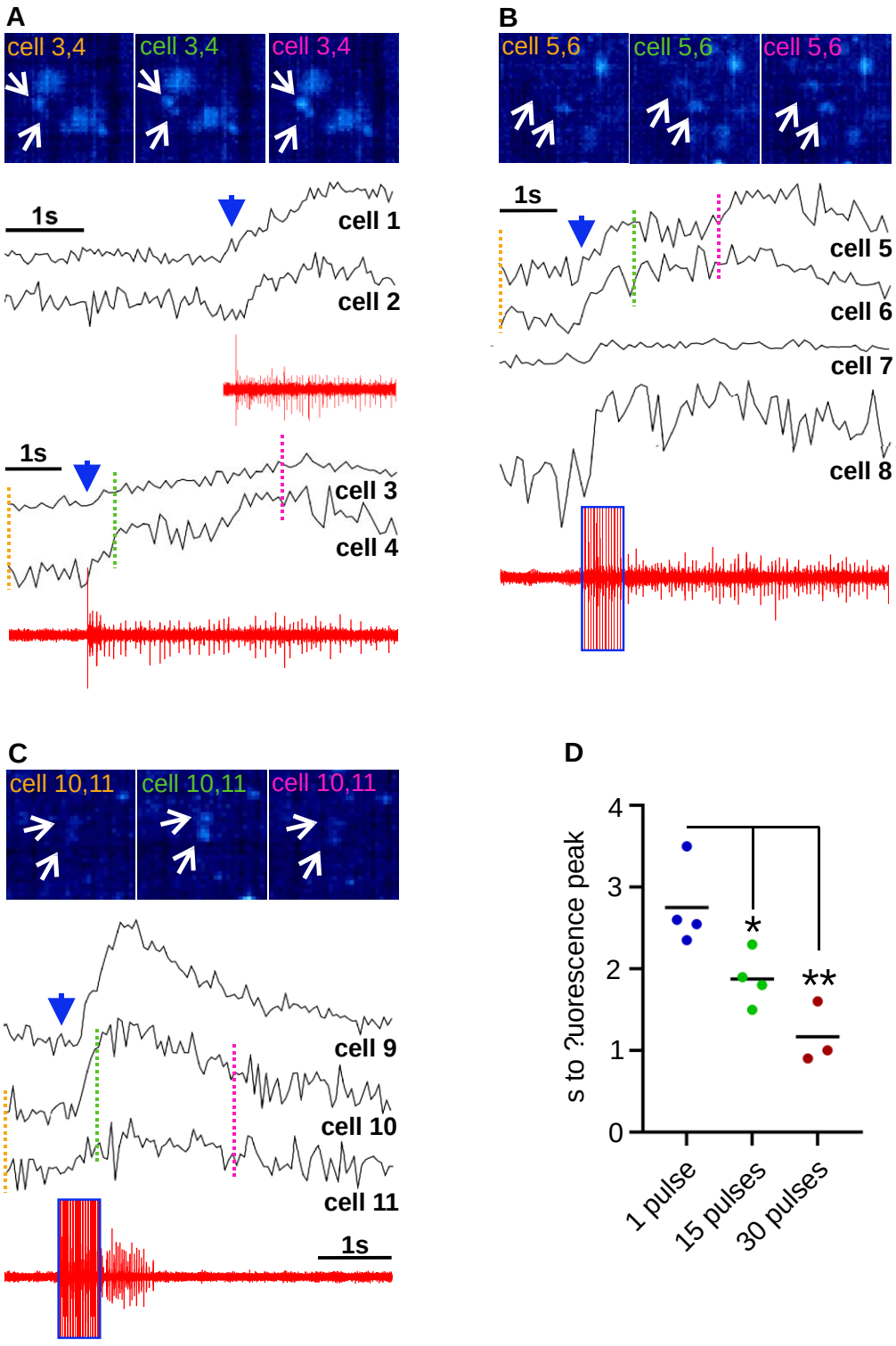

Figure 6.1 Cellular activation after different stimulation detected with calcium imaging.

A) *cells activated by a one-pulse stimulation to the trunk skin. Calcium traces are reported for each cell above the respective VR recording (trace in red). Top panel: examples of cells (white arrows) that increased their fluorescent signal after stimulation, the time when the images were*

captured is indicated with coloured lines on the respective calcium traces (yellow, green and pink dashed lines). Blue arrowheads indicate the time of stimulation.

***B)** cells activated by a 15-pulses stimulation to the trunk skin. Calcium traces are reported for each cell above the respective VR recording (trace in red). Top panel: examples of cells (white arrows) that increased their fluorescent signal after stimulation, the time when the images were captured is indicated with coloured lines on the respective calcium traces (yellow, green and pink dashed lines). Blue arrowhead indicates the start of stimulation, blue box on the VR trace indicates the duration of stimulation.*

***C)** cells activated by a 30-pulses stimulation to the trunk skin. Calcium traces are reported for each cell above the respective VR recording (trace in red). Top panel: examples of cells (white arrows) that increased their fluorescent signal after stimulation, the time when the images were captured is indicated with coloured lines on the respective calcium traces (yellow, green and pink dashed lines). Blue arrowhead indicates the start of stimulation, blue box on the VR trace indicates the duration of stimulation.*

D) Scatter plot of the time from stimulation to peak of fluorescence for cells presented in A, B and C, depending on the type of stimulation received (one, 15 or 30 pulses electrical stimulation). One-way ANOVA, p= 0.003, Tukey's multiple comparisons test: one-pulse vs 15-pulses, p= 0.043, mean difference= 0.8750 s; one-pulse vs 30 pulses stimulation: p=0.0028, mean difference= 1.583 s; 15-pulses vs 30-pulses stimulation p=0.127, mean difference=0.708):

6.3 Discussion

Although the aim of the calcium imaging experiments was to localize putative ExNs based on the activation patterns described in chapter 5, it was not possible to duly stick to this initial scope. This was due to technical difficulties in the sample preparation and in the detection of fluorescence signal. Explanation for both these aspects is given below.

In order to get access to the more ventral neurons, where cells like dINs lie, which have been shown to be activated at swimming initiation (Soffe et al., 2009), the medio-dorsal hindbrain tissue had to be cut and removed. This procedure has been long used to get access to CPG neurons in the hindbrain and in the spinal cord for intracellular recording experiments, and motor response has never been reported to fail after this type of surgery. Normal swimming pattern was recorded in the experiments reported here, so it can be assumed that the CPG circuit was not damaged. Nevertheless, because there are no clues on the position along the dorso-ventral axis of ExNs, it cannot be excluded *a priori* that ExNs were not removed from the preparation or that their axonal projections were severed during surgery. On the other hand, since ependymal cells cover the surface of the hindbrain, the surface of the neurons lying deeper in the brain tissue needed to be exposed to allow the penetration of the Fluo 4AM dye. Overall, even if the chance of removing, or damaging, ExNs was considerably high, the only option for seeing fluorescent signal in neurons seemed to be to remove the medio-dorsal portion of the hindbrain.

The neuronal activation observed in calcium transients was also affected by issues in the detection of changes in fluorescence signal. Although quite a good number of cells seemed to have been permeated by the fluorophore, most of the neurons did not change their fluorescent signal after stimulation. This led to the experimental choice of delivering trains of 30 or 15 pulses to increase the chance of activation, as more excitation in the sensory pathway should be translated into more excitation in hindbrain neurons, thus more activation in more neurons. Stronger stimulation led to swimming initiation, but did not significantly increase the chance of detecting calcium transients in the hindbrain.

Considering the experimental conditions described above, it was not possible to reliably test neurons' activation after a subthreshold stimulation, which is one of the most important features of ExNs. Moreover, because the fluorophore's signal was quickly bleached after one or

two recordings under the blue light used at 100% of intensity, no accurate comparisons coul be made on the same cells responding to different stimulation intensity.

Altogether, it cannot be confirmed that the neurons found to be activated by the different types of stimulation are ExNs. Nevertheless, the pattern of activation might be similar, to certain extent, to that of ExNs, which are activated at swimming initiation. In chapter 5, it has been shown that the ExNs type A population is active only at the start of locomotion, whilst type B population was active during ongoing swimming. The same pattern detected in type B units has been observed after stimulation in the calcium imaging experiments reported here. However, because of the unavailability of a reliable subthreshold stimulation, it cannot be excluded that the neurons activated after stimulation, and that remained active during swimming, are instead CPG neurons. Indeed, CPG neurons are only active during swimming, *i.e.* after a threshold stimulation. Moreover, the main feature that would discriminate between CPG and type B ExNs is the rhythmicity of firing, present in the former and absent in the latter (see chapter 5, fig. 5.7, 5.8). Since the calcium dynamics are slow compared to the quick synaptic activation, the rhythmic firing that is hallmark of CPG neurons could not be detected with this experimental set up.

Neurons activated by a 30-pulse stimulation resemble sensory neurons because of their quick increase in fluorescent signal (fig. 6.1 C). However, because in this experimental trial swimming activity did not last more than 2.2 seconds, it is possible that the decay in fluorescence signal was due to the stopping of motor activity. In this case, there is the possibility that these cells are instead CPG neurons.

Different times of cellular activation have been recorded in neurons responding to different stimulation. Neurons responded quicker to a train of impulse than to a single electrical pulse. In order to discuss these differences, it needs to be taken into consideration that the responding neurons most probably belong to different neuronal populations (see above). That being said, it has previously been shown ((Zhao et al., 1998) and chapter 4 of this work) that tadpoles respond to stronger stimulation with a quicker motor response. The faster activation observed in the experiments reported here indicates that neurons in the tadpole's hindbrain not only can distinguish from a threshold and a suprathreshold stimulation (as observed in chapter 4, fig 4.6), but can also adjust their firing to diverse strength of the stimulus delivered.

Note

Genetically modified tadpoles expressing fluorescent calcium indicator can be used to overcome the issue of low signal detection and quick fluorescence bleaching. In transgenic tadpoles expressing fluorescent GCaMP, the fluorescent signal originates directly from the binding of calcium to the endogenously expressed protein, which will emit green fluorescence when the cell is activated. Unfortunately, such transgenic line was not available at the time when the experiments were carried out, so this solution could not be tested.

7 Results: Anatomical Study of Hindbrain Neuronal Populations

In the previous chapters, evidence for the ExN population to be spread/dispersed along the rostro-caudal axis of the hindbrain have been shown. In lesions experiments (chapter 4), both commissural connections in the hindbrain itself and descending projections to the spinal cord were severed, giving rise to changes in the latency, variability and side preference of motor response. The possibility of ExNs to be spread in the hindbrain has been confirmed by multi-unit extracellular recordings reported in chapter 5, where two main populations of ExNs have been described.

Because of technical issues, Ca^{2++} imaging experiments (chapter 6) did not provide data which are reliable enough to locate ExNs within the hindbrain. In this chapter, immunohistochemistry (IHC) staining has been carried out on the CNS of the *Xenopus* tadpole, in order to identify possible locations for ExNs, the neuronal population thought to 'fill the gap' between the ascending sensory pathway neurons and dINs.

As the molecular identity of the ExNs population is not known, it was not possible to target these cells specifically. In the attempt to find plausible locations for ExNs, which will need to lie in areas where they can be contacted by sensory pathway neurons and have post synaptic connections with descending neurons, IHC staining of markers for different neuronal types were carried out. GABAergic and serotoninergic populations are known to be involved in the stopping pathway (Perrins et al., 2002) and in the process of accelerating ongoing swimming (Sillar et al., 1992), respectively. Both populations were stained in the brain and spinal cord of the *Xenopus* embryo. The expression of the transcription factor Chx10, known to be expressed by locomotion-driving neurons in other species, was also imaged in the tadpole nervous system.

7.1 Materials and Methods

Animal care

Fertilized *Xenopus laevis* eggs were purchased from EXRC (Portsmouth, UK) and raised as described in the 'Materials and Methods' section of Chapter 3. All experiments were carried out on tadpole at developmental stage 37/38 (Nieuwkoop and Faber, 1956).

Sample preparation

Tadpoles at 37/38 developmental stage were briefly anesthetized in MS-222 and fixed in 4% PFA solution in PBS. Fixation was carried out overnight at 4°C. Tadpoles were then washed three times for 20 minutes in PBST (PBS, 0.05% Triton X-100, Sigma Aldrich) on agitation. Following, samples were incubated in a 15% fish gelatin/15% sucrose solution in PBS, overnight at 4°C (gelatin from cold water fish skin, Sigma Aldrich). *Xenopus* embryos were then embedded in the same fish gelatin/sucrose solution. Small (10 x 10 x 5 mm) plastic biopsy molds (Tissue-Tek Cryomold, Sakura) were used to create solid frozen blocks to be cut with a cryostat. One tadpole was positioned in the centre of each gelatin-filled mold; plastic molds were then gradually submerged into a mixture of ethanol and dry ice, to ensure deep freezing of the samples. 20 µm-thick slices were cut from gelatin blocks with a cryostat (Leica CM1950) at a temperature of -20°C. Samples orientation was checked under a light microscope and tissue slices were collected on microscope adhesion slides (Superfrost plus adhesion slides, VWR). Samples were stored at -20°C up to one month.

IHC staining

Slices stored at -20°C were left on bench at RT for roughly 10 minutes to allow tissue to warm up and condensation to dry. Glass slides were then baked at 80°C for 15 minutes on a heat block, in order to re-activate the slide's adhesion mechanism. After allowing the samples to cool down (roughly 10 minutes at RT), slides were submerged into pure acetone for 10 minutes and let dry on bench for 15 minutes. A ring was drawn around the tissue slices with hydrophobic ink pen (Super Pap pen, Agar Scientific, UK) and let dry. Tissue slices were rehydrated with PBS for one hour at RT, and then blocked in 5% BSA (Bovine Serum Albumin Fraction V, Sigma Aldrich) in PBST for one hour at RT.

Primary antibodies were diluted accordingly to table 5.1 in 5% BSA in PBST, and 250/300 µL (depending on the number of tissue slices) of antibody solution were gently placed on the slide. Incubation was carried out over night at 4°C in a non-sealed plastic box lined with wet tissue

paper to avoid drying. Before proceeding with secondary antibody incubation, samples were washed three times for 15 minutes with PBST, on slow agitation. Secondary fluorescent antibodies were diluted accordingly to table X in 5% BSA in PBST. Samples were incubated for one hour at RT in a non-sealed plastic box lined with wet tissue paper. Subsequently, samples were kept in the dark and washed three times for 15 minutes with PBST on slow agitation. After washing, glass slides were carefully dried from drops of PBS, two or three drops (roughly 30 µL) of DAPI-containing mounting media (UltraCruz aqueous mounting media with DAPI, Santa Cruz Biotechnology) were placed on the slides with a micropipette to avoid overloading, and a glass cover slip (rectangular cover glass, VWR) was placed on top. Commercially available nail polish was used to seal the cover slip, and slides were stored in the dark at 4°C until imaging.

All the solutions and procedures described above were adapted and optimised from (Zhang et al., 2016). When available, references for primary antibodies are reported in table 5.1. Of note, because primary and secondary antibodies concentrations were tested and optimised, final conditions of use differ from the ones reported in the references.

Table 5.1 Primary and Secondary Antibodies used in IHC protocols

Target	Primary antibody (catalogue number, company)	Primary antibody dilution	Primary antibody reference	Secondary antibody (catalogue number, company)	Secondary antibody dilution
Chx10	CHX10 polyclonal antibody, bs-6621R, Bioss Antibodies	1:100	--	goat anti-rabbit Alexa Fluor 488, A-11034, Invitrogen	1:100
GABA	anti-GABA antibody, A2052, Sigma Aldrich	1:500	(Viczian et al., 2009)	goat anti-rabbit Alexa Fluor 488, A-11034, Invitrogen	1:500
Serotonin	5-HT (Serotonin) antibody, 20080, Immunostar	1:250	--	goat anti-rabbit Alexa Fluor 488, A-11034, Invitrogen	1:100
TPH	Anti-Tryptophan Hydroxylase antibody, AB1541, Merck Millipore	1:100	(Demarque and Spitzer, 2010)	donkey anti-sheep Alexa Fluor 546, A-21098 Invitrogen	1:100
vGAT	Vesicular GABA Transporter (VGAT) antibody, 2100-VGAT, Phosphosolutions	1:100	(Santos et al., 2018)	goat anti-rabbit Alexa Fluor 594, A-11012 Invitrogen	1:100

Confocal imaging

Images were acquired under a confocal microscope (Zeiss LSM880, AxioObserver), and lasers were selected according to the secondary antibody excitation wavelength (GABA and Chx10, λ=488nm; vGAT, λ=594 nm; TPH, λ=561 nm). Nuclear DAPI staining was imaged at a wavelength of 405 nm. Either a 20x air objective or a 63x oil-immersion objectives was used (Zeiss Plan-Apochromat 20X/0.8 M27 and Plan-Apochromat 63x/1.4 Oil Dic M27, respectively). Image acquisition was carried out in Zen Black software suite (Zeiss).

Data Analysis

Images reconstruction, Z stacks alignment and correction were carried out in Zen Lite (Zeiss). Subsequent images analyses were carried out in ImageJ. Rough depth measurements were calculated by counting the number of tissue slices (20 µm thick) from the first most dorsal slice where brain was visible. Graphs were plotted in GraphPad Prism (version 8) and statistical analyses were also performed in GraphPad Prism Data were tested for normality with Shapiro-Wilk test and when normality criteria were not met, non-parametric analysis was used. Significance level was set at $p<0.05$ for all tests used.

7.2 Results

7.2.1 GABaergic Population

IHC staining for GABA revealed two symmetrical populations in the hindbrain, previously known with the name of MHRs (midhindbrain interneurons, (Boothby and Roberts, 1992, Lambert et al., 2004a)). MHRs have been proven to be involved in the stopping pathway following head touch, as well as in the maintenance of tonic inhibition during periods of attachment through the cement gland (Lambert et al., 2004a, Lambert et al., 2004b). As previously described, the more rostral population lies in the second and third rhombomeres, on both sides of the hindbrain (fig.7.1 A-C), while the more caudal population is found in the sixth and seventh rhombomeres, reaching the level of the second muscle cleft (fig.7.1 A-C).

Both populations appear 40 µm (in dorso-ventral direction) from the dorsal surface of the hindbrain and, while the rostral GABAergic population is present in sections covering tissue for 120 µm, the more caudal population is detectable in a 60 µm thick tissue (fig. 7.1, 7.2 A). This

layout recapitulates well the anatomical shape of the hindbrain, which is thicker in the rostral area, but it narrows (both in dorso-ventral and in medio-lateral direction) towards the obex to join the spinal cord. The GABAergic neurons found in the more rostral populations are shifted towards the midline as the sections are taken more ventrally, and as the lateral space is occupied by GABA positive thick bundles of neuronal projections (fig. 7.1 C,D).

Both populations lie laterally, with cells growing from the outer borders of the hindbrain and enlarging their somata towards the midline (fig. 7.2, B, C). The hindbrain GABAergic cells showed a median cell size of 76.11 μm^2 (IQR=69.08 μm^2, N=105 cells in two animals) and are mostly round shaped, with their median perpendicular axis length being 11.71 µm ('height', measured from the exit point of the axon to the opposite cell border, IQR=5.93 µm) and 8.40 µm ('width', measured at centre of the cell, perpendicular to the height measurement, IQR=2.59 µm) (fig. 7.3 A).

An additional neuronal population stained for GABA was found in the ventral area of the midbrain (fig. 7.1 D-H). As the ones in the hindbrain, the midbrain population is symmetrical and lie laterally. The more dorsal cells appear 80 µm from the dorsal surface of the brain (fig. 7.1, 7.2 A) and occupy the midbrain till the very ventral portion. Although the midbrain and rostral hindbrain GABAergic neurons become close to each other, the somata never come into contact, leaving them as two distinct populations. The midbrain GABAergic cells have a more elongated shape (height= 16.28, 8.61 µm, width= 8.69, 2.83 µm; data reported as median and IQR, N=38 cells in two animals), and they are larger (108.5, 44.30 μm^2; median and IQR) than the GABAergic neurons residing in the hindbrain (fig. 7.3 C, median dfference= 32.41 μm^2; $p<0.0001$, two-tailed Mann-Whitney test). On average, the midbrain population lies at the same distance from the bundle of projections that run on the sides if compared to the distance of the hindbrain population from the lateral borders (fig. 7.3 D, hindbrain population *vs* midbrain population: 16.76, 15.45 µm *vs* 19.20, 21.65 µm; data reported as median and IQR, median difference= 2.45 µm; $p=0.078$, two-tailed Mann-Whitney test).

Staining against the vesicular transporter for GABA (vGAT) revealed that continuous projections leave the hindbrain on both sides and run caudally into the spinal cord, where they lie in the marginal zone (fig. 7.4). These descending projections are tightened in ipsilateral bundles and do not cross to the opposite side in the spinal cord (fig. 7.4 G). Conversely, projections stained for vGAT cross to the opposite side in the ventral sections of the hindbrain, where they form a

broad network (fig. 7.4 H, I; 37.63 ± 6.65 µm along the rostro-caudal axis, 108.60 ± 7.95 µm along left-right direction, data reported as mean ± SEM, 6 consecutive images in dorso-ventral direction, one animal). Rostrally, vGAT-positive neuronal projections cross to the opposite side in one thin bundle that occupies 40 µm (dorso-ventral axis) running along the rostral border of the midbrain (fig. 7.4 E, F; two consecutive images in dorso-caudal direction, one animal, projections cross-sections 2.90 µm in the more dorsal slice, 1.65 µm in the more ventral slice).

(next page)

Figure 7.1 IHC staining of GABAergic neurons

A-H) *Confocal images of longitudinal sections of one tadpole stained for GABA (in green), reported in dorso-ventral order (A=most dorsal, H=most ventral). Nuclear staining with DAPI is in blue. Dashed white lines in A-G indicate MHB; dashed white line in H indicates hindbrain borders. White arrows indicate GABAergic population in the midbrain and hindbrain. oc= otic capsule.*

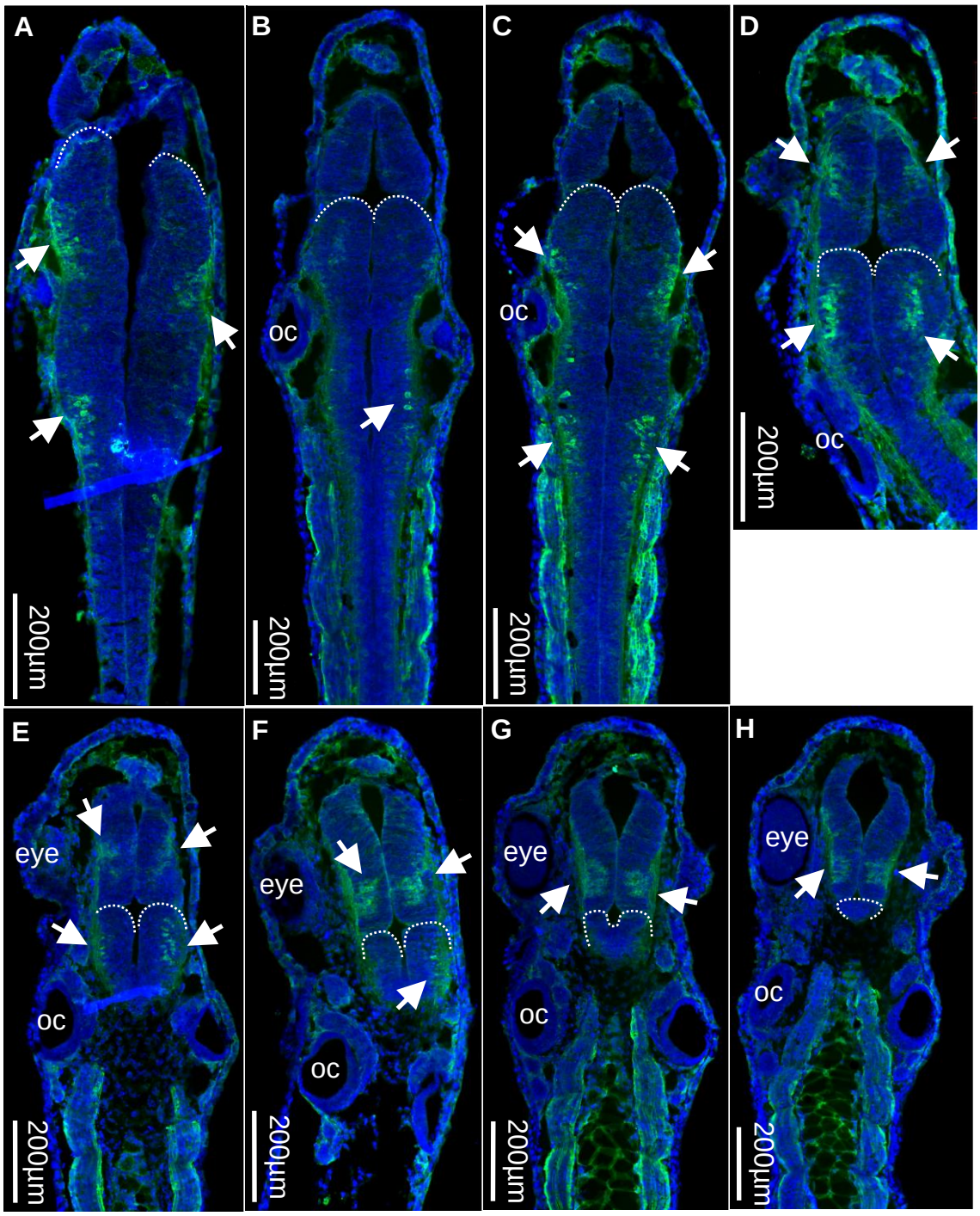

Fig. 7.1 *(figure legend in the previous page)*

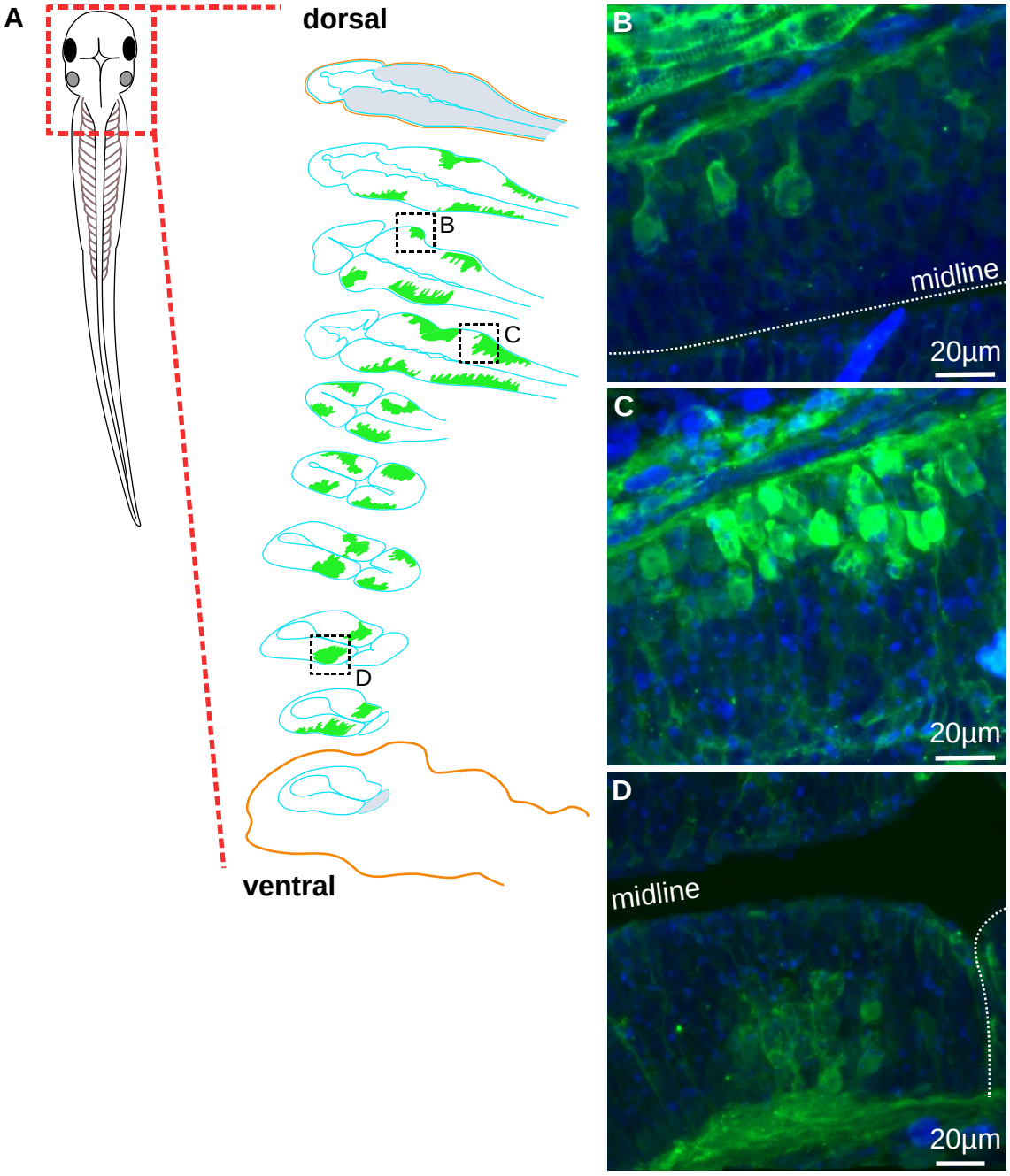

Figure 7.2 Localization of GABAergic populations in the tadpole's brain.

A) *Schematic of GABAergic populations locations in the brain along the dorso-ventral axis. As reference, the hindbrain is reported in grey shade in the top and bottom slice. GABAergic populations are reported in green; brain borders are in blue; skin is reported as orange lines in top and bottom slice as reference.*

B-D) *Confocal images of areas indicated by dashed black square in A. 15 to 20 Z-stacks (1 µm each) were aligned and overlapped at maximum intensity. Dashed white line in B indicates midline; white dashed line in D indicate the MHB.*

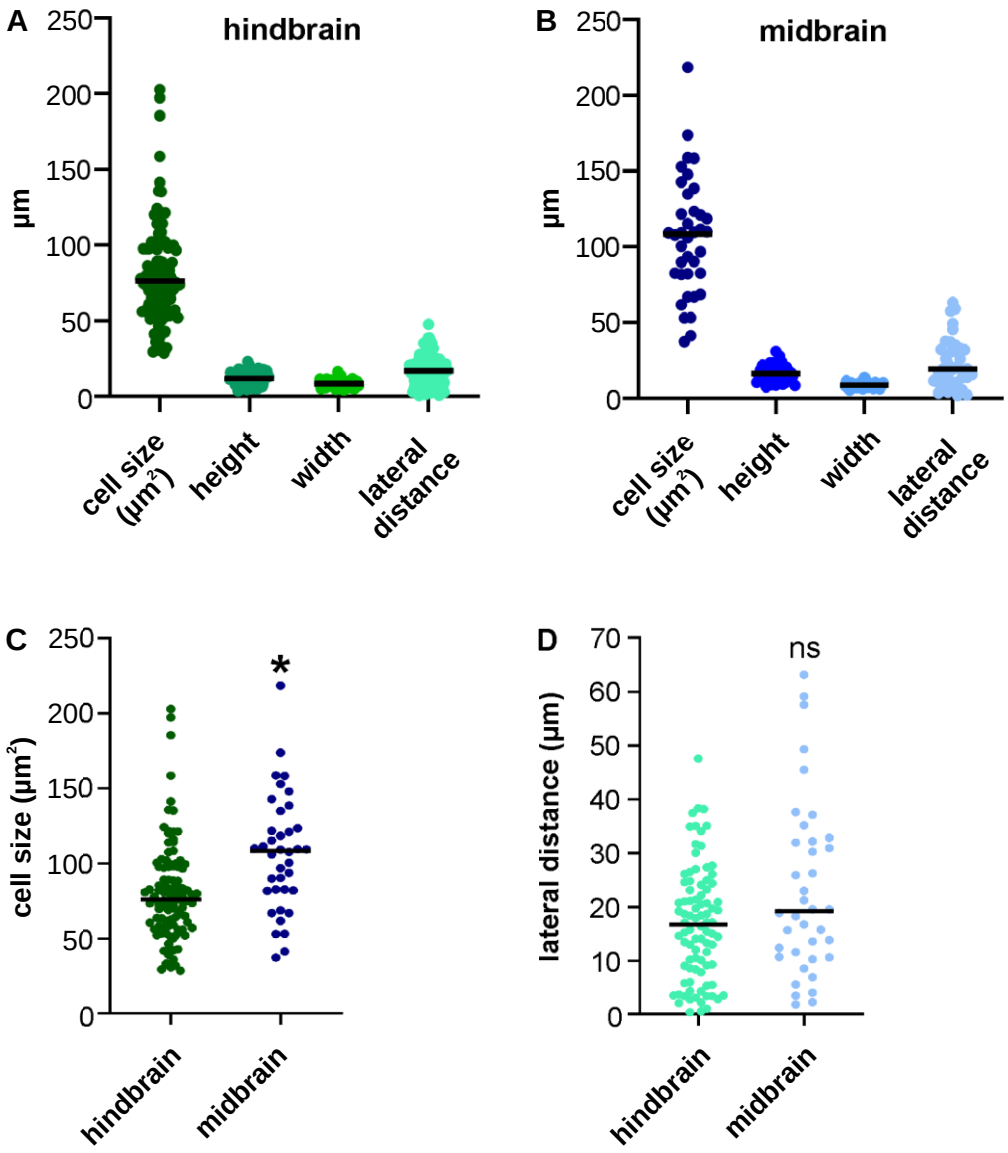

Figure 7.3 Anatomical features of GABA-positive cells in the hindbrain and midbrain.
A,B) *Scatter plot of measurement of cell size, height, width and lateral distance of cells stained against GABA in the hindbrain (A) and midbrain (B). Single cell measurements are reported, transverse black lines indicate* the median.
C) *Scatter plot of measurement of cells size in the hindbrain (green) and midbrain (blue) cells stained against GABA. Mann-Whitney test, two tailed p<0.0001; median difference= 32.41 µm². Single cell measurements are reported in the graph, transverse black lines indicate the median.*
D) *Scatter plot of measurement of lateral distance of cells stained against GABA in hindbrain (green) and midbrain (blue). Mann-Whitney test, two-tailed p=0.078; median difference= 2.45 µm. Single cell measurements are reported, transverse black lines indicate median.*

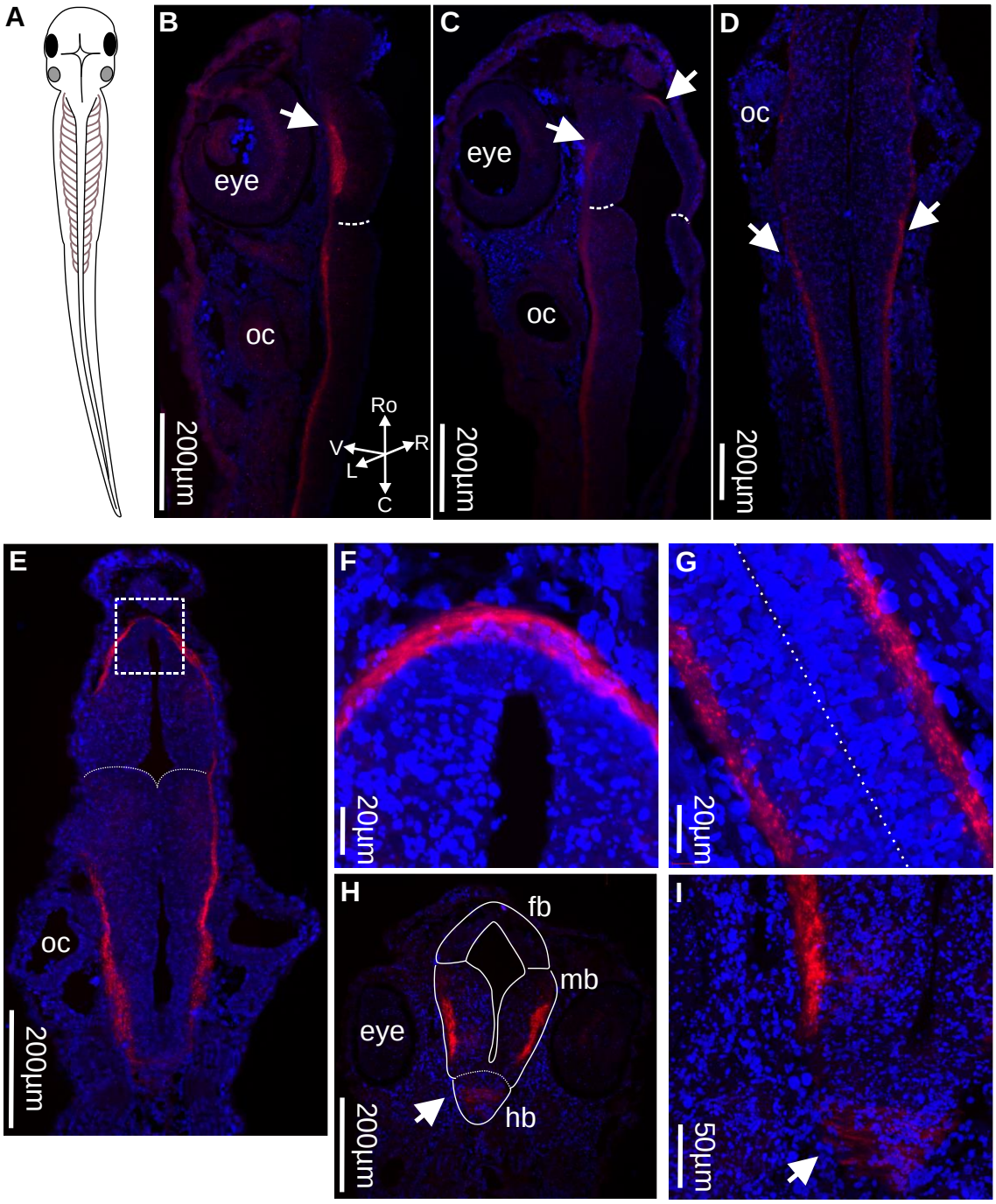

Figure 7.4 IHC staining of vGAT.

A) *Schematic of the tadpole's orientation presented in the confocal images in D-I.*

B-D) *Confocal images of longitudinal sections of one tadpole stained for vGAT (in magenta), nuclear staining with DAPI is in blue. Dashed white lines indicate MHB. White arrows indicate vGAT-positive projections in the midbrain that run caudally in the hindbrain and spinal cord. Axis orientation in B refers to C as well (Ro=rostral, C=caudal, D=dorsal, V=ventral, L=left, R=right). oc= otic capsule.*

E-F) *Images of hindbrain and midbrain stained against vGAT (in magenta), nuclear staining with DAPI is in blue. Dashed white lines in E indicate MHB. Dashed white square in E is enlarged in F. F) vGAT-positive projections running along the rostral tip of the midbrain.*
G) *vGAT-positive projections (in magenta) running continuously in the marginal zone of the spinal cord. Dashed white line indicates the spinal cord midline.*
H-I) *Images of the ventral brain with neuronal projections stained against vGAT, forebrain (fb), midbrain (mb) and hindbrain (hb) are indicated with white lines. Dashed line indicates the MHB, white arrow indicates the area enlarged in I. I) Ventral section of the hindbrain where a broad commissural network of projections stained for vGAT is present (white arrow).*

7.2.1.1 Discussion

Confirmation of known GABAergic populations

The two symmetrical GABAergic populations detected in the hindbrain were identified in early anatomical studies (Roberts et al., 1975), and were later found to be responsible for the stopping of swimming when a pressure is delivered to the head of the tadpoles, as well as for the tonic inhibition of spinal CPG neurons when the cement gland is stimulated (Boothby and Roberts, 1992, Lambert et al., 2004a, Lambert et al., 2004b). Descending projections stained for vGAT run along the two sides of the hindbrain and into the spinal cord, without commissural spinal connections. This anatomical layout suggests that descending and continuous GABAergic bundles make synaptic contact with CPG neurons in the spinal cord, and by inhibiting their rhythmic firing, they can stop swimming (Lambert et al., 2004a, Lambert et al., 2004b). In the brain, vGAT projections are visible in the same location where somata of GABAergic neurons have been detected (fig. 7.1, 7.4), suggesting that the source of GABAergic projections reported in the spinal cord are the GABAergic neurons found in the hindbrain. However, it is not possible to rule out that the midbrain GABAergic population also sends projections in the spinal cord. In fact, the vGAT-stained bundles are formed by single neuronal projections that could not be clearly resolved to the level of single axons or dendrites (fig. 7.4 F as an example). Moreover, ipsilateral projections are reported along the brain both in the midbrain and in the hindbrain, so it is possible that GABAergic neurons in the midbrain have the same role of inhibition over spinal neurons demonstrated for the hindbrain population.

It is worth noting that vGAT is a vesicular transporter that loads not only GABA into neurostransmitter vesicles, but also glycine (Chaudhry et al., 1998). Thus, because cINs and aINs

are glycinergic neurons that lie in the spinal cord of the tadpole lie, the ipsilateral projections found in the spinal cord can be the axons of ipsilateral aINs, which inhibit sensory pathway and other CPG neurons during swimming (Li et al., 2001). On the other hand, cINs have commissural axons. In vGAT staining experiments reported here, commissural axons are not visible in the spinal cord. This could be due to the fact that single axons are too thin to be detected under the 63x objective used for imaging the samples, or that cINs axons in the tadpole do not contain the vGAT protein. The latter explanation is unlikely, as cINs have been repetitively proven to use glycine as neurotransmitter (Soffe, 1989, Yoshida et al., 1998), and as the glycinergic transporter GlyT1 and GlyT2 both act at presynaptic sites, where they reuptake glycine into synaptic vesicles (Liu et al., 1993), thus vGAT remains the protein needed to load GABA into vesicles in other cellular compartments. Experiments of *in situ* hybridization (Wester et al., 2008) against *GlyT2*, *Gad67* (glutamate decarboxylase, used as GABAergic neurons marker) and *vGat* revealed that, in the spinal cord of the *Xenopus* tadpole at hatching stages, cells co-express either *vGat* and *Gad67* transcripts, or *vGat* and *GlyT2* transcripts. However, a high percentage of *vGat*-positive cells, co-expressed also *Gad67* and *GlyT2* transcripts. The authors (Wester et al., 2008) suggested that in the embryonic spinal cord, glycinergic and GABAergic neuronal fates are not solidly established yet, and that the same neurons could use both neurotransmitters simultaneously. So far, inhibitory CPG neurons that are active during swimming have been shown to use only glycine as a neurotransmitter (Li et al., 2001). Also, with the experimental protocols used here, no GABA staining was detected in the spinal cord (fig. 7.1 A-D). For this reason, it seems reasonable to suggest that the vGAT-stained projections in the spinal can be ipsilateral axons of aINs and contralateral axons of cINs. Nevertheless, MHR neurons have been reported to have axons that reach up to the 16th segment in the spinal cord (Perrins et al., 2002), hence it is safe to suggest that at least some of the spinal projections stained for vGAT originate from the more caudal GABAergic population in the hindbrain.

The GABAergic network is in an ideal position for connections to hdINs and possibly ExNs

In the most ventral area of the hindbrain, a broad network of vGAT-positive projections has been detected, and it seems plausible to suggest that these are descending and commissural axons of the hindbrain GABAergic population. Although it is not possible to completely rule out that vGAT-stained cross-connections in the caudal hindbrain are axons growing from glycinergic cINs, this possibility seems unlikely. In fact, the commissural axons of cINs cross the midline in the

spinal cord, at very short distance from their somata, and then they run longitudinally in the marginal zone (Dale et al., 1986, Roberts et al., 1988, Yoshida et al., 1998).

In the tadpole, reticulospinal neurons (also called hdINs) lie in the caudal part of the hindbrain, and they have both descending and ascending axons (Soffe et al., 2009, Li et al., 2006). Their descending axons are instrumental for activating and sustaining the firing of spinal CPG neurons. It has been shown that the GABAergic hindbrain population (MHR) inhibits CPG neurons via the MHRs' descending axons, which are both contralateral and ipsilateral (Boothby and Roberts, 1992, Perrins et al., 2002, Li et al., 2003). This inhibition is activated not only during the stopping pathway (*i.e.* when the tadpole bumps into a solid object with its head), but also it also occurs during tonic inhibition (*i.e.* when the tadpole lies still attached with the cement gland) (Lambert et al., 2004a, Lambert et al., 2004b). The broad network of vGAT-positive crossing projections found in the ventral-caudal hindbrain is located in a position functional for connecting to hdINs, which can be reliably inhibited, thus stopping, or preventing, locomotion on both sides of the tadpole's body.

It has been shown that ExNs are dispersed in the hindbrain, and probably have commissural and ipsilateral projections. Thus, it is possible that ExNs come in contact with the broad network of vGAT-positive inhibitory projections in the ventral area of the hindbrain, so that ExNs would receive tonic inhibition from MHR, as well as the inhibitory signal necessary for the stopping pathway. In this hypothetical scenario, when sensory stimulation reaches the brain via the sensory pathway, ExNs could be in a state of tonic inhibition and the sensory excitation would need to be stronger to elicit firing. Further investigation is needed to decipher a possible role of ExNs within the inhibitory pathway.

The midbrain GABAergic population

The population of GABA-positive neurons found in the midbrain has been reported in early anatomical studies (Roberts et al., 1975) but has not been connected to motor behaviour in the tadpole at stage 37/38. This midbrain population has slightly larger cells than the hindbrain population, and vGAT projections, starting from the same location of these GABAergic neurons, run both caudally and rostrally along the border of the midbrain (7.4 F-H). Caudal projections form a continuous bilateral bundle with the vGAT-positive projections originating from the MHRs. From the staining presented here, it is not possible to detect where the projections originating in the midbrain stop, and where the ones growing from MHRs start.

The midbrain of the tadpole starts to develop into the optic tectum at stage 37/38, when the retinal ganglion cells (RGC) have elongated enough to reach the tectal area (Grant et al., 1980, Holt and Harris, 1983 , Holt, 1984). During this process, GABA has been shown to promote the growth of neurons in the optic tract (Ferguson and McFarlane, 2002). A developmental study on the GABAergic population in the midbrain from stage 42 to stage 47 has shown that these neurons move from a clustered lateral position to a medial dispersed location as the brain undergoes a massive enlargement (Miraucourt et al., 2012). GABA-positive neurons have also been found in the retina of stage 42 tadpoles, contrary to the IHC staining reported here on stage 37/38 tadpoles (Holt, 1984, Miraucourt et al., 2012). This is a further confirmation of the unavailability of visual information to the tadpole's brain at the developmental stage used in this work. When the visual system has completely developed to be functional (stage 47), the tadpole can perform avoidance response when it detects a looming object (Dong et al., 2009, Khakhalin et al., 2014, Gambrill et al., 2016). The avoidance response consists in turning the head and swimming away in a direction opposite to the looming stimulus (Dong et al., 2009, Khakhalin et al., 2014). By studying this behaviour, it has been shown that the GABAergic component of the optic tract is needed to regulate and maintain the excitatory transmission of visual information (Lien et al., 2006, Richards et al., 2010).

Therefore, considering that a functional visual pathway is not developed yet, there is no evidence that the GABAergic population in the midbrain has a role in the initiation of motor response in the tadpole at stage 37/38. However, axons of a few dla and dlc neurons lying in the spinal cord can pass through the hindbrain and reach the midbrain and forebrain (Li et al., 2001). It is possible that the inhibitory populations stained in these experiments are migrating towards the midline and in later stages of development will give rise to a functional optic tract as described above. In this case the sensory information carried by spinal ascending projections could be integrated with visual stimuli in the more developed midbrain.

7.2.2 Serotoninergic Population

Primary antibody against tryptophan hydroxylase (TPH) was used to visualize serotoninergic cells in CNS of the tadpole. TPH is an enzyme involved in the synthesis of serotonin, widely used as a marker for serotoninergic neurons. Only one population of serotoninergic neurons was found in the tadpole's brain, lying in the more ventral area of the hindbrain. Serotoninergic neurons have been previously detected in the *Xenopus* embryo (van Mier et al., 1986), and they have been linked to the increase in swimming rhythm at later larval stages (Sillar et al., 1992).

The IHC staining presented here confirms the presence of a TPH positive neuronal population, found in the ventral areas of the hindbrain (fig. 7.5). This population is formed by two symmetrical clusters of cells which lie laterally at the sides of the hindbrain, at the level of first, second and rostral-third rhombomeres, where they occupy roughly 100 µm along the dorso-ventral axis (fig. 7.5 A, B-F). Although they are very rostral in the hindbrain, TPH-stained cells were never found in the midbrain (fig. 7.5 A, B-F). In the same way, no TPH positive somata could be seen in the spinal cord. TPH-positive neurons lie mostly aligned in three/four rows stacked together (fig. 7.5 G-I), they have a cell size of 143.60 μm^2 (median, IQR=75.9, N=80 cells in two animals) and their shape is elongated (height= 18.04, 5.44 µm; width= 10.74, 2.90 µm; data reported as median and IQR, N=80 cells in two animals, fig. 7.6 A). The lateral position of TPH positive somata changes slightly along the dorsal-ventral direction. The more dorsal TPH-positive neurons have longer axons and can reach more medial location, while the more ventral neurons have shorter axons and lie very close to the hindbrain sides (fig. 7.5 G, H and I; 'long axons cells' lateral distance= 20.81, 19.35 µm, N=17 cells; 'short axon cells' lateral distance= 6.51, 6.30 µm, N=48 cells; data reported as median and IQR; $p<0.0001$ Mann-Whitney test, two tailed, median difference= 14.29 µm, fig. 7.6 B). Although some of the more elongated cells reach in proximity of the midline, no commissural projections were detected.

Because TPH antibody marks only the cell bodies, a primary antibody against serotonin was used to confirm that the same neurons have axons descending in the spinal cord. Indeed, a population with the same features and localization of the neurons marked with antibody against TPH was found in the hindbrain (fig. 7.7). The antibody against serotonin also stained neuronal projections, which confirmed that serotoninergic neurons send ipsilateral descending axons into the rostral spinal cord (fig. 7.7 B). Ipsilateral ascending projections were also detected to reach more rostral area of the hindbrain, stopping at the MHB (fig. 7.7).

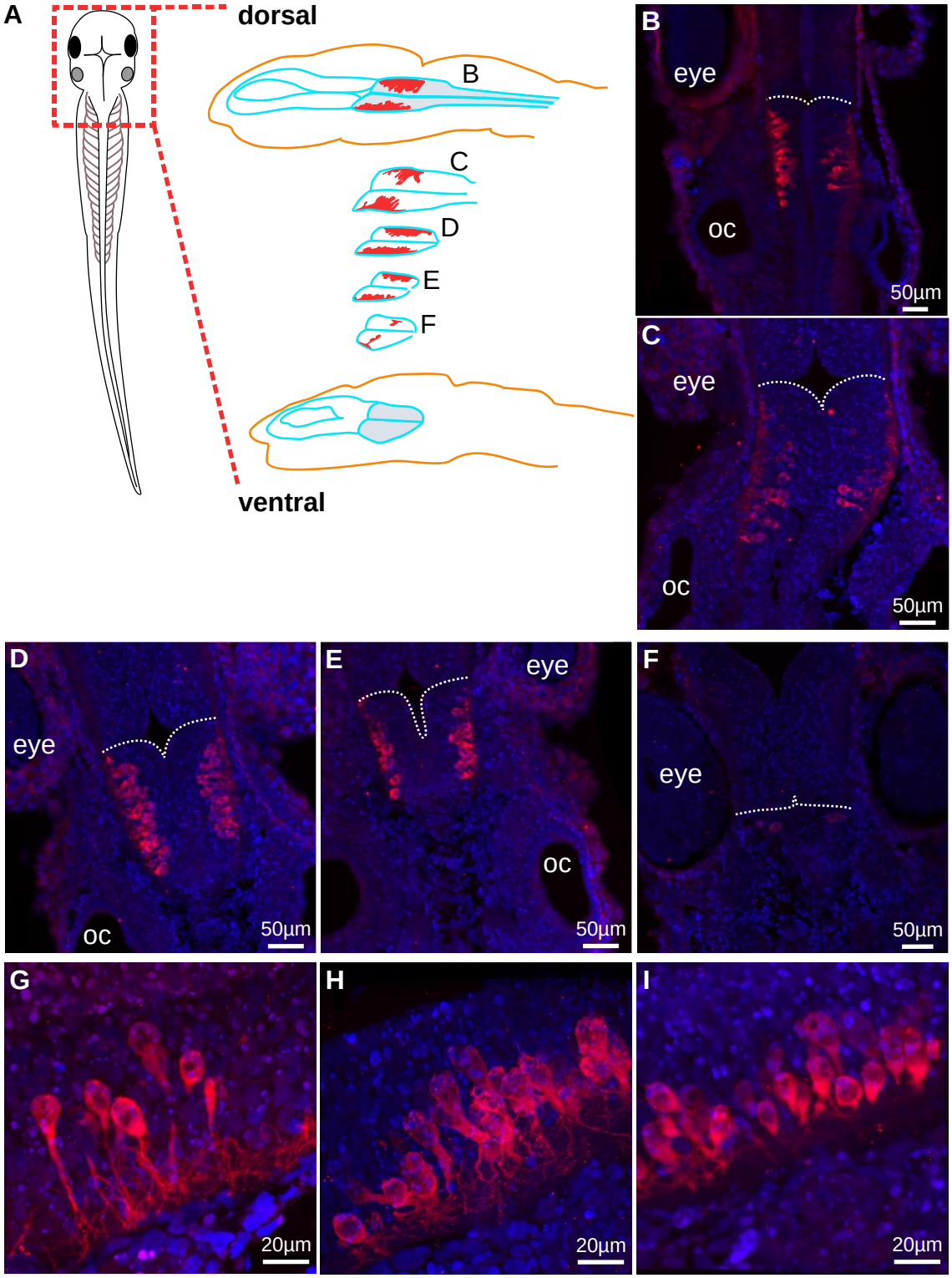

Figure 7.5 Localization of TPH-positive population in the tadpole's hindbrain.

A) *Schematic of TPH-positive population locations in the brain along the dorso-ventral axis. As reference, the hindbrain is reported in grey shade in the top and bottom slice. TPH-positive*

population is reported in red; brain borders are in blue; skin is reported as orange lines in top and bottom slice as reference.

B-F) *Confocal images of TPH-positive neurons (in magenta) in the hindbrain, dorso-ventral order indicated by the B-F letters in A. Nuclear staining with DAPI is in blue. Dashed white lines indicate the MHB, oc=otic capsule.*

G-I) *Examples of TPH-positive neurons in the hindbrain. 15 to 20 Z-stacks (1 µm each) were aligned and overlapped at maximum intensity. Nuclear staining with DAPI is in blue.*

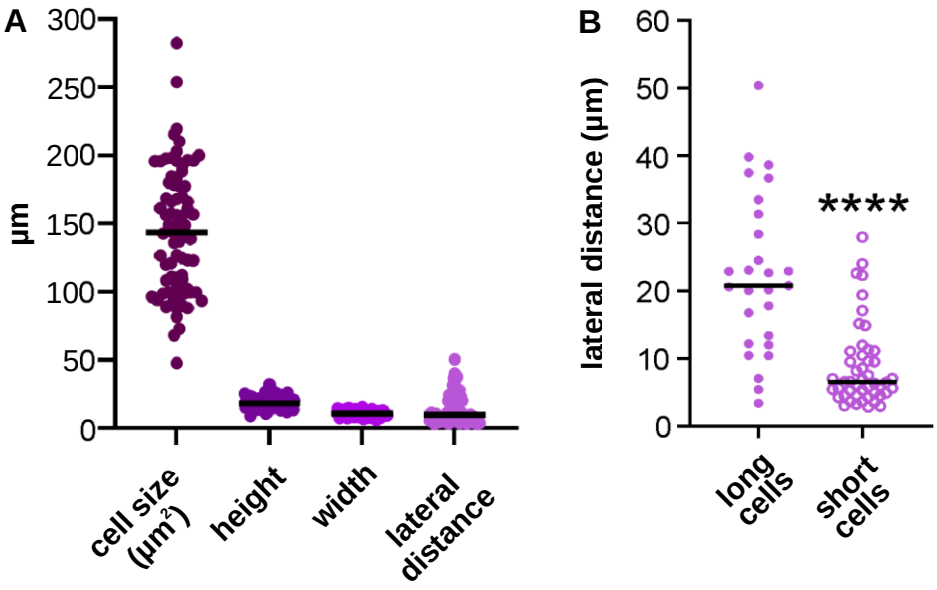

Figure 7.6 Anatomical features of TPH-positive cells in the hindbrain.

A) *Scatter plot of measurement of cell size, height, width and lateral distance of cells stained against TPH. N= 80 cells, cell size= 143.60, 75.9 µm^2, height=18.04, 5.44 µm, width= 10.74, 2.90 µm, lateral distance= 9.63, 15.16 (median and IQR). Single cell measurements are reported, transverse black lines indicate median.*

B) *Scatter plot of measurement of lateral distance of cells stained against TPH. Mann-Whitney test, two-tailed long vs short cells p<0.0001; median difference= 14.29 µm; long cells N=17, 20.81, 19.35 µm; short cells N=48, 6.51, 6.30 µm µm (data reported as median and IQR). Single cell measurements are reported, transverse black lines indicate median.*

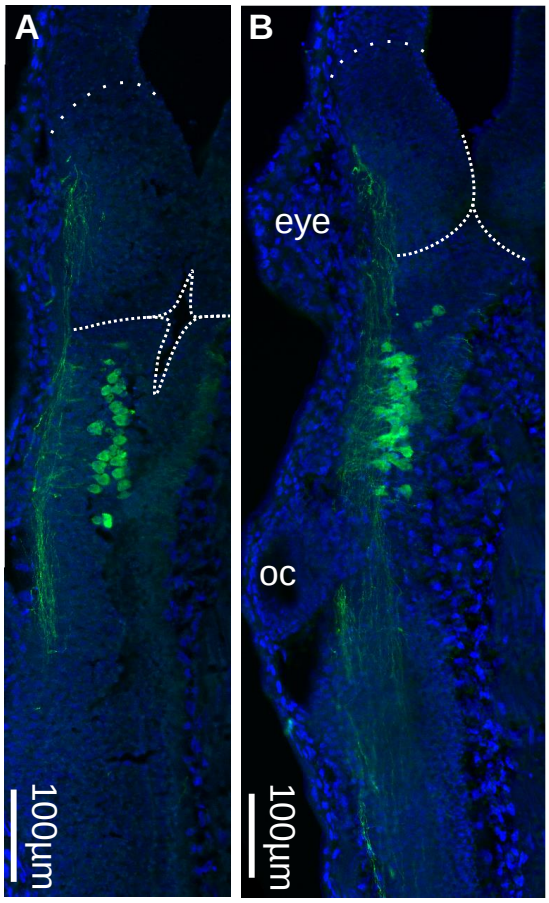

Figure 7.7 Localization of serotoninergic population in the tadpole's hindbrain.
A-B) *Confocal images of hindbrain neurons and neuronal projections stained against serotonin (in green). Cell bodies lie at the same level as TPH-positive population in fig. 7.5, projections run rostrally into the midbrain and caudally into the spinal cord. A dorsal section, B ventral section. Nuclear staining with DAPI is in blue. Dashed white lines indicate the MHB, dotted white lines indicate the border between midbrain and forebrain. oc=otic capsule.*

7.2.2.1 Discussion

The serotoninergic population in the tadpole's hindbrain has been previously reported to appear with a small number of cells at stage 28; they then grow in number at stage 32 and at this stage, their descending axons reach the caudal hindbrain till the more rostral segment of the spinal cord (van Mier et al., 1986). At later larval stages, the hindbrain serotoninergic populations send ipsilateral axons in the spinal cord, which reach the level of the anus (van Mier et al., 1986, Sillar et al., 1992, González et al., 1994). At larval stage 40, serotonin has been demonstrated to increase the swimming burst duration and intensity (Sillar et al., 1992). When serotoninergic neurons are activated during ongoing swimming, the release of serotonin causes a decrease in the IPSPs recorded in motor neurons during mid-cycle inhibition, increasing the burst duration and intensity (Sillar et al., 1992, McDearmid et al., 1997). This mechanism is fully functional *per se* even at stage 37/38. In fact, when serotonin was externally applied to the stage 37/38 tadpole's spinal cord, duration and intensity of bursts increased during swimming, but only in the rostral spinal cord (Sillar et al., 1992). This is in accordance with the anatomy of

serotoninergic descending axons, which at stage 37/38 only reach the fifth myotomal cleft (van Mier et al., 1986, Sillar et al., 1992, González et al., 1994). Although serotoninergic modulation of swimming is not behaviourally functional yet, as it cannot reliably increase swimming bursts along the entire spinal cord, the molecular mechanisms aimed at adapting ongoing swimming behaviour to stimulation are already present at the hatching stage in the *Xenopus* tadpole.

If the hypothesis that ExNs have commissural and ipsilateral projections proposed in this thesis is correct, the serotoninergic population resides in an area of the hindbrain where they can be reached by ExNs axons. Serotonin transmission has not been demonstrated to be involved in swimming initiation in the *Xenopus* tadpole, but instead it increases swim burst duration and intensity (Sillar et al., 1992). Nevertheless, serotoninergic neurons could be indirectly activated by a sensory stimulation. In fact, while swimming, the tadpole can encounter other stimuli, to which it might respond by swimming faster. In this scenario, ExNs will receive sensory information from dla and dlc cells and contact serotoninergic neurons in the hindbrain, hence activating the descending pathway that will lead to the increase in burst duration and intensity recorded in motor neurons (Koutsikou et al., 2018). Another possibility is that dla and dlc axons in the hindbrain contact directly serotoninergic neurons, thus increasing the intensity of motor behaviour in a more direct fashion. Tadpoles also respond to light dimming via the pineal eye pathway (described in chapter 2) by initiating swimming or increasing its speed. At larval stage, when the serotoninergic system is completely functional, the serotoninergic neurons might also receive excitation from the D/MD neurons, which are activated by the pineal eye ganglion cells and project caudally into the hindbrain (Jamieson and Roberts, 1999, Jamieson and Roberts, 2000). Considering the behavioural output of serotoninergic neurons activation, it seems evident that they will receive sensory information, which could be achieved by a direct or indirect synaptic pathway.

The role of serotonin in the adaptation of ongoing movement has been observed also in zebrafish. Similarly to what has been detected in the tadpole, serotoninergic neurons are present in the zebrafish larvae 2 dpf, but they become functional 4 dpf (Brustein et al., 2003). At this stage, the activation of serotoninergic cells leads to an overall increase of the locomotion activity by decreasing periods of rest between swim bouts (Brustein et al., 2003). This feature is also comparable to the effect of serotoninergic neurons in the *Xenopus* tadpole, where the swimming bursts become longer (Sillar et al., 1992).

Interestingly, a more subtle role has been demonstrated for the serotoninergic neurons of the Dorsal Raphe Nucleus (DRN) in zebrafish (Kawashima et al., 2016). Thanks to an experimental setup where larvae can fictively swim in a virtual reality environment, it was shown that TPH-positive neurons are implicated in learning processes (Kawashima et al., 2016). The serotoninergic population in the DRN was proven to not be involved in real-time adaptation, but it was necessary in learning paradigm, *i.e.* when the adaptation of behavioural response is built over time and influences future behaviour (Kawashima et al., 2016).

Crucially, at stage 37/38 the *Xenopus* tadpole does not rely on the visual system, which has not developed yet (Grant et al., 1980, Holt and Harris, 1983 , Holt, 1984). At this early stage, its nervous system is built to respond to sensory stimulation in a 'real-time fashion', as its primary and only necessity is to survive to predators. Nevertheless, it cannot be excluded that the serotoninergic system already present at stage 37/38 will develop to sustain adaptation of behaviour on the basis of learning.

7.2.3 Neurons expressing Chx10

Staining against the transcription factor Chx10 was carried out on longitudinal sections of the tadpole's CNS. In mice and zebrafish, Chx10 is expressed in glutamatergic neurons that drive the excitation of the spinal CPG during locomotion (Kimura et al., 2006, McLean et al., 2008). Similarly, in the *Xenopus* tadpole previous IHC experiments suggested that Chx10 is expressed by dINs (Li and Soffe, 2019, Roberts et al., 2012).

In the IHC staining presented here, cells positive for Chx10 were found in the hindbrain, midbrain and in the spinal cord (fig. 7.8). Such neurons occupy the lateral areas of the CNS, forming a continuous column from the spinal cord into the hindbrain (fig. 7.8 E-G, fig. 7.9 D, E). In the midbrain, Chx10-positive cells appear more ventrally than cells expressing Chx10 in the hindbrain. Cells expressing Chx10 always lie along the sides of the CNS, but they tend to occupy more medial locations in the midbrain than in hindbrain (fig. 7.8 G-I, fig. 7.10 E; p=0.0026, Mann-Whitney test, two-tailed; median difference midbrain vs hindbrain= 9.05 µm; hindbrain lateral distance= 9.40, 12.20 µm, N=52 cells in two animals; midbrain lateral distance= 18.46, 19.64 µm N=18 cells in two animals, data reported as median and IQR). In the spinal cord Chx10-positive cells lie at a constant distance from the midline (fig. 7.10 E; 4.46, 5.06; 17 cells in two animals, data reported as median and IQR). Lateral distance of cells lying in the spinal cord was not compared to hindbrain and midbrain population as, because of the anatomical constraints of the spinal cord, cells could only lie at a smaller lateral distance than the populations in the brain.

Cells expressing Chx10 in the spinal cord were larger than Chx10-positive cells in both hindbrain and midbrain (fig. 7.10 D p<0.0001; spinal cord vs hindbrain p<0.0001, mean rank difference= 35.96 µm^2; spinal cord vs midbrain p<0.0001, mean rank difference= 41.29 µm^2; hindbrain vs midbrain p>0.9999, mean rank difference= 5.33 µm^2; Kruskal-Wallis test followed by Dunn's multiple comparisons test; spinal cord: 87.01, 41.09 µm^2, N=17 cells; hindbrain: 53.75, 26.74 µm^2, N=52 cells; midbrain: 54.74, 13.19 µm^2, N=31 cells; data reported as median and IQR). All three populations showed the same round shape (fig. 7.10 A, B, C; spinal cord: height= 11.92, 3.13 µm, width= 9.36, 2.40 µm; hindbrain: height= 8.99, 2.64 µm, width= 7.80, 2.10 µm; midbrain: height= 8.67, 2.37, width= 7.89, 1.47 µm; data reported as median and IQR).

Although the symmetrical columns of Chx10-expressing cells are located very lateral in the hindbrain and in the spinal cord, a few single cells were detected away from the lateral clusters

and closer to the midline in the mid-ventral hindbrain (fig. 7.9 C). In the hindbrain and midbrain, cells expressing Chx10 are stacked in overlapping rows emerging from the sides (7.8). On the contrary, in the spinal cord Chx10-positive cells lie in a tidier fashion, with only one cell lying next to another (7.9 D, E). Of note, this does not reflect the actual arrangement of these cells in the intact spinal cord, as 20 µm-thick tissue slices are imaged here. Nevertheless, the same arrangement has been observed in all the spinal cord sections, thus confirming a more 'linear' arrangement of Chx10-positive cells in the spinal cord than in the brain.

(next page)

Figure 7.8 IHC staining of the transcription factor Chx10.
A-I) *Confocal images of longitudinal sections of one tadpole stained for Chx10 (green), reported in dorso-ventral order (A=most dorsal, I=most ventral). DAPI is in blue. Dashed white lines in A-G indicate the MHB; dashed white lines in H and I indicate the hindbrain borders. In B hindbrain is broken, but no tissue is lost in the image. In D, tissue in the rostral area of the brain (midbrain and forebrain) is flipped downwards. oc= otic capsule.*

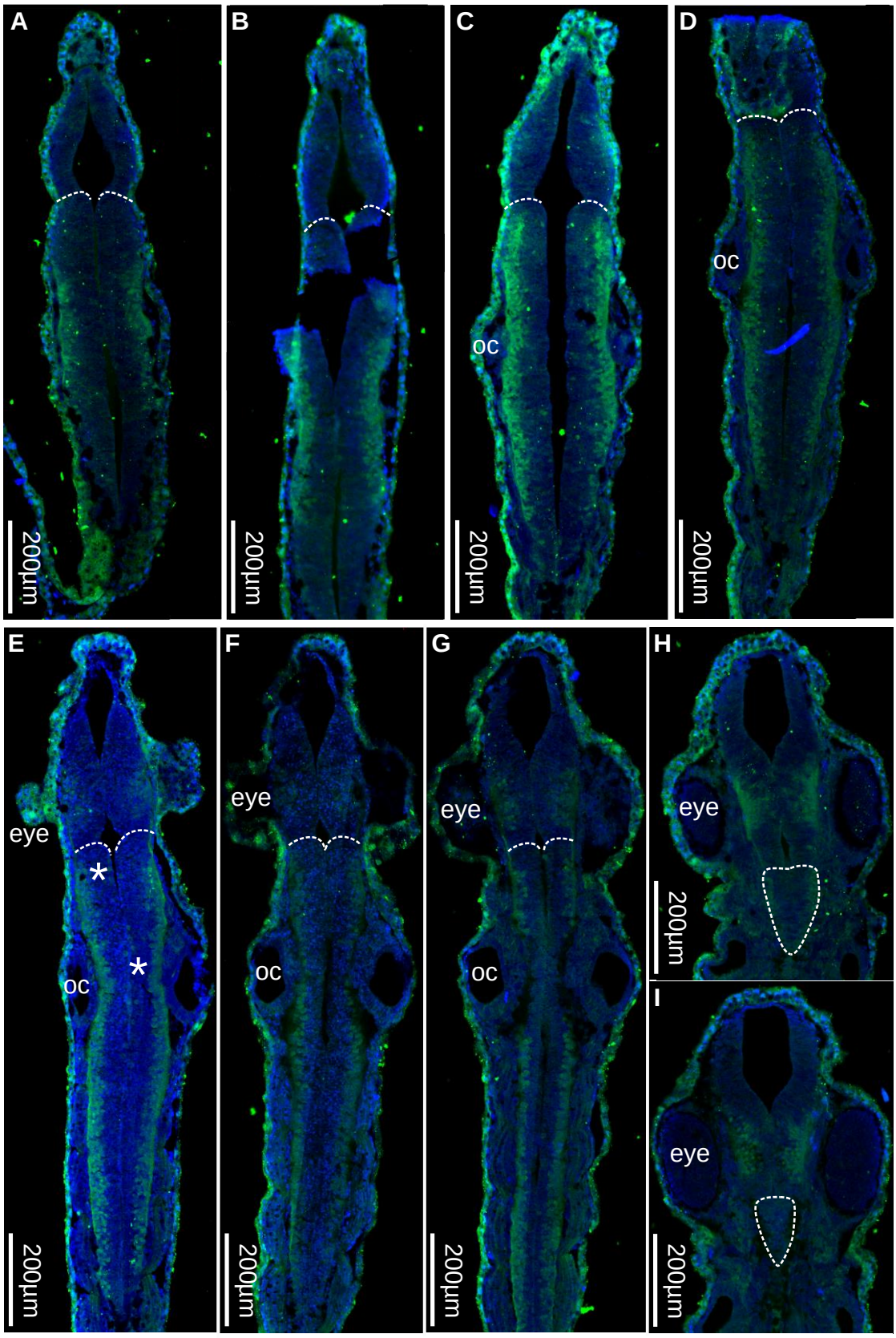
A
B
C
D
oc
oc
200µm
200µm
200µm
200µm
E
F
G
H
I
eye
eye
eye
eye
eye
*
*
oc
oc
oc
200µm
200µm
200µm
200µm
200µm

Figure 7.8

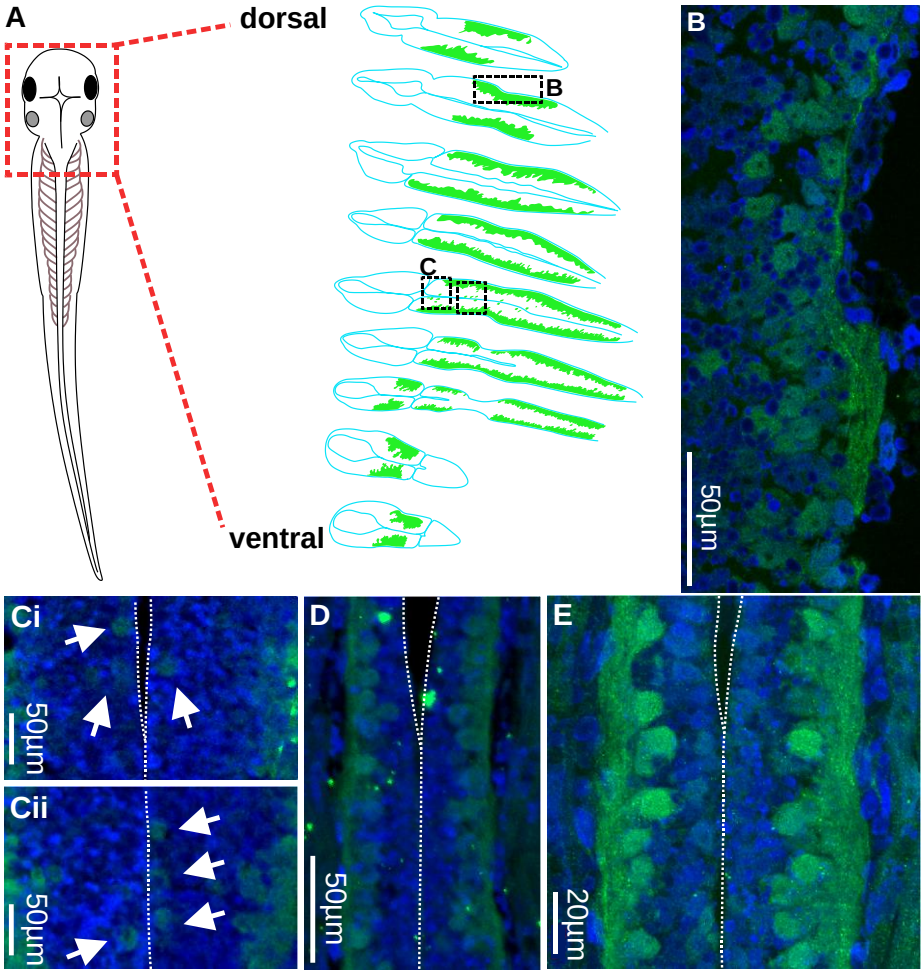

Figure 7.9 Localization of Chx10-positive population in the tadpole's hindbrain.

A) *Schematic of the location of Chx10-positive population (in green) in the brain along the dorso-ventral axis. As reference, the hindbrain is reported in grey shade in the top and bottom slice. TPH-positive population is reported in red; brain borders are in blue; skin is reported as orange lines in top and bottom slice as reference.*

B) *Confocal image of Chx10-positive neurons (in green) in the hindbrain area indicated in A. 20 Z-stacks (1 µm each) were aligned and overlapped at maximum intensity. Nuclear staining with DAPI is in blue.*

C) *Confocal images of Chx10-positive neurons (in green) in the medial area of the hindbrain, as indicated in A. White arrows indicate Chx10-positive cells close to the midline (dashed white lines). Nuclear staining with DAPI is in blue.*

D, E) *Confocal images of Chx10-positive neurons (in green) in the spinal cord. Nuclear staining with DAPI is in blue. Dashed white lines indicates the midline. In E, 20 Z-stacks (1 µm each) were aligned and overlapped at maximum intensity.*

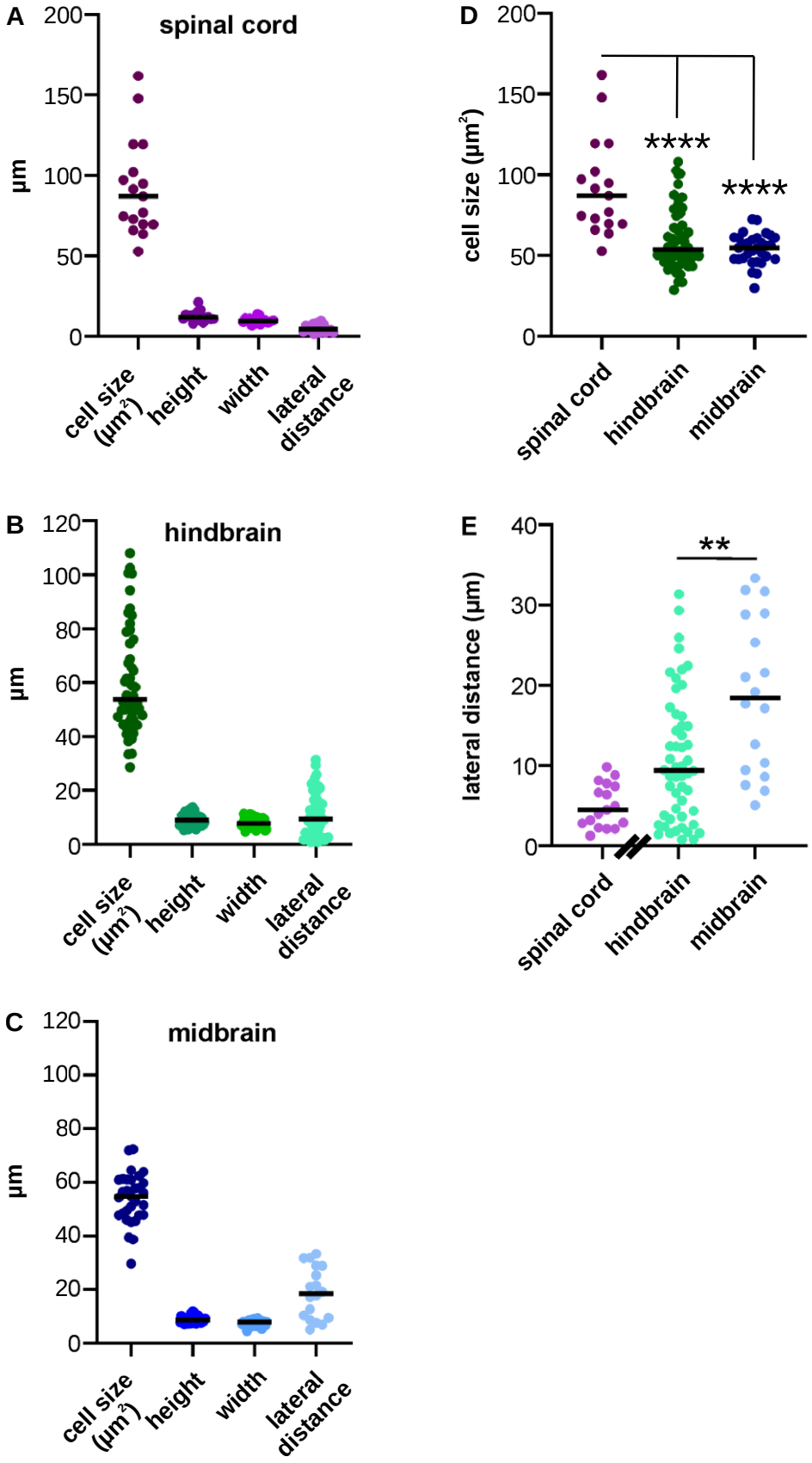
A
spinal cord
µm
200
150
100
50
0
cell size (µm²)
height
width
lateral distance
B
hindbrain
µm
120
100
80
60
40
20
0
cell size (µm²)
height
width
lateral distance
C
midbrain
µm
120
100
80
60
40
20
0
cell size (µm²)
height
width
lateral distance
D
cell size (µm²)
200
150
100
50
0
****
****
spinal cord
hindbrain
midbrain
E
lateral distance (µm)
40
30
20
10
0
**
spinal cord
hindbrain
midbrain

Figure 7.10 Anatomical features of Chx10-positive cells in the spinal cord, hindbrain and midbrain.

A, B, C) *Scatter plot of measurement of cell size, height, width and lateral distance of cells stained against Chx10 in the spinal cord (A), hindbrain (B) and midbrain (C).*
A) Spinal cord N=17 cells, cell size= 87.01, 41.09 µm^2, height= 11.92, 3.13 µm, width= 9.36, 2.40 µm, lateral distance= 4.46, 5.06 µm; B) hindbrain N=52 cells, cell size= 53.75, 26.74 µm^2, height= 8.99, 2.64 µm, width=7.80, 2.10 µm, lateral distance= 9.40, 12.20 µm; C) midbrain N=31 cells, cell size= 54.74, 13.19 µm^2, height=8.67, 2.37 µm, width=7.89, 1.47 µm, lateral distance= 18.46, 19.64 µm. All data reported as median and IQR. Single cell measurements are reported in the graph, transverse black lines indicate median.

D) *Scatter plot of cells size measurements in Chx10-positive cells in the spinal cord (purple), hindbrain (green) and midbrain (blue). Kruskal-Wallis test followed by Dunn's multiple comparisons test p<0.0001; spinal cord vs hindbrain p<0.0001, mean rank difference= 35.96 µm^2; spinal cord vs midbrain p<0.0001, mean rank difference= 41.29 µm^2; hindbrain vs midbrain p>0.9999, mean rank difference= 5.33 µm^2. Spinal cord N=17 cells, hindbrain N=52 cells, midbrain N=31 cells. Single cell measurements are reported, transverse black lines indicate median.*

E) *Scatter plot of measurement of lateral distance of cells stained against Chx10 in the spinal cord (violet), hindbrain (green) and midbrain (blue). Mann-Whitney test, two-tailed hindbrain vs midbrain only p=0.0026; median difference= 9.05 µm. Tilted black lines on the X axis indicate that the lateral distance of cells lying in the spinal cord was not compared to hindbrain and midbrain population (see main text for explanation). Spinal cord N=17 cells, hindbrain N=52 cells, midbrain N=18 cells. Single cell measurements are reported, transverse black lines indicate median.*

7.2.3.1 Discussion

Chx10 is a highly conserved transcription factor that belongs to the family of the homeobox proteins. Cells expressing the transcription factor Chx10 have been previously reported in the *Xenopus* tadpole, and it was suggested that they belonged to the dINs and dINrs neuronal classes (Li and Soffe, 2019, Roberts et al., 2012). Differently from the results reported here, in previous works on the tadpole, Chx10 was only detected in the spinal cord and in the hindbrain, and in a much smaller number of cells (Li and Soffe, 2019). This can be due to technical differences in the staining protocol and in the imaging of the samples. Li and colleagues (Li and Soffe, 2019) performed the IHC staining on whole mount samples, whilst here 20 µm thick sections were cut from fixed and subsequently frozen tadpoles. The thinner tissue might have allowed the antibody to reach more easily their target, while it could not penetrate completely into the

whole mount. In the same work, descending axons were traced under a light microscope equipped with a 100x objective (Li and Soffe, 2019). Here, images were taken with a confocal microscope but at a maximum magnification of 63x, which seems to be not enough to clearly distinguish the axonal projections. Nevertheless, descending bundles can be observed along the sides of both hindbrain and the spinal cord. *In situ* hybridization has been used to mark *chx10* transcripts during the *Xenopus* embryonic development. The neural tube was found to express *chx10* since stage 15, and till stage 32 *chx10* was found to be expressed in the developing hindbrain, in ventral position (D'Autilia et al., 2006). This localization of *chx10* during early development is in agreement with dINs ventral location in the tadpole at stage 37/38.

Chx10 is expressed by different neuronal types

Chx10 expression has been studied in both zebrafish and mice, where the V2a population is Chx10-positive and has been shown to be active during locomotion and, to different extent in the two animals, to drive locomotion.

In zebrafish, the *chx10* homologue *axl* is expressed in the glutamatergic V2a neurons in the spinal cord and in the brain (Kimura et al., 2006, Kimura et al., 2013, Eklöf-Ljunggren et al., 2012, McLean et al., 2008). Both in the spinal cord and in the hindbrain, neurons expressing Chx10 have been reported to be heterogeneous in their activation during swimming (Kimura et al., 2006, Kimura et al., 2013, McLean et al., 2008). Indeed, Chx10 neurons fire rhythmically and excite primary and secondary motor neurons (Kimura et al., 2006, McLean et al., 2008), and in the spinalized zebrafish they can sustain swimming, which correctly alternates on the left and right side and also shows rostro-caudal pattern (Eklöf-Ljunggren et al., 2012). Moreover, the Chx10-expressing population in the zebrafish hindbrain was shown to elicit locomotion when activated optically, and to stop it when it was inactivated (Kimura et al., 2013). Thus, Chx10 neurons in the zebrafish are considered responsible for the initiation of swimming. CiD (circumferential descending) neurons are among the Chx10-positive cells found in zebrafish, and they are known to be involved in eliciting locomotion in the Mauthner cells mechanism (Hale et al., 2016). Based on their similar anatomy (with ipsilateral and descending axons), on their glutamatergic nature, and on the fact that they both express Chx10, the zebrafish CiD neurons and the tadpole dINs have been proposed to be homologous (Li and Soffe, 2019). Interestingly, not all the zebrafish hindbrain neurons expressing Chx10 are rhythmically active during locomotion, with some neurons firing in a more tonic fashion (Kimura et al., 2013). The

population that fires tonically lies in the caudal hindbrain and it is formed by smaller neurons, which have ascending as well as descending axons, and whose firing is not rhythmic and less reliable than the firing of the other Chx10-positive neurons (Kimura et al., 2013). When different areas of the zebrafish hindbrain were activated to monitor locomotion, it was shown that the few Chx10 neurons in the rostral hindbrain are less involved in eliciting locomotion, while the caudal hindbrain elicited swimming more reliably (Kimura et al., 2013).

A similar heterogeneity in the activity of Chx10 neurons was observed in the rodent spinal cord. In the lumbar tract of the mice spinal cord, the majority of Chx10 neurons were shown to fire rhythmically during locomotion, in phase with either the flexor or the extensor activity. Nevertheless, a small portion of V2a spinal neurons were active, but not rhythmically (Dougherty and Kiehn, 2010a). Differently from the descending axons of the zebrafish V2a population, neurons expressing Chx10 in the spinal cord of mice have short projections, which point to the fact that V2a neurons in mammals are diversified and can be divided in sub-populations based on the expression of other transcription factors (Dougherty and Kiehn, 2010a). Recently, Chx10-positive in the GRN (Gigantocellular Reticular Nucleus) of mice have been found to belong to two different subpopulations (Chopek et al., 2021). Neurons expressing Chx10 that are bigger in size project caudally into the spinal cord; thus, they are reticulospinal neurons. On the contrary, smaller Chx10-positive neurons have smaller cell bodies and only have local projections; these have been called local interneurons (Chopek et al., 2021). These local interneurons connect to both other local interneurons and reticulospinal neurons, and they facilitate their excitation (Chopek et al., 2021).

This multifaceted character of the Chx10 populations found in zebrafish and rodents could be present even in the very young *Xenopus* tadpole. The cells stained for Chx10 form a column that runs continuously and bilaterally from the spinal cord into the hindbrain (fig. 7.8), and might enclose slightly different neuronal types, as demonstrated in other vertebrates (Dougherty and Kiehn, 2010a, Chopek et al., 2021). In the previous work where Chx10 was stained in the tadpole (Li and Soffe, 2019), it was proposed that dINs and dINrs were both included in the Chx10-expressing population. If this is confirmed by contingent molecular identification and electrophysiology recording, it might be the first evidence that the Chx10 population consists in more than one neuronal type in the tadpole.

The first evidence for a possible diversified Chx10-positive population in the tadpole can be seen in the different size of the cells in the spinal cord versus the cells found in the brain. Indeed, cells positive for Chx10 in the spinal cord are larger in size than the ones lying in the hindbrain and midbrain (fig. 7.10 D). Neuronal projections could not be resolved in the staining presented here, apart from lateral bundles of projections running along the sides of both brain and spinal cord. Because of previous indication of dINs being positive to Chx10 staining, it seems likely that most of these ipsilateral projections are descending axons. Nevertheless, it cannot be completely ruled out that some ipsilateral ascending projections might also be present. Commissural projections have not been detected, but because of the technical difficulties in imaging single axons at 63x magnification, their presence cannot be completely disregarded. However, it seems reasonable to propose that, if Chx10 neurons have commissural axons, they would cross the midline as single projections, without forming thick bundles. This is because bundles of projections can be seen running ipsilaterally, so they should have been visible also as commissural bundles if they were present. For the same imaging difficulties, the presence of short projections comparable to the ones found in the GRN of mice (Chopek et al., 2021) cannot be either confirmed or denied.

Based on the evidence reported in chapter 5 of this thesis, putative ExNs do not fire rhythmically. Instead, type B population fire tonically at the start of swimming and during locomotion, and this firing activity has been recorded throughout the hindbrain (see fig 5.3 and 5.6, chapter 5). This pattern of activation is similar to the one reported for Chx10-positive neurons in mice (Dougherty and Kiehn, 2010a) and is in accordance with Chx10 neurons stained along the entire length of the hindbrain. Although the data reported in this work do not provide enough evidence for type B neurons to express Chx10, it remains an intriguing possibility which should be further investigated.

Midbrain population

The presence of cells positive for Chx10 expression in the midbrain was rather unexpected. As mentioned above, previous work where the Chx10 population was stained in the tadpole did not report any Chx10-positive cell more rostrally than the hindbrain (Li and Soffe, 2019). Also, it was proposed that the Chx10 population consisted in dINs and dINrs, which have been shown to lie in the spinal cord and in the hindbrain (Roberts et al., 2012, Li et al., 2009), but literature is lacking on the presence dINs and/or dINrs in the midbrain.

In the stage 37/38 tadpole, the midbrain is mostly underdeveloped, and the pathways that stop or initiate locomotion originating from a rostral position rely on the trigeminal nerves to conduct the sensory information to dINs in the hindbrain (*i.e*. the stop response starting from the head bumping into solid object, the tonic inhibition starting from the cement gland and the initiation of swimming via head-skin touch; see chapter 2). One exception is found in the pathway for swimming initiation caused by light dimming (see chapter 2. Once activated, the photoreceptors in the pineal eye excite the D/MD (diencephalic/mesencephalic descending) neurons, which lie in a small bilateral cluster in the ventral midbrain, with a few cells lying in the caudal forebrain. D/MD neurons project caudally into the hindbrain and rostral spinal cord, where they are thought to excite CPG neurons leading to the initiation of swimming (Jamieson and Roberts, 1999, Roberts, 2000). D/MD neurons receive glutamatergic excitation from the pineal ganglion, but direct evidence on the neurotransmitter they use to excite postsynaptic neurons is missing (Jamieson and Roberts, 1999). Nevertheless, the possibility that D/MD are glutamatergic is likely, as CPG excitation is driven by glutamatergic synapses (Roberts et al., 2010). The neurons stained for Chx10 in the midbrain lie in ventral location, which resembles the location where DM/D neurons have previously been found. However, the mean cell size of the midbrain Chx10-positive population reported in the present study is 54.02 ± 1.69 μm^2 (mean ± SEM), which is much smaller than the mean size measured for D/MD neurons (94.61 ± 2.1 μm^2 (mean ± SEM) in (Jamieson and Roberts, 1999)). Of note, the protocols used for samples preparation and staining are different. Jameson and colleagues filled living neurons with carboxyfluorescein, and then imaged the whole mount from the lateral side. Here, the samples were fixed, frozen, and cut along the longitudinal axis of the tadpole, before IHC. Thus, if the Chx10-positive neurons were more elongated in the dorso-ventral direction, this feature could not be observed, possibly leading to a smaller cell size. Overall, it seems possible that the Chx10 population found in the midbrain could represent D/MD neurons, which are indeed descending and excitatory. However, further analysis is needed to confirm this possibility.

Apart from the GABAergic MHR population (Boothby and Roberts, 1992, Perrins et al., 2002, Li et al., 2003), discussed in paragraph 7.2.1 of this chapter) and the little information on D/MD neurons, work on the neuronal populations in the midbrain of the hatchling *Xenopus* embryo is still lacking, which makes difficult to interpret the presence of Chx10-positive neurons. Besides the option of midbrain Chx10-positive cells being D/MD neurons, one possibility is that dINs can also be found in the midbrain, more rostrally than the 'classic' population studied in the spinal

cord and in the hindbrain of the tadpole. Although single axons are not visible in the images discussed here, only ipsilateral bundles of projections running caudally into the hindbrain can be detected. This suggests that the midbrain population might be synaptically connected to the hindbrain population. A third possibility is that the midbrain neurons that are stained for Chx10 are not involved in the locomotion circuit of the tadpole, and instead act in different pathways. This latter option seems unlikely as at the transcription factor Chx10 has been only demonstrated to be expressed in the retina of the *Xenopus* later on during development (D'Autilia et al., 2006), other that in locomotor interneurons.

7.3 Conclusion

In this chapter IHC staining of neuronal populations known to be involved in mechanism of locomotor control has been presented, *i.e.* GABAergic neurons, serotoninergic neurons, and neurons expressing the transcription factor Chx10. None of the populations characterised here are confirmed candidate ExNs, but they all lie in regions of the hindbrain where they could have synapses with ExNs. Future investigations to identify the molecular signature and anatomical location of ExNs are proposed in paragraph 8.4.

8 Conclusions and Outlook

The overall aim of this work was to study the brain mechanisms that control the locomotor response to trunk skin stimulation in the stage 37/38 *Xenopus* tadpole. Previously reported experimental evidence and computational modelling (Koutsikou et al., 2018, Ferrario et al., 2021) indicated that a novel neuronal population might play an instrumental role in the processes of locomotor control in the tadpole. This novel population was called 'extension neurons' (ExNs) based on the assumption that they can cover the role of 'extending' the sensory stimulation until the locomotor response is initiated (Koutsikou et al., 2018). Although the experimental evidence supporting the role of ExNs was already very compelling, direct prove on the existence of such population was not available yet.

Here, a multifaceted approach was used to uncover the putative process that regulates swimming initiation caused by an external stimulation delivered to the trunk skin of the tadpole.

The first objective of this thesis was to confirm the existence of neurons in the hindbrain of the stage 37/38 *Xenopus* tadpole, which have the capability to maintain the long delay to motor response. In order to do so, different regions of the hindbrain were lesioned by mechanically severing the tissue, thus disconnecting neuronal projections and removing the influence of some of the cell bodies that constitute the different areas of the hindbrain (chapter 4). These experiments proved that the hindbrain hosts neurons necessary for the long and variable motor initiation in response to trunk skin stimulation.

The second objective of this work was to identify putative ExN activity at the initiation of swimming. This was achieved by means of hindbrain extracellular recordings, which allowed the characterization of ExN sub-populations (chapter 5). Different neuronal subpopulations were identified, which showed features previously postulated for ExNs.

The last objective was only partially accomplished. Indeed, the anatomical localization of ExNs population could not be precisely defined, as the experimental evidence gained so far point to a neuronal population that is dispersed across the hindbrain (chapter 6 and 7).

8.1 Role of the hindbrain in the maintenance of latency to swim initiation

Behavioural experiments and analysis of fictive swimming initiation were carried out on brain-lesioned tadpoles in order to confirm the involvement of the hindbrain in maintaining the long and variable delay to motor response (Koutsikou et al., 2018). By adjusting the stimulus intensity, it was possible to observe that the *Xenopus* embryo can discern between threshold and suprathreshold stimulation. Indeed, tadpoles respond to a threshold stimulation by starting locomotion after a long and variable delay, and preferentially on the same side of stimulation. On the contrary, strong skin stimulation (suprathreshold stimulation), leads to a locomotor response that is quicker and starts preferentially on the side opposite to stimulation. These different types of motor response have been reported for zebrafish larvae, and it has been demonstrated that they arise from the activation of different circuit in the larval brain (Marquart et al., 2019). In fact, the fast contralateral response displayed by zebrafish larvae is mediated by Mauthner neurons, which can activate directly the CPG in the contralateral spinal cord (Fetcho and Faber, 1988, Kimura et al., 2006). On the contrary, slow motor responses are activated by less intense stimulation in the zebrafish larvae (Eaton et al., 1984, Gahtan et al., 2002, Burgess and Granato, 2007, Koyama et al., 2016), and are mediated by a bilateral population of reticulospinal neurons, which project caudally on the same side of their somata, thus initiating ipsilateral responses (Marquart et al., 2019). The information available on the zebrafish larvae suggest that also in the *Xenopus* embryo the short and long latency motor response might be driven by different neuronal pathways.

The lesions experiments reported in chapter 4 of this thesis demonstrated that the neurons responsible for the activation of the long-latency response lie in the hindbrain, since when this brain area was lesioned in various ways, the tadpoles were not able to sustain delayed motor responses. Indeed, lesioned animals showed the same fast response to both threshold and suprathreshold stimulation, indicating that they lost the ability to adapt their motor response (short latency *versus* long latency) to stimulus intensity.

The ‘correct’ side preference for swim initiation (ipsilateral for threshold stimulation versus contralateral for suprathreshold stimulation) was not completely disrupted in the lesioned animals, but synchronous starts appeared frequently after the delivery of both more and less

intense stimulation. Synchrony is caused by the simultaneous excitation of CPG on both sides of the spinal cord and might be due to a lack of inhibition of descending neurons on one on the two sides. In fact, in order to properly initiate locomotion, the excitatory drive acting on one side of the spinal cord needs to be silenced while excitation is being discharged on the opposite side. This mechanism regulates the pathway mediated by Mauthner cells, where the CPG neurons on the non-bending side receive inhibition (Fetcho and Faber, 1988, Liao and Fetcho, 2008) to allow the fast and reliable motor response. In the experiments presented in this work, where lesions were carried out to disturb the hindbrain functionality, it is not possible to suggest if the synchronous starts reported are due to a lack of inhibition, or to an impaired activation of excitatory neurons. Nevertheless, it is reasonable to propose that the neuronal population that maintains both the long-latency motor response and the asynchronous start of swimming reside in the hindbrain of the stage 37/38 tadpole.

8.2 The extension neurons population in the hindbrain

Behavioural and fictive swimming experiments showed that the tadpole's hindbrain hosts one (or more) neuronal population(s) required for the correct initiation of swimming. Specifically, the surgical disruption of the hindbrain functionality impaired the slow, long-latency response, suggesting that ExNs lie dispersed in the hindbrain. Based on these results, extracellular activity was recorded at the initiation of swimming and after the delivery of a subthreshold stimulation (chapter 5).

Extracellular recordings in the hindbrain revealed neuronal activity with all the features proposed for ExNs (Koutsikou et al., 2018). Firing activity was recorded after stimulation and before the initiation of swimming, at variable latency across firing units and across experimental trials. Furthermore, units responsive to subthreshold stimulation were identified, another key feature proposed for ExNs (Koutsikou et al., 2018). By comparing their firing patterns, two subpopulations were characterized. Type A units are active at swimming initiation, but they turn silent as swimming behaviour becomes sustained by the CPG circuit. Instead, type B units are active both at swimming initiation and during sustained swimming. The existence of two different activation patterns was not hypothesized when ExNs were proposed to account for the long delay in motor response. However, the computational model used to describe ExNs did differentiate among the population, *i.e.* some of the ExNs have direct connections with the

ascending sensory pathway, while some others are activated by the recurrent network formed across the ExN population (Koutsikou et al., 2018, Ferrario et al., 2021).

A mechanism for the activation of the sensorimotor pathway in the tadpole hindbrain has been proposed in chapter 5 of this thesis, based on the firing time and pattern of the ExNs subpopulations recorded in extracellular hindbrain experiments. At this stage, the neuronal connections drawn in the proposed circuit are only speculative, as more experimental work is needed to disentangle and fully characterise this process. However, the firing time and patterns of both type A and type B ExNs seems to explain well the variability and the long delay recorded in dINs at swimming initiation. Furthermore, the additional presence of level 1 and level 2 units (referred to as type A_1 and A_2, type B_1 and B_2 in the text) might provide the tadpole with a system to discern among different stimulation intensities, and to adapt its motor response accordingly. In the experimental data presented in this work, level 1 and level 2 units showed either firing both at threshold stimulation for swimming and at subthreshold stimulation (level 1), or they fired only at threshold stimulation for swimming (level 2). These two patterns were fixed for the single units recorded, suggesting that these two subpopulations indeed respond differently to diverse trunk skin stimulation. At this stage, the reasons for the different activation patterns can only be hypothesized. Level 2 units might have different membrane properties, which will make them less likely to get activated. One example of this mechanism is well-known in the GABAergic striatal neurons expressing the dopamine receptor D1, which are very difficult to activate (Surmeier et al., 2011). These neurons express inward rectifier potassium channels (Kir), which make them stable in hyperpolarized conditions (Ericsson et al., 2011, Zhao et al., 2016). For this reason, only very strong depolarization succeeds in activating these neurons, which in mammals will ultimately disinhibit the glutamatergic neurons in the MLR, leading to locomotor initiation (Roseberry et al., 2016). Although no conclusion about membrane properties can be drawn by the extracellular recordings presented in this thesis, the possibility of a mechanism such as the one regulated by Kir channels in mammals is worth further investigation.

The mechanism proposed in chapter 5 to describe ExNs connections from the ascending sensory pathway neurons (dla and dlc) and to the descending excitatory interneurons (dINs) needs experimental confirmation. One crucial step for the investigation of ExNs pre and post synaptic connections is to anatomically localize their somata in the hindbrain, and to be able to visually follow their axonal and dendritic projections.

8.3 Anatomical localization of the sensorimotor circuit in the hindbrain

The visual localization of the ExNs populations identified in extracellular recordings proved to be a hard task to achieve. The attempt of using calcium imaging in order to correlate cellular activation in the hindbrain to swimming initiation was not successful because of technical difficulties, which have been explained in detail in chapter 6.

The next approach used was to stain neuronal populations in the brain of the tadpole that are correlated to swimming behaviour, namely the GABAergic population, the serotoninergic population and neurons expressing the transcription factor Chx10.

ExNs have been proposed, in previous work (Koutsikou et al., 2018, Ferrario et al., 2021) and in this thesis, to be excitatory, thus likely to be glutamatergic, but there is no evidence on their actual molecular identity. For this reason, a series of IHC staining was carried out to 'scan' the hindbrain in search of regions where neurons acting in such a circuit between sensory pathway and descending interneurons could lie. Results from lesioning experiments (chapter 4) and from extracellular hindbrain recordings (chapter 5) suggested that the ExNs network is dispersed in the hindbrain of the tadpole. The functionality of neuronal circuits strongly relies on the connections among cells, and it is possible that ExNs projections extend in the hindbrain towards all directions (caudally and rostrally, but also ipsilaterally and contralaterally). The IHC experiments described in chapter 7 are based on this assumption, and on the idea that ExNs would contact/be contacted by other neurons involved in the regulation of swimming behaviour.

The hindbrain of the tadpole is indeed a hub for motor control, reached by the descending trigeminal ganglia cells and by the ascending spinal sensory neurons (Roberts et al., 2010 , Roberts et al., 2019). In this scenario, it seems possible that the role played by ExNs in 'extending' the sensory stimulation coming from the trunk skin, might work well also in providing time to allow sensory integration. At the embryonic stage used in this work, the visual system is not developed yet (Beazley et al., 1972, Grant et al., 1980, Holt and Harris, 1983), and the serotoninergic neurons that will increase swimming speed at later stages are not functional yet (Sillar et al., 1992). Nevertheless, the tadpole responds to light dimming via the pineal eye pathway (Jamieson and Roberts, 2000) and to head touch (Perrins et al., 2002, Li et al., 2003,

Buhl et al., 2012). As of now, experimental evidence for mechanism of sensory integration in the *Xenopus* embryo is not available. However, this young organism might be in a stage of development where different sensory pathways start to be integrated. If this is the case the ExNs network might have a role in providing the time necessary for the processing and integration of information detected via diverse sensory pathways.

Staining for serotoninergic and GABAergic populations revealed a region in the medio-ventral hindbrain where both serotoninergic and GABAergic projections lie. Roughly in the same hindbrain region, a few Chx10-positive neurons were identified, located away from the bilateral column of neurons expressing Chx10 found in the spinal cord and along the side of the hindbrain. Chx10-positive neurons in the *Xenopus* tadpole have been proposed to be dINs and dINrs (Li and Soffe, 2019), because of their anatomical position in the hindbrain and in the spinal cord. However, no direct evidence of this molecular identity is available at the moment, and studies in other organisms have started to reveal that neurons expressing Chx10 belong to populations with different roles in locomotion (Kimura et al., 2013, Dougherty and Kiehn, 2010a). ExNs might also express Chx10, as they have been proposed to be excitatory and probably glutamatergic, and they lie disperse in the hindbrain. However, the presence of Chx10-positive neurons in the spinal cord and in the midbrain does not make Chx10 a good molecular marker for the ExNs population.

The step forward towards the localization and anatomical characterization of ExNs might lie in a more functional experimental approach, such as an improved protocol for the calcium imaging experiments. This and other possible future work are presented in next paragraph.

8.4 Future perspectives

In this work, experimental evidence for the existence and the functionality of ExNs has been presented. However, their anatomical position in the hindbrain and their cellular anatomy has not been unveiled. Locating the cell bodies of ExNs is crucial in order to carry out whole-cell recording, which will give insights on their membrane properties and sensorimotor circuit connectivity.

As explained in the previous paragraph, there are no molecular features that can be used as a marker for the ExN population. ExNs are thought to be glutamatergic, but this does not constitute a reliable marker as other neurons are also glutamatergic (such as dINs), and they

also lie in the hindbrain. The same issue is encountered with the expression of Chx10, which indeed is expressed by a large number of cells in the brain and in the spinal cord.

Possible avenues are mainly two: i) employ an imaging protocol that can reliably connect the neuronal activation to the diverse firing patterns observed in type A and type B units (described in chapter 5) and ii) use a molecular approach to define cellular markers which might define the ExNs population.

As described in chapter 6, the calcium imaging experiments carried out in this work were not successful in identifying putative ExNs. Nevertheless, the firing time and pattern are the only features that can be exploited to identify an ExNs so far. For this reason, an experimental design where the imaging of cells is linked to the time and pattern of activation seems to be the more reliable approach. Calcium imaging experiments can be improved by using tadpoles genetically modified to express fluorescent GCaMP, where the fluorescent signal of the calcium transient originates directly from the endogenously expressed protein. In such manner, neuronal activation would be more effectively detected both in terms of number of cells that can show fluorescence, as well as in terms of quality of the fluorescence signal. Indeed, in the transgenic tadpoles of choice, all neurons would express fluorescent GCaMP, overcoming the issue of loading the dye in the deeper brain layers. Moreover, because the fluorescent signal is produced endogenously, less bleaching should occur during multiple experimental trials. Genetically modified tadpoles expressing fluorescent calcium indicator can be used to overcome the issue of low signal detection and quick fluorescence bleaching. In transgenic tadpoles expressing fluorescent GCaMP, the fluorescent signal originates directly from the binding of calcium to the endogenously expressed protein, which will emit green fluorescence when the cell is activated. Unfortunately, such transgenic line was not available at the time when the experiments were carried out, so this solution could not be tested.

The second approach that could be taken to further investigate the ExN population is a molecular approach aimed to identify molecular markers, which might define this new class of neurons. The genetics of the *Xenopus laevis* is not strongly exploited in research, mainly because of the tetraploid genome of this species. The *Xenopus laevis* genome has been shown to consist of two homologues subgenomes, each one being diploid. Evolutionary, the majority of the genetic sequences has been retained in the *Xenopus laevis*, leading to the presence of two homologues copies of each gene (Session et al., 2016). For this reason, the use of transgenic

lines where genes of interest might be inactivated or selectively activated does not seem feasible, at least at this stage in the investigation of mechanism of locomotor control.

However, transcriptomics analysis might be useful to identify particular genes expressed in defined brain regions. Thanks to sequencing, the mRNA content of the hindbrain can be compared to the mRNA expression in the spinal cord, for example. Certainly, a very high percentage of equal expression levels for the same transcripts will be found, as both brain and spinal cord are formed by neurons, and lots of these neurons belong to the same classes in both CNS compartments (such as dINs). However, there might be discrepancies due to different neuronal identities that are not yet known. If ExNs reside in the hindbrain, and not in the spinal cord, and they have a different expression profile compared (for example) to CPG neurons, such analysis could help to unveil these differences. Transcripts that might be upregulated in the hindbrain could then be localised by *in situ* hybridization experiments. Of course, the fact that transcripts are expressed in the hindbrain and not in the spinal cord is not sufficient to identify ExNs, but could add evidence for a molecular identity that is different from CPG neurons.

Lastly, intracellular recording of ExNs will provide clear information on their activation pattern and membrane properties. Although this kind of experiment is the most appropriate to define in detail this novel neuronal type, trying to record from neurons blindly (*i.e.* without previously knowing the cell identity) is a very hard task, especially in the case of novel populations such as ExNs. For this reason, having visual evidence on the anatomical location would be helpful to increase the chances of recording from one actual ExN.

In the event of transcriptomics analysis and subsequent *in situ* hybridization experiments being successful, plasmids carrying a GFP-tagged gene of interest (the one transcribed into the upregulated mRNA) could be injected at egg stage. In this way, intracellular recording might be directed only to the cells expressing the mRNA found to be differently expressed in the hindbrain.

8.5 Implications for research on human pathologies

Impaired motor control and dysfunctional sensorimotor integration are distinctive features of several neurologic pathologies in humans. These range from Parkinson's disease to autistic syndrome, from cerebral palsy to mild cognitive disorder (Khalil et al., 2018, O'Shea, 2008, Wu et al., 2016, Desrochers et al., 2019).

Specifically, dystonia is a movement disorder that causes involuntary movements, which are irregular, lead to dysfunctional contraction of agonist and antagonist muscles, and can either have or have not a tremorous component (Albanese et al., 2013). Studies on patients affected by dystonia have been extensively reviewed in (Desrochers et al., 2019) and include clinical research on posture and balance (Lekhel et al., 1997, Bove et al., 2004, De Pauw et al., 2018), on upper limb movement and coordination (Inzelberg et al., 1995, Berardelli et al., 1996, Kandaswamy et al., 2018), and on lower limb functionality on gait and pace (Hoffland et al., 2014, Barr et al., 2017). All these aspects of motor control and execution were found to be impaired in patients affected by dystonia compared to controls (Desrochers et al., 2019). It has also been shown that the impairment of locomotor functions is very often coupled to non-functional execution of fine movements, for example writing or connecting two dots with a line (Desrochers et al., 2019, Balestrino and Schapira, 2020). Moreover, studies on children affected by autism syndrome showed an impaired ability to make decisions that entail body movement, such as following objects held by others with the eyes and looking at others (Osterling et al., 2002). Motor impairments are very often accompanied by decreased cognitive abilities in patients suffering from Parkinson's disorder, cerebral palsy, and also autism (Balestrino and Schapira, 2020, Khalil et al., 2018, O'Shea, 2008, Wu et al., 2016, Desrochers et al., 2019). Both motor and cognitive symptoms have been recorded and studied in different pathologies, and various cerebral areas have been shown to be involved in the malfunctioning of the sensorimotor and cognitive processes, with the cerebellum and basal ganglia being among the most implicated brain regions (Balestrino and Schapira, 2020, Khalil et al., 2018, O'Shea, 2008, Wu et al., 2016, Desrochers et al., 2019).

One important feature that came to light when different motor impairments were clinically studied is the presence of disturbed cerebral connections, which often fall on the basal ganglia and on the cerebellum (Stinear and Byblow, 2004, Filip et al., 2013).

Although clinical research on human disorders that cause motor impairments is vast and allows to monitor first-hand the symptoms on patients, it is clear that a deep analysis of the molecular mechanisms and of the neuronal circuits that show failures in those pathologies is not possible. In this scenario, basic biological research on simple vertebrate such as the *Xenopus* tadpole can be instrumental to gain a better understanding of the conserved mechanisms of sensorimotor integration and motor control. Indeed, model organisms with simple and less integrated

neuronal network can help in the identification of the building blocks that will then grow and evolve into the neural connections that allows mammals and humans to perform complex movements, and to eventually achieve specific behaviours depending on the external environment.

9 Photoacoustic Microscopy Experiments

(in collaboration with Applied Optics group, University of Kent)

In this chapter, the work carried out in collaboration with Dr. Adrian Bradu's group at School of Physics (Applied Optics group, University of Kent) is presented. The work of researchers in the Applied Optics group is focused on developing new instruments and techniques that allow the detection of biological molecules *in vivo* (Bradu et al., 2009, Podoleanu et al., 2019). To this end, they use photoacoustic microscopy (PAM). The *Xenopus* tadpole was proved to be a good model organism for *in vivo* PAM experiments. Results obtained in PAM experiments on the tadpole are reported in one published article (Dasa et al., 2020) and in one submitted article.

9.1 Principles of Photoacoustic Microscopy

Photoacoustic microscopy relies on the photoacoustic effect to image the samples. When photons travel through a tissue, they are absorbed by the molecules that form the tissue. This absorption induces pressure acoustic waves, which propagate in the sample and that are detected by the transducer. The transducer can map the acoustic waves and reproduce the original deposition of photons in the tissue (Wang and Wu, 2007) (Yao and Wang, 2013). In the last decades, PAM techniques have been implemented in the effort of solving one of the problems in optical microscopy, *i.e.* the optical diffusion limit. The diffusion limit of photons in tissue is ~1 mm. Passed this limit, photons have been scattered multiple times and it becomes harder to acquire images with tight focus (Wang and Wu, 2007). Instead, PAM relies on the conversion of absorbance of photons into acoustic waves, and it can produce less scattered images (Yao and Wang, 2013).

PAM can be employed *in vivo* without the use of staining methods or the introduction of exogenous molecules. Thanks to this feature, the use of PAM in the detection of multiple endogenous molecules related to human diseases has been proposed. (1-5 photoacoustic paper). Biological molecules such as lipids, melanin and haemoglobin have been successfully imaged with PAM, and changes in the amount or localisation of these molecules are observed in pathological conditions. For example, lipidic plaques are found in arteriosclerosis (Wang et al., 2010, Zhang et al., 2010), haemoglobin has been imaged in relation to tumour progression and microvasculature damages (Yao et al., 2011 , Krumholz et al., 2012), and melanin has been

proven to be an exceptional endogenous agent for the detection of skin cancer (Galanzha et al., 2009).

9.2 PAM imaging of the *Xenopus* tadpole

The Xenopus tadpole at stage 37/38 is a very simple organism, but it shows all the biological building blocks of a complex animal. Indeed, lipids are found at high concentration in the yolk sac, the vascular system is present, as well as haemoglobin, and pigmentated cells with high content of melanin are found on the head and along the trunk skin of the tadpole.

In PAM experiments, tadpoles were immobilized in MS-222 (Sigma Aldrich, see Appendix 1) and immersed in tap water, treated with commercially available aquarium conditioner. Details of the microscopy setup are given in the material and methods sections of (Dasa et al., 2020). The technical aspects of PAM experiments are beyond the scope of this thesis and thus are not discussed further.

Lipids were the first molecule imaged in the tadpole because of their high content in the yolk sac. The yolk sac is a well-defined anatomical area, which has the added value of being covered in thin non-pigmented skin, thus allowing easier laser penetration. In accordance with the anatomical localization, images from the lipidic absorbance spectrum were detected in the yolk sac and around the developing otic capsule (fig. 9.1, (Dasa et al., 2020)).

Subsequent PAM experiments on the tadpole were carried out to detect multiple endogenous molecules. These were melanin, haemoglobin, collagen, glucose and lipids, and their detection was achieved with filters for different wavelengths (fig. 9.2). Melanin was detected using filters at 550 and 650 nm, and it was imaged in substantial clusters on the eye, on the cement gland, and along the trunk muscles, while more disperse pigmentation is visible along the dorsal fin and on the tail. In order to detect haemoglobin, filters at 550 and 650 nm were used. Haemoglobin was found along the tadpole's vasculature system, *i.e.* along the dorsal and ventral part of the yolk sac and on the lateral portion of the head. Images of collagen content in the tadpole were obtained with 1200 and 1700 nm filters. Collagen was imaged in the yolk sac, along the trunk muscles and in the developing cranial structures. Glucose images revealed a large presence of this molecule in the tadpole, which was more concentrated on the head, the yolk sac and along the ventral area of trunk muscles. Glucose maps were obtained with filters at 1200 and 1700 nm. Lastly, lipids were imaged using 1200 and 1600 nm filters, and the images

recorded were similar to the lipidic content observed in previous experiment. Indeed, higher concentration of lipids were found in the yolk sac, and to minor extent in the ventral area of the trunk muscles.

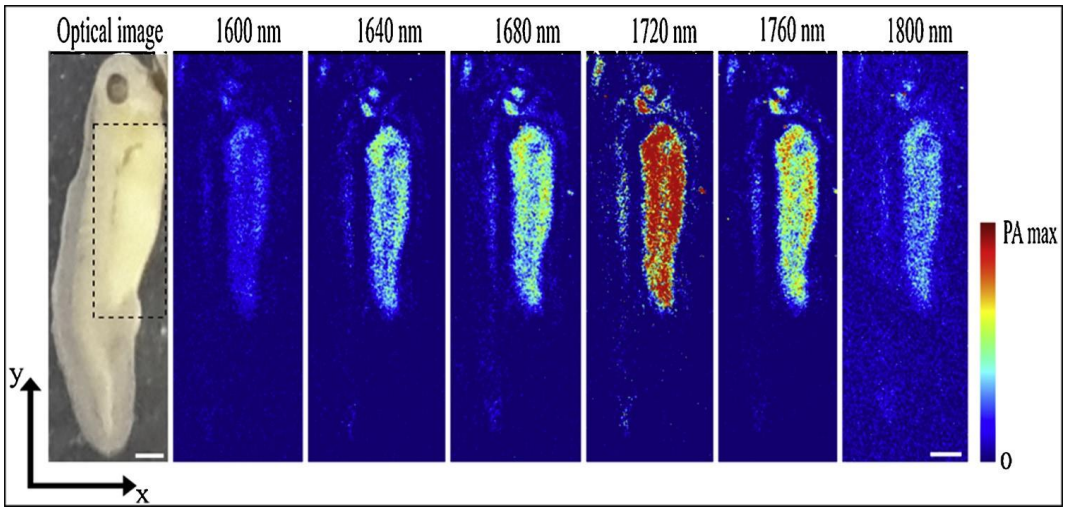

Figure 9.1 PAM images of the Xenopus tadpole.
Optical image and 6 in vivo z-projected en-face MS-PAM images of a tadpole acquired in steps of 40 nm. The highlighted region in the optical image shows the yolk sac. The scale bar represents 1 mm.

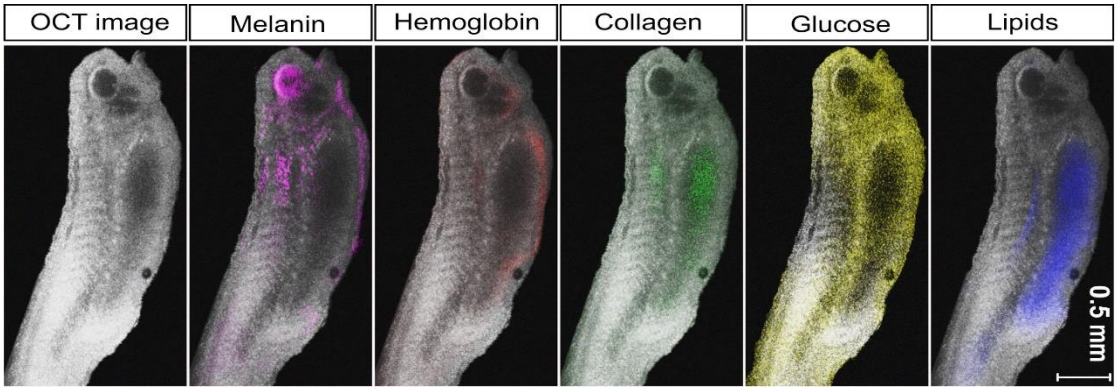

Figure 9.2 OS-PAM images of different endogenous molecules in the Xenopus tadpole.
In vivo OS-PAM images mapping melanin, hemoglobin (Hb), collagen, glucose and lipids in the tadpole at developmental stage 37/38.

9.3 Discussion

Although the PAM imaging studies presented here have been carried out primarily as 'proof of concept' experiments, the outcome was encouraging.

In the last years, PAM has been used to image big tissue and organs, and it has also been employed in neurobiology. By using sophisticated experimental setups, the ratio of oxygenated and non-oxygenated haemoglobin was calculated on PAM images and this was correlated to cellular activity in the mice brain (Ovsepian et al., 2017). In the zebrafish, brain activity was resolved at cellular level in PAM experiments carried out in larvae expressing fluorescent GCaMP5G (Ahrens et al., 2013).

The major advantage of PAM is that imaging can be carried out without the need of a chemical dye, as the image is created thanks to the conversion of light absorbed by the tissue into acoustic waves. This fact assumes a greater importance if this technique will be implemented for clinical purposes, such as cancer detection or tumor progression examination. Indeed, if in pre-clinical and fundamental biology research the use of chemical dye and other invasive techniques are exploited daily, the same cannot be done for diagnostic exams in humans. Innovative research and further experimental work on the possible use of PAM are needed to take this instrument to the use in human healthcare.

10 Bibliography

AGDUHR, E. 1922. Über ein zentrales sinnesorgan (?) bei den vertebraten. *Z. Anat. Entwicklungsgesch,* 66**,** 223–360.

AHRENS, M. B., ORGER, M. B., ROBSON, D. N., LI, J. M. & KELLER, P. J. 2013. Whole-brain functional imaging at cellular resolution using light-sheet microscopy. *Nature Methods,* 10**,** 413-420.

ALBANESE, A., BHATIA, K., BRESSMAN, S. B., DELONG, M. R., FAHN, S., FUNG, V. S. C., HALLETT, M., JANKOVIC, J., JINNAH, H. A., KLEIN, C., LANG, A. E., MINK, J. W. & TELLER, J. K. 2013. Phenomenology and classification of dystonia: A consensus update. *Movement Disorders,* 28**,** 863-873.

ALBIN, R. L., YOUNG, A. B. & PENNEY, J. B. 1989. The functional anatomy of basal ganglia disorders. *Trends in Neurosciences,* 12**,** 366-375.

AMPATZIS, K., SONG, J., AUSBORN, J. & EL MANIRA, A. 2013. Pattern of innervation and recruitment of different classes of motoneurons in adult zebrafish. *The Journal of neuroscience : the official journal of the Society for Neuroscience,* 33**,** 10875-10886.

ANDERSSON, O. & GRILLNER, S. 1981. Peripheral control of the cat's step cycle I. Phase dependent effects of ramp-movements of the hip during “fictive locomotion”. *Acta Physiologica Scandinavica,* 113**,** 89-101.

ANTINUCCI, P., FOLGUEIRA, M. & BIANCO, I. H. 2019. Pretectal neurons control hunting behaviour. *eLife,* 8**,** e48114.

ARBER, S. 2012. Motor Circuits in Action: Specification, Connectivity, and Function. *Neuron,* 74**,** 975-989.

BALESTRINO, R. & SCHAPIRA, A. H. V. 2020. Parkinson disease. *European Journal of Neurology,* 27**,** 27-42.

BARBERA, G., LIANG, B., ZHANG, L., GERFEN, CHARLES R., CULURCIELLO, E., CHEN, R., LI, Y. & LIN, D.-T. 2016. Spatially Compact Neural Clusters in the Dorsal Striatum Encode Locomotion Relevant Information. *Neuron,* 92**,** 202-213.

BARR, C., BARNARD, R., EDWARDS, L., LENNON, S. & BRADNAM, L. 2017. Impairments of balance, stepping reactions and gait in people with cervical dystonia. *Gait & Posture,* 55**,** 55-61.

BARRIOS, J. P., WANG, W.-C., ENGLAND, R., REIFENBERG, E. & DOUGLASS, A. D. 2020. Hypothalamic Dopamine Neurons Control Sensorimotor Behavior by Modulating Brainstem Premotor Nuclei in Zebrafish. *Current Biology,* 30**,** 4606-4618.e4.

BEAZLEY, L., KEATING, M. J. & GAZE, R. M. 1972. The appearance, during development, of responses in the optic tectum following visual stimulation of the ipsilateral eye in Xenopus laevis. *Vision Research,* 12**,** 407-VIII.

BEN-ARI, Y. 2002. Excitatory actions of gaba during development: the nature of the nurture. *Nature Reviews Neuroscience,* 3**,** 728-739.

BERARDELLI, A., HALLETT, M., ROTHWELL, J. C., AGOSTINO, R., MANFREDI, M., THOMPSON, P. D. & MARSDEN, C. D. 1996. Single–joint rapid arm movements in normal subjects and in patients with motor disorders. *Brain,* 119**,** 661-674.

BERG, E. M., BJÖRNFORS, E. R., PALLUCCHI, I., PICTON, L. D. & EL MANIRA, A. 2018. Principles Governing Locomotion in Vertebrates: Lessons From Zebrafish. *Frontiers in Neural Circuits,* 12.

BERNHARDT, R. R., CHITNIS, A. B., LINDAMER, L. & KUWADA, J. Y. 1990. Identification of spinal neurons in the embryonic and larval zebrafish. *Journal of Comparative Neurology,* 302**,** 603-616.

BIANCO, I. H., KAMPFF, A. R. & ENGERT, F. 2011. Prey capture behavior evoked by simple visual stimuli in larval zebrafish. *Frontiers in systems neuroscience,* 5**,** 101-101.

BJÖRNFORS, E. R. & EL MANIRA, A. 2016. Functional diversity of excitatory commissural interneurons in adult zebrafish. *eLife,* 5**,** e18579.

BJURSTEN, L., NORRSELL, K. & NORRSELL, U. 1976. Behavioural repertory of cats without cerebral cortex from infancy. *Exp Brain Res,* May 28**,** 115-30.

BOOTHBY, K. M. & ROBERTS, A. 1992. The stopping response of Xenopus laevis embryos: behaviour, development and physiology. *Journal of Comparative Physiology A,* 170**,** 171-180.

BOOTHBY, K. M. & ROBERTS, A. 1995. Effects of site of tactile stimulation on the escape swimming responses of hatchling Xenopus laevis embryos. *Journal of Zoology,* 235**,** 113-125.

BOVE, M., BRICHETTO, G., ABBRUZZESE, G., MARCHESE, R. & SCHIEPPATI, M. 2004. Neck proprioception and spatial orientation in cervical dystonia. *Brain,* 127**,** 2764-2778.

BRADU, A., MA, L., BLOOR, J. W. & PODOLEANU, A. 2009. Dual optical coherence tomography/fluorescence microscopy for monitoring of Drosophila melanogaster larval heart. *Journal of Biophotonics,* 2**,** 380-388.

BROCARD, F. & DUBUC, R. 2003. Differential Contribution of Reticulospinal Cells to the Control of Locomotion Induced By the Mesencephalic Locomotor Region. *Journal of Neurophysiology,* 90**,** 1714-1727.

BRODIN, L., S, G., R, D., Y, O., S, K. & HÖKFELT, T. 1988. Reticulospinal neurons in lamprey: transmitters, synaptic interactions and their role during locomotion. *Arch Ital Biol,* OCt**,** 317-45.

BROOKS, J. M. & WESSEL, G. M. 2002. The Major Yolk Protein in Sea Urchins Is a Transferrin-like, Iron Binding Protein. *Developmental Biology,* 245**,** 1-12.

BRUSTEIN, E., CHONG, M., HOLMQVIST, B. & DRAPEAU, P. 2003. Serotonin patterns locomotor network activity in the developing zebrafish by modulating quiescent periods. *Journal of Neurobiology,* 57**,** 303-322.

BRUSTEIN, E. & DRAPEAU, P. 2005. Serotoninergic modulation of chloride homeostasis during maturation of the locomotor network in zebrafish. *The Journal of neuroscience : the official journal of the Society for Neuroscience,* 25**,** 10607-10616.

BUCHANAN JAMES, T. & GRILLNER, S. 1987. Newly Identified 'Glutamate Interneurons' and Their Role in Locomotion in the Lamprey Spinal Cord. *Science,* 236**,** 312-314.

BUHL, E., ROBERTS, A. & SOFFE, S. R. 2012. The role of a trigeminal sensory nucleus in the initiation of locomotion. *The Journal of physiology,* 590**,** 2453-2469.

BUHL, E., SOFFE, S. R. & ROBERTS, A. 2015. Sensory initiation of a co-ordinated motor response: synaptic excitation underlying simple decision-making. *J Physiol,* 593**,** 4423-37.

BURGESS, H. A. & GRANATO, M. 2007. Sensorimotor gating in larval zebrafish. *The Journal of neuroscience : the official journal of the Society for Neuroscience,* 27**,** 4984-4994.

BUSS, R. R. & DRAPEAU, P. 2001. Synaptic Drive to Motoneurons During Fictive Swimming in the Developing Zebrafish. *Journal of Neurophysiology,* 86**,** 197-210.

CAGGIANO, V., LEIRAS, R., GOÑI-ERRO, H., MASINI, D., BELLARDITA, C., BOUVIER, J., CALDEIRA, V., FISONE, G. & KIEHN, O. 2018. Midbrain circuits that set locomotor speed and gait selection. *Nature,* 553**,** 455-460.

CARPENTER, R. H. S. 1999. A neural mechanism that randomises behaviour. *Journal of Consciousness Studies,* 6**,** 13-22.

CARPENTER, R. H. S. & WILLIAMS, M. L. L. 1995. Neural computation of log likelihood in control of saccadic eye movements. *Nature,* 377**,** 59-62.

CHAUDHRY, F. A., REIMER, R. J., BELLOCCHIO, E. E., DANBOLT, N. C., OSEN, K. K., EDWARDS, R. H. & STORM-MATHISEN, J. 1998. The vesicular GABA transporter, VGAT, localizes to synaptic vesicles in sets of glycinergic as well as GABAergic neurons. *The Journal of neuroscience : the official journal of the Society for Neuroscience,* 18**,** 9733-9750.

CHOPEK, J. W., ZHANG, Y. & BROWNSTONE, R. M. 2021. Intrinsic brainstem circuits comprised of Chx10-expressing neurons contribute to reticulospinal output in mice. *Journal of Neurophysiology,* 126**,** 1978-1990.

CIONI, C., DE PALMA, F. & STEFANELLI, A. 1989. Morphology of afferent synapses in the mauthner cell of larval Xenopus laevis. *Journal of Comparative Neurology,* 284**,** 205-214.

CLARKE JD FAU HAYES, B. P. H., S. P. & ROBERTS, A. 1984. Sensory physiology, anatomy and immunohistochemistry of Rohon-Beard neurones in embryos of Xenopus laevis. *J Physiol,* Mar**,** 511–525.

CLARKE, J. D., HAYES, B. P., HUNT, S. P. & ROBERTS, A. 1984. Sensory physiology, anatomy and immunohistochemistry of Rohon-Beard neurones in embryos of Xenopus laevis. *The Journal of physiology,* 348**,** 511-525.

CLARKE, J. D. & ROBERTS, A. 1984. Interneurones in the Xenopus embryo spinal cord: sensory excitation and activity during swimming. *The Journal of Physiology,* 354**,** 345-362.

CUI, G., JUN, S. B., JIN, X., PHAM, M. D., VOGEL, S. S., LOVINGER, D. M. & COSTA, R. M. 2013. Concurrent activation of striatal direct and indirect pathways during action initiation. *Nature,* 494**,** 238-242.

D'AUTILIA, S., DECEMBRINI, S., CASAROSA, S., HE, R.-Q., BARSACCHI, G., CREMISI, F. & ANDREAZZOLI, M. 2006. Cloning and developmental expression of the Xenopus homeobox gene Xvsx1. *Development Genes and Evolution,* 216**,** 829-834.

DA SILVA, J. A., TECUAPETLA, F., PAIXÃO, V. & COSTA, R. M. 2018. Dopamine neuron activity before action initiation gates and invigorates future movements. *Nature,* 554**,** 244-248.

DALE, N., OTTERSEN, O. P., ROBERTS, A. & STORM-MATHISEN, J. 1986. Inhibitory neurones of a motor pattern generator in Xenopus revealed by antibodies to glycine. *Nature,* 324**,** 255-257.

DALE, N. & ROBERTS, A. 1984. Excitatory amino acid receptors in Xenopus embryo spinal cord and their role in the activation of swimming. *The Journal of physiology,* 348**,** 527-543.

DALE, N. & ROBERTS, A. 1985. Dual-component amino-acid-mediated synaptic potentials: excitatory drive for swimming in Xenopus embryos. *The Journal of physiology,* 363**,** 35-59.

DALE, N., ROBERTS, A., OTTERSEN, O. P., STORM - MATHISEN, J. & BONE, Q. 1987. The morphology and distribution of 'Kolmer–Agduhr cells', a class of cerebrospinal-fluid-contacting neurons revealed in the frog embryo spinal cord by GABA immunocytochemistry. *Proceedings of the Royal Society of London. Series B. Biological Sciences,* 232**,** 193-203.

DASA, M. K., NTEROLI, G., BOWEN, P., MESSA, G., FENG, Y., PETERSEN, C. R., KOUTSIKOU, S., BONDU, M., MOSELUND, P. M., PODOLEANU, A., BRADU, A., MARKOS, C. & BANG, O. 2020. All-fibre supercontinuum laser for in vivo multispectral photoacoustic microscopy of lipids in the extended near-infrared region. *Photoacoustics,* 18**,** 100163-100163.

DAVIES, S., KITSON, D. & ROBERTS, A. 1982. The development of the peripheral trigeminal innervation in Xenopus embryos. *J Embryol Exp Morphol,* Aug**,** 215-24.

DE PAUW, J., MERCELIS, R., HALLEMANS, A., VAN GILS, G., TRUIJEN, S., CRAS, P. & DE HERTOGH, W. 2018. Postural control and the relation with cervical sensorimotor control in patients with idiopathic adult-onset cervical dystonia. *Experimental Brain Research,* 236**,** 803-811.

DELONG, M. R. 1990. Primate models of movement disorders of basal ganglia origin. *Trends in Neurosciences,* 13**,** 281-285.

DEMARQUE, M. & SPITZER, N. C. 2010. Activity-dependent expression of Lmx1b regulates specification of serotonergic neurons modulating swimming behavior. *Neuron,* 67**,** 321-334.

DESROCHERS, P., BRUNFELDT, A., SIDIROPOULOS, C. & KAGERER, F. 2019. Sensorimotor Control in Dystonia. *Brain Sciences,* 9.

DEVOTO, S. H., MELANCON, E., EISEN, J. S. & WESTERFIELD, M. 1996. Identification of separate slow and fast muscle precursor cells in vivo, prior to somite formation. *Development,* 122**,** 3371-3380.

DI PRISCO, G. V., OHTA, Y., BONGIANNI, F., GRILLNER, S. & DUBUC, R. 1995. Trigeminal inputs to reticulospinal neurones in lampreys are mediated by excitatory and inhibitory amino acids. *Brain Research,* 695**,** 76-80.

DJENOUNE, L. & WYART, C. 2017. Light on a sensory interface linking the cerebrospinal fluid to motor circuits in vertebrates. *Journal of Neurogenetics,* 31**,** 113-127.

DONG, W., LEE, R. H., XU, H., YANG, S., PRATT, K. G., CAO, V., SONG, Y.-K., NURMIKKO, A. & AIZENMAN, C. D. 2009. Visual avoidance in Xenopus tadpoles is correlated with the maturation of visual responses in the optic tectum. *Journal of neurophysiology,* 101**,** 803-815.

DOUGHERTY, K. J. & KIEHN, O. 2010a. Firing and cellular properties of V2a interneurons in the rodent spinal cord. *The Journal of Neuroscience,* 30**,** 24-37.

DOUGHERTY, K. J. & KIEHN, O. 2010b. Functional organization of V2a-related locomotor circuits in the rodent spinal cord. *Annals of the New York Academy of Sciences,* 1198**,** 85-93.

DRAPEAU, P., SAINT-AMANT, L., BUSS, R. R., CHONG, M., MCDEARMID, J. R. & BRUSTEIN, E. 2002. Development of the locomotor network in zebrafish. *Progress in Neurobiology,* 68**,** 85-111.

DUBUC, R., BONGIANNI, F., OHTA, Y. & GRILLNER, S. 1993a. Anatomical and physiological study of brainstem nuclei relaying dorsal column inputs in lampreys. *Journal of Comparative Neurology,* 327**,** 260-270.

DUBUC, R., BONGIANNI, F., OHTA, Y. & GRILLNER, S. 1993b. Dorsal root and dorsal column mediated synaptic inputs to reticulospinal neurons in lampreys: Involvement of glutamatergic, glycinergic, and GABaergic transmission. *Journal of Comparative Neurology,* 327**,** 251-259.

DUBUC, R., BROCARD, F., ANTRI, M., FÉNELON, K., GARIÉPY, J.-F., SMETANA, R., MÉNARD, A., LE RAY, D., VIANA DI PRISCO, G., PEARLSTEIN, É., SIROTA, M. G., DERJEAN, D., ST-PIERRE, M., ZIELINSKI, B., AUCLAIR, F. & VEILLEUX, D. 2008. Initiation of locomotion in lampreys. *Brain Research Reviews,* 57**,** 172-182.

EATON, R. C. & EMBERLEY, D. S. 1991. How stimulus direction determines the trajectory of the Mauthner-initiated escape response in a teleost fish. *Journal of Experimental Biology,* 161**,** 469-487.

EATON, R. C., NISSANOV, J. & WIELAND, C. M. 1984. Differential activation of Mauthner and non-Mauthner startle circuits in the zebrafish: Implications for functional substitution. *Journal of Comparative Physiology A,* 155**,** 813-820.

EKLÖF-LJUNGGREN, E., HAUPT, S., AUSBORN, J., DEHNISCH, I., UHLÉN, P., HIGASHIJIMA, S.-I. & EL MANIRA, A. 2012. Origin of excitation underlying locomotion in the spinal circuit of zebrafish. *Proceedings of the National Academy of Sciences of the United States of America,* 109**,** 5511-5516.

ERICSSON, J., SILBERBERG, G., ROBERTSON, B., WIKSTRÖM, M. A. & GRILLNER, S. 2011. Striatal cellular properties conserved from lampreys to mammals. *The Journal of physiology,* 589**,** 2979-2992.

FARRELL, T. C., CARIO, C. L., MILANESE, C., VOGT, A., JEONG, J.-H. & BURTON, E. A. 2011. Evaluation of spontaneous propulsive movement as a screening tool to detect rescue of Parkinsonism phenotypes in zebrafish models. *Neurobiology of disease,* 44**,** 9-18.

FERGUSON, S. C. D. & MCFARLANE, S. 2002. GABA and development of the Xenopus optic projection. *Journal of Neurobiology,* 51**,** 272-284.

FERRARIO, A., PALYANOV, A., KOUTSIKOU, S., LI, W., SOFFE, S., ROBERTS, A. & BORISYUK, R. 2021. From decision to action: Detailed modelling of frog tadpoles reveals neuronal mechanisms of decision-making and reproduces unpredictable swimming movements in response to sensory signals. *PLOS Computational Biology,* 17**,** e1009654.

FERREIRA-PINTO, M. J., RUDER, L., CAPELLI, P. & ARBER, S. 2018. Connecting Circuits for Supraspinal Control of Locomotion. *Neuron,* 100**,** 361-374.

FETCHO, J. R. 1992. The Spinal Motor System in Early Vertebrates and Some of Its Evolutionary Changes. *Brain, Behavior and Evolution,* 40**,** 82-97.

FETCHO, J. R. & FABER, D. S. 1988. Identification of motoneurons and interneurons in the spinal network for escapes initiated by the mauthner cell in goldfish. *The Journal of neuroscience : the official journal of the Society for Neuroscience,* 8**,** 4192-4213.

FETCHO, J. R., HIGASHIJIMA, S.-I. & MCLEAN, D. L. 2008. Zebrafish and motor control over the last decade. *Brain Research Reviews,* 57**,** 86-93.

FIDELIN, K., DJENOUNE, L., STOKES, C., PRENDERGAST, A., GOMEZ, J., BARADEL, A., DEL BENE, F. & WYART, C. 2015. State-Dependent Modulation of Locomotion by GABAergic Spinal Sensory Neurons. *Current Biology,* 25**,** 3035-3047.

FILE, S. E. & WARDILL, A. G. 1975. Validity of head-dipping as a measure of exploration in a modified hole-board. *Psychopharmacologia,* 44**,** 53-59.

FILIP, P., LUNGU, O. V. & BAREŠ, M. 2013. Dystonia and the cerebellum: A new field of interest in movement disorders? *Clinical Neurophysiology,* 124**,** 1269-1276.

FOSTER, R. G. & ROBERTS, A. 1982. The pineal eye inXenopus laevis embryos and larvae: A photoreceptor with a direct excitatory effect on behaviour. *Journal of comparative physiology,* 145**,** 413-419.

FREEZE, B. S., KRAVITZ, A. V., HAMMACK, N., BERKE, J. D. & KREITZER, A. C. 2013. Control of basal ganglia output by direct and indirect pathway projection neurons. *The Journal of neuroscience : the official journal of the Society for Neuroscience,* 33**,** 18531-18539.

GABRIEL, J. P., MAHMOOD, R., WALTER, A. M., KYRIAKATOS, A., HAUPTMANN, G., CALABRESE, R. L. & EL MANIRA, A. 2008. Locomotor Pattern in the Adult Zebrafish Spinal Cord In Vitro. *Journal of Neurophysiology,* 99**,** 37-48.

GAHTAN, E. & O'MALLEY, D. M. 2003. Visually guided injection of identified reticulospinal neurons in zebrafish: A survey of spinal arborization patterns. *Journal of Comparative Neurology,* 459**,** 186-200.

GAHTAN, E., SANKRITHI, N., CAMPOS, J. B. & O'MALLEY, D. M. 2002. Evidence for a Widespread Brain Stem Escape Network in Larval Zebrafish. *Journal of Neurophysiology,* 87**,** 608-614.

GAHTAN, E., TANGER, P. & BAIER, H. 2005. Visual prey capture in larval zebrafish is controlled by identified reticulospinal neurons downstream of the tectum. *The Journal of neuroscience : the official journal of the Society for Neuroscience,* 25**,** 9294-9303.

GALANZHA, E. I., SHASHKOV, E. V., SPRING, P. M., SUEN, J. Y. & ZHAROV, V. P. 2009. In vivo, noninvasive, label-free detection and eradication of circulating metastatic melanoma cells using two-color photoacoustic flow cytometry with a diode laser. *Cancer research,* 69**,** 7926-7934.

GAMBRILL, A. C., FAULKNER, R. & CLINE, H. T. 2016. Experience-dependent plasticity of excitatory and inhibitory intertectal inputs in Xenopus tadpoles. *Journal of neurophysiology,* 116**,** 2281-2297.

GARCIA-RILL, E., SKINNER, R. D. & FITZGERALD, J. A. 1983. Activity in the mesencephalic locomotor region during locomotion. *Experimental Neurology,* 82**,** 609-622.

GERFEN CHARLES, R., ENGBER THOMAS, M., MAHAN LAWRENCE, C., SUSEL, Z., CHASE THOMAS, N., MONSMA FREDERICK, J. & SIBLEY DAVID, R. 1990. D1 and D2 Dopamine Receptor-regulated Gene Expression of Striatonigral and Striatopallidal Neurons. *Science,* 250**,** 1429-1432.

GERFEN, C. R. & SURMEIER, D. J. 2011. Modulation of striatal projection systems by dopamine. *Annual review of neuroscience,* 34**,** 441-466.

GLENN NORTHCUTT, R. 1979. Experimental determination of the primary trigeminal projections in lampreys. *Brain Research,* 163**,** 323-327.

GOLD, J. I. & SHADLEN, M. N. 2007. The Neural Basis of Decision Making. *Annual Review of Neuroscience,* 30**,** 535-574.

GONZÁLEZ, A., MARÍN, O., TUINHOF, R. & SMEETS, W. J. A. J. 1994. Ontogeny of catecholamine systems in the central nervous system of anuran amphibians: An immunohistochemical study with antibodies against tyrosine hydroxylase and dopamine. *Journal of Comparative Neurology,* 346**,** 63-79.

GOULDING, M. 2009. Circuits controlling vertebrate locomotion: moving in a new direction. *Nature Reviews Neuroscience,* 10**,** 507-518.

GRANT, P., RUBIN, E. & CIMA, C. 1980. Ontogeny of the retina and optic nerve in Xenopus laevis. I. Stages in the early development of the retina. *Journal of Comparative Neurology,* 189**,** 593-613.

GREEN, C. S. & SOFFE, S. R. 1996. Transitions between two different motor patterns in Xenopus embryos. *Journal of Comparative Physiology A,* 178**,** 279-291.

GRILLNER, S. 2006. Biological Pattern Generation: The Cellular and Computational Logic of Networks in Motion. *Neuron,* 52**,** 751-766.

GRILLNER, S. & EL MANIRA, A. 2020. Current Principles of Motor Control, with Special Reference to Vertebrate Locomotion. *Physiol Rev,* 100**,** 271-320.

GRILLNER, S., HELLGREN, J., MÉNARD, A., SAITOH, K. & WIKSTRÖM, M. A. 2005. Mechanisms for selection of basic motor programs – roles for the striatum and pallidum. *Trends in Neurosciences,* 28**,** 364-370.

GRILLNER, S. & MATSUSHIMA, T. 1991. The neural network underlying locomotion in lamprey-synaptic and cellular mechanisms. *Neuron,* 7**,** 1-15.

GRILLNER, S. & ROBERTSON, B. 2016. The Basal Ganglia Over 500 Million Years. *Current Biology,* 26**,** R1088-R1100.

GRILLNER, S., WALLÉN, P., SAITOH, K., KOZLOV, A. & ROBERTSON, B. 2008. Neural bases of goal-directed locomotion in vertebrates—An overview. *Brain Research Reviews,* 57**,** 2-12.

GRILLNER, S. & ZANGGER, P. 1979. On the central generation of locomotion in the low spinal cat. *Experimental Brain Research,* 34**,** 241-261.

HALE, M. E., KATZ, H. R., PEEK, M. Y. & FREMONT, R. T. 2016. Neural circuits that drive startle behavior, with a focus on the Mauthner cells and spiral fiber neurons of fishes. *Journal of Neurogenetics,* 30**,** 89-100.

HALE, M. E., RITTER, D. A. & FETCHO, J. R. 2001. A confocal study of spinal interneurons in living larval zebrafish. *Journal of Comparative Neurology,* 437**,** 1-16.

HAYES, B. P., ROBERTS, A. & BOYCOTT, B. B. 1983. The anatomy of two functional types of mechanoreceptive 'free' nerve-ending in the head skin of Xenopus embryos. *Proceedings of the Royal Society of London. Series B. Biological Sciences,* 218**,** 61-76.

HIGASHIJIMA, S.-I., MASINO, M. A., MANDEL, G. & FETCHO, J. R. 2004. Engrailed-1 expression marks a primitive class of inhibitory spinal interneuron. *The Journal of neuroscience : the official journal of the Society for Neuroscience,* 24**,** 5827-5839.

HIKOSAKA, O. & WURTZ, R. H. 1983. Effects on eye movements of a GABA agonist and antagonist injected into monkey superior colliculus. *Brain Research,* 272**,** 368-372.

HOFFLAND, B. S., VEUGEN, L. C., JANSSEN, M. M. H. P., PASMAN, J. W., WEERDESTEYN, V. & VAN DE WARRENBURG, B. P. 2014. A Gait Paradigm Reveals Different Patterns of Abnormal Cerebellar Motor Learning in Primary Focal Dystonias. *The Cerebellum,* 13**,** 760-766.

HOLT, C. E. 1984. Does timing of axon outgrowth influence initial retinotectal topography in Xenopus? *The Journal of neuroscience : the official journal of the Society for Neuroscience,* 4**,** 1130-1152.

HOLT, C. E. & HARRIS, W. A. 1983. Order in the initial retinotectal map in Xenopus: a new technique for labelling growing nerve fibres. *Nature,* 301**,** 150-152.

HOWE, M. W. & DOMBECK, D. A. 2016. Rapid signalling in distinct dopaminergic axons during locomotion and reward. *Nature,* 535**,** 505-510.

HUBBARD, JEFFREY M., BÖHM, URS L., PRENDERGAST, A., TSENG, P.-EN B., NEWMAN, M., STOKES, C. & WYART, C. 2016. Intraspinal Sensory Neurons Provide Powerful Inhibition to Motor Circuits Ensuring Postural Control during Locomotion. *Current Biology,* 26**,** 2841-2853.

HULL, M. J., SOFFE, S. R., WILLSHAW, D. J. & ROBERTS, A. 2016. Modelling Feedback Excitation, Pacemaker Properties and Sensory Switching of Electrically Coupled Brainstem Neurons Controlling Rhythmic Activity. *PLoS Comput Biol,* 12**,** e1004702.

INZELBERG, R., FLASH, T., SCHECHTMAN, E. & KORCZYN, A. D. 1995. Kinematic properties of upper limb trajectories in idiopathic torsion dystonia. *Journal of Neurology, Neurosurgery & Psychiatry,* 58**,** 312.

IRONS, T. D., KELLY, P. E., HUNTER, D. L., MACPHAIL, R. C. & PADILLA, S. 2013. Acute administration of dopaminergic drugs has differential effects on locomotion in larval zebrafish. *Pharmacology, biochemistry, and behavior,* 103**,** 792-813.

JACKSON, H. E. & INGHAM, P. W. 2013. Control of muscle fibre-type diversity during embryonic development: The zebrafish paradigm. *Mechanisms of Development,* 130**,** 447-457.

JAMES, L. J. & SOFFE, S. R. 2011. Skin impulse excitation of spinal sensory neurons in developing Xenopus laevis (Daudin) tadpoles. *Journal of Experimental Biology,* 214**,** 3341-3350.

JAMIESON, D. & ROBERTS, A. 1999. A Possible Pathway Connecting the Photosensitive Pineal Eye to the Swimming Central Pattern Generator in Young Xenopus laevis Tadpoles. *Brain, Behavior and Evolution,* 54**,** 323-337.

JAMIESON, D. & ROBERTS, A. 2000. Responses of young Xenopus laevis tadpoles to light dimming: possible roles for the pineal eye. *The Journal of experimental biology,* 203 Pt 12**,** 1857-67.

JIN, X., TECUAPETLA, F. & COSTA, R. M. 2014. Basal ganglia subcircuits distinctively encode the parsing and concatenation of action sequences. *Nature Neuroscience,* 17**,** 423-430.

JORDAN, L. M. 1998. Initiation of Locomotion in Mammals. *Annals of the New York Academy of Sciences,* 860**,** 83-93.

JORGENSEN, P., STEEN, J. A. J., STEEN, H. & KIRSCHNER, M. W. 2009. The mechanism and pattern of yolk consumption provide insight into embryonic nutrition in Xenopus. *Development (Cambridge, England),* 136**,** 1539-1548.

JUÁREZ-MORALES, J. L., SCHULTE, C. J., PEZOA, S. A., VALLEJO, G. K., HILINSKI, W. C., ENGLAND, S. J., DE JAGER, S. & LEWIS, K. E. 2016. Evx1 and Evx2 specify excitatory neurotransmitter fates and suppress inhibitory fates through a Pax2-independent mechanism. *Neural development,* 11**,** 5-5.

JUNG, H. & DASEN, JEREMY S. 2015. Evolution of Patterning Systems and Circuit Elements for Locomotion. *Developmental Cell,* 32**,** 408-422.

KAHN, J. A., ROBERTS, A. & BOYCOTT, B. B. 1982a. Experiments on the central pattern generator for swimming in amphibian embryos. *Philosophical Transactions of the Royal Society of London. B, Biological Sciences,* 296**,** 229-243.

KAHN, J. A., ROBERTS, A. & KASHIN, S. M. 1982b. The neuromuscular basis of swimming movements in embryos of the amphibian Xenopus laevis. *Journal of Experimental Biology,* 99**,** 175-184.

KANDASWAMY, D., M, M., ALEXANDER, M., PRABHU, K., S, M. G. & KROTHAPALLI, S. B. 2018. Quantitative Assessment of Hand Dysfunction in Patients with Early Parkinson's Disease and Focal Hand Dystonia. *JMD,* 11**,** 35-44.

KATZ, P. S. 2016. Evolution of central pattern generators and rhythmic behaviours. *Philos Trans R Soc Lond B Biol Sci,* 371**,** 20150057.

KAWASHIMA, T., ZWART, M. F., YANG, C.-T., MENSH, B. D. & AHRENS, M. B. 2016. The Serotonergic System Tracks the Outcomes of Actions to Mediate Short-Term Motor Learning. *Cell,* 167**,** 933-946.e20.

KHAKHALIN, A. S., KOREN, D., GU, J., XU, H. & AIZENMAN, C. D. 2014. Excitation and inhibition in recurrent networks mediate collision avoidance in Xenopus tadpoles. *European Journal of Neuroscience,* 40**,** 2948-2962.

KHALIL, R., TINDLE, R., BORAUD, T., MOUSTAFA, A. A. & KARIM, A. A. 2018. Social decision making in autism: On the impact of mirror neurons, motor control, and imitative behaviors. *CNS Neuroscience & Therapeutics,* 24**,** 669-676.

KIEHN, O. 2006. Locomotor circuits in the mammalian spinal cord. *Annu Rev Neurosci,* 29**,** 279-306.

KIEHN, O. 2016. Decoding the organization of spinal circuits that control locomotion. *Nature Reviews Neuroscience,* 17**,** 224-238.

KIMURA, Y., OKAMURA, Y. & HIGASHIJIMA, S.-I. 2006. alx, a zebrafish homolog of Chx10, marks ipsilateral descending excitatory interneurons that participate in the regulation of spinal locomotor circuits. *The Journal of neuroscience : the official journal of the Society for Neuroscience,* 26**,** 5684-5697.

KIMURA, Y., SATOU, C., FUJIOKA, S., SHOJI, W., UMEDA, K., ISHIZUKA, T., YAWO, H. & HIGASHIJIMA, S.-I. 2013. Hindbrain V2a Neurons in the Excitation of Spinal Locomotor Circuits during Zebrafish Swimming. *Current Biology,* 23**,** 843-849.

KLAUS, A., MARTINS, G. J., PAIXAO, V. B., ZHOU, P., PANINSKI, L. & COSTA, R. M. 2017. The Spatiotemporal Organization of the Striatum Encodes Action Space. *Neuron,* 95**,** 1171-1180.e7.

KLIETHERMES, C. L. & CRABBE, J. C. 2006. Pharmacological and genetic influences on hole-board behaviors in mice. *Pharmacology Biochemistry and Behavior,* 85**,** 57-65.

KNUDSEN, E. I. 2011. Control from below: the role of a midbrain network in spatial attention. *European Journal of Neuroscience,* 33**,** 1961-1972.

KOLMER, W. 1921. Das "sagitallorgan" der wirbeltiere *Z. Anat. Entwicklungsgesch,* 60**,** 652–717.

KOLMER, W. 1925. Weitere beitrage zur kenntnis des sagittalorgans der wirbeltiere. Verh. . *Anat. Ges. JENA* 60**,** 252–257.

KOUTSIKOU, S., MERRISON-HORT, R., BUHL, E., FERRARIO, A., LI, W. C., BORISYUK, R., SOFFE, S. R. & ROBERTS, A. 2018. A simple decision to move in response to touch reveals basic sensory memory and mechanisms for variable response times. *J Physiol,* 596**,** 6219-6233.

KOYAMA, M., KINKHABWALA, A., SATOU, C., HIGASHIJIMA, S.-I. & FETCHO, J. 2011. Mapping a sensory-motor network onto a structural and functional ground plan in the hindbrain. *Proceedings of the National Academy of Sciences of the United States of America,* 108**,** 1170-1175.

KOYAMA, M., MINALE, F., SHUM, J., NISHIMURA, N., SCHAFFER, C. B. & FETCHO, J. R. 2016. A circuit motif in the zebrafish hindbrain for a two alternative behavioral choice to turn left or right. *eLife,* 5**,** e16808.

KOYAMA, M. & PUJALA, A. 2018. Mutual inhibition of lateral inhibition: a network motif for an elementary computation in the brain. *Current Opinion in Neurobiology,* 49**,** 69-74.

KREITZER, A. C. & MALENKA, R. C. 2008. Striatal Plasticity and Basal Ganglia Circuit Function. *Neuron,* 60**,** 543-554.

KRUMHOLZ, A., WANG, L., YAO, J. & WANG, L. V. 2012. Functional photoacoustic microscopy of diabetic vasculature. *Journal of biomedical optics,* 17**,** 060502-060502.

KYRIAKATOS, A., MAHMOOD, R., AUSBORN, J., PORRES, C. P., BÜSCHGES, A. & EL MANIRA, A. 2011. Initiation of locomotion in adult zebrafish. *The Journal of neuroscience : the official journal of the Society for Neuroscience,* 31**,** 8422-8431.

LAMBERT, T. D., HOWARD, J., PLANT, A., SOFFE, S. & ROBERTS, A. 2004a. Mechanisms and significance of reduced activity and responsiveness in resting frog tadpoles. *Journal of Experimental Biology,* 207**,** 1113-1125.

LAMBERT, T. D., LI, W. C., SOFFE, S. R. & ROBERTS, A. 2004b. Brainstem control of activity and responsiveness in resting frog tadpoles: tonic inhibition. *Journal of Comparative Physiology A,* 190**,** 331-342.

LEE, R. K. K., EATON, R. C. & ZOTTOLI, S. J. 1993. Segmental arrangement of reticulospinal neurons in the goldfish hindbrain. *Journal of Comparative Neurology,* 329**,** 539-556.

LEKHEL, H., POPOV, K., ANASTASOPOULOS, D., BRONSTEIN, A., BHATIA, K., MARSDEN, C. D. & GRESTY, M. 1997. Postural responses to vibration of neck muscles in patients with idiopathic torticollis. *Brain,* 120**,** 583-591.

LEMON, R. N. 2008. Descending Pathways in Motor Control. *Annual Review of Neuroscience,* 31**,** 195-218.

LI, W.-C., SAUTOIS, B., ROBERTS, A. & SOFFE, S. R. 2007. Reconfiguration of a vertebrate motor network: specific neuron recruitment and context-dependent synaptic plasticity. *The Journal of neuroscience : the official journal of the Society for Neuroscience,* 27**,** 12267-12276.

LI, W.-C. & SOFFE, S. R. 2019. Stimulation of Single, Possible CHX10 Hindbrain Neurons Turns Swimming On and Off in Young Xenopus Tadpoles. *Frontiers in cellular neuroscience,* 13**,** 47-47.

LI, W. C., HIGASHIJIMA, S.-I., PARRY, D. M., ROBERTS, A. & SOFFE, S. R. 2004a. Primitive roles for inhibitory interneurons in developing frog spinal cord. *The Journal of neuroscience : the official journal of the Society for Neuroscience,* 24**,** 5840-5848.

LI, W. C., PERRINS, R., SOFFE, S. R., YOSHIDA, M., WALFORD, A. & ROBERTS, A. 2001. Defining classes of spinal interneuron and their axonal projections in hatchling Xenopus laevis tadpoles. *J Comp Neurol,* 441**,** 248-65.

LI, W. C., PERRINS, R., WALFORD, A. & ROBERTS, A. 2003. The neuronal targets for GABAergic reticulospinal inhibition that stops swimming in hatchling frog tadpoles. *Journal of Comparative Physiology A,* 189**,** 29-37.

LI, W. C., ROBERTS, A. & SOFFE, S. R. 2009. Locomotor rhythm maintenance: electrical coupling among premotor excitatory interneurons in the brainstem and spinal cord of young Xenopus tadpoles. *J Physiol,* 587**,** 1677-93.

LI, W. C., SOFFE, S. R. & ROBERTS, A. 2002. Spinal inhibitory neurons that modulate cutaneous sensory pathways during locomotion in a simple vertebrate. *The Journal of neuroscience : the official journal of the Society for Neuroscience,* 22**,** 10924-10934.

LI, W. C., SOFFE, S. R. & ROBERTS, A. 2004b. Dorsal Spinal Interneurons Forming a Primitive, Cutaneous Sensory Pathway. *Journal of Neurophysiology,* 92**,** 895-904.

LI, W. C., SOFFE, S. R. & ROBERTS, A. 2004c. Glutamate and acetylcholine corelease at developing synapses. *Proceedings of the National Academy of Sciences of the United States of America,* 101**,** 15488-15493.

LI, W. C., SOFFE, S. R., WOLF, E. & ROBERTS, A. 2006. Persistent responses to brief stimuli: feedback excitation among brainstem neurons. *J Neurosci,* 26**,** 4026-35.

LIAO, J. C. & FETCHO, J. R. 2008. Shared versus specialized glycinergic spinal interneurons in axial motor circuits of larval zebrafish. *The Journal of neuroscience : the official journal of the Society for Neuroscience,* 28**,** 12982-12992.

LIEN, C.-C., MU, Y., VARGAS-CABALLERO, M. & POO, M.-M. 2006. Visual stimuli–induced LTD of GABAergic synapses mediated by presynaptic NMDA receptors. *Nature Neuroscience,* 9**,** 372-380.

LIU, K. S. & FETCHO, J. R. 1999. Laser Ablations Reveal Functional Relationships of Segmental Hindbrain Neurons in Zebrafish. *Neuron,* 23**,** 325-335.

LIU, Q. R., LÓPEZ-CORCUERA, B., MANDIYAN, S., NELSON, H. & NELSON, N. 1993. Cloning and expression of a spinal cord- and brain-specific glycine transporter with novel structural features. *Journal of Biological Chemistry,* 268**,** 22802-22808.

LIU, Y.-C. & HALE, M. E. 2017. Local Spinal Cord Circuits and Bilateral Mauthner Cell Activity Function Together to Drive Alternative Startle Behaviors. *Current Biology,* 27**,** 697-704.

LJUNGGREN, E. E., HAUPT, S., AUSBORN, J., AMPATZIS, K. & EL MANIRA, A. 2014. Optogenetic activation of excitatory premotor interneurons is sufficient to generate coordinated locomotor activity in larval zebrafish. *The Journal of neuroscience : the official journal of the Society for Neuroscience,* 34**,** 134-139.

MARQUART, G. D., TABOR, K. M., BERGERON, S. A., BRIGGMAN, K. L. & BURGESS, H. A. 2019. Prepontine non-giant neurons drive flexible escape behavior in zebrafish. *PLoS biology,* 17**,** e3000480-e3000480.

MASINO, M. A. & FETCHO, J. R. 2005. Fictive Swimming Motor Patterns in Wild Type and Mutant Larval Zebrafish. *Journal of Neurophysiology,* 93**,** 3177-3188.

MAUTHNER, L. 1859. Untersuchungen uuml ber den Bau des Ruumlckenmarks der Fische. Eine vorlauml ufige Mittheilung. *Sitzgsber Kaiserl Akad Wiss Wien Math-Naturw Classe,* 34**,** 31–6.

MCDEARMID, J. R., SCRYMGEOUR-WEDDERBURN, J. F. & SILLAR, K. T. 1997. Aminergic modulation of glycine release in a spinal network controlling swimming in Xenopus laevis. *The Journal of physiology,* 503 (Pt 1)**,** 111-117.

MCLEAN, D. L., FAN, J., HIGASHIJIMA, S.-I., HALE, M. E. & FETCHO, J. R. 2007. A topographic map of recruitment in spinal cord. *Nature,* 446**,** 71-75.

MCLEAN, D. L. & FETCHO, J. R. 2004a. Ontogeny and innervation patterns of dopaminergic, noradrenergic, and serotonergic neurons in larval zebrafish. *Journal of Comparative Neurology,* 480**,** 38-56.

MCLEAN, D. L. & FETCHO, J. R. 2004b. Relationship of tyrosine hydroxylase and serotonin immunoreactivity to sensorimotor circuitry in larval zebrafish. *Journal of Comparative Neurology,* 480**,** 57-71.

MCLEAN, D. L. & FETCHO, J. R. 2009. Spinal interneurons differentiate sequentially from those driving the fastest swimming movements in larval zebrafish to those driving the slowest ones. *The Journal of neuroscience : the official journal of the Society for Neuroscience,* 29**,** 13566-13577.

MCLEAN, D. L., MASINO, M. A., KOH, I. Y. Y., LINDQUIST, W. B. & FETCHO, J. R. 2008. Continuous shifts in the active set of spinal interneurons during changes in locomotor speed. *Nature Neuroscience,* 11**,** 1419-1429.

MCPHERSON, ADAM D., BARRIOS, JOSHUA P., LUKS-MORGAN, SASHA J., MANFREDI, JOHN P., BONKOWSKY, JOSHUA L., DOUGLASS, ADAM D. & DORSKY, RICHARD I. 2016. Motor Behavior Mediated by Continuously Generated Dopaminergic Neurons in the Zebrafish Hypothalamus Recovers after Cell Ablation. *Current Biology,* 26**,** 263-269.

MÉNARD, A., AUCLAIR, F., BOURCIER-LUCAS, C., GRILLNER, S. & DUBUC, R. 2007. Descending GABAergic projections to the mesencephalic locomotor region in the lamprey Petromyzon marinus. *Journal of Comparative Neurology,* 501**,** 260-273.

MENELAOU, E. & MCLEAN, D. L. 2012. A gradient in endogenous rhythmicity and oscillatory drive matches recruitment order in an axial motor pool. *The Journal of neuroscience : the official journal of the Society for Neuroscience,* 32**,** 10925-10939.

MENELAOU, E. & MCLEAN, D. L. 2019. Hierarchical control of locomotion by distinct types of spinal V2a interneurons in zebrafish. *Nature Communications,* 10**,** 4197.

MIRAUCOURT, L. S., SILVA, J. S. D., BURGOS, K., LI, J., ABE, H., RUTHAZER, E. S. & CLINE, H. T. 2012. GABA expression and regulation by sensory experience in the developing visual system. *PloS one,* 7**,** e29086-e29086.

MOGENSON, G. J., SWANSON, L. W. & WU, M. 1985. Evidence that projections from substantia innominata to zona incerta and mesencephalic locomotor region contribute to locomotor activity. *Brain Research,* 334**,** 65-76.

MONTORZI, M., FALCHUK, K. H. & VALLEE, B. L. 1995. Vitellogenin and lipovitellin: zinc proteins of Xenopus laevis oocytes. *Biochemistry,* 34**,** 10851-10858.

MYERS, P. Z. 1985. Spinal motoneurons of the larval zebrafish. *Journal of Comparative Neurology,* 236**,** 555-561.

MYERS, P. Z., EISEN, J. S. & WESTERFIELD, M. 1986. Development and axonal outgrowth of identified motoneurons in the zebrafish. *The Journal of neuroscience : the official journal of the Society for Neuroscience,* 6**,** 2278-2289.

NIEUWKOOP, P. & FABER, J. 1956. Normal table of Xenopus laevis (Daudin) a systematical and chronological survey of the develop ment from the fertilized egg till the end of metamorphosis (2nd edition). *North-Holland Pub. Co*.

NOGA, B. R., KETTLER, J. & JORDAN, L. M. 1988. Locomotion produced in mesencephalic cats by injections of putative transmitter substances and antagonists into the medial reticular

formation and the pontomedullary locomotor strip. *The Journal of neuroscience : the official journal of the Society for Neuroscience,* 8**,** 2074-2086.

NOORANI, I. & CARPENTER, R. H. S. 2016. The LATER model of reaction time and decision. *Neuroscience & Biobehavioral Reviews,* 64**,** 229-251.

NORDLANDER, R. H., BADEN, S. T. & RYBA, T. M. J. 1985. Development of early brainstem projections to the tail spinal cord of xenopus. *Journal of Comparative Neurology,* 231**,** 519-529.

O'MALLEY, D. M., KAO, Y.-H. & FETCHO, J. R. 1996. Imaging the Functional Organization of Zebrafish Hindbrain Segments during Escape Behaviors. *Neuron,* 17**,** 1145-1155.

O'SHEA, T. M. 2008. Diagnosis, Treatment, and Prevention of Cerebral Palsy. *Clinical Obstetrics and Gynecology,* 51.

OHLENDORF, D. H., BARBARASH, G. R., TROUT, A., KENT, C. & BANASZAK, L. J. 1977. Lipid and polypeptide components of the crystalline yolk system from Xenopus laevis. *Journal of Biological Chemistry,* 252**,** 7992-8001.

OPRIS, I., DAI, X., JOHNSON, D. M. G., SANCHEZ, F. J., VILLAMIL, L. M., XIE, S., LEE-HAUSER, C. R., CHANG, S., JORDAN, L. M. & NOGA, B. R. 2019. Activation of Brainstem Neurons During Mesencephalic Locomotor Region-Evoked Locomotion in the Cat. *Front Syst Neurosci,* 13**,** 69.

ORLOVSKIĬ, G. N. 1970. Relations between reticulo-spinal neurons and locomotor regions of the brain stem. *Biofizika,* Jan-Feb**,** 171-8.

ORLOVSKY, G., DELIAGINA, T. & GRILLNER, S. 1999. Neuronal Control of Locomotion: From Mollusc to Man. *Oxford University Press*.

OSTERLING, J. A., DAWSON, G. & MUNSON, J. A. 2002. Early recognition of 1-year-old infants with autism spectrum disorder versus mental retardation. *Development and Psychopathology,* 14**,** 239-251.

OVSEPIAN, S. V., OLEFIR, I., WESTMEYER, G., RAZANSKY, D. & NTZIACHRISTOS, V. 2017. Pushing the Boundaries of Neuroimaging with Optoacoustics. *Neuron,* 96**,** 966-988.

PARKER, J. G., MARSHALL, J. D., AHANONU, B., WU, Y.-W., KIM, T. H., GREWE, B. F., ZHANG, Y., LI, J. Z., DING, J. B., EHLERS, M. D. & SCHNITZER, M. J. 2018. Diametric neural ensemble dynamics in parkinsonian and dyskinetic states. *Nature,* 557**,** 177-182.

PÉREZ-FERNÁNDEZ, J., STEPHENSON-JONES, M., SURYANARAYANA, S. M., ROBERTSON, B. & GRILLNER, S. 2014. Evolutionarily conserved organization of the dopaminergic system in lamprey: SNc/VTA afferent and efferent connectivity and D2 receptor expression. *Journal of Comparative Neurology,* 522**,** 3775-3794.

PERRINS, R. & ROBERTS, A. 1994. Nicotinic and muscarinic ACh receptors in rhythmically active spinal neurones in the Xenopus laevis embryo. *The Journal of physiology,* 478 (Pt 2)**,** 221-228.

PERRINS, R. & ROBERTS, A. 1995a. Cholinergic and electrical motoneuron-to-motoneuron synapses contribute to on-cycle excitation during swimming in Xenopus embryos. *Journal of Neurophysiology,* 73**,** 1005-1012.

PERRINS, R. & ROBERTS, A. 1995b. Cholinergic contribution to excitation in a spinal locomotor central pattern generator in Xenopus embryos. *Journal of Neurophysiology,* 73**,** 1013-1019.

PERRINS, R. & SOFFE, S. R. 1996. Local effects of glycinergic inhibition in the spinal cord motor systems for swimming in amphibian embryos. *Journal of Neurophysiology,* 76**,** 1025-1035.

PERRINS, R., WALFORD, A. & ROBERTS, A. 2002. Sensory activation and role of inhibitory reticulospinal neurons that stop swimming in hatchling frog tadpoles. *The Journal of neuroscience : the official journal of the Society for Neuroscience,* 22**,** 4229-4240.

PFLIEGER, J. F. & DUBUC, R. 2004. Vestibulo-reticular projections in adult lamprey: Their role in locomotion. *Neuroscience,* 129**,** 817-829.

PODOLEANU, A., CERNAT, R. & BRADU, A. 2019. Down-conversion en-face optical coherence tomography. *Biomedical optics express,* 10**,** 772-788.

RICHARDS, B. A., VOSS, O. P. & AKERMAN, C. J. 2010. GABAergic circuits control stimulus-instructed receptive field development in the optic tectum. *Nature Neuroscience,* 13**,** 1098-1106.

ROBERTS, A. 1969. Conducted Impulses in the Skin of Young Tadpoles. *Nature,* 222**,** 1265-1266.

ROBERTS, A. 1978. Pineal eye and behaviour in Xenopus tadpoles. *Nature,* 273**,** 774-775.

ROBERTS, A. 1980. The function and role of two types of mechanoreceptive 'free' nerve endings in the head skin of amphibian embryos. *Journal of comparative physiology,* 135**,** 341-348.

ROBERTS, A. 1996. Trigeminal pathway for the skin impulse to initiate swimming in hatchling Xenopus embryos. *J Physiol* 493**,** 40-41.

ROBERTS, A. 2000. Early functional organization of spinal neurons in developing lower vertebrates. *Brain Research Bulletin,* 53**,** 585–593.

ROBERTS, A. & ALFORD, S. T. 1986. Descending projections and excitation during fictive swimming in Xenopus embryos: Neuroanatomy and lesion experiments. *Journal of Comparative Neurology,* 250**,** 253-261.

ROBERTS, A., BLIGHT, A. R. & BOYCOTT, B. B. 1975. Anatomy, physiology and behavioural rôle of sensory nerve endings in the cement gland of embryonic Xenopus. *Proceedings of the Royal Society of London. Series B. Biological Sciences,* 192**,** 111-127.

ROBERTS, A., BORISYUK, R., BUHL, E., FERRARIO, A., KOUTSIKOU, S., LI, W. C. & SOFFE, S. R. 2019. The decision to move: response times, neuronal circuits and sensory memory in a simple vertebrate. *Proc Biol Sci,* 286**,** 20190297.

ROBERTS, A. & CLARKE, J. D. 1982. The neuroanatomy of an amphibian embryo spinal cord. *Phil. Trans. R. Soc. Lond. B,* 296**,** 195-212.

ROBERTS, A., DALE, N., OTTERSEN, O. P. & STORM-MATHISEN, J. 1987. The early development of neurons with GABA immunoreactivity in the CNS of Xenopus laevis embryos. *Journal of Comparative Neurology,* 261**,** 435-449.

ROBERTS, A., DALE, N., OTTERSEN, O. P. & STORM-MATHISEN, J. 1988. Development and characterization of commissural interneurones in the spinal cord of Xenopus laevis embryos revealed by antibodies to glycine. *Development,* 103 3**,** 447-61.

ROBERTS, A., LI, W.-C. & SOFFE, S. 2010. How neurons generate behaviour in a hatchling amphibian tadpole: an outline. *Frontiers in Behavioral Neuroscience,* 4.

ROBERTS, A., LI, W.-C. & SOFFE, S. R. 2008. Roles for inhibition: studies on networks controlling swimming in young frog tadpoles. *Journal of Comparative Physiology A,* 194**,** 185-193.

ROBERTS, A., LI, W.-C. & SOFFE, S. R. 2012. A functional scaffold of CNS neurons for the vertebrates: The developing Xenopus laevis spinal cord. *Developmental Neurobiology,* 72**,** 575-584.

ROBERTS, A. & SILLAR, K. T. 1990. Characterization and Function of Spinal Excitatory Interneurons with Commissural Projections in Xenopus laevis embryos. *European Journal of Neuroscience,* 2**,** 1051-1062.

ROBERTS, A. & STIRLING, C. A. 1971. The properties and propagation of a cardiac-like impulse in the skin of young tadpoles. *Zeitschrift für vergleichende Physiologie,* 71**,** 295-310.

ROBERTSON, B., SAITOH, K., MÉNARD, A. & GRILLNER, S. 2006. Afferents of the lamprey optic tectum with special reference to the GABA input: Combined tracing and immunohistochemical study. *Journal of Comparative Neurology,* 499**,** 106-119.

RONAN, M. & NORTHCUTT, R. G. 1990. Projections ascending from the spinal cord to the brain in petromyzontid and myxinoid agnathans. *Journal of Comparative Neurology,* 291**,** 491-508.

ROSEBERRY, T. K., LEE, A. M., LALIVE, A. L., WILBRECHT, L., BONCI, A. & KREITZER, A. C. 2016. Cell-Type-Specific Control of Brainstem Locomotor Circuits by Basal Ganglia. *Cell,* 164**,** 526-37.

ROVAINEN, C. M. 1979. Neurobiology of lampreys. *Physiological Reviews,* 59**,** 1007-1077.

RYCZKO, D. & DUBUC, R. 2013. The Multifunctional Mesencephalic Locomotor Region. *Current Pharmaceutical Design,* 19**,** 4448-4470.

RYCZKO, D. & DUBUC, R. 2017. Dopamine and the Brainstem Locomotor Networks: From Lamprey to Human. *Frontiers in Neuroscience,* 11**,** 295.

RYCZKO, D., GRÄTSCH, S., ALPERT, M. H., CONE, J. J., KASEMIR, J., RUTHE, A., BEAUSÉJOUR, P.-A., AUCLAIR, F., ROITMAN, M. F., ALFORD, S. & DUBUC, R. 2020. Descending Dopaminergic Inputs to Reticulospinal Neurons Promote Locomotor Movements. *The Journal of neuroscience : the official journal of the Society for Neuroscience,* 40**,** 8478-8490.

SAINT-AMANT, L. & DRAPEAU, P. 1998. Time course of the development of motor behaviors in the zebrafish embryo. *Journal of Neurobiology,* 37**,** 622-632.

SAKURAI, A. & KATZ, P. S. 2015. Phylogenetic and individual variation in gastropod central pattern generators. *Journal of Comparative Physiology A,* 201**,** 829-839.

SAKURAI, A. & KATZ, P. S. 2016. The central pattern generator underlying swimming in Dendronotus iris: a simple half-center network oscillator with a twist. *J Neurophysiol,* 116**,** 1728-1742.

SANTOS, R. A., FUERTES, A. J. C., SHORT, G., DONOHUE, K. C., SHAO, H., QUINTANILLA, J., MALAKZADEH, P. & COHEN-CORY, S. 2018. DSCAM differentially modulates pre- and postsynaptic structural and functional central connectivity during visual system wiring. *Neural development,* 13**,** 22-22.

SATOU, C., KIMURA, Y. & HIGASHIJIMA, S.-I. 2012. Generation of multiple classes of V0 neurons in zebrafish spinal cord: progenitor heterogeneity and temporal control of neuronal diversity. *The Journal of neuroscience : the official journal of the Society for Neuroscience,* 32**,** 1771-1783.

SATOU, C., SUGIOKA, T., UEMURA, Y., SHIMAZAKI, T., ZMARZ, P., KIMURA, Y. & HIGASHIJIMA, S.-I. 2020. Functional Diversity of Glycinergic Commissural Inhibitory Neurons in Larval Zebrafish. *Cell Reports,* 30**,** 3036-3050.e4.

SAUTOIS, B., SOFFE, S. R., LI, W.-C. & ROBERTS, A. 2007. Role of type-specific neuron properties in a spinal cord motor network. *Journal of Computational Neuroscience,* 23**,** 59-77.

SCHALTENBRAND, G. & COBB, S. 1931. CLINICAL AND ANATOMICAL STUDIES ON TWO CATS WITHOUT NEOCORTEX. *Brain,* 53**,** 449-488.

SEKI, K., PERLMUTTER, S. I. & FETZ, E. E. 2003. Sensory input to primate spinal cord is presynaptically inhibited during voluntary movement. *Nature Neuroscience,* 6**,** 1309-1316.

SESSION, A. M., UNO, Y., KWON, T., CHAPMAN, J. A., TOYODA, A., TAKAHASHI, S., FUKUI, A., HIKOSAKA, A., SUZUKI, A., KONDO, M., VAN HEERINGEN, S. J., QUIGLEY, I., HEINZ, S., OGINO, H., OCHI, H., HELLSTEN, U., LYONS, J. B., SIMAKOV, O., PUTNAM, N., STITES, J., KUROKI, Y., TANAKA, T., MICHIUE, T., WATANABE, M., BOGDANOVIC, O., LISTER, R.,

GEORGIOU, G., PARANJPE, S. S., VAN KRUIJSBERGEN, I., SHU, S., CARLSON, J., KINOSHITA, T., OHTA, Y., MAWARIBUCHI, S., JENKINS, J., GRIMWOOD, J., SCHMUTZ, J., MITROS, T., MOZAFFARI, S. V., SUZUKI, Y., HARAMOTO, Y., YAMAMOTO, T. S., TAKAGI, C., HEALD, R., MILLER, K., HAUDENSCHILD, C., KITZMAN, J., NAKAYAMA, T., IZUTSU, Y., ROBERT, J., FORTRIEDE, J., BURNS, K., LOTAY, V., KARIMI, K., YASUOKA, Y., DICHMANN, D. S., FLAJNIK, M. F., HOUSTON, D. W., SHENDURE, J., DUPASQUIER, L., VIZE, P. D., ZORN, A. M., ITO, M., MARCOTTE, E. M., WALLINGFORD, J. B., ITO, Y., ASASHIMA, M., UENO, N., MATSUDA, Y., VEENSTRA, G. J. C., FUJIYAMA, A., HARLAND, R. M., TAIRA, M. & ROKHSAR, D. S. 2016. Genome evolution in the allotetraploid frog Xenopus laevis. *Nature,* 538**,** 336-343.

SHIK ML FAU - SEVERIN, F. V., SEVERIN FV FAU - ORLOVSKIĬ, G. N. & ORLOVSKIĬ, G. N. 1966. Control of walking and running by means of electric stimulation of the midbrain. *Biofizika,* 11**,** 659-66.

SHIK, M. L., ORLOVSKIĬ, G. N. & SEVERIN, F. V. 1968. [Locomotion of the mesencephalic cat evoked by pyramidal stimulation]. *Biofizika,* Jan-Feb**,** 127-35.

SHIK, M. L. & ORLOVSKY, G. N. 1976. Neurophysiology of locomotor automatism. *Physiological Reviews,* 56**,** 465-501.

SILLAR, K. T. 2009. Mauthner cells. *Current Biology,* 19**,** R353-R355.

SILLAR, K. T. & ROBERTS, A. 1988. Unmyelinated cutaneous afferent neurons activate two types of excitatory amino acid receptor in the spinal cord of Xenopus laevis embryos. *The Journal of neuroscience : the official journal of the Society for Neuroscience,* 8**,** 1350-1360.

SILLAR, K. T. & ROBERTSON, R. M. 2009. Thermal activation of escape swimming in post-hatching Xenopus laevis frog larvae. *The Journal of experimental biology,* 212**,** 2356-2364.

SILLAR, K. T., WEDDERBURN, J. F. S. & SIMMERS, A. J. 1992. Modulation of swimming rhythmicity by 5-hydroxytryptamine during post-embryonic development in Xenopus laevis. *Proceedings of the Royal Society of London. Series B: Biological Sciences,* 250**,** 107-114.

SIROTA, M. G., DI PRISCO, G. V. & DUBUC, R. 2000. Stimulation of the mesencephalic locomotor region elicits controlled swimming in semi-intact lampreys. *European Journal of Neuroscience,* 12**,** 4081-4092.

SMOLENAARS, M. M. W., MADSEN, O., RODENBURG, K. W. & VAN DER HORST, D. J. 2007. Molecular diversity and evolution of the large lipid transfer protein superfamily^{s⃞}. *Journal of Lipid Research,* 48**,** 489-502.

SOFFE, S. R. 1987. Ionic and pharmacological properties of reciprocal inhibition in Xenopus embryo motoneurones. *The Journal of physiology,* 382**,** 463-473.

SOFFE, S. R. 1989. Roles of Glycinergic Inhibition and N-Methyl-D-Aspartate Receptor Mediated Excitation in the Locomotor Rhythmicity of One Half of the Xenopus Embryo Central Nervous System. *European Journal of Neuroscience,* 1**,** 561-571.

SOFFE, S. R. 1990. Active and Passive Membrane Properties of Spinal Cord Neurons that Are Rhythmically Active during Swimming in Xenopus Embryos. *European Journal of Neuroscience,* 2**,** 1-10.

SOFFE, S. R. 1991. Triggering and gating of motor responses by sensory stimulation: behavioural selection in Xenopus embryos. *Proceedings of the Royal Society of London. Series B: Biological Sciences,* 246**,** 197-203.

SOFFE, S. R. 1993. Two distinct rhythmic motor patterns are driven by common premotor and motor neurons in a simple vertebrate spinal cord. *The Journal of neuroscience : the official journal of the Society for Neuroscience,* 13**,** 4456-4469.

SOFFE, S. R. 1996. Motor patterns for two distinct rhythmic behaviors evoked by excitatory amino acid agonists in the Xenopus embryo spinal cord. *Journal of Neurophysiology,* 75**,** 1815-1825.

SOFFE, S. R. 1997. The pattern of sensory discharge can determine the motor response in young Xenopus tadpoles. *Journal of Comparative Physiology A,* 180**,** 711-715.

SOFFE, S. R., CLARKE, J. D. & ROBERTS, A. 1984. Activity of commissural interneurons in spinal cord of Xenopus embryos. *Journal of Neurophysiology,* 51**,** 1257-1267.

SOFFE, S. R. & ROBERTS, A. 1982a. Activity of myotomal motoneurons during fictive swimming in frog embryos. *Journal of Neurophysiology,* 48**,** 1274-1278.

SOFFE, S. R. & ROBERTS, A. 1982b. Tonic and phasic synaptic input to spinal cord motoneurons during fictive locomotion in frog embryos. *Journal of Neurophysiology,* 48**,** 1279-1288.

SOFFE, S. R., ROBERTS, A. & LI, W. C. 2009. Defining the excitatory neurons that drive the locomotor rhythm in a simple vertebrate: insights into the origin of reticulospinal control. *J Physiol,* 587**,** 4829-44.

SOFFE, S. R., ZHAO, F. Y. & ROBERTS, A. 2001. Functional projection distances of spinal interneurons mediating reciprocal inhibition during swimming in Xenopus tadpoles. *European Journal of Neuroscience,* 13**,** 617-627.

STEPHENSON-JONES, M., SAMUELSSON, E., ERICSSON, J., ROBERTSON, B. & GRILLNER, S. 2011. Evolutionary Conservation of the Basal Ganglia as a Common Vertebrate Mechanism for Action Selection. *Current Biology,* 21**,** 1081-1091.

STEPIEN, A. E. & ARBER, S. 2008. Probing the Locomotor Conundrum: Descending the ‘V’ Interneuron Ladder. *Neuron,* 60**,** 1-4.

STERNBERG, JENNA R., SEVERI, KRISTEN E., FIDELIN, K., GOMEZ, J., IHARA, H., ALCHEIKH, Y., HUBBARD, JEFFREY M., KAWAKAMI, K., SUSTER, M. & WYART, C. 2016. Optimization of a Neurotoxin to Investigate the Contribution of Excitatory Interneurons to Speed Modulation In Vivo. *Current Biology,* 26**,** 2319-2328.

STINEAR, C. M. & BYBLOW, W. D. 2004. Impaired inhibition of a pre-planned response in focal hand dystonia. *Experimental Brain Research,* 158**,** 207-212.

SURMEIER, D. J., CARRILLO-REID, L. & BARGAS, J. 2011. Dopaminergic modulation of striatal neurons, circuits, and assemblies. *Neuroscience,* 198**,** 3-18.

SURMEIER, D. J., SONG, W. J. & YAN, Z. 1996. Coordinated expression of dopamine receptors in neostriatal medium spiny neurons. *The Journal of neuroscience : the official journal of the Society for Neuroscience,* 16**,** 6579-6591.

SVARA, F. N., KORNFELD, J., DENK, W. & BOLLMANN, J. H. 2018. Volume EM Reconstruction of Spinal Cord Reveals Wiring Specificity in Speed-Related Motor Circuits. *Cell Reports,* 23**,** 2942-2954.

SVOBODA, K. & LI, N. 2018. Neural mechanisms of movement planning: motor cortex and beyond. *Current Opinion in Neurobiology,* 49**,** 33-41.

THOMPSON, J. R. & BANASZAK, L. J. 2002. Lipid− protein interactions in lipovitellin. *Biochemistry,* 41**,** 9398-9409.

TRIPODI, M., STEPIEN, A. E. & ARBER, S. 2011. Motor antagonism exposed by spatial segregation and timing of neurogenesis. *Nature,* 479**,** 61-66.

TUNSTALL, M. J. & ROBERTS, A. 1991. Longitudinal coordination of motor output during swimming in Xenopus embryos. *Proceedings of the Royal Society of London. Series B: Biological Sciences,* 244**,** 27-32.

TUNSTALL, M. J. & ROBERTS, A. 1994. A longitudinal gradient of synaptic drive in the spinal cord of Xenopus embryos and its role in co-ordination of swimming. *The Journal of physiology,* 474**,** 393-405.

VAN MIER, P., JOOSTEN, H. W. J., VAN RHEDEN, R. & TEN DONKELAAR, H. J. 1986. The development of serotonergic raphespinal projections in Xenopus laevis. *International Journal of Developmental Neuroscience,* 4**,** 465-469.

VAN MIER, P. & TEN DONKELAAR, H. J. 1984. Early development of descending pathways from the brain stem to the spinal cord in Xenopus laevis. *Anatomy and Embryology,* 170**,** 295-306.

VAN RAAMSDONK, W., POOL, C. W., HEYTING, C., TEKRONNIE, G. & VEEKEN, K. 1982. Effects of immobilization and partial denervation on the differentiation of muscle fiber types in the zebrafish, Brachydanio rerio. *Anatomy and Embryology,* 164**,** 63-74.

VIANA DI PRISCO, G., BOUTIN, T., PETROPOULOS, D., BROCARD, F. & DUBUC, R. 2005. The trigeminal sensory relay to reticulospinal neurones in lampreys. *Neuroscience,* 131**,** 535-546.

VIANA DI PRISCO, G., PEARLSTEIN, E., LE RAY, D., ROBITAILLE, R. & DUBUC, R. 2000. A Cellular Mechanism for the Transformation of a Sensory Input into a Motor Command. *The Journal of Neuroscience,* 20**,** 8169.

VICZIAN, A. S., SOLESSIO, E. C., LYOU, Y. & ZUBER, M. E. 2009. Generation of functional eyes from pluripotent cells. *PLoS biology,* 7**,** e1000174-e1000174.

WANG, B., SU, J. L., KARPIOUK, A. B., SOKOLOV, K. V., SMALLING, R. W. & EMELIANOV, S. Y. 2010. Intravascular Photoacoustic Imaging. *IEEE Journal of Selected Topics in Quantum Electronics,* 16**,** 588-599.

WANG, L. & WU, H.-I. 2007. Biomedical optics : principles and imaging. *Wiley-Interscience,* xiv**,** 362.

WANG, W.-C. & MCLEAN, DAVID L. 2014. Selective Responses to Tonic Descending Commands by Temporal Summation in a Spinal Motor Pool. *Neuron,* 83**,** 708-721.

WESTER, M. R., TEASLEY, D. C., BYERS, S. L. & SAHA, M. S. 2008. Expression patterns of glycine transporters (xGlyT1, xGlyT2, and xVIAAT) in Xenopus laevis during early development. *Gene Expression Patterns,* 8**,** 261-270.

WIGGIN, T. D., PECK, J. H. & MASINO, M. A. 2014. Coordination of fictive motor activity in the larval zebrafish is generated by non-segmental mechanisms. *PloS one,* 9**,** e109117-e109117.

WILEY, H. & WALLACE, R. 1981. The structure of vitellogenin. Multiple vitellogenins in Xenopus laevis give rise to multiple forms of the yolk proteins. *Journal of Biological Chemistry,* 256**,** 8626-8634.

WILSON, D. M. & WYMAN, R. J. 1965. MOTOR OUTPUT PATTERNS DURING RANDOM AND RHYTHMIC STIMULATION OF LOCUST THORACIC GANGLIA. *Biophysical journal,* 5**,** 121-143.

WU, M., BRUDZYNSKI, S. M. & MOGENSON, G. J. 1993. Functional interaction of dopamine and glutamate in the nucleus accumbens in the regulation of locomotion. *Canadian Journal of Physiology and Pharmacology,* 71**,** 407-413.

WU, Q., CHAN, J. S. Y. & YAN, J. H. 2016. Mild cognitive impairment affects motor control and skill learning. *Reviews in the Neurosciences,* 27**,** 197-217.

WYART, C., BENE, F. D., WARP, E., SCOTT, E. K., TRAUNER, D., BAIER, H. & ISACOFF, E. Y. 2009. Optogenetic dissection of a behavioural module in the vertebrate spinal cord. *Nature,* 461**,** 407-410.

XU, L., GUAN, N. N., HUANG, C.-X., HUA, Y. & SONG, J. 2021. A neuronal circuit that generates the temporal motor sequence for the defensive response in zebrafish larvae. *Current Biology,* 31**,** 3343-3357.e4.

YANG, L., WANG, F. & STRÄHLE, U. 2020. The Genetic Programs Specifying Kolmer–Agduhr Interneurons. *Frontiers in Neuroscience,* 14**,** 1064.

YAO, J., MASLOV, K. I., ZHANG, Y., XIA, Y. & WANG, L. V. 2011. Label-free oxygen-metabolic photoacoustic microscopy in vivo. *Journal of biomedical optics,* 16**,** 076003-076003.

YAO, J. & WANG, L. V. 2013. Photoacoustic Microscopy. *Laser & photonics reviews,* 7**,** 10.1002/lpor.201200060.

YOSHIDA, M. 1997. Oligodendrocyte maturation in Xenopus laevis. *Journal of Neuroscience Research,* 50**,** 169-176.

YOSHIDA, M., ROBERTS, A. & SOFFE, S. R. 1998. Axon projections of reciprocal inhibitory interneurons in the spinal cord of young Xenopus tadpoles and implications for the pattern of inhibition during swimming and struggling. *Journal of Comparative Neurology,* 400**,** 504-518.

ZHANG, C., MASLOV, K. & WANG, L. V. 2010. Subwavelength-resolution label-free photoacoustic microscopy of optical absorption in vivo. *Optics Letters,* 35**,** 3195-3197.

ZHANG, S., LI, J., LEA, R. & AMAYA, E. 2016. Assessing Primary Neurogenesis in Xenopus Embryos Using Immunostaining. *Journal of visualized experiments : JoVE***,** e53949-e53949.

ZHAO, B., ZHU, J., DAI, D., XING, J., HE, J., FU, Z., ZHANG, L., LI, Z. & WANG, W. 2016. Differential dopaminergic regulation of inwardly rectifying potassium channel mediated subthreshold dynamics in striatal medium spiny neurons. *Neuropharmacology,* 107**,** 396-410.

ZHAO, F. Y., WOLF, E. & ROBERTS, A. 1998. Longitudinal distribution of components of excitatory synaptic input to motoneurones during swimming in young Xenopus tadpoles: experiments with antagonists. *The Journal of physiology,* 511 (Pt 3)**,** 887-901.

11 Appendix

11.1 Appendix 1
Supplementary Materials and Methods

11.1.1 Tools making

Handmade tungsten tools were used to perform animal surgery. Fine (diameter 0.3 mm) tungsten wires were cut and sharpened through an in-house electrolysis kit. The kit consisted of a Ag/AgCl electrode disk connected to the negative pole of a 9V battery; a short wire was connected to the positive pole of the battery and it was tied onto a metal clip. The tungsten wire was hold with the clip and submerged into a KOH 3M solution, together with the Ag/AgCl electrode disk. In this way, the metal particles were transferred from the tungsten to the solution, leaving the wire sharper. The same procedure was employed to make very small needle used to pin the animals to the Sylgard block during surgery. In this case, the tungsten was 0.075 mm in diameter.

11.1.2 Animal surgery

Animals were anesthetized and immobilized in MS-222 (5 minutes at RT, for behavioural experiments) or in α-bungarotoxin (50 minutes at RT, for electrophysiology experiments) before surgery. All animal surgery procedures were performed on a rotating Sylgard block in a custom-made dissecting dish. The dish was filled with saline solution and dissections were performed under a stereomicroscope (Leica M205 C), equipped with an external dimmable halogen lamp (max output 150 W; Lumina, Chiu Technical Corporation) illuminating the animal from the side. Animals were pinned to the Sylgard block with three fine home-made tungsten needles along the body: one through the eye, the second through the notochord just caudal to the obex, the third through the notochord slightly rostral to the level of the anus. In such way, the tadpole lied on its side and the whole body was elongated enough to perform accurate surgery. For head skin removal, a fine tungsten needle was inserted underneath the skin at the level of the obex. The skin was then cut longitudinally towards the forebrain to expose the hindbrain and the midbrain. All brain lesions described in chapter 4 were performed after skin was removed from the tadpoles' head. In all electrophysiology experiments, trunk skin was removed from both

sides of the body to allow suction electrodes to reach the myotomal clefts. For trunk skin removal, two cuts were performed on the fin and one sharp tungsten tool was sled in between the skin and trunk muscles along both sides of the tadpole's body. Skin on the tail and on the most caudal part of the trunk was left intact to allow the stimulation electrode to be attached to the skin at the level of the anus.

11.1.3 Solutions used for animal surgery

Saline

Saline solution was used during animal surgery and electrophysiology recordings. The recipe was as follows: NaCl 115 mM, HEPES 10 mM, $NaHCO_3$ 2.4 mM, KCl 3 mM, $MgCl_2$ 1mM, $CaCl_2$ 2mM. The salts were dissolved in de-ionized water and pH was adjusted to 7.4 with NaOH 3 M.

MS222 (ethyl 3-aminobenzoate methanesulfonate)

MS-222 powder was purchased from Sigma-Aldrich and stored at -20°C. The powder was dissolved in saline with at a concentration of 0.01%. The MS-222 was made fresh every day before use.

α-Bungarotoxin

α-bungarotoxin (from *Bungarus multicintum*) was purchase from Invitrogen. 0.1 mM (in de-ionized water) stock aliquots were kept frozen at -20°C. Aliquots were diluted with de-ionized water to reach a 0.01 mM working solution, which was kept refrigerated at 4°C for up to two weeks.

12 Appendix 2

Supplementary Material Chapter 4

Table 1

	25% percentile	median	75% percentile	IQR
Controls	79.76	109.5	153.6	73.84
Midline lesion	82.14	150.0	231.5	149.36
MHB lesion	143.5	201.2	287.5	144
0 cleft lesion	74.41	163.1	235.1	160.69
2nd cleft lesion	114.3	160.7	278.0	163.7
L-R staggered lesion	110.7	157.1	295.2	184.5
R-L staggered lesion	107.1	192.9	302.4	195.3

Table 1. *Median, 25% and 75% percentiles and interquartile range (IQR) values of latency (ms) to swim response after touch stimulation was manually delivered to control and hindbrain lesioned animals in behavioural experiments.*

Table 2

	25% percentile	median	75% percentile	IQR
Controls	91.02	100.9	117.8	26.78
Midline lesion	38.21	53.93	72.92	34.71
MHB lesion	36.24	48.12	61.40	25.16
0 cleft lesion	24.84	33.80	39.61	14.77
2nd cleft lesion	33.20	39.36	46.00	12.8
L-R staggered lesion	27.95	41.50	46.41	18.46
R-L staggered lesion	34.57	38.12	40.01	5.44

Table 2. *Median, 25% and 75% percentiles and interquartile range (IQR) values of latency (ms) to swim response after a threshold stimulation was delivered to control and hindbrain lesioned animals in electrophysiology experiments.*

Table 3

	25% percentile	median	75% percentile	IQR
Controls				
Ipsilateral response	93.12	101.90	112.00	18.88
Contralateral response	23.63	67.44	132.80	109.17
Midline lesion				
Ipsilateral response	40.17	53.93	58.73	18.56

Contralateral response	32.45	57.49	94.69	62.24
Synchronous response	42.20	95.71	149.20	107.00
MHB lesion				
Ipsilateral response	39.58	49.75	63.97	106.17
Contralateral response	36.52	50.65	83.59	47.07
Synchronous response	35.88	36.24	39.78	3.90
0 cleft lesion				
Ipsilateral response	33.96	37.77	46.75	12.79
Contralateral response	23.73	25.03	34.40	10.67
Synchronous response	35.09	35.09	35.09	0.00
2nd cleft lesion				
Ipsilateral response	24.85	39.69	50.67	25.82
Contralateral response	33.83	39.61	41.81	7.98
Synchronous response	34.45	36.45	47.37	12.92
L-R staggered lesion				
Ipsilateral response	27.54	36.97	46.41	18.87
Contralateral response	33.57	42.56	46.32	12.75
Synchronous response	27.95	27.95	27.95	0.00
R-L staggered lesion				
Ipsilateral response	36.95	39.07	46.99	10.04
Contralateral response	24.07	24.07	24.07	0.00
Synchronous response	34.57	37.15	39.73	5.16

Table 3. *Median, 25% and 75% percentiles and interquartile range (IQR) values of latency (ms) to swim response after a threshold stimulation was delivered to control and hindbrain lesioned animals in electrophysiology experiments. Latency to swim initiation is reported according to the side of first burst (ipsilateral or contralateral to the side of stimulus delivery) or to synchronous response.*

Table 4

	25% percentile	**median**	**75% percentile**	**IQR**
Controls	24.35	27.82	95.81	71.46
Midline lesion	26.48	30.94	44.57	18.09
MHB lesion	24.28	35.16	56.94	32.66
0 cleft lesion	21.35	27.36	32.97	11.62
2nd cleft lesion	24.18	26.90	37.62	13.44
L-R staggered lesion	23.09	24.91	38.68	15.59
R-L staggered lesion	26.22	33.71	39.47	13.25

Table 4. *Median, 25% and 75% percentiles and interquartile range (IQR) values of latency (ms) to swim response after a suprathreshold stimulation was delivered to control and hindbrain lesioned animals in electrophysiology experiments.*

Table 5

	25% percentile	median	75% percentile	IQR
Controls				
Ipsilateral response	96.96	107.9	120.3	23.34
Contralateral response	23.93	25.48	32.67	8.74
Midline lesion				
Ipsilateral response	32.28	46.77	52.69	20.41
Contralateral response	24.94	26.61	35.73	3.41
Synchronous response	26.92	30.22	36.54	9.62
MHB lesion				
Ipsilateral response	23.34	36.45	53.24	29.90
Contralateral response	24.81	43.61	95.71	70.90
Synchronous response	12.69	25.75	36.10	23.41
0 cleft lesion				
Ipsilateral response	20.26	25.87	34.35	14.09
Contralateral response	23.92	28.41	33.81	9.89
Synchronous response	24.09	27.47	31.43	7.34
2nd cleft lesion				
Ipsilateral response	24.11	26.29	45.41	21.3
Contralateral response	23.54	25.21	35.81	12.27
Synchronous response	24.44	28.12	32.17	7.73
L-R staggered lesion				
Ipsilateral response	21.23	25.73	46.99	25.76
Contralateral response	22.77	23.65	29.33	6.56
Synchronous response	23.71	24.52	44.30	20.59
R-L staggered lesion				
Ipsilateral response	33.58	36.78	37.87	4.29
Contralateral response	25.78	29.41	45.36	19.58
Synchronous response	32.73	32.73	32.73	0.00

Table 5. *Median, 25% and 75% percentiles and interquartile range (IQR) values of latency (ms) to swim response after a suprathreshold stimulation was delivered to control and hindbrain lesioned animals in electrophysiology experiments. Latency to swim initiation is reported according to the side of first burst (ipsilateral or contralateral to the side of stimulus delivery) or to synchronous response.*

13 Appendix 3

Submitted paper

Title:
Novel, highly distributed and diverse hindbrain neuronal activity contributes to sensory processing and motor control in the *Xenopus laevis* tadpole.

Running title: Hindbrain descending motor control

Author names and Affiliations:

Giulia Messa and Stella Koutsikou
Medway School of Pharmacy, University of Kent, Anson Building, Central Avenue, Chatham Maritime, Kent ME4 4TB, UK

Corresponding authors:

Stella Koutsikou;
S.Koutsikou@kent.ac.uk

Giulia Messa; gm452@kent.ac.uk

Number of pages: 16 Number of figures: 8

Number of words: abstract (203), introduction (612), discussion (1253)

Conflict of interest

The authors declared no conflict of interest for this work.

Acknowledgements

The authors would like to thank Professor Alan Roberts FRS for his helpful comments on the draft of this manuscript and acknowledge the financial support from the Physiological Society UK through a research grant awarded to SK.

Abstract

An animal's survival depends heavily on the selection and execution of timely and well-coordinated motor responses. The brainstem controls the activity of spinal neural circuits to produce and modify movements. However, important questions remain unanswered about the origin of this descending control and how brainstem neuronal activity integrates sensory inputs and determines specific motor functions. Here, we record hindbrain extracellular activity in response to trunk skin stimulation, which in turn leads to fictive swimming in the hatchling *Xenopus laevis* tadpole. We identify four distinct classes of single unit activity, distributed along the hindbrain rostro-caudal axis, whose firing patterns correlate to distinct motor states. We observe different firing patterns in response to stimulation that leads to fictive swimming *versus* the application of a weak stimulus which does not evoke movement. We identify differences in the temporal activation of the four classes of hindbrain activity in relation to the initiation of fictive swimming. We propose a simple network encompassing the novel neuronal populations embedded within the currently known sensory pathway and central pattern generators of the tadpole brainstem. By identifying the contribution of the individual supraspinal neuronal populations we build a better understanding of how the brain controls and modulates movement in this simple animal.

Significance Statement

Initiation, maintenance, adjustment and stopping of locomotion depends heavily on brainstem descending control over spinal neural circuits. Our study identifies novel, diverse and highly distributed hindbrain neuronal activity that correlates to distinct motor outputs in the *Xenopus laevis* tadpole. These newly identified firing patterns provide (i) explanation for the long and variable delays to the initiation of swimming, as seen in complex neural circuits of the adult vertebrate brain, active during motor decisionmaking, and (ii) critical information for the design and interpretation of new studies using the *Xenopus* tadpole, already a pioneering experimental model in the field of motor research.

Introduction

In nature animals must select, execute, and adapt their motor behavior to specific aims such as feeding, escaping from a predator, or finding a mate. From nudibranchs (Sakurai and Katz, 2016) to lamprey (Stephenson-Jones et al., 2011), from cats (Opris et al., 2019) to humans (MacKinnon, 2018), all animals are required to coordinate and timely activate central and peripheral neuronal circuits in order to perform the most advantageous movement. Most of the sensory input animals receive leads to motor activity.

In adult vertebrates, the combined activation of neural circuits in the forebrain, brainstem and spinal cord generates a fine-tuned and rich repertoire of motor behaviors, including locomotion (Goulding, 2009; Ruder and Arber, 2019). Although the spinal neural circuits have been extensively studied in higher vertebrates (Kiehn, 2006; Kiehn, 2016), unravelling the supraspinal control of movement (Armstrong, 1988; Dietz, 2010; Shik and Orlovsky, 1976) remains challenging, and the neuron-to-neuron pathways that coordinate motor decision and movement initiation have not been fully elucidated yet (Arber, 2012; Bouvier et al., 2015; Caggiano et al., 2018; Ferreira-Pinto et al., 2018; Parker, 2010).

Likewise, the spinal neuronal circuits responsible for swimming in the *Xenopus laevis* tadpole have been extensively characterized. The reticulospinal descending interneurons (dINs) that drive CPG (Central pattern Generators) activity have been anatomically and functionally described (Li et al., 2001; Li et al., 2006; Roberts et al., 2010). Furthermore, we have recently shown that the tadpole initiates stimulusevoked swimming after a delay of 50-150ms (Buhl et al., 2015; Koutsikou et al., 2018; Roberts et al., 2019). This delay is characterised by slow and variable accumulation of synaptic excitation in dINs (Koutsikou et al., 2018), which resembles the accumulation of excitation proposed for complex brain circuits active during motor decision-making (Carpenter, 1999; Gold & Shadlen, 2007). This finding allowed us to infer the existence of candidate neurons pre-synaptic to dINs, namely hindbrain extension neurons (hexNs; (Koutsikou et al., 2018)). It has been proposed that hexNs extend the short-lived sensory signal carried by the sensory and sensory pathway neurons (Rohon-Beard cells and dorsolateral ascending -dla- and dorsolateral commissural -dlc- neurons, respectively (Clarke et al., 1984; Roberts and Clarke, 1982), thus allowing the animal to make the simple motor decision, to swim or not to swim. Ultimately, and only if the stimulus delivered is strong enough, this build-up of excitation in the dINs reaches a firing threshold, which in turn marks the start of swimming (Buhl et al., 2015; Li et al., 2006). The accumulation of excitation on dINs has been mimicked through modelling of an excitatory recurrent network embedded within the brainstem sensory pathways (Ferrario et al., 2021; Koutsikou et al., 2018).

Despite the evidence above which is indicative of the fundamental elements of descending motor control being present at early developmental stages, the neurons processing and extending sensory information and subsequently activating motor pathways in the *Xenopus* tadpole are currently undefined. We implemented a top-down approach to uncover the extracellular firing characteristics of candidate hexNs, responsible for the accumulation of excitation in dINs prior to swim initiation and in response to trunk skin stimulation.

We identified novel firing patterns distributed across the tadpole's hindbrain indicating increased neuronal activity in the time between the sensory stimulation and motor output. We classified four hexN subpopulations based on their firing activity, which differentially contributed to the accumulation of excitation in the hindbrain prior to swimming initiation. These newly identified neuronal populations exhibit all features necessary for motor the decision-making process (*e.g.*, to swim or not to swim) in the tadpole. We propose a simple hindbrain neural network that includes the newly identified hexN subpopulations embedded within the existing well-defined sensory, sensory-pathway and CPG neuronal circuitry of the tadpole's CNS.

Materials and Methods

Ethics, animal care and preparation

Xenopus laevis embryos were supplied by the European *Xenopus* Resource Centre (EXRC; Portsmouth, UK). Animal care and all experimental procedures on *Xenopus* tadpoles were approved by the University of Kent Animal Welfare and Ethical Review Body (AWERB)

committee. *Xenopus* tadpoles were used at developmental stage 37/38 (Nieuwkoop & Faber, 1956) and all experiments were conducted at room temperature (19-22°C).

Tadpoles were briefly anesthetized in 0.1% MS-222 (ethyl 3-aminobenzoate methanesulfonate, SigmaAldrich), and subsequently immobilized by immersion in a 10 □M □-bungarotoxin (Invitrogen) solution for 50 minutes. Both solutions mentioned above were made in saline (NaCl 115 mM, HEPES 10 mM, NaHCO3
2.4 mM, KCl 3 mM, MgCl2 1mM, CaCl2 2mM) adjusted to pH 7.4. Animals were then mounted onto a rotating Sylgard block submerged in saline, and dissection was carried out as previously described (Buhl et al., 2015; Li et al., 2001). Briefly, the skin covering the brain and trunk muscles on both sides was removed, giving access to the entire hindbrain and myotomal clefts (Buhl et al., 2015; Li et al., 2001). The trigeminal nerves were severed at both sides of the body to prevent initiation of swimming in response to propagation of skin impulse (James and Soffe, 2011; Roberts, 1996; Roberts et al., 1971).

Electrophysiology

Extracellular ventral root recordings, indicative of fictive swimming, in combination with extracellular recordings of hindbrain neuronal activity, were performed on immobilized *Xenopus* tadpoles at stage 37/38. Two borosilicate glass suction electrodes (tip diameter □50□m) filled with saline were attached to both sides of the tadpole's body (Fig. 1*A*, *B*), approximately at the level of the 5th myotomal cleft (Buhl et al., 2015; Li et al., 2001). A third glass suction electrode (tip opening □30□m) filled with saline was used to record extracellular hindbrain neuronal activity (Fig. 1*A*, *B*). The hindbrain recording electrode was randomly positioned in one of the three hindbrain areas depicted in fig. 1C. The electrode's location was annotated based on its position relative to anatomical landmarks, *i.e.* the midbrain-hindbrain border (MHB), otic capsules and the obex (Fig. 1*C*). Ventral root and hindbrain extracellular activity were amplified, filtered, and digitized via a Power1401 (CED, Cambridge, UK) and recorded in Signal 7 (CED, Cambridge, UK). Electrical stimulation was delivered in single square pulses through a glass suction electrode, wrapped in silver wire and filled with saline. This stimulating electrode was attached to the trunk skin at the level of the anus (Fig. 1*B*). Both intensity (V) and duration (ms) of the stimulus were set in each experiment as the smallest values required to evoke fictive swimming. All animals initiated fictive swimming after a stimulation within the range of 3.5-4.5 V and 0.25-0.4 ms.

Experimental design and statistical analyses

In order to discriminate neuronal activity correlated to swim initiation only, ventral root and hindbrain neuronal activity were recorded in four motor states: 1) at rest, when no stimulus was applied to the tadpole's skin and ventral root activity was absent; 2) stimulation/no start, when the stimulus delivered was not strong enough to produce fictive swimming; 3) stimulation/start, when the stimulus delivered triggered fictive swimming; 4) swimming, during sustained fictive swimming (Fig. 1*D*).

Spike sorting, based on single spikes' size and shape, was carried out on all hindbrain extracellular recordings using Spike2 version 10.00 (CED, Cambridge, UK), and single units were visually evaluated for spike shape consistency. The number of spikes fired by individual units

was counted during 150 ms trials in each of the four motor states (Fig. 1*D*). Randomly chosen 150 ms repetitions throughout a recording were analyzed for 'rest' and 'swimming' states. For the two states where stimulation was applied ('stimulation/start' and 'stimulation/no start'), the time frame analyzed was stimulation (t=0) + 150 ms. A minimum number of 4 trials were analyzed for each of the four motor states, in each experiment. Twoway ANOVA with Geisser-Greenhouse correction was run (GraphPad Prism 9) on the number of spikes counted for each unit in the four motor states described above.

Stimulation and swimming were the two factors tested in the two-way ANOVA. Depending on the statistical outcome of the two-way ANOVA, units considered for further classification and firing pattern analysis were: 1) units which showed a p value <0.05 for the interaction between stimulation and swimming; 2) units which showed a p value <0.05 for the swimming factor (swim effect). Coefficient of variations (CV=standard deviation/mean) were used to create the heat maps presented. CV was calculated for each time bin (5 ms) on the number of spikes fired by each unit during the same 5 ms.

Kolmogorov-Smirnov test or Kruskal-Wallis test were performed on latency data of spikes fired by units of interest, while Wilcoxon matched pairs signed rank test or repeated measures one-way ANOVA with Bonferroni correction were carried out on firing frequency data.

Results

Extracellular hindbrain neuronal activity was recorded from immobilised tadpoles in response to electrical trunk skin stimulation above and below the threshold for swimming. Single unit hindbrain neuronal activity was studied in four distinct motor states: 1) at rest, 2) following stimulation which did not initiate swimming (stim/no start), 3) following stimulation which led to swim initiation (stim/start), and 4) during sustained swimming (swimming) (Fig. 1*D*). Spike sorting analysis (see Materials and Methods) was used to isolate and subsequently categorise single units. All units were mapped along the rostro-caudal axis of the tadpole's hindbrain, which was divided into three sectors defined by anatomical landmarks (in rostrocaudal order: midbrain-hindbrain border, otic capsule and obex, respectively) as shown in Fig. 1*C*.

Novel hindbrain firing patterns involved in control of swimming and its initiation

We identified two novel firing patterns that were correlated with swim initiation in the tadpole. This was achieved by counting the number of spikes fired by individual units during 150 ms trials in each of the four experimental motor states (Fig. 1*D*). Two-way ANOVA was then run in order to categorize the different units according to changes in their firing rates during the different motor states.

25 units recorded from 6 animals (27.8% of total units; N=90 units in total from 18 animals) showed significantly higher activity at the start of swimming in response to trunk skin stimulation ('stimulus X swim interaction' units, p<0.05, two-way ANOVA; 150 ms continuous recording was analysed with t = 0 at the point of stimulation, Fig. 2*Ai*, *Aii*). We named these units, with firing rate significantly higher only at motor initiation, 'type A units'. Type A units were highly active only when the electrical stimulus was strong enough to induce swimming in the tadpole (the experimental condition referred to as 'stimulation/start'), while they were

mainly silent at rest, during sustained swimming, and when the stimulation failed to trigger swimming (Fig. 2*Ai*, *Aii*). 11 units recorded in 8 animals (12% of total units; N=90 units in total from 18 animals) showed increased firing activity following trunk skin stimulation, both at the initiation of, and during sustained swimming ('swim effect' units, $p<0.05$, two-way ANOVA; Fig. 2*Bi*, *Bii*). These units, which were more active both at the start of movement, as well as during continuous swimming, were named 'type B units'. Type B units were mostly inactive when the animal was not swimming, *i.e.* at rest and when stimulation did not lead to swimming (Fig. 2*Bi*, *Bii*).

Fifty-four (54) out of ninety (90) units did not change their firing rate in response to trunk skin stimulation, or during swimming ('non-significant units', $p>0.05$, two-way ANOVA). These units showed stable, low firing in every motor state tested (rest, stimulation/no start, stimulation/start and swimming, Fig. 3*Ai*, *Aii*), so we concluded that they were not implicated in the control of swim initiation. Thus, such units were excluded from further analysis.

Both type A and type B units were recorded throughout the hindbrain (Fig. 3*B*), with an overall prevalence for type A over swim type B (27.8% type A *vs* 12.2% type B units, Fig. 3*Bi*). In the rostral area of the hindbrain (sector 1, Fig. 1*C*), 30.3% of the recorded units were type A units (10/33 units), while 6.1% (2/33 units) fell into type B category (Fig. 3*Bii*). At the level of the otic capsule (sector 2, Fig. 1*C*), 19.4% of the units were found to be type A units (7/36 units) and 8.3% were type B units (3/36 units) (Fig. 3*Biii*). The highest percentage of type A and B units was recorded in the most caudal area of the hindbrain (sector 3, Fig. 1*C*), where 38.1% of the units recorded were type A units (8/21 units), and 28.6% (6/21 units) were type B units. (Fig. 3*Biv*). Percentages were calculated over the total number of units recorded within a single hindbrain sector. 'Non-significant units' were also recorded throughout the hindbrain: 63.6% in the rostral area (21/33 sector's units), 72.2% (26/36 sector's units) at the otic capsule level, 33.3% (7/21 sector's units) in the caudal area (Fig. 3*Bii-iv*, percentages calculated over the total number of units recorded within each hindbrain sector).

We recorded from three CPG units, one in each hindbrain sector, and we fully characterised them in order to rule out the possibility of type A or type B units exhibiting CPG-like activity. All three CPG units were silent when fictive swimming was not present. Indeed, CPG units did not show any firing activity in trials with sub-threshold stimulation or during resting conditions (Fig. 4*A* and *B*, 'stimulation/start' and 'rest' conditions, respectively). When the stimulus delivered was sufficient to initiate swimming, CPG units were activated (Fig. 4*A*), and they fired rhythmically, with the same firing rate as for the ventral root bursts (Fig. 4*B*, 'stimulation/start' and 'swimming'). CPG rhythmic firing continued during ongoing swimming (Fig. 4*A* and *B*, 'swimming'). Importantly, all CPG units were activated at the same time as the first ventral root burst, and they were always silent prior to the start of fictive swimming (Fig. 4*C*).

None of type A or type B units presented in this study showed features of rhythmic activity as observed in the CPG units showed in Fig. 4. Moreover, contrary to CPG characteristic features, type A and type B units fired spikes before the initiation of swimming, as discussed below. Based on this evidence, we are confident that none of type A or type B units studied here can be assigned to the CPG category.

Type A units are activated earlier than type B units, and both firing patterns are distributed throughout the hindbrain

Following trunk skin stimulation, type A unit firing increased to a peak (0.48 ± 0.21 Hz, mean ± SEM) 11 ms before swimming started, and then slowly decreased to become silent during sustained swimming (Fig. 5*Ai*). Type B units also increased their activity rate before the start of swimming (Fig. 5*Ai*), but there was no clear peak in their overall firing activity. Type B unit firing rates were stable as swimming became continuous (0.06 ± 0.08 Hz 10 ms before vs 0.06 ± 0.09 Hz 10 ms after swimming initiation; data expressed as mean ± SEM). In addition, type A unit firing in response to trunk skin stimulation demonstrated an overall earlier onset in comparison to firing of type B units (Fig. 5Aii; *p<0.0001,* Kolmogorov-Smirnov test). Type A units recorded in the central area of the hindbrain (otic capsule level, sector 2, Fig. 1*C*) were the major contributors to the firing rate peak at swimming initiation (1.28 ± 2.23 Hz occurring 10 ms before the start of movement, Fig. 5*Bi*). Type A units detected in the rostral and caudal sectors increased their firing in a less steep fashion (Fig. 5*Bi*), nevertheless still contributing to the overall augmented activity, which was prolonged after the initiation of swimming (0 to ~150 ms after the start, Fig. 5*Bi*). However, the onset and distribution of spikes fired at the start of movement by type A units across the three hindbrain sectors did not differ (Fig. 5*Bii*). Type B units recorded in the three hindbrain areas showed prolonged firing at the initiation of swimming, resulting in a constant activity that persisted during sustained swimming (Fig. 5*Ci*). Similarly, to type A units, the onset and distribution of the spikes fired by type B units did not differ among the three hindbrain areas (Fig. 5*Cii*). Both type A and type B units showed a distribution of firing activity throughout the three hindbrain sectors, leading us to consider the two populations to be dispersed throughout the hindbrain.

Subpopulations of type A and type B units are differentially activated

Based on their distinctive firing patterns, we identified two subgroups among type A units. The first group, 'type A, level 1' (referred to as type A_1), showed increased firing in the stimulation/start trials (Fig. 6*Ai* and *Aii*), but was also active when the stimulus delivered was not strong enough to cause swim initiation (stim/no start, Fig. 6*Bi* and *Bii*). On the contrary, the second group, named type A, level 2' (referred to as type A_2), was active only when the stimulation led to a motor response (Fig. 6*Ai*, *Aii* and 6*Bi*, *Bii*). In the time prior to swim initiation, spikes by type A_1 units fired at shorter latencies compared to those fired by type A_2 units (Fig. *6C*, negative area of the graph; *p*=0.0187, Kolmogorov-Smirnov test). After swimming had started, the temporal distribution of spikes fired by type A_1 and A_2 units did not differ (Fig. *6C*, positive area of the graph; *p*=0.0923, Kolmogorov-Smirnov test). Similarly, the type B population could be divided into two subpopulations. 'Type B, level 1' (referred to as type B_1) units were active when stimulation was delivered to the animal, irrespective of the motor outcome (Fig. 7*Ai*, *Aii* and 7*Bi*, *Bii*). On the other hand, 'type B, level 2' (referred to as type B_2) firing was detected only when the electrical stimulus led to swimming (Fig. 7*Ai*, *Aii* and 7*Bi*, *Bii*). Contrary to type A units, both type B_1 and type B_2 units showed the same temporal distribution of spikes prior to movement initiation (Fig. 7*C*, negative area of the graph; *p*=0.1182, Kolmogorov-Smirnov test), as well as after swimming had become continuous (Fig. 7*C*, positive area of the graph; *p*=0.0803, Kolmogorov-Smirnov test).

Discussion

This work presents the first direct evidence of the distributed and diverse hindbrain neuronal excitability accounting for the long and variable latency to swim initiation in the *Xenopus laevis* tadpole. Using threshold and subthreshold trunk skin electrical stimuli evoking distinct motor outputs, we categorised hindbrain units based on their firing patterns and latencies in relation to the initiation of swimming. We identified two distinct groups of the recently proposed hindbrain extension neurons (hexNs; (Koutsikou et al., 2018)), and based on their firing properties, we divided them in two main groups, named type A and type B units.

We showed that both hexN types had the ability to extend the sensory memory based on their variable firing latency and frequency, following stimulation above and below the threshold for swimming (Fig. 2A, 5, 6, 7). Their firing patterns are also in agreement with well-established theories on sensory memory and motor decision-making, based on the existence of (Koutsikou et al, 2018) and their contribution to a variable accumulation of excitation to a threshold for movement initiation (Brody & Hanks, 2016; Carpenter & Williams, 1995; Gold & Shadlen, 2007; Noorani & Carpenter, 2016).

Furthermore, these units' firing patterns cannot be ascribed to any of the well-known cell types of the tadpole central nervous system. The firing of both types of units differed significantly from the early and mostly single-spike firing of sensory (Rohon-Beard cells) and sensory pathway neurons (dla and dlc) (A. Roberts & Clarke, 1982), as well as the rhythmic and late firing of dINs and other CPGs (Li et al., 2001; Li et al., 2006). Although Rohon-Beard cells, dlc and dla neurons fire reliably before swimming starts, they do so at short and consistent latencies. Moreover, these sensory pathway neurons fire only one or two action potentials and turn silent as soon as stimulation stops (Li et al., 2001; Li et al., 2004). Conversely, both type A and type B units fire multiple action potentials earlier than the start of swimming, and they do that at different latencies and rates of firing across trials. Type A and B units are also able to maintain their firing activity during the first few swimming cycles (type A units), and as fictive swimming progresses (type B units).

Both Type A and B units also showed different firing patterns to those of dINs. In the tadpole, dINs are key in the initiation and maintenance of locomotor activity (Li et al., 2006). They fire rhythmically, in phase with ipsilateral VR bursts, and they are activated only if the stimulation is strong enough to cause swim initiation. On the contrary, type A and B units did not fire rhythmically, and they were also active following subthreshold stimulation, which did not lead to the initiation of swimming.

Altogether, the features of early and variable firing activity recorded for type A and B units agree with both the latency of synaptic potentials previously recorded on dINs, as well as their long and variable firing (Buhl et al., 2015; Ferrario et al., 2021; Koutsikou et al., 2018). This suggests that both type A and type B units could act pre-synaptically to dINs.

Furthermore, we identified subtypes of both Type A and B units. The subtypes were categorised as 'first level' (A_1 and B_1) and 'second level' (A_2 and B_2) units based on their firing patterns in

response to subthreshold stimuli. First level units across both groups fired in response to subthreshold stimuli, at a lower frequency when compared to their firing following suprathreshold stimulation. This is in full agreement with the presence of synaptic potentials and accumulation of excitation on dINs (Koutsikou et al., 2018), even when the stimulus does not lead to dIN firing and thus to initiation of fictive swimming.

Based on our current findings, we propose a supraspinal mechanism of descending motor control, which includes the newly identified hindbrain units, as depicted in figure 8. We suggest that type A units work as sensory processors in the hindbrain of the tadpole, being postsynaptic to sensory pathway neurons (dlas and dlcs), whilst type B units act at later stages (motor planning centre), providing the necessary overall excitation to hindbrain dINs. This is supported by the longer latency of type B average spiking in comparison to type A firing. Initially, the sensory information received by Rohon-Beard cells in the skin is carried to the brain by dla and dlc neurons. It is then weighted and integrated by the proposed sensory processing centre in the hindbrain, comprised by first and second level type A units (Fig. 8). When the stimulus delivered is strong enough to lead to movement, type A_1 and A_2 units fire and excite both subpopulations of type B units, the proposed motor planning centre (stimulation/start; Fig. 8*A*), which will in turn provide the cumulative excitation to dINs, allowing them to reach their firing threshold. The firing of dINs will lead to motor neuron excitation and the initiation of swimming (Li et al., 2006; Li et al., 2009).

All first level units were active also when the trunk skin stimulus applied was below the threshold for swimming (stimulation/no start, Fig. 8*B*), in contrast to second level units which were inactive under similar conditions. In the model we propose that the firing of first level units will still lead to depolarisation of dINs as previously reported by Koutsikou and colleagues (Koutsikou et al., 2018), but only below their firing threshold, thus not allowing swim initiation.

We hypothesise that the type A_2 population is less likely to fire due to its electrical membrane properties, providing the neuronal circuit with the means to discriminate between stimulus intensities. In this scenario, all type A units will receive synaptic input from dla and dlc neurons. However, type A_2 units will not be activated due to their higher firing threshold. On the contrary, type A_1 units will be activated at lower stimulus intensities. Once active, type A_2 units would excite second level type B units, which will provide, together with first level type B, strong excitation to dINs (Fig. 8*A*). A different firing probability for first *versus* second level type A populations might also explain the slightly delayed firing of second level units before swimming starts, compared to first level units of the same type (Fig. 6, 7).

Although it is not possible to precisely locate the neuronal somata through extracellular recordings, we discovered that type B unit firing was preferentially localised in the caudal portion of the hindbrain, while type A unit firing was similarly dispersed along the hindbrain (Fig. 3*B*). This anatomical layout might partially reflect the function of the distinct neuronal populations, *i.e.* type B units would be excited, and thus controlled, by type A units. This layout across the tadpole hindbrain is in agreement with studies in complex vertebrate brains, where neurons involved in motor decision-making and planning have diverse spatial and temporal firing profiles, and they are intermingled across different brain areas (Svoboda & Li, 2018).

In this study we provide the first direct evidence of the spatial and temporal 'extension' of sensory information across the tadpole's hindbrain. We attribute to this hindbrain neuronal activity a major role in the accumulation of excitation on reticulospinal neurons, whose firing, or lack of, will in turn manifest into the tadpole's binary motor decision to swim or not to swim, respectively. We believe that the identification of the neuron-to-neuron pathways and how individual cells modulate aspects of the tadpole's behavior are the important next steps in unravelling the role of supraspinal brainstem control on motor output.

References

Arber, S. (2012). Motor circuits in action: specification, connectivity, and function. *Neuron, 74*(6), 975-989. doi:10.1016/j.neuron.2012.05.011

Armstrong, D. M. (1988). The supraspinal control of mammalian locomotion. *J Physiol, 405*, 1-37. doi:10.1113/jphysiol.1988.sp017319

Bouvier, J., Caggiano, V., Leiras, R., Caldeira, V., Bellardita, C., Balueva, K., . . . Kiehn, O. (2015). Descending Command Neurons in the Brainstem that Halt Locomotion. *Cell, 163*(5), 1191-1203. doi:10.1016/j.cell.2015.10.074

Brody, C. D., & Hanks, T. D. (2016). Neural underpinnings of the evidence accumulator. *Current Opinion in Neurobiology, 37*, 149-157. doi:https://doi.org/10.1016/j.conb.2016.01.003

Buhl, E., Soffe, S. R., & Roberts, A. (2015). Sensory initiation of a co-ordinated motor response: synaptic excitation underlying simple decision-making. *J Physiol, 593*(19), 4423-4437. doi:10.1113/JP270792

Caggiano, V., Leiras, R., Goni-Erro, H., Masini, D., Bellardita, C., Bouvier, J., . . . Kiehn, O. (2018). Midbrain circuits that set locomotor speed and gait selection. *Nature, 553*(7689), 455-460. doi:10.1038/nature25448

Carpenter, R. H. S. (1999). A neural mechanism that randomises behaviour. *Journal of Consciousness Studies, 6*(1), 13-22.

Carpenter, R. H. S., & Williams, M. L. L. (1995). Neural computation of log likelihood in control of saccadic eye movements. *Nature, 377*(6544), 59-62. doi:10.1038/377059a0

Clarke Jd Fau Hayes, B. P. H., S. P., & Roberts, A. (1984). Sensory physiology, anatomy and immunohistochemistry of Rohon-Beard neurones in embryos of Xenopus laevis. *J Physiol, Mar*(348), 511–525.

Dietz, V. (2010). Behavior of spinal neurons deprived of supraspinal input. *Nat Rev Neurol, 6*(3), 167-174. doi:10.1038/nrneurol.2009.227

Ferrario, A., Palyanov, A., Koutsikou, S., Li, W., Soffe, S., Roberts, A., & Borisyuk, R. (2021). Whole animal modelling reveals neuronal mechanisms of decision-making and reproduces unpredictable swimming in frog tadpoles. doi:10.1101/2021.07.13.452162

Ferreira-Pinto, M. J., Ruder, L., Capelli, P., & Arber, S. (2018). Connecting Circuits for Supraspinal Control of Locomotion. *Neuron, 100*(2), 361-374. doi:10.1016/j.neuron.2018.09.015

Gold, J. I., & Shadlen, M. N. (2007). The Neural Basis of Decision Making. *Annual Review of Neuroscience, 30*(1), 535-574. doi:10.1146/annurev.neuro.29.051605.113038

Goulding, M. (2009). Circuits controlling vertebrate locomotion: moving in a new direction. *Nature Reviews Neuroscience, 10*(7), 507-518. doi:10.1038/nrn2608

James, L. J., & Soffe, S. R. (2011). Skin impulse excitation of spinal sensory neurons in developing Xenopus laevis (Daudin) tadpoles. *Journal of Experimental Biology, 214*(20), 3341-3350. doi:10.1242/jeb.058446

Kiehn, O. (2006). Locomotor circuits in the mammalian spinal cord. *Annu Rev Neurosci, 29*, 279-306. doi:10.1146/annurev.neuro.29.051605.112910

Kiehn, O. (2016). Decoding the organization of spinal circuits that control locomotion. *Nature Reviews Neuroscience, 17*(4), 224-238. doi:10.1038/nrn.2016.9

Koutsikou, S., Merrison-Hort, R., Buhl, E., Ferrario, A., Li, W. C., Borisyuk, R., . . . Roberts, A. (2018). A simple decision to move in response to touch reveals basic sensory memory and mechanisms for variable response times. *J Physiol, 596*(24), 6219-6233. doi:10.1113/JP276356

Li, W. C., Perrins, R., Soffe, S. R., Yoshida, M., Walford, A., & Roberts, A. (2001). Defining classes of spinal interneuron and their axonal projections in hatchling Xenopus laevis tadpoles. *J Comp Neurol, 441*(3), 248-265. doi:10.1002/cne.1410

Li, W. C., Roberts, A., & Soffe, S. R. (2009). Locomotor rhythm maintenance: electrical coupling among premotor excitatory interneurons in the brainstem and spinal cord of young Xenopus tadpoles. *J Physiol, 587*(Pt 8), 1677-1693. doi:10.1113/jphysiol.2008.166942

Li, W. C., Soffe, S. R., & Roberts, A. (2004). Dorsal Spinal Interneurons Forming a Primitive, Cutaneous Sensory Pathway. *Journal of Neurophysiology, 92*(2), 895-904. doi:10.1152/jn.00024.2004

Li, W. C., Soffe, S. R., Wolf, E., & Roberts, A. (2006). Persistent responses to brief stimuli: feedback excitation among brainstem neurons. *J Neurosci, 26*(15), 4026-4035. doi:10.1523/JNEUROSCI.4727-05.2006

MacKinnon, C. D. (2018). Sensorimotor anatomy of gait, balance, and falls. *Handb Clin Neurol., 159*, 3-26. doi:10.1016/B978-0-444-63916-5.00001-X

Nieuwkoop, P., & Faber, J. (1956). Normal table of Xenopus laevis (Daudin) a systematical and chronological survey of the development from the fertilized egg till the end of metamorphosis (2nd edition). *North-Holland Pub. Co*.

Noorani, I., & Carpenter, R. H. S. (2016). The LATER model of reaction time and decision. *Neuroscience & Biobehavioral Reviews, 64*, 229-251. doi:https://doi.org/10.1016/j.neubiorev.2016.02.018

Opris, I., Dai, X., Johnson, D. M. G., Sanchez, F. J., Villamil, L. M., Xie, S., . . . Noga, B. R. (2019). Activation of Brainstem Neurons During Mesencephalic Locomotor Region-Evoked Locomotion in the Cat. *Front Syst Neurosci, 13*, 69. doi:10.3389/fnsys.2019.00069

Parker, D. (2010). Neuronal network analyses: premises, promises and uncertainties. *Philos Trans R Soc Lond B Biol Sci, 365*(1551), 2315-2328. doi:10.1098/rstb.2010.0043

Roberts, A. (1996). Trigeminal pathway for the skin impulse to initiateswimming in hatchling Xenopus embryos. *Journal of Physiology, 493P*, 40-41P.

Roberts, A., Borisyuk, R., Buhl, E., Ferrario, A., Koutsikou, S., Li, W. C., & Soffe, S. R. (2019). The decision to move: response times, neuronal circuits and sensory memory in a simple vertebrate. *Proc Biol Sci, 286*(1899), 20190297. doi:10.1098/rspb.2019.0297

Roberts, A., & Clarke, J. D. (1982). The neuroanatomy of an amphibian embryo spinal cord. *Phil. Trans. R. Soc. Lond. B, 296*, 195-212.

Roberts, A., Li, W.-C., & Soffe, S. (2010). How neurons generate behaviour in a hatchling amphibian tadpole: an outline. *Frontiers in Behavioral Neuroscience, 4*(16). doi:10.3389/fnbeh.2010.00016

Roberts, A. S., Charles A. (1971). The Properties and Propagation of a Cardiac-like Impulse in the Skin of Young Tadpoles. *Z. vergl. Physiologie, 71*, 295-310.

Ruder, L., & Arber, S. (2019). Brainstem Circuits Controlling Action Diversification. *Annual Review of Neuroscience, 42*(1), 485-504. doi:10.1146/annurev-neuro-070918-050201

Sakurai, A., & Katz, P. S. (2016). The central pattern generator underlying swimming in Dendronotus iris:
a simple half-center network oscillator with a twist. *J Neurophysiol, 116*(4), 1728-1742. doi:10.1152/jn.00150.2016

Shik, M. L., & Orlovsky, G. N. (1976). Neurophysiology of locomotor automatism. *Physiol Rev, 56*(3), 465501. doi:10.1152/physrev.1976.56.3.465

Stephenson-Jones, M., Samuelsson, E., Ericsson, J., Robertson, B., & Grillner, S. (2011). Evolutionary conservation of the basal ganglia as a common vertebrate mechanism for action selection. *Curr Biol, 21*(13), 1081-1091. doi:10.1016/j.cub.2011.05.001

Svoboda, K., & Li, N. (2018). Neural mechanisms of movement planning: motor cortex and beyond. *Current Opinion in Neurobiology, 49*, 33-41. doi:https://doi.org/10.1016/j.conb.2017.10.023

Figure legends

Figure 1. Experimental design

A. Lateral view of stage 37/38 *Xenopus laevis* tadpole; anatomical features are indicated on the head (eye and otic capsule) and along the body (spinal cord and trunk muscles). Grey dotted line on the head represents the area where the skin was removed to expose the brain.

B. Dorsal view of developmental stage 37/38 *Xenopus* tadpole with extracellular suction electrodes positioned as per experimental conditions. Grey dotted line marks the area where the skin was removed to make the hindbrain accessible. In different experiments, the brain electrode (hindbrain) was positioned in one of the three hindbrain sectors as depicted in Fig. 1*C*. The two VR (ventral root) electrodes were positioned at the 5th inter-myotomal cleft on both sides of the tadpole's body (left VR, right VR). The stimulating electrode (stimulus) was attached to the skin on the right side of the body at the level of the anus. Scale bar as in A.

C. The *Xenopus* tadpole's hindbrain as it appears when the skin is removed. The hindbrain was visually divided into three sectors along the rostro-caudal axis using well-defined anatomical landmarks, i.e. MHB (yellow arrow), otic capsules (blue arrow) and obex (green arrow): rostral sector (1), otic capsule level (2) and caudal sector (3).

D. Examples of recordings during the four different motor states (200 ms): rest, stimulation/no start of swimming, stimulation/start of swimming, sustained swimming. Raw traces for hindbrain extracellular activity (hb, black trace) and right and left VR recording (rVR

and lVR, grey traces) are presented. Red arrowheads indicate stimulus delivery, blue arrowhead indicates the start of swimming.

Figure 2. Type A and type B units are activated at the start of swimming.

Ai. Average heat map of type A units recorded in the hindbrain (25 units in 11 animals, minimum of 4 trials per motor state per unit). Coefficients of variation (CV=standard deviation/mean) were calculated for each time bin (5 ms) on the number of spikes fired by single units in the four motor states. **Aii**. Examples of spikes fired by a single type A unit recorded in the four motor states investigated (rest, stimulation/no start, stimulation/start, swimming). 150 ms are reported for each example. Red lines indicate spikes fired by the unit, and they are presented above the respective extracellular hindbrain raw trace recording (black trace). Fictive swimming is shown by rhythmic right and left VR bursts (grey trace, rVR and lVR). Red arrowheads represent the delivery of the electrical stimulus; blue arrowhead indicates the start of swimming.

Bi. Average heat map of type B units recorded in the hindbrain (11 units in 8 animals, minimum of 4 trials per motor state per unit). Coefficients of variation (CV=standard deviation/mean) were calculated for each time bin (5 ms) on the number of spikes fired by single units in the four motor states. **Bii.** Examples of spikes fired by a single type B unit recorded in the four motor states investigated (rest, stimulation/no start, stimulation/start, swimming) 150 ms are reported for each example. Green lines indicate spikes fired by the unit, and they are presented above the respective extracellular hindbrain recording raw trace
(black trace). Fictive swimming is shown by rhythmic right and left VR bursts (grey trace, rVR and lVR). Red arrowheads represent the delivery of the electrical stimulus; blue arrowhead indicates the start of swimming

Figure 3

A. Neural activity of non-significant units is not correlated to swim behaviour.

Ai. Average heat map of non-significant units recorded in the hindbrain (54 units in 14 animals, minimum of 4 trials per motor state per units). Coefficients of variation (CV=standard deviation/mean) were calculated for each time bin (5 ms) on the number of spikes fired by single units during the same 5 ms in the four motor states. **Aii.** Examples of spikes fired by a single non-significant unit recorded in the four motor states investigated (rest, stimulation/no start, stimulation/start, swimming) 200 ms are reported for each example. Orange lines indicate spikes fired by the unit, and they are presented above the respective extracellular hindbrain raw trace recording (black trace). Fictive swimming is shown by rhythmic bursts of the right VR (grey trace, rVR). Red arrowheads represent the delivery of the electrical stimulus; blue arrowhead indicates the start of swimming. **B. Hindbrain unit distribution.**

Bar charts representing percentages for non-significant (grey), type B (green) and type A units (violet) across the entire hindbrain (**Bi**), and in different hindbrain sectors as depicted in Fig. 1C

(**Bii**, rostral sector; **Biii**, otic capsule level; **Biv**, caudal sector). Percentages were calculated over the total number of units recorded in the hindbrain (Bi, 54/90 = 60.0% non-significant units; 11/90 = 12.2% type B units, 25/90 = 27.8% type A units), and over the total number of units recorded in each of the hindbrain sectors (Bii, rostral sector, 21/33 = 63.6% non-significant units, 2/33 = 6.1% type B units, 10/33 = 30.3% type A units; Biii, otic capsule level, 26/36 = 72.2% non-significant units, 3/36 = 8.3% type B units, 7/36 = 19.4% type A units; Biv, caudal sector, 7/21 = 33.3% non-significant units; 6/21 = 28.6% type B units, 8/21 = 38.1% type A units)

Figure 4. Central Patter Generator (CPG) units.

A. Average heat map of CPG units recorded in the hindbrain (3 units in 3 animals, minimum of 4 trials per motor state per unit). Coefficients of variation (CV=standard deviation/mean) were calculated for each time bin (5 ms) on the number of spikes fired by single units in the four motor states.

B. Examples of spikes fired by a single non-significant unit recorded in the four motor states investigated (rest, stimulation/no start, stimulation/start, swimming). 200 ms are reported for each example. Green lines indicate spikes fired by the unit, and they are presented above the respective extracellular hindbrain raw trace recording (black trace). Fictive swimming is shown by rhythmic bursts of the right VR (grey trace, rVR). Red arrowheads represent the delivery of the electrical stimulus; blue arrowhead indicates the start of swimming.

C. Scatter plot of spikes fired by one rostral CPG (blue), one CPG recorded at the otic capsule level (red) and one caudal CPG (green) at the initiation of swimming. Dotted grey line (ms=0) marks the start of fictive swimming. Black solid lines indicate median values. Kruskal-Wallis test, p=0.356; rostral CPG unit 261.9 ± 141.5 ms; CPG unit at the otic capsule level 248.4 ± 143.9 ms; caudal CPG unit 205.9 ± 120.6 ms. Values expressed as median ± SD. 69 spikes from 1 rostral unit, 110 spikes from 1 unit at the otic capsule level, 15 spikes from 1 caudal unit.

Figure 5 A) Type A and Type B units are activated at different latencies

Ai) Firing rates of type A (violet line) and type B units (green line) recorded before movement initiation and in the first 500 ms of sustained swimming. Dotted grey line (ms=0) marks the start of fictive swimming. Data are presented as mean (solid lines) ± SEM (shaded area). Wilcoxon matched pairs signed rank test, *p<0.0001*; type A units 0.0925 ± 0.0139, type B units 0.0299 ± 0.0031 (mean ± SEM). Type A units N=25, type B units N=11; minimum 4 trials/unit. ****p<0.0001*

Aii) Scatter plot of spikes fired by type A units (violet) and type B units (green) before movement initiation and during the first 500 ms of sustained swimming. Dotted grey line (ms=0) marks the start of fictive swimming. Black solid lines indicate median values (median ± SD= 72.69 ± 104.4 ms for type A units; median ± SD = 160.8 ± 144.3 ms for type B units). Kolmogorov-Smirnov test, *p<0.0001*; 1145 spikes from 25 type A units, 288 spikes from 11 type B units. ****p<0.0001*

B, C) Type A and type B units show different firing rates throughout the hindbrain

Bi) Firing rates of type A units recorded in the rostral sector (blue), at the otic capsule level (red) and in the caudal sector (green) of the hindbrain. Dotted grey line (ms=0) marks the start of fictive swimming. Data are presented as mean (solid lines) ± SEM (shaded area). Repeated measures one-way ANOVA with Bonferroni correction for multiple comparisons, *p=0.0003*; rostral vs OC level, mean diff.=0.0725; rostral vs caudal, mean diff.= 0.0376; OC level vs caudal, mean diff.= 0.1101. Rostral sector N=10 units; otic capsule level N=7 units; caudal sector N=8 units; minimum 4 trials per unit. ****p<0.001*

Bii) Scatter plot of spikes fired by type A units recorded in the rostral sector (blue), at the otic capsule level (red) and in the caudal sector (green) of the hindbrain. Dotted grey line (ms=0) marks the start of fictive swimming. Black solid lines indicate median values (median ± SD = 71.94 ± 93.29 ms for rostral units; median ± SD = 65.97 ± 117.5 ms for otic capsule level units; median ± SD= 78.32 ± 109.5 ms for caudal units). Kruskal-Wallis test, *p=0.0618*; 558 spikes from 10 rostral units, 284 spikes from 7 otic capsule level units, 303 spikes from 8 caudal units.

Ci) Firing rates of type B units recorded in the rostral sector (blue), at the otic capsule level (red) and in the caudal sector (green) of the hindbrain. Dotted grey line (ms=0) marks the start of fictive swimming. Data are presented as mean (solid lines) ± SEM (shaded area). Repeated measures one-way ANOVA with Bonferroni correction for multiple comparisons, *p<0.0001*; rostral vs OC level, mean diff.= 0.0390; rostral vs caudal, mean diff.= 0.0137; OC level vs caudal, mean diff.= -0.0254. Rostral sector N=2 units; otic capsule level N=3 units; caudal sector N=6 units; minimum 4 trials per unit. *****p<0.0001*

Cii) Scatter plot of spikes fired by type B units recorded in the rostral sector (blue), at the otic capsule level (red) and in the caudal sector (green) of the hindbrain. Dotted grey line (ms=0) marks the start of fictive swimming. Black solid lines indicate median values (median ± SD = 127.8 ± 148.6 ms for rostral units; median ± SD = 190.2 ± 160.7 ms for otic capsule level units; median ± SD = 162.2 ± 134.1 ms for caudal units). Kruskal-Wallis test, *p=0.2837*; 63 spikes from 2 rostral units, 73 spikes from 3 oc level units, 152 spikes from 6 caudal units.

Fig. 6. Subpopulations of type A units are activated differently

Ai) Firing rates of first (type A_1, pink line) and second level (type A_2, violet line) type A units recorded before movement initiation and in the first 500 ms of sustained swimming. Dotted grey line (ms=0) marks the start of fictive swimming. Data are presented as mean (solid lines) ± SEM (shaded area). Wilcoxon matched pairs signed rank test, *p=0.0511*; type A_1 units 0.0695 ± 0.0100 ms, type A_2 units 0.1094 ± 0.0180 ms (mean ± SEM). First level type A_1 units N=11, type A_2 units N=14; minimum 4 trials/unit.

Aii) Examples of spikes fired by one type A_1 unit (top trace, pink lines) and one type A_2 unit (bottom trace, violet lines), recorded in the stimulation/start motor state. Spikes fired by the units are presented above the respective extracellular hindbrain recording raw trace (hb, black trace). Fictive swimming is shown by rhythmic VR bursts (grey trace, VR). For clarity, only the VR with the first burst, marking swimming initiation, is shown here. Red arrowheads represent the delivery of the electrical stimulus; blue arrowhead indicates the start of swimming.

Bi) Firing rates of type A_1 (pink line) and type A_2 (violet line) units recorded in the first 500 ms after stimulation. Data are presented as mean (solid lines) ± SEM (shaded area). Wilcoxon matched pairs signed rank test, *p<0.0001*; type A_1 units 0.0149 ± 0.0018 ms, type A_2 units 0.0000 ± 0.0000 (mean ± SEM). Type A_1 units N=11, type A_2 units N=14; minimum 4 trials/unit. ****p<0.0001*

Bii) Examples of spikes fired by one type A_1 unit(top trace, pink lines) and one type A_2 unit (bottom trace, no lines), recorded in the in the stimulation/no start motor state. Spikes fired by the units are presented above the respective extracellular hindbrain recording raw trace (hb, black trace). The absence of fictive swimming is shown by the silent VR (grey trace, VR). As both VR were silent in this case, for clarity only one VR is shown here. Red arrowheads represent the delivery of the electrical stimulus.

C) Scatter plot of spikes fired by type A_1 units (pink) and type A_2 units (violet) before movement initiation and during the first 500 ms of sustained swimming. Dotted grey line (ms=0) marks the start of fictive swimming. Black solid lines indicate median values. Kolmogorov-Smirnov test on data recorded before swim initiation, *p=0.0187*; type A_1 units -25.75 ± 50.27 ms; type A_2 units -17.19 ± 26.90 ms (median ± SD). 60 spikes from 11 type A_1 units, 120 spikes from 14 type A_2 units. Kolmogorov-Smirnov test on data recorded after swim initiation, *p=0.0923*; type A_1 units 91.09 ± 94.18 ms; type A_2 units 88.95 ± 104.5 ms (median ± SD). 450 spikes from type A_1 units, 565 spikes from type A_2 units. **p<0.05*

Fig. 7. Subpopulations of type B units are activated differently

Ai) Firing rates of type B_1 (blue line) and type B_2 (green line) units recorded before movement initiation and in the first 500 ms of sustained swimming. Dotted grey line (ms=0) marks the start of fictive swimming. Data are presented as mean (solid lines) ± SEM (shaded area). Wilcoxon matched pairs signed rank test, *p<0.0394*; type B_1 units 0.0237 ± .0035, type B_2 units 0.0350 ± 0.0042 (mean ± SEM). Type B_1 units N=5, type B_2 units N=6; minimum 4 trials/unit. **p<0.05*

Aii) Examples of spikes fired by one type B_1 unit (top trace, blue lines) and one type B_2 (bottom trace, green lines), recorded in the in the stimulation/start motor state. Spikes fired by the units are presented above the respective extracellular hindbrain recording raw trace (hb, black trace). Fictive swimming is shown by rhythmic VR bursts (grey trace, VR). For clarity, only the VR with the first burst, marking swimming initiation, is shown here. Red arrowheads represent the delivery of the electrical stimulus; blue arrowhead indicates the start of swimming.

Bi) Firing rates of type B_1 (blue line) and type B_2 (green line) units recorded in the first 500 ms after stimulation. Data are presented as mean (solid lines) ± SEM (shaded area). Wilcoxon matched pairs signed rank test, *p<0.0001*; type B_1 units 0.0111 ± 0.0017, type B_2 units 0.0000 ± 0.0000 (mean ± SEM). Type B_1 units N=5, type B_2 units N=6; minimum 4 trials/unit. ****p<0.0001*

Bii) Examples of spikes fired by one type B_1 (top trace, blue lines) and one type B_2 unit (bottom trace, no lines), recorded in the in the stimulation/no start motor state. Spikes fired by the units are presented above the respective extracellular hindbrain recording raw trace (hb, black trace).

The absence of fictive swimming is shown by the silent VR (grey trace, VR). For clarity, only one VR is shown here. Red arrowheads represent the delivery of the electrical stimulus.

C) Scatter plot of spikes fired by type B_1 (blue) and type B_2 units (green) before movement initiation and during the first 500 ms of sustained swimming. Dotted grey line (ms=0) marks the start of fictive swimming. Black solid lines indicate median values. Kolmogorov-Smirnov test on data recorded before swim initiation, *p=0.1182*; type B_1 units -15.65± 11.20 ms; type B_2 units -30.61 ± 38.49 ms (median ± SD). 8 spikes from 5 type B_1 units, 21 spikes from 6 type B_2 units. Kolmogorov-Smirnov test on data recorded after swim initiation, *p=0.0803*; type B_1 units 183.5 ± 152.7 ms; type B_2 units 183.9 ± 125.3ms (median ± SD). 75 spikes from 5 type B_1 units, 184 spikes from 6 type B_2 units.

Fig. 8. Proposed neural mechanism for motor descending control

A) Scheme of the proposed neural circuit active when a suprathreshold stimulus is delivered to the tadpole (stimulation/start). Solid arrows represent known synaptic connections, solid line boxes indicate known circuits (sensory pathway and swimming). Dotted arrows and boxes represent proposed connections and circuits in the hindbrain (sensory processing, motor planning, descending motor control). A higher firing rate in the various synaptic connections is represented by thicker arrows, compared to the same arrows in B. Red star represents stimulation that is strong enough to lead to swim initiation.

Scheme of the proposed neural circuit active when a subthreshold stimulus is delivered to the tadpole (stimulation/no start). Solid arrows represent known synaptic connections, solid line boxes indicate known circuits (sensory pathway and swimming). Dotted arrows and boxes represent proposed connections and circuits in the hindbrain (sensory processing, motor planning, descending motor control). A lower firing rate in the various synaptic connections is represented by thinner arrows, compared to the same arrows in B. Red star represents a weaker stimulation than in A, which does not lead to swim initiation. Red 'X' indicates that the tadpole does not start to swim.

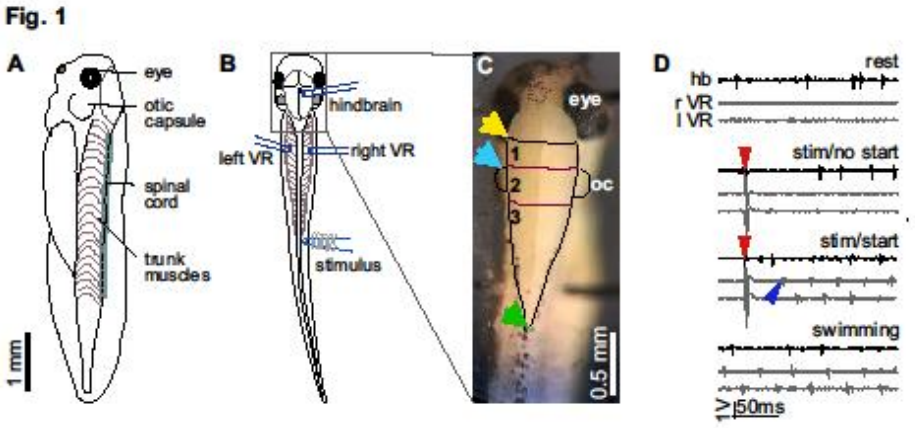

Fig. 2

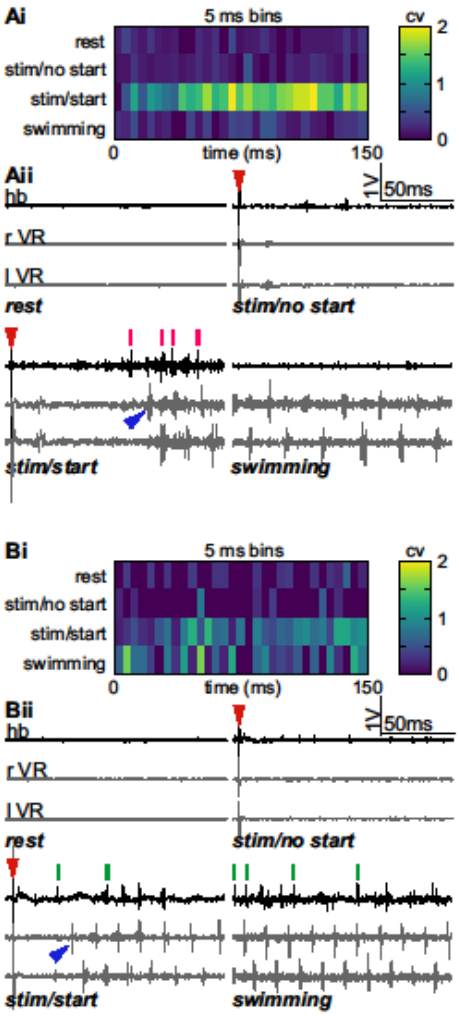
Ai
5 ms bins
cv
2
1
0
rest
stim/no start
stim/start
swimming
0
time (ms)
150
Aii
hb
1V
50ms
r VR
l VR
rest
stim/no start
stim/start
swimming
Bi
5 ms bins
cv
2
1
0
rest
stim/no start
stim/start
swimming
0
time (ms)
150
Bii
hb
1V
50ms
r VR
l VR
rest
stim/no start
stim/start
swimming

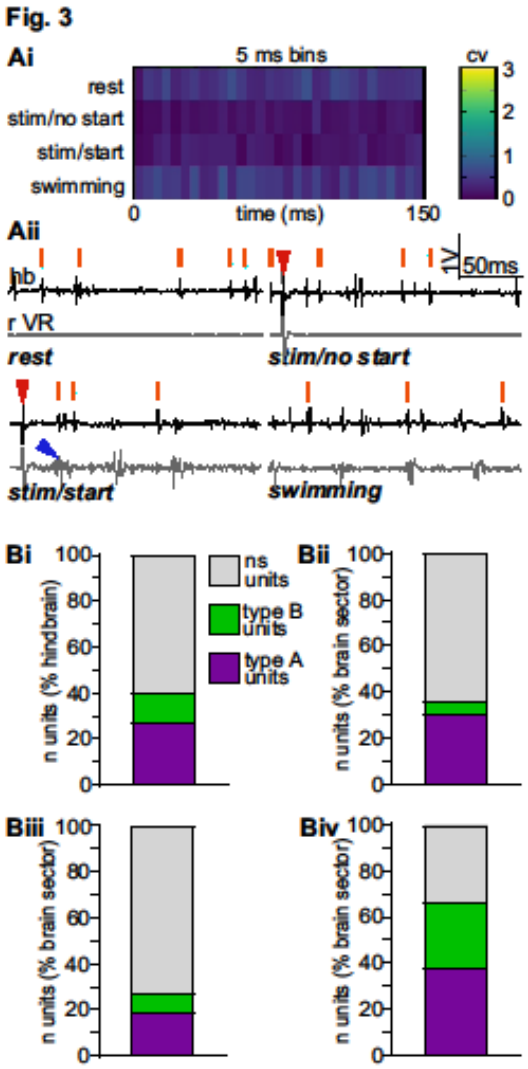
Fig. 3
Ai
5 ms bins
cv
rest
stim/no start
stim/start
swimming
0
time (ms)
150
3
2
1
0
Aii
hb
r VR
1V
50ms
rest
stim/no start
stim/start
swimming
Bi
Bii
Biii
Biv
n units (% hindbrain)
n units (% brain sector)
ns units
type B units
type A units
100
80
60
40
20
0

Fig. 4

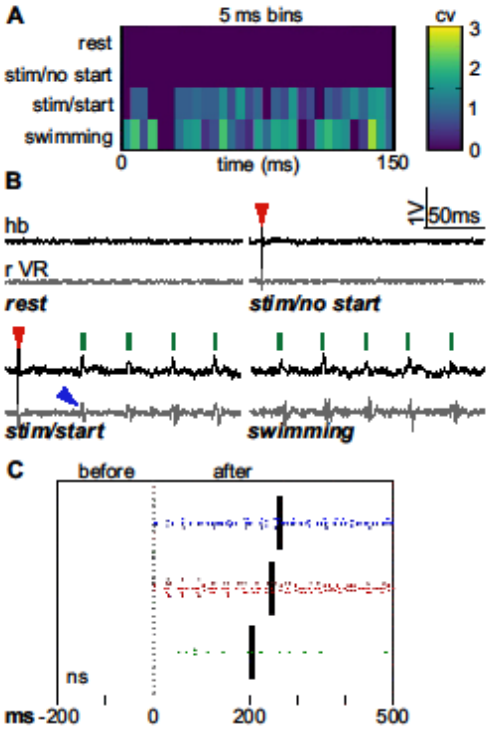
A
5 ms bins
cv
3
2
1
0
rest
stim/no start
stim/start
swimming
0
time (ms)
150
B
hb
r VR
≥50ms
rest
stim/no start
stim/start
swimming
C
before
after
ns
ms -200
0
200
500

Fig. 5

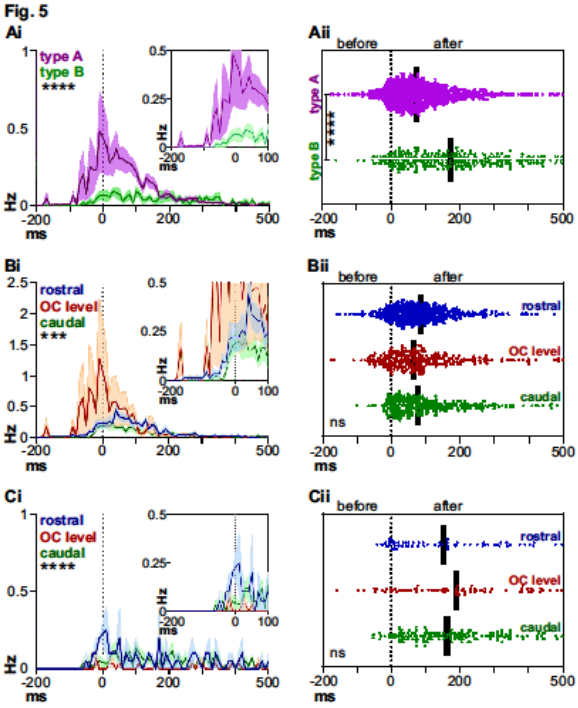
Ai
type A
type B
****
Hz
ms
Aii
before
after
type A
type B
****
Bi
rostral
OC level
caudal
***
Bii
rostral
OC level
caudal
ns
Ci
rostral
OC level
caudal
****
Cii
rostral
OC level
caudal
ns

Fig. 6

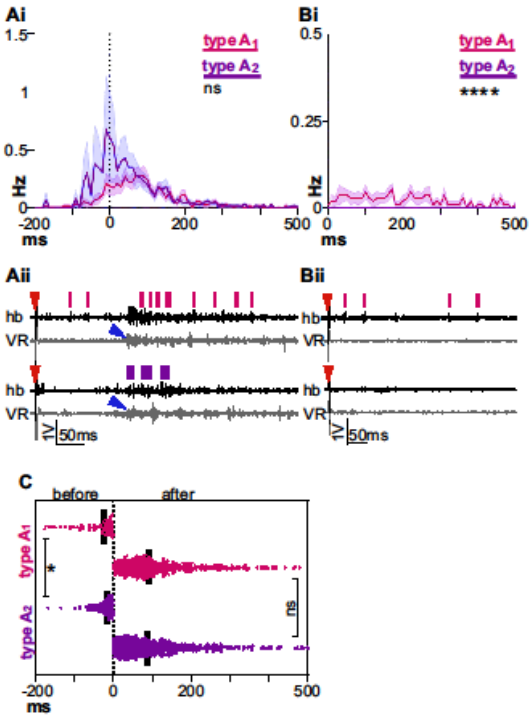

Fig. 7

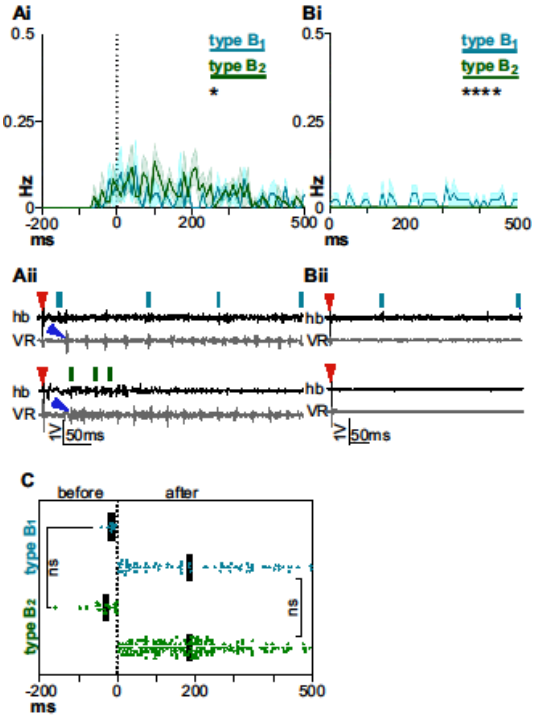

Fig. 8